Université d'Ottawa BIBLIOTHÈQUES ANNEXE DE LA BIBLIOTHÈQUE uOttawa LIBRARY ANNEX LIBRARIES

# KILOVOLT COLLISIONS OF SMALL IONS

by

Jozsef Bordas Nagy

A Thesis

Presented to the University of Ottawa

in fulfillment of the

thesis requirement for the degree of

Ph.D.

in

Chemistry

Jozsef Bordas Nagy, Ottawa, Canada, 1989

UMI Number: DC53726

INFORMATION TO USERS

The quality of this reproduction is dependent upon the quality of the copy submitted. Broken or indistinct print, colored or poor quality illustrations and photographs, print bleed-through, substandard margins, and improper alignment can adversely affect reproduction.
In the unlikely event that the author did not send a complete manuscript and there are missing pages, these will be noted. Also, if unauthorized copyright material had to be removed, a note will indicate the deletion.

UMI®

UMI Microform DC53726
Copyright 2011 by ProQuest LLC
All rights reserved. This microform edition is protected against unauthorized copying under Title 17, United States Code.

ProQuest LLC
789 East Eisenhower Parkway
P.O. Box 1346
Ann Arbor, MI 48106-1346

Acknowledgements

I would like to thank my supervisor, Professor John L. Holmes for his support, encouragement and enthusiasm throughout my studies. The many discussions we had together were always stimulating, enjoyable and very essential for me in making progress in research. I learnt very much about ion-chemistry in particular and doing research in general from Professor Holmes.

Many thanks to Dr. A.A. Mommers, Sander, for knowing so much about the ZAB and being so creative in modifying it and most of all, for being so generous with helping me when I got stuck.

Thanks to Professor Fred P. Lossing, Dr. Clem Kazakoff and Dr. John Krause for their advice and assistance throughout the years I spent in the mass spec lab. Thanks to my fellow graduate students Marcia Blanchette, Jeff Ridal and Marcel Hop for their constant willingness to help and their friendship.

I would like to thank Eva Szabo for the many drawings of highest quality she made for me and for her patience.

## ABSTRACT

Collision induced processes resulting from gas present in the field-free regions of mass spectrometers have been known to take place since the early days of mass spectrometry. But it is only in the last decade that instrumental development and extensive exploratory investigations of collision induced processes has led to the widespread application of these processes to problems in ion-physics, ion-chemistry and analytical mass spectrometry. The type of collision experiment that is described in this thesis is as follows. Ions are generated in an electron impact or chemical ionization ion source; the ions are accelerated out of the source to keV kinetic energies; an ion of a particular mass to charge ratio is then selected by a magnet or by a combination of a magnet and an electric sector and enters a field-free, drift region containing one or more differentially pumped areas into which collision gases can be admitted. The fast ionic products of the collision processes that take place between the fast projectile ions and the thermal collision gas(es), are momentum or kinetic energy analyzed. A general survey is presented of the scientific literature concerning the fundamental aspects and applications of these processes in Chapters 1.2.1-1.2.6. Chapters 2.1-2.8 deal with the research carried out by ourselves using a VG Analytical ZAB 2F double focusing mass spectrometer at the University of Ottawa. This work was focused around two main topics.

The first related to the generation of high-Rydberg fragment species in keV collisions of small ions with static target gases. By applying a field ionization device, added to the apparatus in our laboratory, fast high-Rydberg species were selectively field ionized resulting in a well-defined ion beam which could be kinetic energy analyzed by scanning the electrostatic sector of the mass spectrometer. The

analysis of the field-induced kinetic-energy spectra allowed us to establish general mechanisms for these processes.

The second topic related to fundamental aspects of a novel mass spectrometric technique, the so-called neutralization-reionization mass spectrometry (NRMS). In this technique, fast, mass selected beams of ions are neutralized in charge transfer collisions with a target gas, yielding a fast beam of neutrals. By applying an electric field the surviving ionic species are deflected; the fast neutral species are made to collide with a second collision gas and the ionic products from these collisions are kinetic energy analyzed. These experiments may yield information about the structure and stability of neutral species which are difficult to study by more conventional experimental methods. The results presented in this thesis have already appeared or are under publication in the international scientific literature. Below we list these publications together with the corresponding chapter of this thesis.

## LIST OF PUBLICATIONS

*Field Ionization of High Velocity Neutral Species; Rydberg States in Noble Gas Atoms; The Measurement of Translational Energy Loss in Neutralization Reionization Mass Spectra*, Jozsef Bordas-Nagy, John L. Holmes and Alexander A. Mommers, *Organic Mass Spectrometry*, **21** 629 (1986). **Chapters 2.1 and 2.2.**

*Kinetic Energy Spectroscopy of High-Rydberg Fragments from keV Collisions of* $H_2^+$ , $D_2^+$ , $N_2^+$ *and* $C_2^+$ *Ions with Rare-Gas Atoms*, Jozsef Bordas-Nagy and John L. Holmes, *Chemical Physics Letters*, **132** 200 (1986). **Chapters 2.3 and 2.5.**

*The Elusive Methylene Ylides*, Cornelis.E.C.A. Hop, Jozsef Bordas-Nagy, John L. Holmes and Johann K. Terlouw, *Organic Mass Spectrometry*, **23** 155 (1988).

*Kinetic Energy Spectra of High-Rydberg Fragments from keV Collisions Between Small Ions and Inert Gas Atoms*, Jozsef Bordas-Nagy and John L. Holmes, *International Journal of Mass Spectrometry and Ion Processes*, **82** 81 (1988). **Chapters 2.4 and 2.5.**

*The Effect of Vibrational Energy Content on the Neutralization Reionization Mass Spectra of* $H_2^+$ *Ions*, Jozsef Bordas-Nagy and John L. Holmes, *Organic Mass Spectrometry*, **23** 334 (1988). **Chapter 2.7.**

*keV Collisions of Methonium Ions; The Properties of* $CH_5$ *and* $CH_5^{2+}$ *and the Generation of High-Rydberg Fragments therefrom*, Jozsef Bordas-Nagy, Cornelis E.C.A. Hop and John L. Holmes, *International Journal of Mass Spectrometry and Ion Processes*, **85** 241 (1988). **Chapter 2.8.**

*keV Collisions of* $[H_3]^+$ *and Isotopomer Ions*, Jozsef Bordas Nagy and John L. Holmes, *Chemical Physics*, in press. **Chapter 2.6.**

- *Dissociation Processes in 10keV Collisions between* $[H_3]^+$ *and Rare Gas Atoms*, Jozsef Bordas Nagy and John L. Holmes, *Advances in Mass Spectrometry*, **11** (1988), in press.

## SUMMARY OF RESULTS

1 We have shown, through a series of experiments, that it is possible to field ionize fast, high-Rydberg (HR) species in a mass spectrometer by a pair of charged, very fine meshes which intersect perpendicularly the main ion beam path. It has also been shown that the resulting ion beam is still well defined and amenable to kinetic energy analysis.

2 A method has been established for the determination of the zero point of the scale of the kinetic energy loss suffered by a fast, mass selected beam of ions that undergo successive neutralization and reionization collisions. The neutralization of a fast beam of, $Kr^+$ ions residing in their high lying metastable electronic states, by collision with Ar atoms followed by reionization with He collision gas will give rise to a neutralized-reionized $Kr^+$ beam which has the same kinetic energy as that of the primary ion beam, within a ±0.3eV uncertainty.

3 By using the field ionization device we obtained kinetic energy spectra of H(HR) fragments from keV collisions of $[H_2]^+$ and $[D_2]^+$ with the rare gases and diatomic molecules. From the analysis of these spectra two major mechanisms for the generation of H(HR) fragments in these collisions have been established. One is the excitation of the electron of $[H_2]^+$ into a HR state which can be described as a system of two protons surrounded by an electron in far removed orbit. The two protons will repel

each other and after they separated the electron will join one them to give H(HR) fragment together with an $H^+$ counterfragment. The other involves electron capture by the $[H_2]^+$ ion into a HR orbit around it accompanied by a simultaneous (vibrational and/or electronic) excitation of the $[H_2]^+$ core. The excited $[H_2]^+$ core will dissociate into $H^+$+H fragments and the HR electron will join the $H^+$ to give a H(HR) fragment.

4 The kinetic energy spectra of H(HR) fragments from $[H_2]^+$/He collisions was used to characterize the vibrational energy distributions in $[H_2]^+$ ion beams of different origin.

5 Kinetic energy spectra of HR fragments from collisions of small ions, such as $[N_2]^+$, $[O_2]^+$, $[NO]^+$, $[CH]^+$, $[CH_4]^+$ etc. , with rare gas targets have been obtained. Based on the results of these experiments, the mechanisms established for the collisional generation of HR fragments in keV collisions of $[H_2]^+$ were generalized.

6 Collisions between $[H_3]^+$ and isotopomer ions of 10keV translational energy and He have been investigated. The analysis of the kinetic energy spectra of the ionic fragments from these collisions revealed a unique mechanism for the generation of $H^+$ ions in these collisions. This involves a vertical electronic transition to the first singlet excited state of $[H_3]^+$ followed by a non-adiabatic transition to the ground electronic potential surface over which the dissociation to $H^+$ + $H_2$ fragments will take place. Collision gases other than He were also applied. From these investigations it was established that for He and for Ne as target species

Wigner's total spin-conservation rule is strictly obeyed, while for Ar and the heavier rare gases this selection rule breaks down. The kinetic energy spectra HR fragments from $[H_3]^+$/He collisions have also been measured and analysed to obtain information about the processes generating these fragments.

7 $[H_2]^+$ ion beams of different vibrational energy content were used to investigate the effect of the vibrational excitation of the projectile ion on NR mass spectra. It was found that the intensity of the primary ions that survive neutralization reionization depended only weakly on their vibrational excitation.

8 The neutralization and reionization of isotopomeric methonium ions ($[CH_5]^+$, $[CD_5]^+$ and $[CD_4H]^+$) of keV translational energy have been investigated using a variety of collision gases. It was concluded that no stable $CH_5$ radicals are generated in charge transfer neutralization of $[CH_5]^+$ ion beams. Interferences, that can affect the experiments aimed at proving the stability of neutral species using NRMS have also been discussed. The analysis of the kinetic energy spectra of the ionic and HR species from 10keV collisions of $[CH_5]^+$ were used to obtain information about the processes generating these fragments as well as about dissociative electronic states of $[CH_5]^+$ and $[CH_5]^{2+}$.

## Contents

# 1.1 The Mass Spectrometer

All experiments described in this thesis have been carried out using a VG Analytical ZAB 2F double focussing mass spectrometer of reversed geometry [1]. In this section the major characteristics of this instrument will be discussed. Fig.1 shows the general layout of the ZAB 2F. The major parts are the ion source, first field-free region, magnetic sector analyzer, second field-free region, electrostatic analyzer and electron multiplier for ion detection. In the following section brief descriptions of these parts will be given.

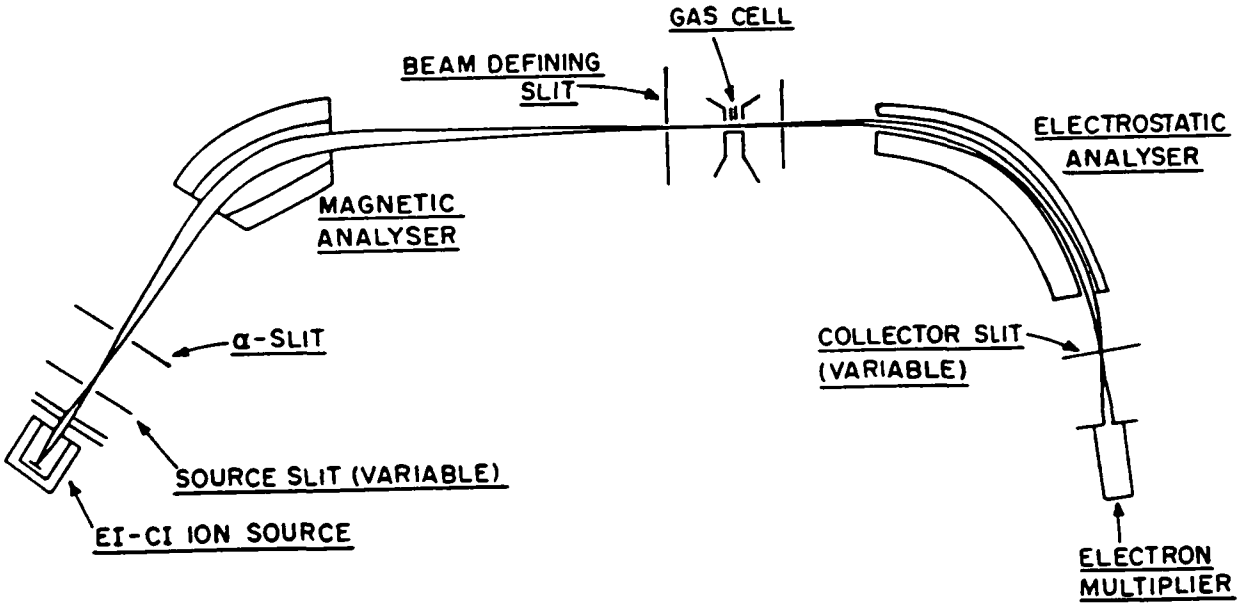


Figure 1. Simplified diagram of the VG Analytical ZAB 2F double focusing mass spectrometer.

### 1.1.1 The ion source

The apparatus is equipped with a Nier-type ion source. A schematic representation of it is shown in Fig.2.

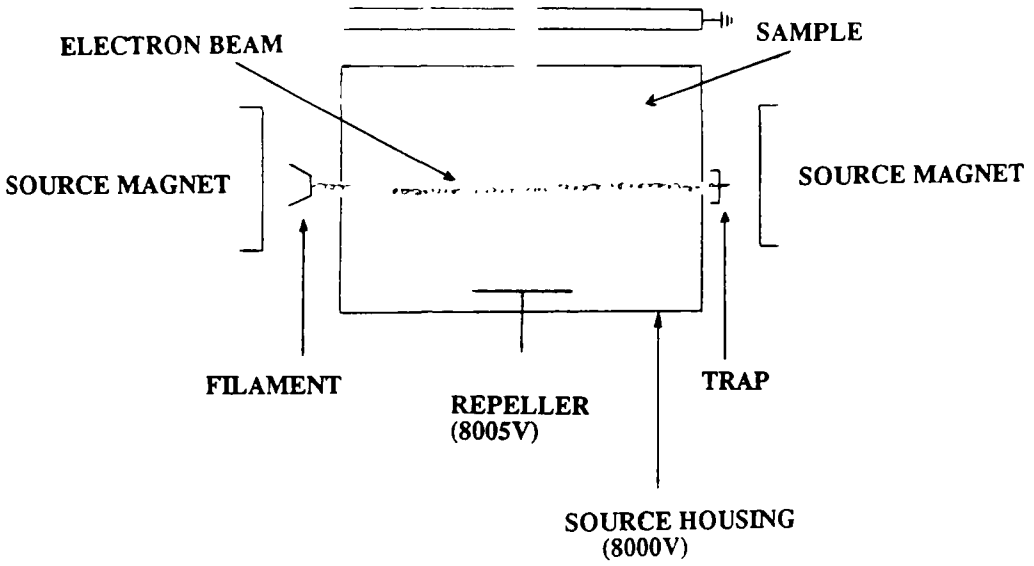


Figure 2. Simplified diagram of the ionization chamber.

Electrons are produced from an incandescent helical filament made of tungsten. The electrons are accelerated towards the ionization chamber. The kinetic energy of the electrons can be varied by changing the potential difference between the filament and the ionization chamber. The region within the ionization chamber is essentially free of electric fields and the electrons traverse it at constant velocity. Electrons which pass through a slit at the far end of the ionization chamber are accelerated towards an electrode (trap) and collected. In order to constrain the electron current passing through the ionization chamber into a narrow beam, a magnetic field from a permanent magnet is aligned along the direction of electron flow. Electrons with a velocity component at right angles to the magnetic field will move in tight helices

along the axis of the field.

Samples can be introduced through four kinds of inlet systems.They are the septum, the Granville-Phillips inlet, the probe and the gas inlet line. The septum inlet is for injection of liquid samples by means of a microsyringe. The septum temperature can be varied so that a satisfactory source pressure can be obtained for liquids of various boiling points. The Granville-Phillips inlet system allows entry of gases, volatile liquids or solids. It is capable of maintaining a constant source pressure for long periods of time. The direct probe is used for involatile solids. Sample pressures can be controlled by heating or cooling the probe, and by manipulating the distance of the probe tip to the source chamber. There is also a gas line fitted to the source chamber that allows direct entry of gases from a high pressure cylinder to the source. The gas pressure is controlled by a needle valve located between the gas cylinder and the source chamber.

Ions are generated when fast electrons (typically of 70 eV kinetic energy) interact with the outer shell electrons of the sample molecule. An electron is ejected from the sample molecule and a positive ion is generated.

$$M + e^- \rightarrow M^+ + 2e^- \qquad (1.1)$$

A 70 eV electron traverses a molecular diameter of the order of $10^{-7}$ cm in a time of $1x10^{-16}$ sec. The act of ionization must be completed in this order of time. The fastest molecular vibrational periods are of the order of $10^{-14}$ sec and so the atoms can be considered to be effectively at rest during ionization. Thus the ionization is an electronically vertical process. The ions formed are in various electronic states but due to intramolecular relaxation processes this electronic energy is transferred into electronic ground state vibrational energy, for a discussion see [2]. The ions

source, which is in the order of 1 μs, giving rise to fragment ions.

$$M_1^+ \rightarrow M_2^+ + M_3 \qquad (1.2)$$

The production and relative intensity of fragment ions can be explained by the quasi equilibrium theory (QET) of mass spectra [3,4]. QET is formulated using the assumptions:

(1) The rate of dissociation is slow relative to the rate of redistribution of the initial excitation energy among all degrees of freedom.

(2) All degrees of freedom have equal a priori probability.

(3) Fragmentation will occur when sufficient energy is accumulated in the critical vibrational mode(s) which leads to the decomposition. The rate constant of a particular reaction in this case is a function of the excess energy, $\epsilon^*$, above the minimum energy, $\epsilon_0$, required for the reaction to occur, and the frequency factor, v, for the reaction. This is summarized by a simplified QET equation

$$k = v(\epsilon^* - \epsilon_o)^{s-1} \qquad (1.3)$$

The ions will leave the ionization chamber under the influence of the repeller electrodes and have a small kinetic energy corresponding to about 1.0 eV. Outside the ionization chamber they will fall through a potential gradient, the accelerating voltage, $V_{acc}$, and are accelerated towards a plate containing a slit, known as the source slit. The source slit is at ground potential and the ionization chamber is operated at a positive potential above ground. The kinetic energy of an ion falling through this potential gradient depends on its charge, z, and $V_{acc}$

$$\frac{1}{2}mv^2 = zV_{acc} \qquad (1.4)$$

where m is the mass and v is the terminal velocity of the ion. The ion accelerator contains an arrangement of focussing plates designed to concentrate the ion beam on the source slit and to minimize the penetration of the accelerating field gradient into the ionization chamber, which would disperse the ion kinetic energies. *After acceleration all ions have the same kinetic energy regardless of their masses.*

### 1.1.2 The magnetic analyzer

The source generated, accelerated ions will pass through a magnetic field perpendicular to their motion, produced by an electromagnet. They will follow a circular path with a radius r determined by

$$mv = Bzr \qquad (1.5)$$

Substituting 1.4 into 1.5 we obtain

$$m/z = (B^2r^2)/(2V_{acc}) \qquad (1.6)$$

It follows, that by varying B (the current through the electromagnet coils), ions of different mass to charge ratios can selectively be transmitted through the magnet, since $V_{acc}$ and r are constant. The magnet also focusses an ion beam having an angular divergence in the xy plane. There is no focussing action in the z-axial direction parallel to the magnetic field.

Low resolution mass spectra can be obtained by scanning the magnet and using the first electron multiplier to detect the ions.

### 1.1.3 The electrostatic analyzer (ESA)

The ESA consist of two parallel curved plates, a section of a circle with a radius, $r_e$. When the two plates are placed at different potentials a radial electric field is created between them. If a beam of ions of various energies is injected midway between the plates and moving perpendicular to the direction of the electric field, there will be some ions which will describe a circular trajectory along the curve of radius, $r_e$, which is a line of equipotential. This condition is met when the kinetic energy of these ions, $mv^2/2$, is such that the electrostatic force on the ions is exactly balanced by the centripetal force. That is

$$mv^2/r_e = zF \qquad (1.6)$$

where F is the field strength. For source generated ions 1.4 can be substituted into 1.6 to obtain

$$r_e = (2V_{acc})/F \qquad (1.7)$$

or more generally

$$r_e = (2E_k)/F \qquad (1.8)$$

where $E_k$ is the kinetic energy of the ion. The mass, m, and the charge, z, carried by the ion do not appear in this equation so that ions of all masses carrying any number of charges will follow the same radius through the electric sector, provided only that they have been accelerated through $V_{acc}$.

only that they have been accelerated through $V_{acc}$.

The radial electric field will also produce a focusing action on a diverging monoenergetic beam of ions in the xy plane. In the z-axial direction, (perpendicular to the electric field), there is no focusing action.

High resolution mass spectra can be obtained by setting F in appropriate proportion of $V_{acc}$ and scanning the magnet. This is known as the double-focusing mode, which has enhanced mass resolution compared to the single-focusing mode, because the ESA focuses the small spread in the kinetic energies of the ions.

### 1.1.4 Field-free regions

There are drift regions before and after the magnetic sector called the first and second field-free regions, respectively. Both of these regions can be exploited for experimental purposes.

In both field-free regions unimolecular ion fragmentations can occur. When the frequency factor for a fragmentation is low and/or the rate constant only increases slowly as a function of the ion internal energy, fragmentation may take place as the ion traverses the instrument. The ions which fragment in the flight tubes of the mass spectrometer are called metastable ions. If the fragmentation occurs in the first or second field-free regions, the resulting metastably generated ions can be detected. Metastable peaks can be important observations in mass spectrometry and may provide valuable information towards identifying isomeric ion structures.

The second field-free region of the ZAB 2F mass spectrometer at the University of Ottawa contains accessories which permit one to carry out a variety of experiments with a particular ion, mass selected into the second field-free region by the magnet. The layout of these accessories are shown in Fig.3.

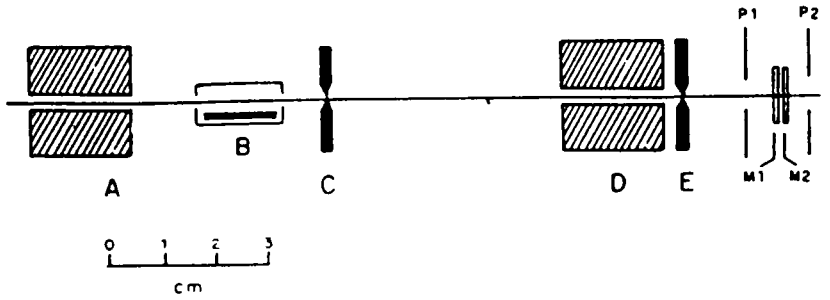


Figure 3. Layout of accessories in the second field-free region of the ZAB 2F mass spectrometer. A, first collision cell; B, deflector electrode; C and E, beam defining slits; D, second collision cell M1 and M2, nickel meshes; P1 and P2, grounded plates.

There are two collision cells into which collision gases can be admitted. That close to the magnet was assembled at our laboratory the other is a standard feature of the ZAB 2F [1] supplied by the manufacturer, VG Analytical. The two cells are 2cm long and 10 cm apart, centre to centre. Pressures for the two collision cells are measured by two ionization gauges mounted above the diffusion pumps symmetrically located just upstream and downstream of the two cells. Between the collision cells there is an ion deflector electrode which is placed inside a grounded metal cage, in order to prevent field penetration to other regions of the mass spectrometer, see Fig.3. When the deflector electrode is charged only fast neutrals can continue their flight through the apparatus. Beams of fast neutrals can be generated either by unimolecular dissociation of ions between the magnet and the deflector or in collisions between fast ions and gas molecules in the first cell. The high velocity neutrals can be reionized by collisions with gas molecules in the second cell. The neutrals which are in high-Rydberg (HR) states can be selectively field ionized by using the field ionization assembly, which was added to the apparatus in our laboratory [5]. The design and the operation of the field ionization assembly will be described in detail in section 2.1.

### 1.1.5 The Detectors

The detectors, positioned as shown in Fig.1, are off-axis electron multipliers. The ion beam is deflected onto a negatively charged (-5kV) conversion dynode (a polished dural cylinder), which liberates electrons, which in turn are accelerated across to the electron multiplier. The resulting signal is amplified, allowing ion currents of down to $10^{-16}$ A to be detected.

## 1.2. keV Collisions between Ions and Neutrals

Collision-induced processes between ion beams of keV kinetic energy and neutral targets have been studied in mass spectrometers since the early days of the technique. Aston was the first to recognize the possibility of using a mass spectrometer for such studies [6,7]. In the last two decades these processes have increasingly been exploited to gain information about the projectile and/or target species participating in these collisions, (for reviews see refs. [8-12]). The following processes have been most studied:

(i) Collision-induced dissociation (CID) of fast primary ion beams, which is usually described as a two step process

$$M_1^+ + N \rightarrow M_1^+(*) + N \rightarrow M_2^+ + M_3 + N \qquad (1.9)$$

where $M_1^+$ is the fast projectile ion, N is the stationary neutral target, $M_1^+(*)$ designates a dissociative excited state of $M_1^+$ created during the collision between $M_1^+$ and N, $M_2^+$ and $M_3$ are the fragments resulting from the dissociation of $M_1^+(*)$.

(ii) Measurement of the spectrum of translational energy loss undergone by the projectile ion in collision with a specific target at zero scattering angle. The measured kinetic energy loss can be correlated with excitation energies of different excited states of the projectile and/or target.

(iii) Charge transfer neutralization of fast ion beams by the process

$$M_1^+ + N \rightarrow M_1 + N^+ \qquad (1.10)$$

which can be a source of a beam of fast neutral $M_1$ species, on which further experiments can be carried out.

(iv) Other charge permutation processes, such as

double electron capture

$$M_1^+ + N \rightarrow M_1 + N^{2+} \qquad (1.11)$$

charge reversal

$$M_1^- + N \rightarrow M_1^+ + N + 2e^- \qquad (1.12)$$

charge stripping

$$M_1^+ + N \rightarrow M_1^{2+} + N + e^- \qquad (1.13)$$

The following sections contain discussions of the present status and understanding of the above mentioned processes as well as descriptions of their more important applications to chemical research. The collision-induced dissociation and charge transfer neutralization of fast ions will receive the most attention because these are the topics which are directly related to the work presented in this thesis.

### 1.2.1 Collision Induced Dissociation of Diatomic Ions of keV Kinetic Energy

Investigations of the CID of the diatomic ions played a very important role in the understanding of the CID of polyatomic ions. This is because diatomic systems are the most amenable to experimental and theoretical study; consequently the basic

processes operative in the CID of polyatomic ions was first established for diatomic projectiles and the resulting principles were then applied to the understanding of more complex systems. In order to fully characterize the collision induced dissociation, that can be generally described with the equation

$$AB^+ + N \rightarrow AB^+(*) + N \rightarrow A^+ + B + N \qquad (1.14)$$

the following variables have to be measured [13]: total cross section, velocity ($v_g$) and scattering angle ($\theta_g$) of the center of mass (c.o.m.) of the pair $A^+$+B; velocity ($u_a$) and scattering angle ($\Phi$) distributions of $A^+$ with respect to this c.o.m.; possible excitation of $A^+$, B and N after collision; and it is also desirable to have some information about the initial internal energy of the projectile ion. Fig.4 contains a vector diagram showing the relationship between the above mentioned variables.

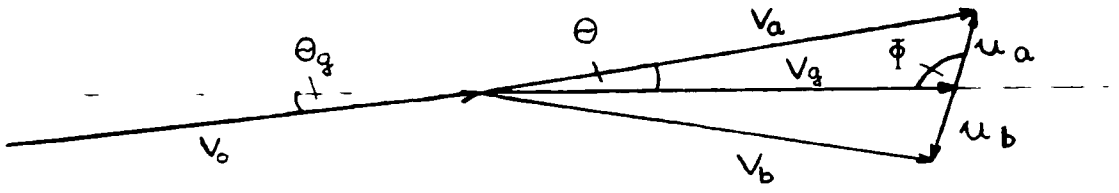


Figure 4. Velocity vector diagram for the collision induced dissociation process described by equation 1.14.

The *velocity* $v_g$ *of the c.o.m.* after the collision (i.e. the velocity of $AB^+(*)$) indicates a *translational energy loss* $\Delta E$

$$\Delta E = \tfrac{1}{2} m_{ab}(v_o^2 - v_g^2) \qquad (1.15)$$

which for any scattering angle $\theta_g$ includes an *elastic energy loss*

$$\Delta E_{el} = (m_{ab}/m_n) \tan^2\theta_g E_o \{1/[1+((m_n+m_{ab})/2m_n)\tan\theta_g)^2]\} \quad (1.16)$$

where $m_{ab}$ and $m_n$ are the masses of $AB^+$ and N, respectively; $E_o$ is the incident translational energy ($E_o=\frac{1}{2}m_{ab}v_o^2$). $\Delta E$ given by (1.15) also includes an *inelastic energy loss*

$$\Delta E_{inel} = E^* \{1-(m_{ab}/(m_{ab}+m_n)) (\tan^2\theta_g)/(1-(m_{ab}\tan\theta_g/m_n)^2\}^{1/2} \quad (1.17)$$

where $E^*$ is *the excitation energy* from $AB^+$ to $AB^+(*)$ plus possibly, the excitation energy of N. In eqs (1.16) and (1.17) the approximation $\sin\theta=\tan\theta=\theta$ was made.

The *velocities* $u_a$ and $u_b$ of $A^+$ and B with respect to the c.o.m. for diatomic $AB^+$ are directly related to the *excess energy* W of $AB^+(*)$ (see equation (1.14)) above the energy of $A^+$+B in the electronic states where they appear:

$$W = \frac{1}{2} (m_a u_a^2 - m_b u_b^2) = (m_a m_{ab} u_a^2)/(2m_b) \quad (1.18)$$

A very large number of experimental investigations on the CID of diatomic ions have appeared in the literature. For example Durup et al. [14] list 60 papers on the CID of $[H_2]^+$ that were published before 1968. The majority of investigations involved experimental arrangements that can generally be described as containing the following parts:

(i) An electron impact (EI) ion source for the generation of ions, in some cases with well controlled electron energies for appearance energy measurements.

(ii) An acceleration region, followed in most cases, by some kind of mass selection.

(iii) A differentially pumped collision cell into which the (thermal) target gas is

admitted.

(iv) Determination of the laboratory velocity distribution of the ionic fragment, $v_a$ in Fig.4, which is achieved either by momentum analysis by a magnetic sector or spectrograph, or by kinetic energy analysis by an electric sector. The angle of the velocity vector relative to the primary beam direction, $\theta_s=\theta_g+\theta$ in Fig. 4, is determined by electrostatically deflecting, with varying degrees, either the primary beam or the fragments. A thorough review of the different experimental arrangements applied can be found in reference [15].

For the information obtained in these experiments to be physically significant, two conditions have to be satisfied [16]. In the first place, the separating particles should not be electronically excited; if they are excited then additional information should be available about the two fragments and the target atom. The second, more stringent, requirement concerns the contribution of the scattering of the c.o.m. of the incident molecule to the scattering of the fragments in the laboratory frame. This contribution should either be negligible or should be obtainable from the measured momentum distribution. If these two conditions are met, the laboratory momentum distribution of the fragments can be transformed to a momentum distribution in the c.o.m. of the dissociating molecule. In this way dissociation cross sections are obtained which are differential with respect to the orientation of the molecule and with respect to the translational energy of the separating fragments, but averaged over all impact parameters.

Experimental results allows a classification of the different mechanisms of CID. Such a classification was first given by Durup [13] in 1970. It has been augmented in subsequent reviews [16,17]. Los in 1973 [17] described four limiting processes together with subcases. These are:

(1) Electronic excitation of $AB^+$ to $AB^+(^*)$

(a) through vertical transition, i.e. obeying the Franck-Condon principle, with or without an excitation of target N and with essentially no deflection of the c.o.m.. This process occurs at relatively large impact parameters and involve little momentum transfer perpendicular to the incident flight direction. Note that the Franck-Condon principle involves not only the conservation of internuclear distance which is automatically satisfied at keV impact energies due to the large difference between the collision time ($\approx 10^{-16}$s) and molecular vibrational period ($10^{-14}$sec), but also the conservation of nuclear momenta. This means that if significant momentum transfer takes place during the collision, the Franck-Condon principle and the assumption of electronic verticality, is no longer applicable. If the electronic excitation takes place at small impact parameters there is, simultaneously, significant momentum transfer to the nuclei of the projectile. This is quite likely to happen when

(b) the excitation occurs as the result of a diabatic passage through an avoided crossing between two potential surfaces for the triatomic system: molecule + atomic collision partner. In this case there will be a high transition probability particularly at some (often small) value of the impact parameter, corresponding to the location of the avoided crossing. This circumstance favours the simultaneous occurrence of momentum transfer and electronic transition, which result in $AB^+(^*)$ being both electronically and vibrationally excited.

(2) Vibrational and/or rotational excitation, which can be due to two different mechanisms.

(a) Momentum transfer by the target atom to one or both of the nuclei composing the incident ion, resulting in vibrational-rotational excitation of $AB^+$

above the dissociation limit of its initial electronic state; the momentum transfer vector is essentially perpendicular to the incident flight direction, and the c.o.m. of $AB^+$ is usually significantly deflected.

(b) Excitation of $AB^+$ above its dissociation limit also can be caused by the adiabatic distortion of the electron clouds of the two colliding particles, e.g. through the induced polar forces during the collision.

(3) Predissociation that can be caused by

(a) perturbation of the $AB^+$ projectile by the target inducing a radiationless transition to a dissociative state of the same energy, and by

(b) direct collisional excitation to a predissociated state.

Durup [13] and Los [17] also mention a fourth mechanism that can be active in the CID of ions. This is a completely inelastic collision, that is an intermediate $[ABN]^+$ complex is formed during the collision and all the relative translational energy of the colliding particles is converted into internal energy of the complex, which after some time breaks up into separate atoms. However, this process is only operative at or near thermal energies, therefore it will not be discussed here.

We shall now proceed to discuss experimental and theoretical work on particular systems that provide evidence for the processes listed above and also a more detailed picture of them.

### CID of $[H_2]^+$ molecules

There is convincing evidence that the CID of $[H_2]^+$ ions, in the keV energy range, is mainly due to electronic excitation to the antibonding $2p\sigma_u$ state, as illustrated in Fig.5.

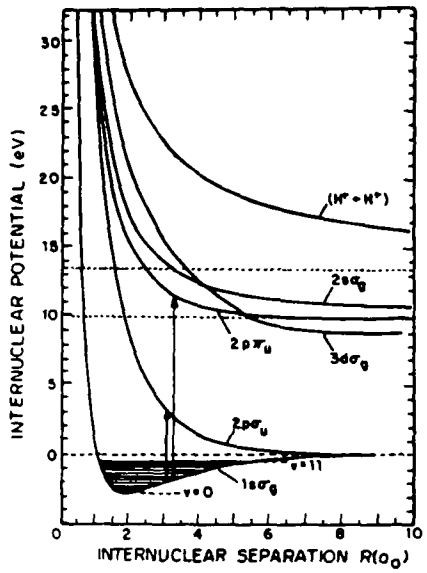


Figure 5. Relevant $[H_2]^+$ potential curves. Vertical arrows indicate transitions according to the classical picture of Franck-Condon principle.

This has been found to be particularly true for lighter rare gas atoms (He, Ne). Decisive proof in this respect has been provided by measurements of the angular and velocity distributions of the proton fragments. The angular distribution shows a pronounced anisotropy which is strongly dependent on the c.o.m. velocity of $H^+$, $u_h$. The comparison of this variation with theoretical predictions, supplies very strong evidence on the particular excitation mechanism responsible for CID. It was pointed out first by Dunn in 1962 [18], that measurements of the angular distributions can provide means of identifying the final dissociative states. He argued that in the case of the first Born approximation, which is believed to be valid for impact energies near to and greater than 10 keV. the initial and final motions of the colliding particles are approximated by plane waves. The incoming and outgoing plane waves combine to a plane wave along the momentum transfer vector **K**, where **K** is the difference between the initial and final wave propagation vectors $\mathbf{K}=\mathbf{k}_i-\mathbf{k}_f$. Dunn showed that in this case the entire system has a symmetry axis parallel to **K**, and that symmetry in the initial state should be preserved in the final state, leading to angular selection rules. For $[H_2]^+$ he found that the $1s\sigma_g \rightarrow 2p\sigma_u$ is allowed for

parallel orientations of the molecular axis with **K**, but forbidden for perpendicular orientation. The reverse is true for $1s\sigma_g \rightarrow 2p\pi_u$ transitions.

The qualitative arguments of Dunn imply that the excitation is often strongly anisotropic with respect to **K**. If the so called axial recoil assumption is valid, i.e., when the dissociation takes place along the instantaneous orientation of the molecular axis, the resulting fragments will thus be distributed anisotropically with respect to **K**. As **K** will in general not be distributed isotropically with respect to the axis of the incident beam, the momentum distribution of the dissociation fragments will be anisotropic with respect to the incident beam direction. As a consequence, the measurement of the angular distribution of the dissociation fragments can be a useful tool in establishing with which molecular state the observed fragments are correlated.

Theoretical calculations using the Born approximation confirmed the above qualitative arguments. The most demonstrative example showing how the angular dependence of the dissociative excitation varies with the specific transition involved has been given by the Born calculations of Green and Peek [19] for $[H_2]^+$ colliding on He and Ar targets. They calculated explicitly the dissociation cross section, $\sigma(\Phi,R)$, as a function of $\Phi$, the angle between the initial beam direction and the orientation of the internuclear axis in $[H_2]^+$ at the moment of the collisional excitation, and R, the internuclear distance in $[H_2]^+$. The transitions examined were $1s\sigma_g \rightarrow 2p\sigma_u$, $1s\sigma_g \rightarrow 2p\pi_u$ and $1s\sigma_g \rightarrow 2s\sigma_g$. They found that in the case of the $1s\sigma_g \rightarrow 2p\sigma_u$ transition, for small R the excitation probability has maxima for orientations parallel to the original beam direction ($\Phi$=0°,180°), but for large R it is maximized at perpendicular orientations ($\Phi$=90°). Fig.6 shows some characteristic results obtained for this transition.

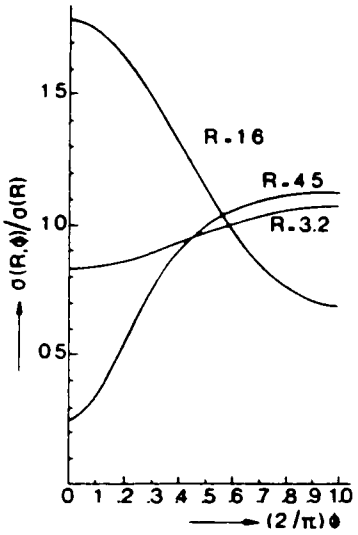


Figure 6. Born approximation calculation [19] for dissociative $1s\sigma_g \rightarrow 2p\sigma_u$ excitation of 10 keV $[H_2]^+$ incident on Ar. The quite different dependence of the cross section on the angle $\Phi$ between the molecular axis and the beam direction is shown for three internuclear distances (in a.u.).

In the case of transitions to the $2p\pi_u$ and $2s\sigma_g$ states the calculations did not indicate such strong variation of the angular dependence of the excitation probability for different internuclear distances. It was found to be peaked at $\Phi$=90° independent of R.

In 1968 Gibson et al. [20] measured the cross section, $\sigma(v_h,\theta_s)$, for $H^+$ production in 3-10 keV collisions between $[H_2]^+$ and rare gas targets as a function of the laboratory scattering angle ($\theta_s$) and the laboratory velocity ($v_h$) of the fragment protons. By considering the vector diagram in Fig.4 it can be seen that protons detected at a certain $\theta_s$ angle and having a certain $v_h$ velocity can be uniquely attributed to dissociations at a definite angle $\Phi$ with a definite c.o.m. dissociation velocity $u_h$ assuming that:

(i) $\theta_g \approx 0$, i.e., the c.o.m. is not deflected in the collision and so $\theta_s \approx \theta$. It will be seen below that this assumption is valid.

(ii) The orientation of the internuclear distance does not change in the course of excitation-dissociation process. That this assumption is valid can be easily seen by

comparing the characteristic times for these processes.

collision time$\approx 10^{-16}$sec

vibrational period$\approx$dissociation time$\approx 10^{-14}$sec

rotational period$\approx 10^{-12}$sec

Furthermore, $u_h$ can be directly related to a unique value of R, in the following way. From equation (1.18) W, the kinetic energy released in the dissociation giving $H^+$ with $u_h$ c.o.m. velocity, can be obtained. For a specific value of W a corresponding value of R can be determined, assuming Franck-Condon $1s\sigma_g \rightarrow 2p\sigma_u$ transitions and using calculated potential curves for the two states involved. The above discussion shows that $\sigma(v_h,\theta_s)$ distributions can be transformed into $\sigma(R,\Phi)$ distributions. Gibson et al. [20] carried out this transformation on their data, and compared the resulting $\sigma(R,\Phi)$ distributions to theoretical calculations. In Fig.7 some of the experimental results of Gibson et al. are shown together with the theoretical calculations of Peek and Green (cited by McClure [21]).

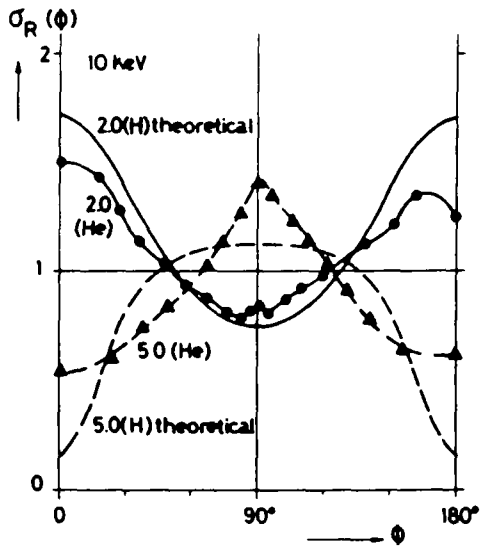


Figure 7. Angular dependence of the experimental c.o.m. dissociation cross section, $\sigma_R(\Phi)$, for 10 keV $[H_2]^+$ incident on He [20], compared with theoretical Born calculations for an H-atom target [21]. The calculations were made under the assumption that the dissociation is due to $1s\sigma_g \rightarrow 2p\sigma_u$ transition. The parameter R is indicated in atomic units.

It is obvious that there is a good qualitative agreement between the theoretical predictions based on Born calculations for $1s\sigma_g \rightarrow 2p\sigma_u$ transitions and the experimental results. This agreement is conclusive proof that the most important process in the CID of $[H_2]^+$ is the $1s\sigma_g \rightarrow 2p\sigma_u$ excitation, because only this transition shows such large relative variation of the angular dependence of the excitation probability on the internuclear distance. Experimental verification of the relatively low cross sections for excitations to the higher electronic states was given by Sauers et al. [22]. They measured the laboratory angular distributions of the metastable H(2s) fragments together with the H(1s) and $H^+$ fragments for the CID of $[H_2]^+$ on various targets (He, Ar, $H_2$ and $N_2$) in the energy range 4-12 keV. Indeed, the laboratory cross sections for H(2s) formation was a factor of 10 smaller than that for H and $H^+$ formation.

Vogler and Seibt [23] also measured , with a parabola mass spectrograph, the laboratory momentum distribution, angle ($\theta$) and velocity ($v_h$), of $H^+$ fragments for the CID of $[H_2]^+$ ions at an incident energy of 20.4 keV. The target gases used were the rare gases and $H_2$ and $N_2$. Vogler and Seibt analysed their data in a different way than Gibson et al [20]. They determined parallel $u_=$ and perpendicular $u_\perp$ , to the initial beam direction, components of the c.o.m. velocity of $H^+$ fragments. They generated diagrams in which the differential cross section for $H^+$ production was plotted against $u_=$. A series of curves were obtained in this way by changing u as a parameter. Fig.8 shows one of the diagrams from that work.

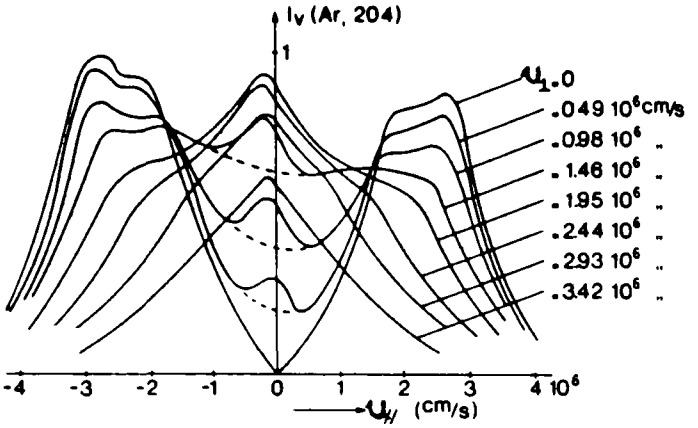


Figure 8. Center-of-mass proton velocity distribution for the collision induced dissociation of 20 4 keV $[H_2]^+$ incident on Ar [23]. For the lower three nonzero values of the velocity perpendicular to the beam direction the contribution from vibrational dissociation is indicated by the dashed lines.

It was concluded that the wings extending to large $u_\perp$ values were mostly due to vertical $1s\sigma_g \rightarrow 2p\sigma_u$ transitions with some contribution from ionizing collisions reaching the $[H_2]^{2+}$ potential curve.

Vogler and Seibt noted a marked anomaly in these differential cross sections. It was found that the differential cross section shows a narrow peak at angles perpendicular to the beam direction, which is not expected for pure electronic excitations. For example the plots in Fig.8 clearly exhibit an additional contribution to the fragment distribution at $u_{=}\approx 0$ and $u_\perp = 0$, which for lower values of $u_\perp$ can be estimated by graphical substraction. Vogler and Seibt proposed that a vibrational dissociation due to impulsive momentum change of one or both protons led to a distribution of fragments perpendicular to the beam direction with almost no velocity change parallel to the beam. Generally, this excitation is expected to be associated with scattering angles of the c.o.m. which are large compared with those

appearing in electronic excitation. Since the momentum change of the $[H_2]^+$ ion must be nearly perpendicular to its initial momentum, based on symmetry considerations, one can expect classically that the fragments have velocities perpendicular to the beam direction in the c.o.m. frame. This agrees with classical calculations by Green [24] and by Meierjohann [25]. The calculations of Meierjohann also showed that the sharp peaks at $u_{=}\approx 0$ are slightly displaced towards lower velocities ($u_{=}<0$), a shift which increases with larger $u_{\perp}$ values. These shifts are also observed in the experiments of Gibson et al. [20] and Durup et al. [14]. It is clear that these shifts are not due to an electronic excitation of the target as originally proposed, but merely to the momentum change of the molecule.

In 1977 Meierjohann and Vogler [26] obtained velocity distributions of fragments from CID of 10 keV $[H_2]^+$ on He detecting the $H^+$+H fragments in coincidence. Their experimental arrangement contained two detectors placed symmetrically around the incident beam direction as shown in the kinematic diagram of the experiment in Fig.9.

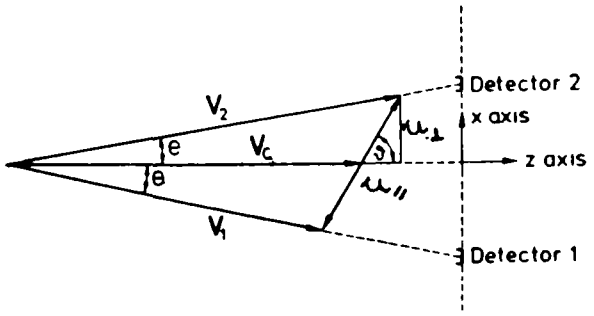


Figure 9. Kinematic diagram relevant to the coincidence experiments of Meierjohann and Vogler [26].

By moving the detectors along the x axis θ and so $u_{\perp}$ was changed, and by measuring the flight time difference between the $H^+$+H pairs reaching the detectors, applying delayed coincidence technique, a $u_{=}$ distribution was obtained. From Fig.9 it is clear, that *only when* the c.o.m. is not deflected can both fragments be detected

coincidentally. With this experimental arrangement there was no narrow component observed at $u_{=}\approx 0$ in the differential cross sections. Therefore, the narrow feature, observed when only one fragment is detected, must be due to dissociative collisions accompanied by considerable deflection of the c.o.m. In other words the apparent velocity distribution around $v_{=}=0$ is really an angular distribution around $\Phi=90°$.

In 1984 Baldreich et al. [27] modified the apparatus used by Meierjohann and Vogler. In the modified version the analyzer tube of the apparatus could be turned horizontally around a vertical axis through the collision chamber. The consequence of turning the analyzer tube around the collision chamber by $\theta_t$ angle is that the z axis in the kinematic diagram in Fig.9 will no longer be aligned with the incident beam direction, there will be a $\theta_t$ angle between them. Therefore, only those $H^+$+H fragments can be recorded coincidentally for which the collisional excitation process involve a c.o.m. deflection $\theta_g=\theta_t$. For $\theta_g>0.15°$ Baldreich et al. [27] did no longer observed the features of the velocity distributions identified as arising from vertical $1s\sigma_g \rightarrow 2p\sigma_u$ transitions, i.e., the wings in the velocity distributions extending to large values of $u_{=}$ and associated with large c.o.m. energies, $\epsilon_{=}$=3-4 eV. Only narrow features around $\epsilon_{=}$=0eV extending to $\epsilon_{=}\approx 0.3$ eV appeared in the distributions. *This is decisive evidence that the dissociative electronic transitions in the CID of* $[H_2]^+$ *involve negligible deflections of the c.o.m., i.e., negligible amounts of momentum transfer. This observation is believed to be extendable to the vertical excitation of other di- and polyatomic ions, assuming they have high enough velocity for the Born approximation to be valid.*

Several groups have carried out experiments in which they measured the laboratory kinetic energy distribution of $H^+$ fragments from the CID of $[H_2]^+$ at zero laboratory scattering angle [14,28]. Because the observations are made at zero scattering angle, only backward and forward scattered (relative to the incident beam

direction) fragments are detected. From this condition and by applying the laws of conservation of momentum and energy a simple relationship can be obtained between the observed laboratory kinetic energy, $E_h$, for a $H^+$ fragment and the c.o.m. kinetic energy release, W, associated with the dissociation event from which it originates

$$E_h = \tfrac{1}{2}(E_o - E^*) \pm \{W(E_o - E^*)\}^{1/2} \qquad (1.19)$$

or for the more general case of $AB^+ \rightarrow A^+ + B$ dissociation

$$E_a = (m_a/m_b)(E_o - E^*)^2 \pm (m_a m_b/m_{ab})^{1/2}\{W(E_o - E^*)\}^{1/2} + (m_b/m_{ab})W \quad (1.20)$$

where $E_o$ is the initial velocity of the projectile E* is the excitation energy, the plus sign refers to forward and the minus sign to backward scattering. Therefore, using equation (1.19) (or 1.20) measured laboratory kinetic energy distributions can be transformed into c.o.m. kinetic energy release distributions. Fig.10 shows some of the results obtained by Durup et al. [14] who determined W distributions at zero scattering angle for the CID of $[H_2]^+$.

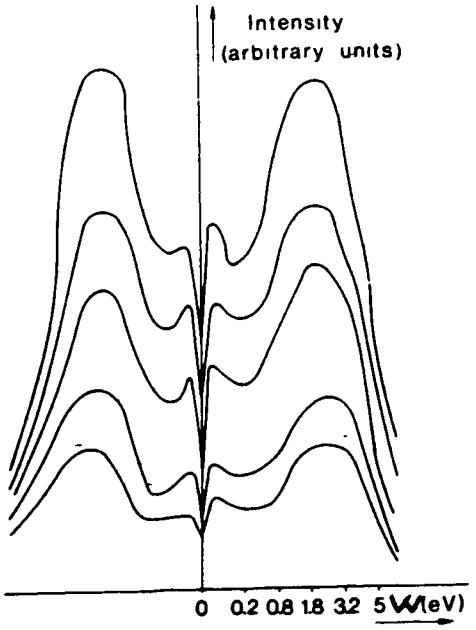


Figure 10. Center-of-mass distribution of the kinetic energy (W) of forward and backward scattered proton fragments for 5 keV $[H_2]^+$ incident on Kr; ionizing electron energies, from bottom to top: 18.4, 20.4, 21.4, and 22.8 eV [14].

The surprising feature of these curves is that a secondary maximum appears at W values of ≈0.1eV, besides the main maximum at W≈3eV which is due to electronic excitation. These secondary maximum peaks do not appear in He and Ne; for Ar they depend on the primary beam energy and for Kr and Xe and some molecular target gases they appear in the whole energy range from 3-5 keV. Anderson and Swan [29,30] subsequently investigated these secondary maxima very thoroughly. From careful analysis of their data they concluded that these components are due to vibrational dissociation, but in this case it is not caused by the momentum transfer mechanism discussed above for the production of protons appearing perpendicular to the main beam direction. Anderson and Swan established that these forward and backward scattered peaks must be due to the vibrational dissociation mechanism proposed by Russek [31].In 1970, in his paper on the theoretical treatment of CID in keV collisions, Russek [31] pointed out that the electrons in this impact energy range can adjust adiabatically during the collision (unlike the nuclei which cannot), the more so for larger impact parameters. The consequence of this is that vibrational and rotational excitation can occur, up to the continuum, due to polarization induced forces at large impact parameters. In this modified Born approximation, the nuclear motion is treated exactly as in the usual Born approximation, the electrons, however, are dealt with adiabatically. It was shown by Russek that this will lead to the same expressions for electronic excitation as in the usual Born approximation, but that an (until then) unrecognized mechanism may cause a vibrational dissociation. In contrast to the mechanism which occurs at small impact parameters (see above), this vibrational excitation will not lead to deflection of the molecular c.o.m., and the fragments will be detected with small velocities

with respect to the c.o.m.

Another interesting observation was made by Durup et al. [14] by measuring very carefully the appearance energy of different W values, by adjusting the ionizing electron energy in the ion source. Fig.11 shows the results of their measurements for $H_2$ target.

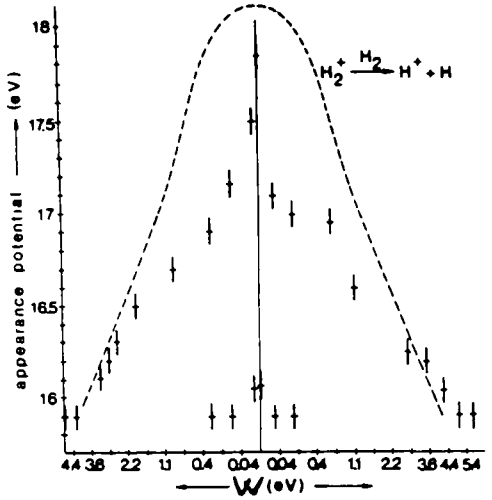


Figure 11. Appearance potentials as a function of W for $H^+$ from the collision induced dissociation of 3 keV $[H_2]^+$ incident on $H_2$ [14]. The dashed curve corresponds to theoretical appearance potentials assuming vertical transitions in keeping with the classical picture of Franck-Condon principle.

It was found that for the heavier rare gases and for molecular gases, there were fragments with W≈0eV even at the lowest ionizing energies, see Fig.11. At these low ionizing energies only the lowest vibrational energy levels of $[H_2]^+$ can be populated. Vertical electronic transitions to the $2p\sigma_u$ state would result in dissociations with W>5eV. and so only vibrational dissociation in the ground electronic state of $[H_2]^+$ can give rise to these fragments. Fig.11 also shows the theoretical appearance potential curve expected from the classical picture of the Franck-Condon principle, i.e., transitions occur from the outer turning points of the vibrational levels because classically the molecule spends most of its vibrational period near this turning point, see Fig.5. Of course, quantum-mechanically this is a

very false picture because the probability distribution of the internuclear distance in the $v^{th}$ vibrational level have v+1 maxima which have comparable intensity. The W distribution of fragments from vertical electronic excitation to a repulsive state, as it has been discussed by Fournier et al. [32-34], is determined firstly by the Franck-Condon overlap integral between the initial vibrational level and the repulsive potential curve. An illustration of this is shown in Fig.12.

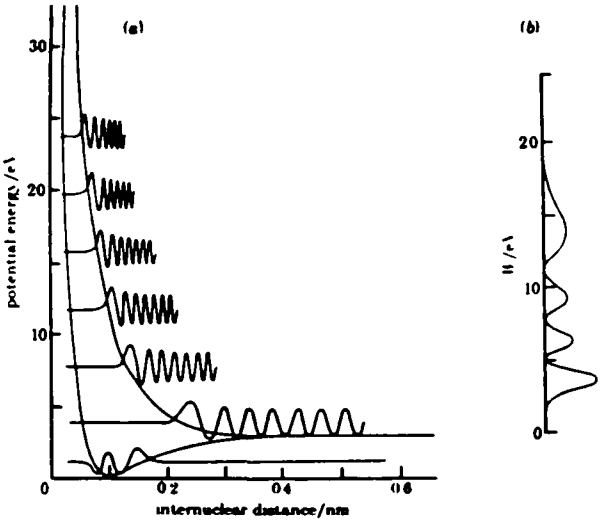


Figure 12 Illustration of the calculation of Franck-Condon overlap integral [34] (a) The potential energy curve of $[H_2]^+$ in the $1s\sigma_g$ ground state showing the wavefunction for v=3 Also shown is the $2p\sigma_u$ repulsive curve and a representation of the outgoing wavefunctions at intervals of 2 eV (b) The W distribution calculated for transition to the $2p\sigma_u$ state from the v=3 vibrational level of the $1s\sigma_g$ ground state

It can be seen that the W distribution obtained from the Franck-Condon overlaps has the largest maximum close to the W corresponding to a transition from the outer turning of the actual vibrational level. Moreover, the probability of collision induced transition is strongly decreasing with the increase of the excitation energy involved. It can be seen that even in the quantum-mechanical description W's corresponding to the classical picture of Franck-Condon principle are strongly favoured.

## CID of $[HeH]^+$ molecules

The second, and last, molecule to be discussed in some detail is $[HeH]^+$, the simplest heteronuclear molecule. The CID of this molecule-ion reflects several interesting processes not observed for $[H_2]^+$ projectiles. The ion $[HeH]^+$ has a ground state, dissociating into He and a proton, with a rather narrow and deep potential well of about 2eV and an equilibrium internuclear distance of 0.76Å. Potential curves for the first 14 electronic states of $[HeH]^+$ have been calculated by Michels [35] and by Green et al. [36]. The first two excited states $A^1\Sigma$ and $a^3\Sigma$ show very shallow potential wells, sustaining a few vibrational levels, with large equilibrium distances. The repulsive part of these states is steep. The excitation energy for a vertical transition from the bottom of the ground state potential well to these states is in the order of 10eV. The next higher states lie about 10eV higher and are all strongly repulsive at internuclear distances on the order of the equilibrium ground state separation.

Because of these features it can be expected that dissociative electronic excitation would yield very broad distributions of the fragment ions, whether $H^+$ or $He^+$, in the center of mass. Surprisingly, however, the c.o.m. momentum distribution of proton fragments in collisional dissociation is very narrow; W ranges from zero to 1eV. Fig.13 shows the laboratory velocity distributions of protons from the CID of $[HeH]^+$ incident on He as obtained by Schopman et al. [37].

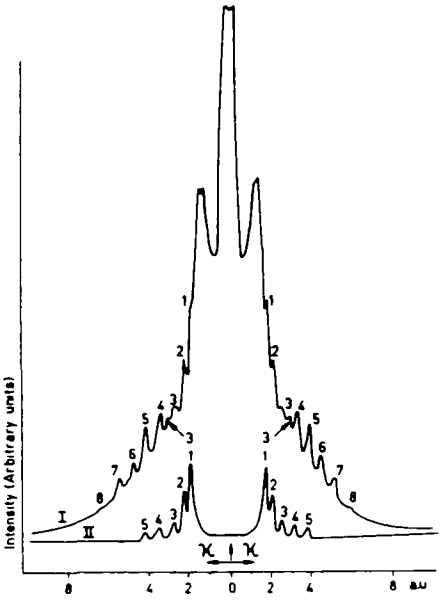


Figure 13 Laboratory momentum distribution of forward and backward scattered $H^+$ fragments from 10 keV $[^4HeH]^+$ Lower trace distribution at residual gas pressure (unimolecular dissociation) Upper trace distribution observed when $10^{-3}$ torr of He is introduced into the collision chamber (unimolecular+collision induced dissociation), [37]

Because the W range is small, it has been concluded that the electronic excitation mechanism can be neglected. The distribution is so narrow that reliable angular measurements are not available. This indicates that the Russek mechanism of vibrational dissociation is responsible for the proton production in these collisions. This is strongly supported by the measurements of Schopman and Los [38] who found that the intensity of the central peak is proportional to the square of the polarizability of the target, as predicted by the theoretical work of Russek [31].

Apart from the general shape, Fig.13 shows that fine structure is superimposed upon the continuous velocity distribution, which is partly present in the (unimolecular) background, too. This background spectrum, which has also been observed by Houver et al. [39], is due to unimolecular dissociation. Peek [40]

explained the appearance of the fine structure in the spectra as a result of rotational predissociation, which is caused by tunneling through the rotational barrier of high angular momentum states lying above the dissociation limit. Peek showed that the quasibound states form a series with respect to lifetime. The different states of one series, which is formed by steps $\Delta v=-1$, $\Delta J=2$, have approximately the same lifetime and show moreover a quadratic energy dependence in the continuum. Lifetimes between different series, however, differ by about two orders of magnitude. The peaks in the background belong to one series with a relatively long lifetime, being excited in the ion source and decaying in the collision chamber. The peaks which are added in the collision induced spectrum belong to another series with relatively short lifetimes, being excited in the collision chamber where they also decay. Good agreement was found between the calculations of Peek with respect to lifetime and energy and the experimental measurements for $[^4HeH]^+$ and $[^3HeH]^+$.

Fig.14 shows the W distribution, averaged over scattering angle, as obtained by Schopman, Los and Maas [41] for 10keV $[HeH]^+$ colliding on He.

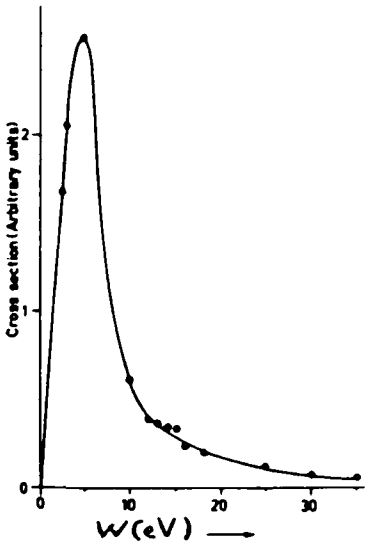


Figure 14. The dissociation cross section integrated over angle, of 10 keV $[HeH]^+$ incident on He and dissociating into $He^+$+H, as a function of the kinetic energy of the fragments W [41].

It peaks around W=5eV which strongly indicates that electronic excitation to a repulsive state is the most important process for $He^+$ production. However, a few percent of the total dissociation cross section belongs to some processes with W≈25eV or even higher. Because in a vertical electronic transition this high internal energy cannot be obtained, it can be concluded that high W values arise from violent collisions involving large amounts of momentum transfer. The angular distributions, shown in Fig.15 of the W=5eV and the W=25eV components support the above conclusions about their origin.

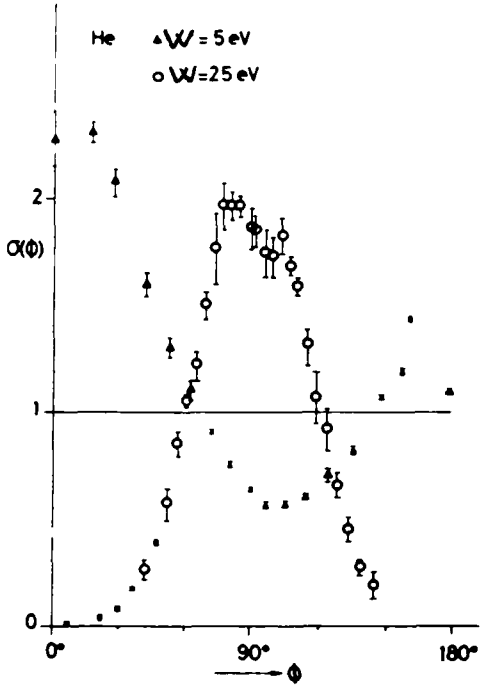


Figure 15. Doubly differential c.o.m. cross section at two different W values for the collision induced dissociation into $He^+$ and H of 10 keV $[HeH]^+$ incident on He [43].

The lower W value shows a spectrum where maxima are found in the forward and backward directions, as expected from Dunn's rules for electronic transitions [18]. Contrary to the dissociation of $[H_2]^+$, however, there is no symmetry with respect to the 90° direction. The forward dissociation is more intense than the backward one. The same results have been observed for the asymmetric molecules $[CO]^+$ and

$[NO]^+$ [42] in contrast to the dissociations of symmetric molecules such as $[O_2]^+$ and $[N_2]^+$ which again are symmetric in the forward and backward directions. It was even observed by Pham Dong and Durup [43] that the dissociation of $[HD]^+$ shows a slightly more pronounced forward scattering of the $D^+$ fragment. At a W value of 25eV, the second curve in Fig.15, the dissociation is almost completely perpendicular to the beam, just as expected for dissociative excitations involving large quantities of momentum transfer.

**In summary. It was seen in this chapter that the collision induced dissociation of diatomic ions has been studied very thoroughly, both experimentally and theoretically. The basic excitation mechanisms leading to dissociation have been identified and well characterized. In the keV impact energy range electronic excitations play the major role, especially for small, atomic targets of low polarizability. For molecular and/or highly polarizable target species vibrational excitation can become the major process.**

### 1.2.2 Translational Spectroscopy

This term usually covers two different kinds of observation made on an ion beam, after it passed through a gas target, with the aim of obtaining spectroscopic information relating to either the projectile or target species. One is the measurement of the translational energy spectrum of the primary ion beam at high resolution (up to 0.1 eV). In such a spectrum, relatively less intense signals will appear around the peak corresponding to the unscattered ion beam. The energy displacement on the translational energy scale of these weak peaks relative to the primary beam position, is directly correlated to the energy of the collision induced transitions between quantized energy levels (electronic, vibrational) of the target and/or the projectile. The second kind of experiment is the recording of the laboratory kinetic energy spectrum of fast ionic fragments generated by the collisions. This laboratory kinetic energy spectrum can be transformed into a center of mass (c.o.m.) kinetic energy release distribution, which in turn can be used to identify the states from which the particular dissociations take place. In the following discussion these methods will be illustrated by some appropriate examples.

#### Translational Energy Change Spectroscopy

In this method a beam of fast (keV range) ions is collided with a target gas and the kinetic energy spectrum of the resulting, undissociated ions is recorded at zero scattering angle. Because only ions which do not experience deflection are detected, the collision events that are observed take place at large impact parameters; so-called grazing collisions. The collisions induce transitions between the quantized energy levels of the ion and/or of the molecules of the target gas. The transitions manifest themselves as discrete changes in the translational energy of the ion beam and which are experimentally measured by an electrostatic sector

analyzer. Considering relationships, such as (1.16) and (1.17), between kinetic energy change, scattering angle and interconversion between internal and translational energy, it can be seen that at zero scattering angle and keV initial ion kinetic energy the measured kinetic energy change is practically equal to the energy of the collision induced transition. In practical applications of the method, either the projectile or the target is chosen to be a species with very little internal structure in order to avoid ambiguities in assigning the observed transitions to either the target or the projectile. That is, collision induced transitions in either the target or the projectile are observed as described by the following equations

$$P^+ + T(i) \rightarrow P^+ + T(f) + \Delta E_t \qquad (1.21)$$

$$P^+(i) + T \rightarrow P^+(f) + T + \Delta E_t \qquad (1.22)$$

where $P^+$ is the fast projectile ion, T is the static target species, i designates the initial state before collision, f the final state reached in the collision, and $\Delta E_t$ is the translational energy change. Target molecules are always in their ground electronic state and mostly at the ground vibrational level; therefore transitions in the target always refer to higher energy states, that is $\Delta E_t$ is always $<0$ and only energy *loss* peaks, which appear at lower kinetic energy than the main ion beam position, are observed. However, quite often a significant fraction of the projectile ions are in metastable, excited electronic and/or vibrational states. In such cases therefore, there is a possibility for transitions to lower energy states, which should result in a kinetic energy **gain** in the collision, $\Delta E_t>0$. This produces peaks at higher kinetic energies than the main beam position. Such peaks are indeed observed, and the processes generating them are called superelastic collisions. Of course, transitions to higher energy states of the projectile can also occur, so that in

kinetic energy change spectra of structured ionic projectiles, peaks can appear at both sides of the primary beam position.

Early work in this area was carried out by Park [44,45], who measured cross sections for proton excitations of different electronic states of He, $N_2$ and $O_2$ at 20-120 keV collision energy and with only a modest (2eV) energy resolution. At about the same time Moore and Doering [46] reported kinetic energy spectra with much better energy resolution, 0.15eV fwhm. In their first experiment they obtained the kinetic energy loss spectra of 500eV protons incident on $H_2$. They resolved peaks corresponding to the excitation of the v=1,2,3 vibrational states of the ground electronic state of $H_2$. This was a relatively easy task considering that the vibrational spacing in $H_2$ is ca. 0.5 eV. In general, for diatomic molecules, spacing of individual vibrational bands are usually of the order of 0.1 eV, or larger. Therefore, it is possible in principle to resolve the individual vibrational components of an electronic transition induced by ion impact. Moore [47-49] has carried out experiments of this kind for $H^+$ incident on $N_2$ and CO. A high resolution energy-loss spectrum of 2.9 keV protons incident on $N_2$ is shown in Fig.16 as obtained by Moore [49].

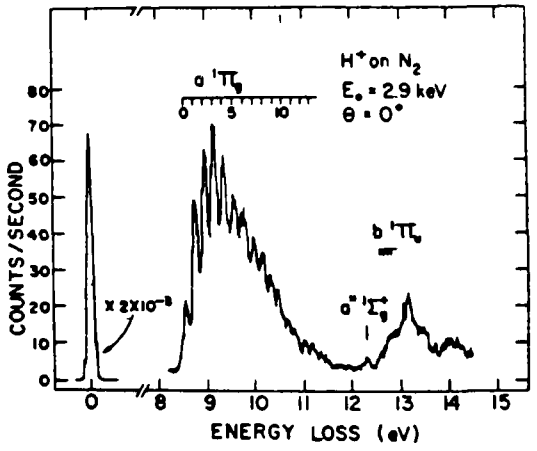


Figure 16. Energy loss spectrum of 2.9keV protons on $N_2$, [49].

The features displayed in this spectrum have been identified with known states of $N_2$. The dominant feature was assigned to the $X^1\Sigma_g^+ \rightarrow a^1\pi_g$ transition. The identification was made from the location and spacing of individual vibrational states of the band system. The relative intensities of the first six vibrational components were found to be in good agreement with theoretical predictions based on Franck-Condon factors. In general, Moore [49] concluded that the Franck-Condon principle gave a good description of the observed vibrational band intensities at projectile velocities of 2-7 $10^7$ cm/s.

Moore [50,51] has also investigated another fundamental aspect of collisional excitation; the validity of the Wigner total-spin-conservation rule [52]. Massey and Burhop [53] stated the Wigner rule in the following manner.

Two ions, atoms or molecules, with initial electron-spin quantum numbers $s_1$ and $s_2$ posses a total-spin angular momentum S which is the vector sum of the spins of the individual systems. The resultant total-spin quantum number is

$$S = |S| = (s_1 + s_2), \ldots, |s_1 \quad s_2| \tag{1.23}$$

Assuming very weak coupling between electron-spin and orbital angular momentum during a collision, the Wigner rule states that the only transitions likely to occur are those for which total electron-spin is conserved. Thus if the final spin quantum numbers of the individual particles are $s_3$ and $s_4$, then one of the numbers $(s_3+s_4)$, ..., $|s_3-s_4|$ , must be included in the set, $(s_1+s_2)$, ..., $|s_1-s_2|$ , which was initially possible for S. Moore recorded the kinetic energy change spectra of $N^+$ ions of 1-4keV kinetic energy incident on the rare gases, and on $N_2$ and $O_2$. The kinetic energy peaks observed were assigned to electronic transitions in the projectile $N^+$ and/or in the target species. Moore observed that in the case of He, Ne, Ar and $N_2$

targets the probability for spin-conserving transitions was three orders of magnitude higher than that for spin-non-conserving transitions. On the other hand for Kr, Xe and $O_2$ targets spin-non-conserving transitions had high probability.

Moore and Doering [54,55] obtained energy loss spectra of $H^+$ and $He^+$ ions incident on vapours of organic molecules. According to spin conservation rules, $H^+$ impact can only excite singlet-singlet transitions in target molecules. However, $He^+$ impact can excite both singlet-singlet and optically forbidden singlet-triplet transitions. In the latter case the excitation of the triplet states occur predominantly through electron exchange. If the target molecule in a singlet ground state exchanges one of its electrons for a projectile electron with opposite spin, the target is left in a triplet state with two electrons of the same spin but with different principal quantum numbers. It can be seen that this kind of interaction does not require spin-orbit interaction because the total spin of the $He^+$-target-molecule system does not change. In the case of the proton as projectile, this electron exchange mechanism cannot be operative for obvious reasons. An example of the observations that have been obtained by Moore and Doering is shown in Fig.17.

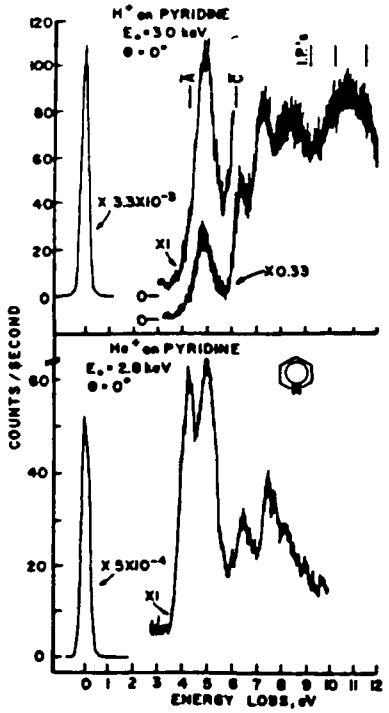


Figure 17. 3.0keV $H^+$- and $He^+$-impact energy loss spectra of pyridine

The results are those obtained for pyridine [55]. Pyridine is expected to have three triplet states lying just below or just above the lowest excited singlet state. However, singlet-triplet transitions cannot be observed in the optical spectrum of pyridine vapour. This problem can be overcome by ion impact excitation. The spectrum for $H^+$ contains peaks that have been identified as arising from transitions to singlet excited states, observed before in optical spectra. The kinetic energy loss spectrum of $He^+$ incident on pyridine vapour also contains singlet-singlet transition peaks but there is a new feature at 4.1eV, 0.2eV below the first singlet transition energy, which has been attributed to the excitation of the lowest lying triplet state of pyridine.

In 1972 Herrero and Doering [56] recorded the translational energy change spectra of $[H_2]^+$ incident on He, Ne, Ar, Kr, and $H_2$. Fig.18 shows the energy change spectrum for Kr target.

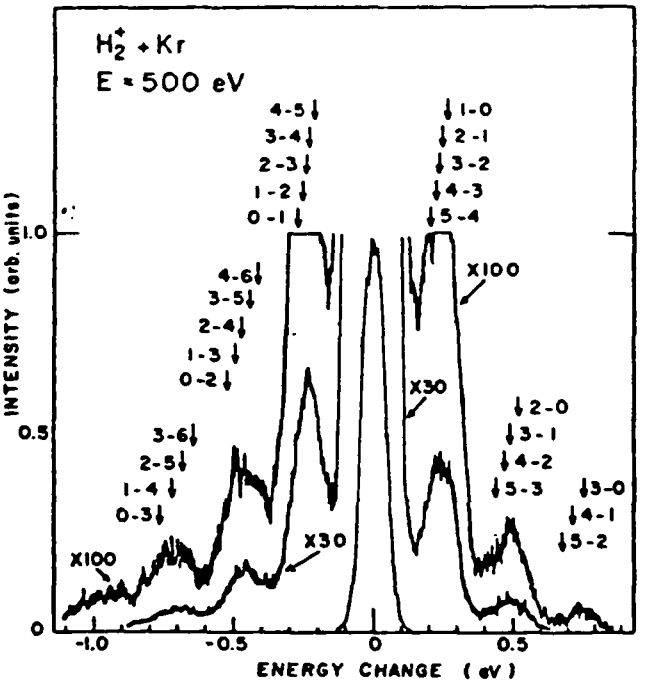


Figure 18. Energy change spectrum produced by 500eV $[H_2]^+$ on Kr [56]. The transmitted unscattered primary beam appears at 0eV. The position in energy of the various vibrational transitions within the $[H_2]^+$ ground electronic state are shown above the peaks.

It is apparent that energy gain peaks corresponding to superelastic collisions also appear in the spectrum. Transitions involving $\Delta v=\pm1,\pm2,\pm3$ are present. Since vibrational transitions of the same $\Delta v$ but from different vibrational levels have slightly different energies, then by observing the exact position of the maximum of each transition corresponding to particular $\Delta v$ values, some conclusions may be drawn about the vibrational energy content of the $[H_2]^+$ beam. Comparing the positions in energy of various individual transitions with positions of peak maxima in Fig.18, it can be concluded that vibrational energy levels up to v=4 are highly populated in the $[H_2]^+$ beam obtained by Herrero and Doering from their duoplasmatron ion source. Further work in this area, preceding 1977, has been reviewed [57].

It must be noted that a greater energy resolution for measuring kinetic energy spectra than that achieved by Doering and coworkers, has been realised by two other groups one working in Japan [58] and the other in West-Germany [59]. These groups obtained 20-40meV energy resolution in their specially built apparatus and were able to observe mode specific excitations of vibrational states of triatomic molecules. Itoh et al. [60] reached 7meV ultimate resolution with their apparatus, which permitted the observation of peaks in the kinetic energy loss spectra of $Li^+$ ions due to the collisional excitation of rotational transitions in target $H_2$ molecules.

In a recent series of publications Bowers and coworkers [61-64], using a commercial instrument (VG Analytical ZAB 2F) to obtain high resolution kinetic energy change spectra (0.1eV fwhm), have presented some ingenious applications of translational energy loss spectroscopy. They showed for several systems how this method can be used as a complimentary tool to optical spectroscopy and also for ion beam diagnostics; i.e. to determine the absence or presence of particular

metastable, excited states in ion beams. For example, O'Keefe et al. [62,63] measured the kinetic energy change spectra of $[NO]^+$ ion beams, generated by two different methods, incident on He at 8keV kinetic energy. The two methods used to generate $[NO]^+$ were (i) 70 eV EI of NO gas and (ii) charge transfer from $Ar^+$ to the NO molecule, respectively. Fig.19 shows the spectra obtained.

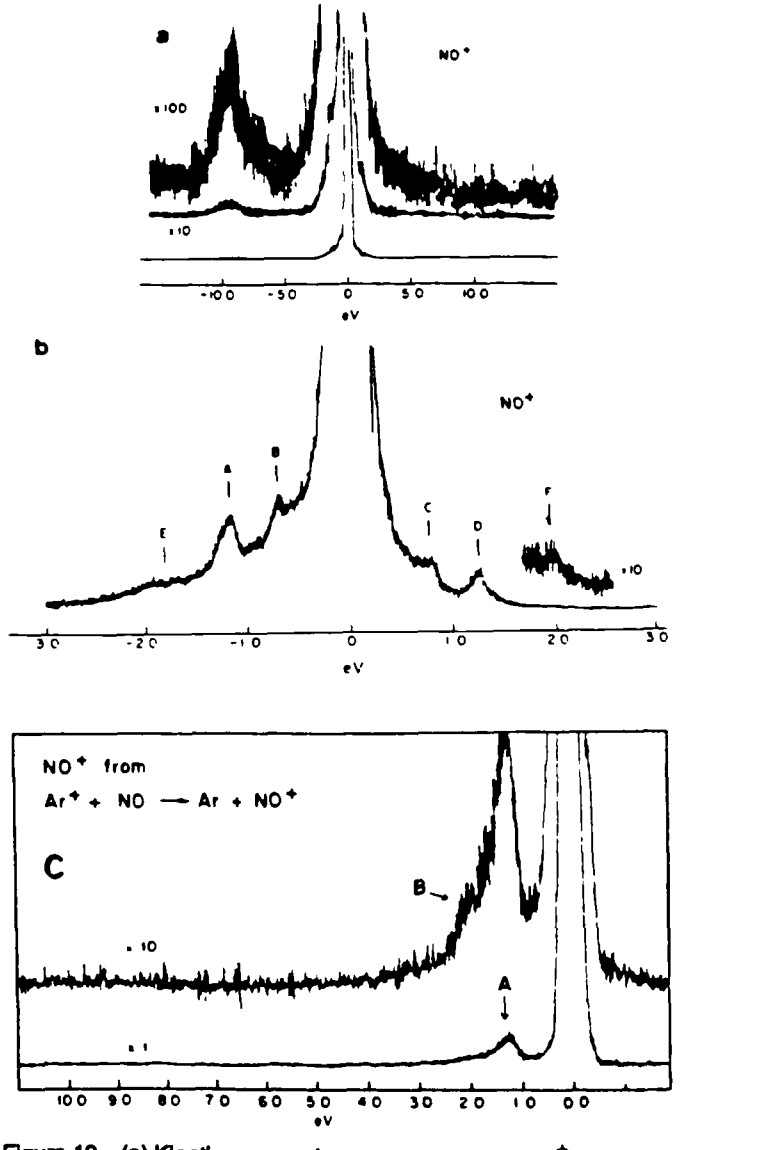


Figure 19. (a) Kinetic energy change spectrum of $[NO]^+$ ions formed by electron impact of NO, [62]. (b) High-resolution kinetic energy change spectrum of $[NO]^+$ ions fromed by electron impact of NO, [62]. (c)High-resolution kinetic energy change spectrum of $[NO]^+$ ions formed by charge exchange $Ar^+$, [63].

When $[NO]^+$ is obtained from the 70eV EI of NO gas the kinetic energy change spectrum contains several features, see Fig.19a,b. There is a peak, obtained at a somewhat reduced resolution for sensitivity reasons (Fig.19a), positioned around $\Delta E_t$=9eV. This value was found to agree well with the energy known for the $A^1\pi \leftarrow X^1\Sigma^+$ transition. Fig.19b shows the high resolution kinetic energy change spectrum for $[NO]^+$ projectiles formed by 70eV EI. Three well resolved energy loss peaks and the same number of energy gain peaks were recorded. The appearance of superelastic peaks indicated that metastable states were populated in the ion beam. The energy loss and gain peaks could be arranged into pairs having the same magnitude but opposite sign of $\Delta E_t$. These peak pairs, together with the corresponding $\Delta E_t$, were: B-C, $\Delta E_t$=±0.6eV; A-D, $\Delta E_t$=±1.2eV; E-F, $\Delta E_t$=±1.9eV. O'Keefe et al. [62] concluded that these features were the results of upward and downward transitions between pairs of excited electronic states of $[NO]^+$. To assign particular states to the observed transitions they relied on the assumption that electronic transitions induced by collisions with He must be spin-conserving and therefore only transitions within either the singlet or triplet manifold took place. From these considerations and using calculated potential curves for the electronic states of $[NO]^+$, they assigned peaks B and C to the transitions $w^3\Delta \rightarrow b^3\pi$ and $w^3\Delta \leftarrow b^3\pi$, respectively; similarly A-D were assigned to transitions $b'^3\Sigma^- \rightarrow b^3\pi$ and E-F to transitions $b^3\pi$(and/or $w^3\Delta$)$\rightarrow a^3\Sigma^+$, in the last case the peaks were less well resolved than the others, resulting in the ambiguity of the assignment. The above observations showed that the 70eV EI of NO gives a beam of $[NO]^+$ which contains the ground $X^1\Sigma^+$ state and the metastable $a^3\Sigma^+$, $b'^3\Sigma^-$, $w^3\Delta$ and $b^3\pi$ states. This was expected on the basis of the photoelectron spectrum of NO and the lifetimes of the excited states of $[NO]^+$. When $[NO]^+$ is formed in the charge exchange reaction between $Ar^+$ and NO the kinetic energy change spectrum contains fewer features,

see Fig.19c. Two energy loss peaks, peak A and the weak B feature corresponding to 1.25±0.05eV and 1.95±0.05eV $\Delta E_t$ values, respectively, were recorded. No superelastic peaks were observed indicating that only the lowest triplet or singlet state was populated. The population of the lowest singlet state was discounted based on the absence of a peak at $\Delta E_t$=9eV, and so it was concluded that only $a^3\Sigma^+$, the lowest triplet state was populated. This is in keeping with the energetics of the charge transfer reaction because, as indicated in Fig.20, the charge transfer into this state is a resonant process. In Fig.20 the origin of peaks A and B are also clearly illustrated.

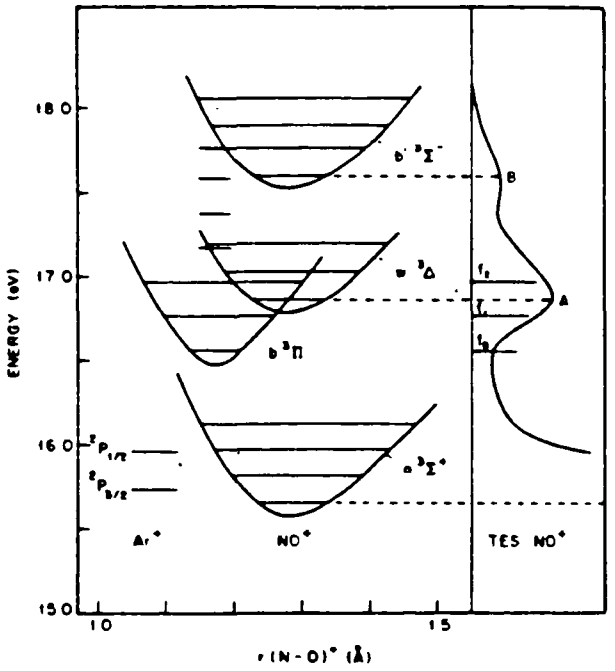


Figure 20. Potential curves for the low lying triplet states of $[NO]^+$ The energy of the two components of $Ar^+$ $^2P_{3/2}$ and $^2P_{1/2}$, and the $[NO]^+$ kinetic energy change from Fig.19c are also shown. The spectrum has been positioned assuming that the ions in the main beam are mainly in the $a^3\Sigma^+$, v=0 state. The symbols $f_0$, $f_1$ and $f_2$ represent the relative intensities of Franck-Condon factors for $b^3\pi$, v'=0,1 and 2←$a^3\Sigma^+$,v'=0 transition. Taken from reference 63.

Another noteworthy result from Bower's laboratory concerns the kinetic energy change spectroscopy of $[C_2]^+$ ions generated by the 70 eV EI of different precursor molecules [64]. Based on similar arguments to those presented above, O'Keefe et al.

[64] concluded that the 70eV EI of $C_2N_2$ produces $[C_2]^+$ ions in the lowest doublet excited state ($1^2\pi_u$), whereas 70eV EI of $C_2H_2$ gives $[C_2]^+$ ions in the quartet ground $X^4\Sigma_g^-$ state. The spectra obtained by O'Keefe et al. [64] together with the assignments of the peaks are shown Fig.21.

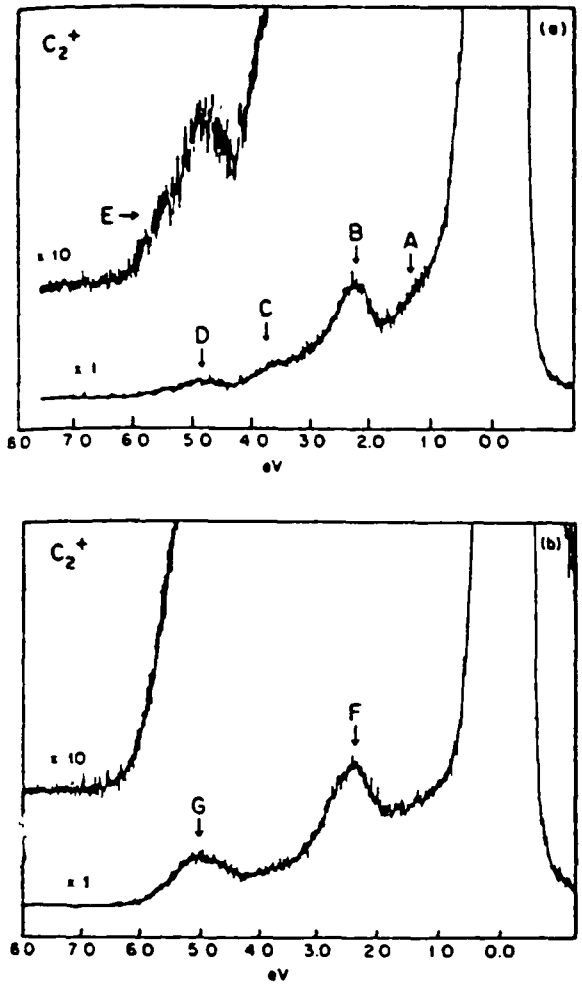


Excitation energies and assignments of spin doublet transitions in $C_2^+$

| Observed transition | Energy (eV) | Assignment | |
|---|---|---|---|
| A | 0.5–2.0 | $^2\Delta_g$, $^2\Sigma_g^-$, $^2\Sigma_g^+$, $2^2\Pi_u$ | $\leftarrow 1^2\Pi_u$ |
| B | 2.3 | $1^2\Pi_g$ | $\leftarrow 1^2\Pi_u$ |
| C | 3.0–4.0 | $1^2\Sigma^+$, $1^2\Delta_u$ | $\leftarrow 1^2\Pi_u$ |
| D | 5.0 | $1^2\Sigma_u^-$ | $\leftarrow 1^2\Pi_u$ |
| E | 5.8 | $2^2\Pi_g$ | $\leftarrow 1^2\Pi_u$ (?) |

Excitation energies and assignments of spin quartet transitions in $C_2^+$

| Observed transition | Energy (eV) | Assignment |
|---|---|---|
| shoulder on the main beam | 0.5–2.0 | $1^4\Sigma_u^- \leftarrow 1^4\Pi_g$<br>$1^4\Pi_g \leftarrow X^4\Sigma_g^-$ |
| F | 2.50 | $1^4\Sigma_u^- \leftarrow X^4\Sigma_g^-$ |
| G | 5.0 | $1^4\Pi_u \leftarrow 1^4\Pi_g$ |

Figure 21. (a) Kinetic energy change spectrum of $[C_2]^+$ taken at a main beam energy of 8keV. The $[C_2]^+$ ions were formed by electron impact of $C_2N_2$.The transition energies are listed in the table shown parallel. (b)Same as in (a) except $[C_2]^+$ was formed by electron impact of $C_2H_2$. The transition energies are listed in the table shown parallel. Taken from reference 64.

It is noteworthy that until very recently [65] these results were the only experimental observations of electronic transitions in the $[C_2]^+$ molecule, which is thought to be a very important interstellar species.

**Kinetic Energy Release Spectroscopy**

Another kind of information obtained from collisions that can have spectroscopic value is the c.o.m. kinetic energy release (KER) distribution associated with collision induced dissociations. In the case of diatomic projectile ions the KER equals the energy difference between the products and the state from which the dissociation takes place and therefore its measurement can be helpful in identifying dissociative states. At zero scattering angle, the laboratory kinetic energy corresponding to forward and backward scattered fragments is correlated to the c.o.m. KER involved in the particular dissociation through equation 1.20. The difference between the laboratory kinetic energy of the forward and backward scattered fragments from 1.20 is obtained as

$$E_a^f \; E_a^b = \Delta E_a = 4\{m_a m_b (E_o - E^*)/(m_{ab})\}^{1/2} (W)^{1/2} \qquad (1.24)$$

From equation 1.20 it is also apparent that $E_a^f$ and $E_a^b$ are nearly symmetrically positioned around the laboratory kinetic energy value corresponding with zero KER.

It can be seen from 1.24 that the separation between the forward and backward laboratory kinetic energies, $\Delta E_a$, is much larger than the kinetic energy released in the center of mass frame, W. For keV primary ion beam energies there is ca two orders of magnitude difference between these two variables. Therefore, a certain energy resolution in the laboratory frame, as determined by the resolution of the electrostatic sector analyzer and the beam collimation, corresponds to a much better resolution in the determination of W, the c.o.m. KER. The relationship between the two kinds of resolution is

$$\Delta W = \{m_{ab}/(m_a m_b E_o)\}^{1/2} W^{1/2} \Delta E \qquad (1.25)$$

where $\Delta E$ is the energy resolution in the laboratory frame and $\Delta W$ is that in the c.o.m. frame. Equations 1.24 and 1.25 are generally valid for polyatomic ions of mass $m_{ab}$, dissociating into two fragments of masses $m_a$ and $m_b$. However, in this case the obtained W values are less straightforward to interpret because one or both of the fragments are polyatomic and there is a possibility for the formation of vibrationally-rotationally excited fragments.

The work by Goh and Swan [66] on $[H_3]^+$ is an interesting example of the application of the method described above. Goh and Swan measured the kinetic energy spectra of $[H_2]^+$ fragments from collisions between $[H_3]^+$ having kinetic energies 750-2000eV and He as target. Fig.22 shows a spectrum obtained at 750eV collision energy.

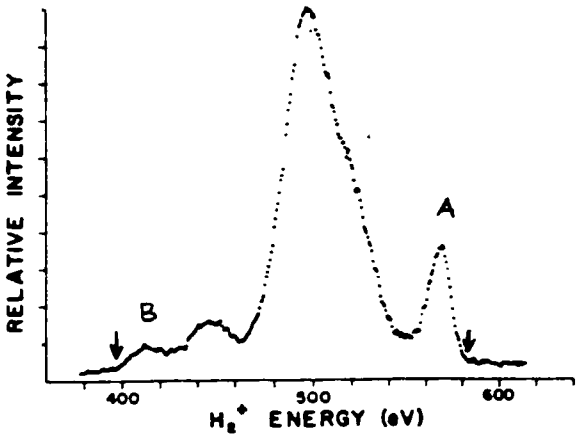


Figure 22. The energy spectrum of $[H_2]^+$ ions arising from the dissociation of 750 eV $[H_3]^+$ ions following collisions with He as target gas. Taken from reference 66.

There is a well resolved pair of peaks, A/B, positioned approximately symmetrically around 500eV, the position of the $[H_2]^+$ fragment arising from the dissociation of $[H_3]^+$ of 750eV kinetic energy with zero KER, and separated by ca 150eV. These observations indicate that A/B arises from the dissociation of $[H_3]^+$ from a repulsive electronic state into $[H_2]^+$+H. Goh and Swan took the energy values at the points where A and B reach the baseline, indicated by the arrows, as the maximum ($E^f_{max}$)

and minimum ($E^b_{min}$) laboratory kinetic energy for the forward and backward scattered fragments, respectively. By substituting $E^f_{max}$ and $E^f_{min}$ into equation 1.20 they obtained the maximum KER W=13.0±0.2eV and the maximum excitation energy E*=19.3±0.3eV for the CID process generating A/B. That W and E* are maximum values means that they correspond to the collision induced dissociative excitation of $[H_3]^+$ from its vibrational ground state. Therefore, it was concluded that the difference between E* and W, E*-W=6.3±0.3eV, corresponded to the binding energy of the $[H_3]^+$ relative to $[H_2]^+$+H(1s), in good agreement with high level theoretical calculations.

The other example that will be considered here in some detail shows how various collisional processes can be used to populate different dissociative states of ions, spectroscopic information about which can be subtracted from the laboratory kinetic energy spectra of the fragments. In 1984, Holmes and Szulejko [67] investigated predissociative states of $[OH]^+$ ions that were populated by the collision induced charge reversal of $[OH]^-$ ions. They used a double-focusing mass spectrometer of reversed geometry in their experiments (VG Analytical ZAB 2F model). $[OH]^-$ions were generated by 50eV EI of $H_2O$ in the ion source under chemical ionization conditions. Negative ions were accelerated out of the ion source to 8keV kinetic energy and collided with He target gas introduced into the first field-free region (after the ion source, before the magnet). $[OH]^+$ ions, generated from charge reversal induced by collisions with the He, were mass selected by the magnet into the second field-free region. There the $[OH]^+$ ions collided with another He target gas (admitted into a differentially pumped collision cell located in the second field-free region at the focal point) and $H^+$ ions therefrom were kinetic energy analysed by the electrostatic sector analyzer. The spectrum obtained is shown in Fig.23.

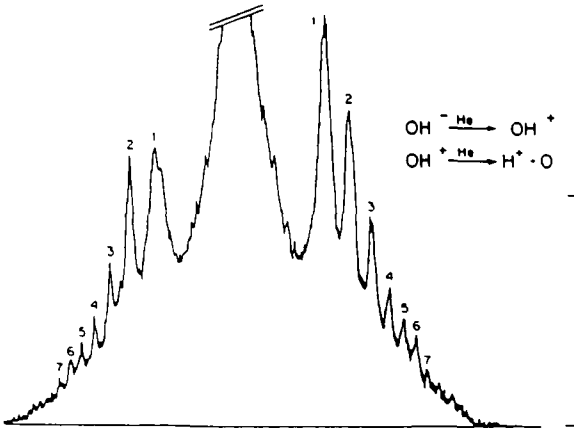


$OH^+ a\,^1\Delta$ state

| horn ($n$) | $T_n^{exp}$ | $v$ | $E_v^{calc}$ | $T_{n,v}$ |
|---|---|---|---|---|
| 0 | 0.06 a) | 9 | 3.01 | 0.03 |
| 1 | 0.29 | 10 | 3.25 | 0.27 |
| 2 | 0.50 | 11 | 3.47 | 0.49 |
| 3 | 0.70 | 12 | 3.68 | 0.70 |
| 4 | 0.89 | 13 | 3.88 | 0.90 |
| 5 | 1.06 | 14 | 4.06 | 1.08 |
| 6 | 1.22 | 15 | 4.22 | 1.24 |
| 7 | 1.36 | 16 | 4.37 | 1.39 |

Figure 23. Ion kinetic-energy spectrum for the collision induced reaction $[OH]^+ \rightarrow H^+$. The $[OH]^+$ ions were generated by the collisionally induced charge reversal of $[OH]^-$. The analysis of the fine structure is given in the table shown parallel. Taken from reference [67].

There is a very well resolved fine structure in the $H^+$ spectrum shown above indicating that predissociations from discrete vibrational-rotational levels of some of the electronic states of $[OH]^+$ are taking place. The analyses of the fine structure showed that it must have originated from the predissociation, induced by intersecting repulsive electronic states, of certain vibrational levels of the $a^1\Delta$ state, the lowest singlet electronic state of $[OH]^+$. The table beside the spectrum in Fig.23 shows the observed values of KER associated with the peak pairs building up the fine structure and also the calculated values for the predissociation of specific vibrational levels of the $a^1\Delta$ state as obtained from spectroscopic data fitted to the observed values. It has to be emphasized that collisions of $[OH]^+$ ions generated by 70eV EI of $H_2O$ in the ion source of the mass spectrometer did not produce any such fine structure. Holmes and Szulejko explained this by the fact that the $[H_2O]^+$ ions were known to dissociate only to give $[OH]^+$ ion in its triplet ground state $X^3\Sigma^-$ and collisional excitation from this state into the $a^1\Delta$ state was forbidden by spin conservation rules. On the other hand, charge reversal of $[OH]^-$ can populate any states of $[OH]^+$ and it is quite plausible that charge reversal of $[OH]^-$ in the first field free region populates the $a^1\Delta$ state of $[OH]^+$ and lower,

non-predissociating, vibrational levels will survive the flight time to the collision cell in the second field free region, where they are excited to higher, predissociating, vibrational levels.

The work of Curtis and Boyd on diatomic dications, $[CO]^{2+}$ [68] and $[N_2]^{2+}$, $[O_2]^{2+}$ and $[NO]^{2+}$ [69], should also be mentioned. In their investigations Curtis and Boyd used a double focusing mass spectrometer (VG Analytical 7070F model). Doubly charged ions were generated by EI of corresponding diatomic molecules. The electric sector potential and the magnetic sector field were held constant, the accelerating voltage was scanned to obtain the kinetic energy spectra of fragments formed in the first field free region. Kinetic energy spectra were recorded with and without collision gas; the collision gas was introduced into a cell in the first field free region. The peaks in the fragment spectra obtained with no collision gas present were assigned to unimolecular dissociations taking place on the μs timescale due to tunneling through the potential barriers of quasibound electronic states of the diatomic dications. Peaks appearing when collision gas was introduced were considered to arise from collision induced, vertical, electronic transitions to repulsive parts of the potential curves of excited electronic states. Curtis and Boyd had difficulties in assigning their observations to specific electronic states of the dications because of the paucity of experimental and theoretical information on these species. Their work highlighted a serious lack of knowledge in this respect and initiated further studies of dications [70-73].

**In summary. The measurement of the translational energy change of an ion beam after collision, can provide valuable information on collisional processes as well as give spectroscopic information about the projectile ion or the target species. From the measurement of the kinetic energy spectrum of the fragments from collision induced dissociation the center of mass kinetic energy release distributions**

**can be obtained, which in turn can be used to obtain information on the dissociation mechanisms and on the spectroscopy of the projectile ion.**

### 1.2.3 Collision Induced Dissociation of Polyatomic Ions

CID of polyatomic ions has been studied since Aston first recognized that these processes can be studied in a mass spectrometer [6,7]. A real upsurge of interest in these processes was catalyzed by a paper by Jennings in 1968 [74] and extended investigations of CID of organic ions by McLafferty and coworkers [75-78]. Subsequent modifications to commercial instruments (which allow collision gas introduction) and the development of a reversed geometry double focusing mass spectrometer [79,80], (magnetic sector first followed by the electric sector) have facilitated these studies. It has been recognized that using such an instrument, a peak in the normal mass spectrum can be separated by the magnetic field and caused to dissociate in a special chamber to which some kind of collision gas is admitted; separation of the resulting ions by the electrostatic analyzer yields the collision activated (CA) mass spectrum of that particular ion. Because it has been found that in many cases this spectrum is characteristic of the ion's structure, collision activated mass spectrometry (CA/MS) has been applied extensively in studies aimed at identifying isomeric ion structures and in separation and identification of mixture components [10]. In order to meaningfully apply this method, some knowledge relating to fundamental processes in the CID of polyatomic ions is necessary. The most important questions relate to the excitation mechanism, energy deposition in collision, the role of ion internal energy, effects of the nature of the target gas species and target gas pressure. The information relating to these questions has been reviewed before [9,10,81]. A brief summary of the current understanding of these effects is given in the following.

**Excitation mechanism**

The CID of polyatomic ions is considered to be a two step process. In the first step electronic and/or vibrational excitation occurs. This excitation energy deposited in collision into the ion will quickly be redistributed randomly among all degrees of freedom of the ground electronic state before dissociation takes place in a second, separate step. Because randomization of excitation energy is complete before dissociation the standard QET theory of unimolecular ion decay [3,4] will govern the relative abundances of fragment ions in CA/MS. Evidence for the validity of QET has been obtained by McLafferty and coworkers [77,78] who compared the normal EI mass spectra of a large number of compounds to the CA/MS of their molecular ions and found very close similarity between the two kinds of spectra. It was also pointed out that if collision induced dissociation proceeded via a repulsive state or from violent collision corresponding to a spectator stripping mechanism, then in both cases energy randomization could not take place; rearrangement peaks would be conspicuously absent from the CA mass spectra, which was not found to be the case.

The primary excitation step can involve electronic excitation and/or vibrational excitation by either momentum transfer or polarization forces, as has been discussed for the CID of diatomic ions in section 1.2.1. Information about the nature of the excitation process in the CID of the polyatomic ions has been inferred mostly from the measurement of the fragment ion abundances as a function of the ion kinetic energy. (Note that polyatomic ions lack the symmetries of diatomic ions and therefore angular anisotropies in fragment ion abundances, similar to those which helped to identify CID mechanism for diatomic ions as discussed in section 1.2.1, are not present.) In 1984, McLuckey et al. [82] carried out a study of collision energy effects on the CA mass spectra of several ions over a translational energy range of

10-6000eV. They took special precautions to eliminate all discrimination effects that could influence the comparisons. Relative fragment ion abundances were determined for methane, propane and n-butylbenzene molecular ions as a function of translational energy. Fig.24 shows the relative abundances of fragment ions as a function of the logarithm of the collision energy and also, for comparison, as a function of molecular ion internal energy, as obtained from photoion-photoelectron coincidence (PIPECO) measurements [83].

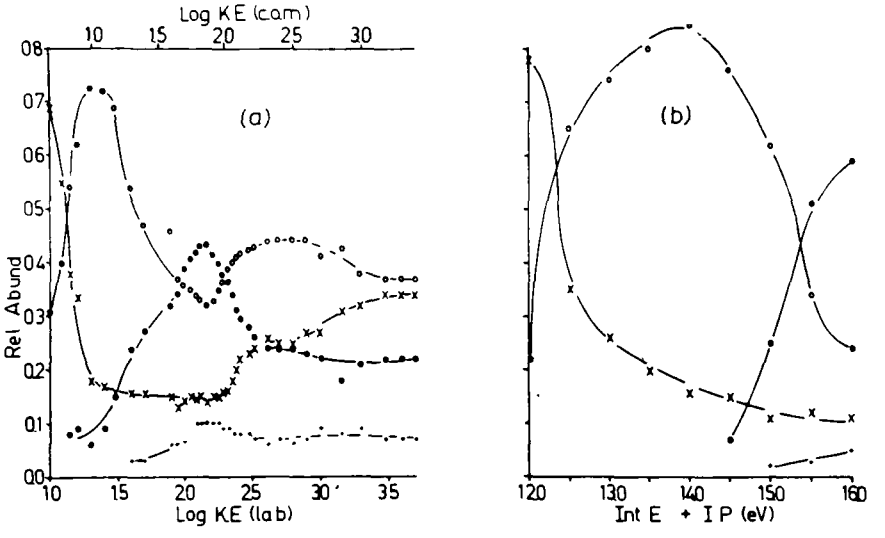


Figure 24. Plots of selected fragment ion relative abundances from the propane molecular ion. (a) As a function of the logarithm of the collision energy in collisions with Ar and (b) as a function of internal energy as obtained from PIPECO measurements. Taken from reference [82].

It can be seen that up to ca 200eV collision energy a particular value of internal energy can be assigned to the observed relative intensities using the PIPECO data. The energy deposition was found to increase until it reached a maximum at around 140eV. This translational energy corresponds to an interaction time of $2\text{-}3\text{x}10^{-14}$s which is in the order of a carbon-carbon bond vibration time. Linder and coworkers [84] had previously presented evidence that the probability for exciting a particular vibrational mode is maximized when the collision time equals one half of the period

of vibration. On this basis McLuckey et al. [82] concluded that at low collision energies (up to ca 400-500eV), vibrational excitation is the most important mechanism for energy deposition. At collision energies greater than ca. 400eV, relative fragment ion abundances did not change markedly. Also, the combination of relative fragment ion abundances at any collision energy >400eV did not correspond closely to any particular value of internal energy. This was explained as a consequence of the relatively broad distribution of excitation energies resulting from a distribution of impact parameters which are integrated into the measurement by collecting products over a finite range of scattering angles and also taken as an indication of a change in excitation mechanism from vibrational to electronic excitation. McLuckey et al. [82] further argued that a wide range of impact parameters was also sampled at low kinetic energies, but the range of excitation energies was limited by a lower c.o.m. collision energy. The observation in this case, and others [85,86], that general trends in relative ion abundances as a function of internal energy are qualitatively reproduced in collision energy resolved CA mass spectra in the low collision energy region probably reflects a relatively narrow distribution of deposited energies under these collision energies.

**The energy deposition function, $P_c(E)$**

In collisions of several keV kinetic energy the major internal energy deposition mechanism is generally thought to be electronic excitation. Massey derived a relationship between the collision time and the energy defect of the collision induced electronic transition, which is named after him as Massey's adiabatic criterion [87,88]. The principle of the derivation is very simple. Massey considered three ranges of ion velocity: (a) At low ion velocity the electrons can adjust adiabatically to the perturbation resulting from the interaction between ion and

target, making a transition unlikely; (b) at high velocity the electronic transition time is long compared to the collision time, which again makes a transition unlikely; (c) there is an intermediate range of velocities where the collision and electronic transition times are comparable, which maximizes the transition probability. The optimum collision time is simply derived from Heisenberg's uncertainty principle $\Delta t(opt.) \approx h/\Delta E(opt.)$ and from this, $\Delta E(opt.)$, the kinetic energy defect which has the highest probability at a primary ion kinetic energy, $E_o$, is obtained as

$$\Delta E(opt.) = (a/h)(2E_o/m)^{1/2} \qquad (1.26)$$

where m is the mass of the projectile ion, a is the characteristic distance along which the interaction, which induces the electronic excitation, takes place.

Using the above criterion and some simplifying assumptions, Kim and McLafferty [89] calculated energy deposition probability functions ($P_c(E)$), Fig.25 contains the results of some of their model calculations.

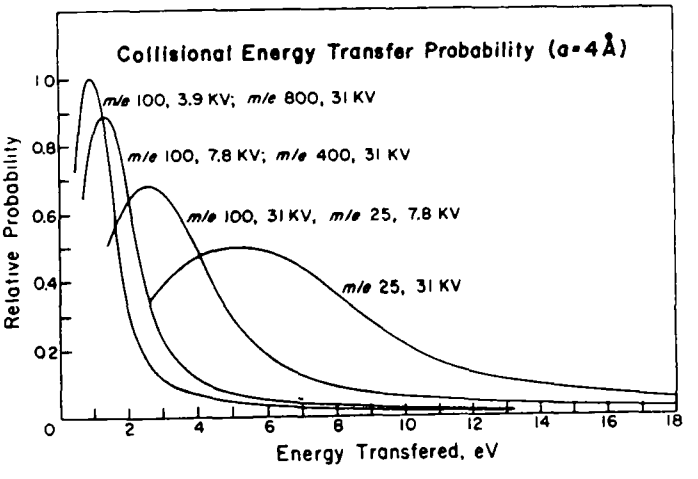


**Figure 25. Collisional energy transfer probability functions $P_c(E)$ calculated assuming an adiabatic parameter, a, of 4Å. Taken from reference [89].**

These diagrams can only be applied in a qualitative way. The major features, that were found to be correct in experiments, are (i) $P_c(E)$ is a smooth distribution without discontinuities (ii) the maximum shifts towards higher energy defects with increasing ion velocity (iii) the tailing of the distribution towards larger energy defects becomes relatively more important with increasing velocity. Also, the magnitude of the most probable energy deposition is thought to be of similar order as those given by these calculations.

**Influence of primary ion internal energy**

Early studies by McLafferty and coworkers [77,78], in which they varied the ionizing electron energy to change the ion internal energy, showed that only peaks associated with the fragmentation of lowest activation energy, which were mainly processes that gave rise to a metastable peak, showed variation of their relative intensity in CA mass spectra. The relative intensities of peaks associated with high activation energy processes was not affected considerably by the change of internal energy. It has been pointed out by McLafferty [9] that this behaviour is not unexpected in the light of the above discussions on the shape of the energy deposition function, $P_c(E)$. The CID energy distribution is a smooth function and the maximum probability for ion internal energies is well below that range of energies which governs the high energy fragmentation pathways. Thus an increase in the internal energy possessed by the projectile ion before collision will only shift the $P_c(E)$ function to slightly higher values; for the high energy part this will increase all probabilities with the same relative amount, leaving unchanged the relative abundances of fragments from these high energy processes. In more recent

measurements by McLafferty and Proctor [90,91], of fragment ion yields from the CID of isomeric $[C_7H_7]^+$ [90] and $[C_3H_7O_2]^+$ [91] ions it was shown that even the energy effect on ion yields relative to the primary beam intensity was small, 0-12%. Note that there has been some controversy about the general validity of the above conclusions. Namely, in 1978 Porter et al. [92] presented results that showed that the CA mass spectra of benzoyl cations depended on their internal energy. However, two years later, McLafferty et al [93] showed that there was no such internal energy effect. The present consensus is that in CA mass spectra the relative ion abundances of fragment ions resulting from all reactions of high critical energy are independent of the internal energy of the precursor ion, provided that isomerization is not important at the internal energies sampled.

**Collision gas effects**

For most applications He is the target gas of choice in CA/MS. It is favored because, as has been shown by Laremie et al. [94], (i) its uniquely high ionization energy minimizes the precursor ion loss due to charge transfer (ii) its small diameter minimizes ion losses due to scattering. Laremie et al. [94] found a linear relationship (with negative slope) between the logarithm of the cross section for neutralization of 7.0keV $[CH_4]^+$ and the logarithm of the ionization potential of the target. They also found that scattering losses decreased with decreasing size of the target.

Another favorable property of He as collision gas is that it has a high relative cross section for electronic excitation, especially those involving large energy defects. For example, Kim and McLafferty [89] determined the relative CID efficiencies for different targets of the reaction $[CH_4]^+ \rightarrow C^+$ at 7.8keV collision

energy. This reaction was chosen because its high critical energy (12.4eV) minimizes the vibrational energy transfer contribution to the excitation step. Surprisingly they found a steep linear relationship between the efficiency for this reaction and the ionization energy of the target species. However, for a special kind of high energy process in CA/MS, the so-called charge stripping (CS) process, which gives rise to doubly charged ions in the CA mass spectra, other collision gases such as $N_2$ or $O_2$ have been found to be more efficient than He [95-97].

The effect of collision gas pressure on CA mass spectra has also been investigated. It has been found that increasing collision gas pressure so that precursor ions undergo multiple collisions not only increases the CID efficiency, but also increases the intensity of those fragment ions formed via high energy processes [77,94,98]. It has also been shown that the structural specificity is not lost under high collision gas pressure conditions. For example, Bockhoff and McLafferty [99] found for CA/MS studies of $[C_7H_7]^+$ isomers that even though the spectra of the isomers changed with collision gas pressure, quantitative results were identical within experimental error, provided that the pressure used for analysis was the same as used to obtain the reference spectra of the ion isomers. However, it should be noted that at extremely high pressures where multiple collisions are dominant, the tendency towards generating stripped C groups ($C_1$, $C_2$, $C_3$...etc.) can become strong enough that structure characteristic fragment peaks will disappear from the CA mass spectra.

There have been theoretical studies of multiple collision conditions [98,100]. Kim [100] showed that probability for multiple collisions could be approximated by a Poisson distribution, the probability for n subsequent collisions ($P_n$) is given as

$$P_n = (1/n!)(I/I_o)[\ln(I/I_o)]^n \qquad (1.27)$$

where $I_0$ is the main beam intensity without collision gas and I is that with collision gas present. Using the results of Kim, Holmes [10] derived a diagram which contains $P_n$ as a function of collision gas pressure and also of main beam reduction. The diagram is shown in Fig.26.

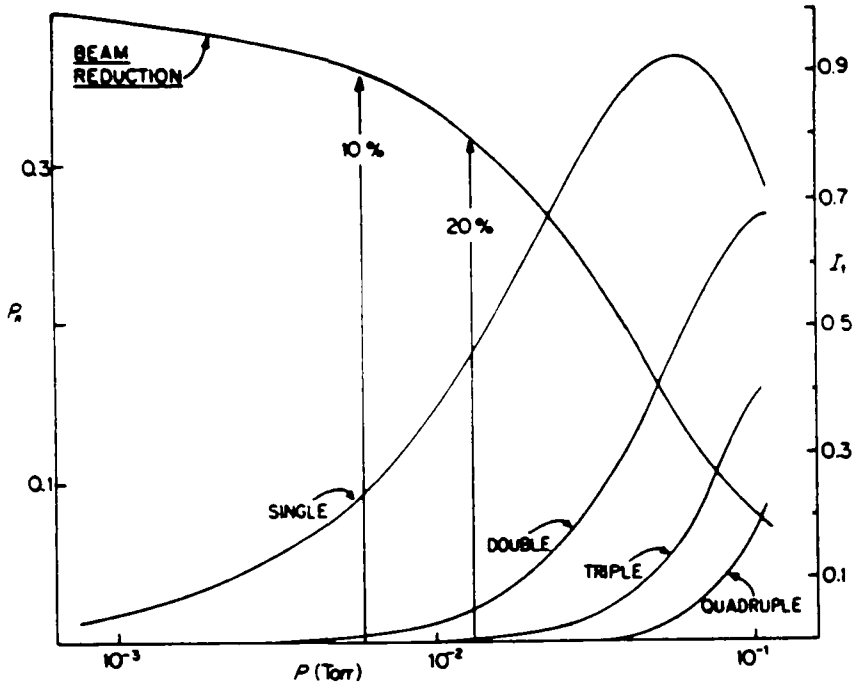


Figure 26. Total collision probability and the fractions of single and multiple collision processes as a function of collision gas pressure. (for an ion of collision cross-section $5x10^{-16}cm^2$, collision path 1cm.) Taken from reference [10]

Based on the above results Holmes [10] concluded that for maximum sensitivity without too much loss of structure identifying features due to multiple collisions, a main ion beam reduction of ca. 30-40% is optimal. If only single collision processes are desirable a beam reduction of <10% is necessary.

Finally, it should noted that there have been investigations of the conditions for using CA/MS for determining quantitative percent compositions of isomeric ion mixtures. In 1982 Bass and Bowers [101] presented a thorough examination of the

problem. They relied on the superposition principle of CA mass spectra introduced by McLafferty and coworkers [102], to derive rigorous expressions relating the percent composition to either the normalized peak height of a given m/z peak, or to the ratio of two peak heights, in the corresponding CA mass spectrum. The above mentioned superposition principle states that if the CA mass spectra of the individual isomers are independent of their internal energy content, then the CA mass spectrum of the mixture represents the superposition of the individual spectra from the corresponding amounts of the pure isomers. Bass and Bowers [101] showed that the peak ratio method does not lead to the simple linear interpolation formula used by McLafferty and coworkers (see equation (2) in reference [101]) but to a slightly more involved expression (equation (8) in reference [101]). The work of Bass and Bowers emphasized that *for a correct analysis it is always necessary to determine the normalized to either the main beam or the total fragment ion intensity- peak heights in the spectrum of each of the pure isomers.*

**In summary. The processes associated with the CID of polyatomic ions have been characterized in much less detail than those for the CID of diatomic molecules. However, it has been shown that similar mechanisms are operative in both cases. The effect of experimental parameters on the CID of polyatomic ions has been thoroughly studied and the conditions for obtaining CA mass spectra for structure elucidation studies, and isomeric ion mixture analyses, have been established.**

### 1.2.4. Charge Transfer Neutralization of Ion Beams

From the 1930's there has been a continuing interest and development in the understanding of charge transfer phenomena in atomic and molecular collisional processes, as well as the exploitation of these phenomena in practical applications and scientific research. The processes studied can be generally described by the following reaction

$$P^{n+}(i) + N(i) \rightarrow P^{(n-k)+}(f) + N^{k+}(f) \qquad (1.28)$$

where $P^{n+}$ stands for a projectile ion (atom or molecule) with n positive charges on it and N is a neutral collision partner. The reaction involves a transfer of k electrons from N to $P^{n+}$. The reactants and the products can be in variety of states (i stands for initial, f for final states).

The field has a very extended scope, covering relative velocities of collision partners from meV up to the MeV range; from singly charged projectile ions up to completely stripped nuclei. The discussion here will be restricted to systems and experimental conditions which have direct relevance to the work described in this thesis. That means focusing on electron capture processes between singly charged ions of keV kinetic energy and a neutral target gas. First, the current understanding of charge transfer collisions between atomic-ions and atoms will be reviewed. This being the simplest, is the best understood system and ideas established for it are often applied to systems which are more difficult to understand, such as electron capture by diatomic and polyatomic ions that will be discussed subsequently.

**Ion-Atom Charge Exchange**

There are two fundamentally different types of charge exchange reactions depending upon the nature of the interacting species. One is the symmetric resonant charge exchange which refers to charge exchange processes between like atoms and ions, as described by the reaction

$$A^+ + A \rightarrow A + A^+ \qquad (1.29)$$

Experimental evidence shows that the cross section for a symmetric resonant charge transfer process decreases as the relative kinetic energy ($E_k$) of the interacting species increases [103,104]. Another general trend is that for different reacting systems, at a given relative velocity, the cross sections increase with increasing ease of ionization of the atom A.

These general characteristics has been reproduced with nearly quantitative precision by semiclassical impact parameter calculations introduced by Gurnee and Magee in 1957 [105]. The most significant characteristics of this method are that the relative motion of the colliding particles is treated classically and all other degrees of freedom are treated by quantum mechanics. Classical mechanics can be used for the relative motion in a collision problem if the trajectories of the particles are well defined both before and after the collision. Thus the wavelength associated with the momentum, Mv and the momentum transfer, $\Delta p$ must be small compared to the impact parameter, $R_o$. These conditions apply up to high keV collision energies. The simplest theoretical treatments further assume that the transferred electron moves independently of all others and therefore has only two states, symmetric and antisymmetric. The charge exchange cross section $\sigma$ is given by

$$\sigma = 2\pi \int P(b) b \, db = 2\pi \int b \sin^2\Gamma(b) \, db \qquad (1.30)$$

where b is the impact parameter. The probability of charge transfer P(b) is given by $\sin^2\Gamma(b)$, where

$$\Gamma(b) = (1/\hbar v) \int \{R(E_g - E_u)/(R^2 - b^2)^{1/2}\} \, dR \qquad (1.31)$$

v being the impact velocity, R the internuclear separation, $E_g$ the energy of the symmetric state and $E_u$ the energy of the antisymmetric state. A qualitative picture illustrating the physical process of exchange is as follows. When $A^+$ and A approach, the $A_2^+$ system can be approximately given by the normalized sum of two wave functions, $\Phi_g$ and $\Phi_u$, describing states of energies $E_g$ and $E_u$. As $A^+$ approaches A, the instantaneous time dependencies of these wavefunctions are in and out of phase with an instantaneous beat frequency $(E_g - E_u)/h$. Integration of this beat frequency over the collision time determines whether the electron ends up on one nucleus or the other as the two particles recede from the collision. The term $\sin^2\Gamma(b)$ oscillates with sufficient rapidity that it is customarily replaced by its average value of 1/2. In Fig.27 experimental and theoretical results for the $He^+$ + He system are shown as an example

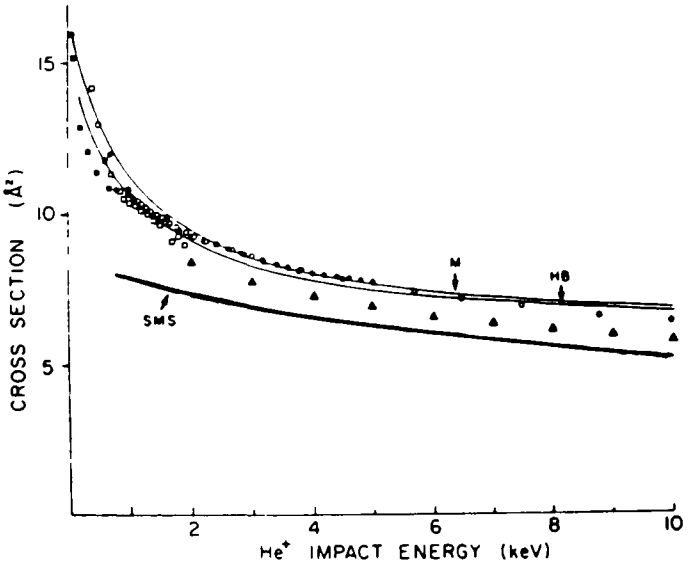


Figure 27. Cross sections for electron transfer in $He^+$+He interaction as a function of $He^+$ impact energy, [106]. Experimental data are from (■)[107], (▲) [108], (●) [109], (◆) [110]. Theoretical calculations are given by solid lines,from top to bottom, [111], [112] and [113].

It is apparent that the cross section decreases with increasing kinetic energy and that the theoretical calculations are in good quantitative agreement with experimental results. Theoretical calculations also confirm the general experimentally observed trend, that the cross section increases with decreasing ionization energy of A. Fig.28 shows a comparison of experimental and theoretical results regarding this characteristic of resonant charge exchange collisions.

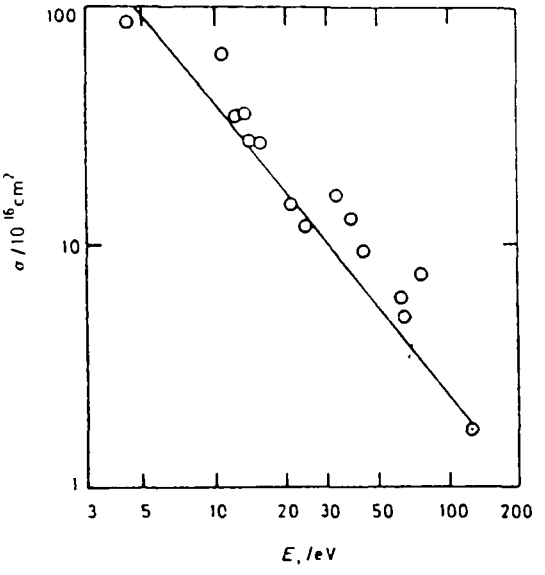


Figure 28. Correlation between cross section σ for symmetrical charge exchange reactions $A^+ + A \rightarrow A + A^+$, and ionization energy $E_i$ for the process $A \rightarrow A^+ + e^-$, [114].

Electron transfer between unlike atoms is a fundamentally different process from resonance charge transfer. In the symmetric resonant process (equation 1.29), even though there are two $A_2^+$ states involved in the collision there is only one asymptotic state at R=∞, $A^+ + A$. However in the non-resonant reaction

$$A^+ + B \rightarrow A + B^+ \qquad (1.32)$$

there are two different asymptotic states, $(A^+ + B)$ and $(A + B^+)$. Each of these are asymptotic forms of different electronic states of $AB^+$. Charge exchange requires an electronic transition from one electronic state to the other. For this electronic transition involving an energy defect $\Delta E$ between the two states, Massey's adiabatic criterion, described in the previous section, can be applied. It states that the cross section of a non-resonant charge transfer process will increase with increasing relative kinetic energy of the collision partners up to a maximum value beyond which the cross section decreases. The relative kinetic energy, (and the relative velocity ($v_{max}$)), at which the maximum cross section is reached can be obtained from equation (1.26). The value for $v_{max}$ can be obtained as

$$v_{max} = (a/h)\,\Delta E \qquad (1.33)$$

The energy defect, $\Delta E$, substituted in (1.33) should, in principle, be the energy difference between the two electronic states of $AB^+$ for the internuclear distance at which the transition takes place. This is difficult to estimate. However, Hasted [115,116] used the $\Delta E$ value corresponding to infinite separation, i.e. the difference between the ionization energies of A and B, and still obtained a good correlation for $v_{max}$ with a constant value of 7Å for a large number of asymmetric systems.

Several authors have carried out calculations for charge transfer between unlike atoms by a general method, similar to that applied for resonance transfer [103,117]. The dependence of charge transfer cross section on impact energy has the expected form. With increasing kinetic energy, the cross section rises to a maximum and then falls. Fig.29 shows the comparison of experimental and theoretical results on the velocity dependence of charge exchange between $H^+$ and different target atoms.

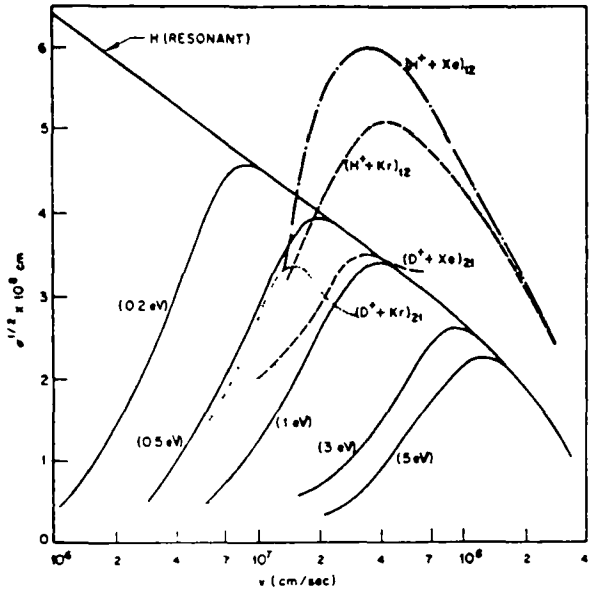


Figure 29. Calculated and measured cross sections for $H^+ + A \rightarrow H + A^+ + \Delta E$ reaction, where $\Delta E$ is the difference between the ionization energies of H and A, [103]. Solid lines are theoretical calculations others are experimental results.

For asymmetric charge transfer between unlike atoms which have widely different ionization energies there can be many reaction channels involving excited state products for which the energy balance is much closer to resonance than that for ground state products. In this case it is expected that mostly these excited state channels will be populated in the reaction. A good example of this is the charge transfer reaction between $He^+$ and Cs. The ground state product channel, $He(^1S_o)+Cs^+(^1S_o)$, is exothermic by 20.69eV, but the processes leading to excited neutral He in the $2^3S$, $2^1S$, $2^3P$ and $2^1P$ levels have respective energy defects of -0.88, -0.08, 0.27 and 0.52eV, respectively. Reynaud et al. [118] have performed time-of-flight measurements to determine the translational energy change of $He^+$ projectiles undergoing the reaction $He^+ + Cs \rightarrow He + Cs^+$. Fig.30 shows their results and the assignments of the observed translational energy change peaks to particular excited state products.

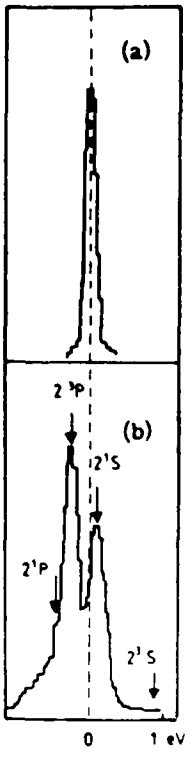


Figure 30. (a) Time of flight spectrum of He atoms from the $He^+$ + He collision giving the zero point of the translational energy change spectrum; (b) translational energy change spectrum of He atoms from $He^+$ + Cs collisions, [118].

This example shows that excited states can play an important role in charge transfer reactions when they are associated with resonant or near-resonant processes. Their importance is discussed in greater detail, in several recent reviews [114, 119, 120].

### Charge exchange in molecular systems

The simplest, symmetric molecular charge transfer reaction is that between $[H_2]^+$ ions and $H_2$ molecules illustrated by reaction (1.34)

$$[H_2]^+(X^1\Sigma_g^+,v_o') + H_2(X^2\Sigma_g^+,v_o'') \rightarrow [H_2](X^2\Sigma_g^+,v'') + H_2^+(X^1\Sigma_g^+,v') \quad (1.34)$$

Because the vibrational energy levels of a molecule are more closely spaced

than the electronic energy levels of atoms, there are a large number of charge transfer channels having a relatively small energy defect. The existence of these, so-called "near-resonant" channels, significantly influences the total charge transfer probability for molecular systems. Fig.31 shows the measured and calculated cross section for the deuterium analogue of reaction (1.34) as a function of the square root of the $[D_2]^+$ impact energy.

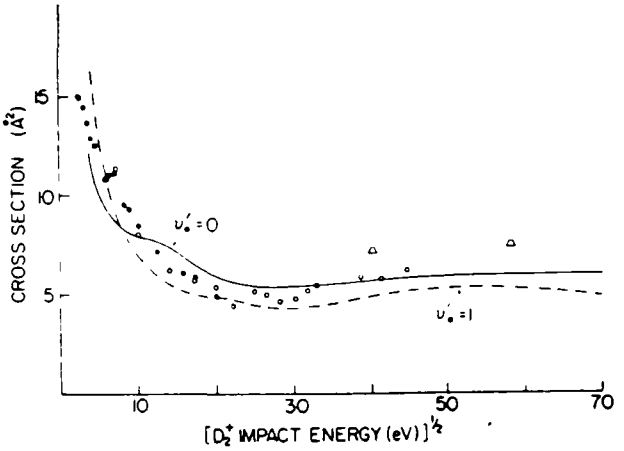


Figure 31. Cross sections for the electron transfer in $[D_2]^+(X^2\Sigma^+_g,v_o')+D_2(X^1\Sigma^+_g,v_o''=0)$ collisions as a function of square root of $[D_2]^+$ impact energy, [106]. Experimental data are from (•) [121], (Δ) [122], (o) [123]. The solid and dashed curves are the computations of Moran et al. [124] for the $v_o''=0$ and 1 levels of reactant $[D_2]^+(X^2\Sigma^+)$ ions.

It can be seen from Fig.31 that after an initial decrease at low impact energies the cross section does not change appreciably, unlike for atomic systems where the cross section for charge transfer decreases exponentially over a wide range of impact energies. The theoretical treatment of the reaction, to be discussed below, gives the underlying reasons for this behaviour.

The theoretical treatment generally used to describe molecular charge transfer is the so-called multistate impact parameter method. It has been pioneered by Bates and Reid [125] and was subsequently improved upon by Moran and coworkers [126] and applied to a wide range of problems [106]. In this approach a set of coupled

partial differential equations resulting from the time dependent Schroedinger equation are solved numerically. From the solutions, the cross section for each charge transfer channel is obtained and these are summed to obtain the total cross section. Two parameters appear to influence the importance of a particular channel. They are the corresponding energy balance and the value of the vibrational Franck-Condon overlap integral between the initial and final states. The theoretical calculations of Moran et al. [124] for the reaction

$$[H_2]^+(X^2\Sigma_g^+,v_o'=0)+H_2(X^1\Sigma_g^+,v_o''=0)\rightarrow H_2(X^2\Sigma_g^+,v'')+[H_2]^+(X^2\Sigma_g^+,v') \quad (1.35)$$

clearly demonstrate this point. Fig.32 is a diagram showing the cross section as a function of the square root of the impact energy for the individual charge exchange channels defined by particular values of v'' and v'. The energy defects and Franck-Condon factors are shown in the table beside the diagram.

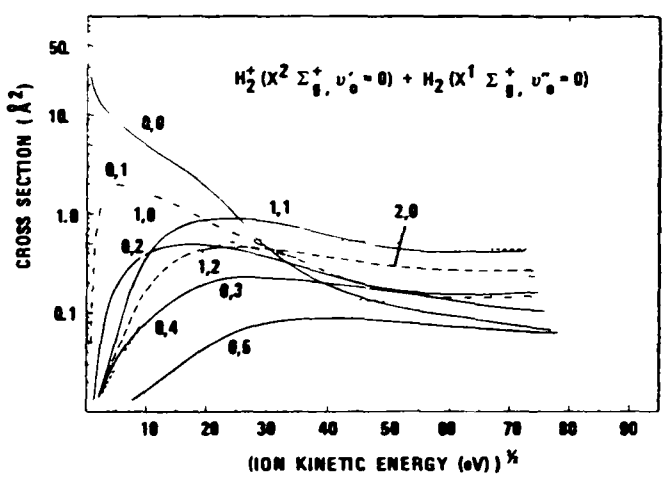


| Product vibrational levels v'',v' | Energy defect (eV) | Overlap |
|---|---|---|
| 0,0 | 0.00 | 0.090 |
| 0,1 | 0.27 | -0.121 |
| 1,0 | 0.52 | 0.159 |
| 0,2 | 0.53 | 0.126 |
| 0,3 | 0.77 | -0.118 |
| 1,1 | 0.79 | -0.211 |
| 0,4 | 0.99 | 0.104 |
| 2,0 | 1.00 | 0.175 |
| 1,2 | 1.04 | 0.220 |
| 0,5 | 1.21 | -0.089 |

Figure 32. Multistate $[H_2]^+(X_2\Sigma^+_g,v_o'=0)+H_2(X^1\Sigma^+_g,v_o''=0)$ electron transfer cross sections for the production of specific product-ion states as a function of the square root of $[H_2]^+$ impact energy. The vibrational quantum numbers of the respective neutral and ion products are given for ten near resonant electron transfer channel. The table contains energy defects and vibrational overlaps for the specific channels. Taken from reference [124].

It can be seen that the cross section for the totally resonant channel, (0,0), for which the Franck-Condon factor is only 0.098, decreases rapidly with increasing impact energy. Above 1keV it becomes one of the least efficient channels, and the most efficient channels (1,0), (2,0) and (0,2) involve fairly large energy defects (around 1eV) but have very favorable Franck-Condon factors. From these and similar calculations it has been concluded that electron transfer cross sections at low impact energies tend to be controlled by the magnitude of the energy defect and to a lesser extent by the overlap integrals. However, at higher impact energies the magnitude of the vibrational overlaps exerts a dominant role on the product channel distribution. This has been shown by the calculations of Moran and Flannery [127] to result in the generation of vibrationally excited hydrogen ions and molecules in the charge transfer process. This conclusion is confirmed by the results of merged beam experiments carried out on fast beams of hydrogen molecules obtained by charge transfer neutralization of the corresponding ion beam [128-130].

Several other symmetric diatomic charge transfer systems have been investigated both experimentally and theoretically, such as $[N_2]^+ + N_2$, $[O_2]^+ + O_2$, $[NO]^+ + NO$, $[CO]^+ + CO$ (for a review see reference [106]). Similar general characteristics have been obtained for these systems as for the $[H_2]^+ + H_2$ system.

Asymmetric molecular charge transfer systems have also been studied. It has been found that the same factors, the vibrational overlap and the energy balance, (as for symmetric systems), influence the cross section for asymmetric charge transfer reactions. A good example is the $[O_2]^+ + N_2$ charge exchange studied by Wilcox and Moran [131]. Ionization of ground state $O_2$ molecules to form ground state $[O_2]^+(X^2\pi_g)$ ions requires 12.0eV. If electrons of 16.1eV or greater kinetic energy are used to ionize $O_2$ molecules in an EI ion source, a certain fraction of the $[O_2]^+$ ions, depending on the ionizing electron energy, are formed in the

metastable $a^4\pi_u$ electronic state. Fig.33 shows the relative electron transfer cross sections for 1keV $[O_2]^+$+$N_2$ reactions as a function of the ionizing electron energy.

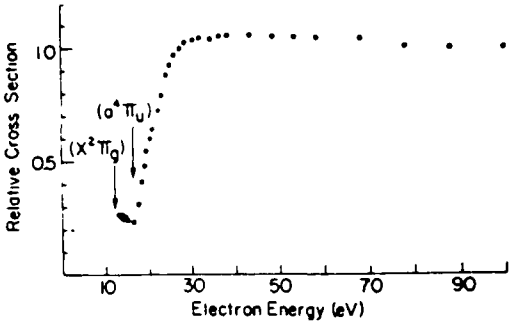


Figure 33. Relative electron transfer cross sections for 1 keV $[O_2]^+$+$N_2$ reaction as a function of ionizing electron energy used to form $[O_2]^+$ ions. Energetic thresholds for forming $[O_2]^+(X^2\pi_g, v_o'=0)$ and $[O_2]^+(a^4\pi_u, v_o'=0)$ ion states are indicated by the arrows. Taken from reference [131].

There is a rapid increase in the relative electron transfer cross section above 16.1eV. the energetic onset for producing $[O_2]^+(a^4\pi_u)$ ions. Cross sections continue to increase as the $a^4\pi_u$ fraction of the ion beam is increased and indicates a greater efficiency for $[O_2]^+(a^4\pi_u)$ ions compared to the ground electronic state ions. Wilcox and Moran [131] have also obtained from their measurements the absolute cross sections for the ground and the excited state $[O_2]^+$ as a function of ion impact energy. The results are shown in Fig.34.

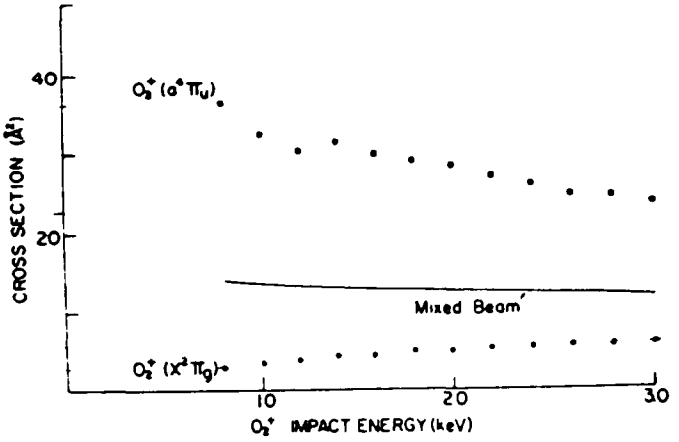


Figure 34. Electron transfer cross sections in $[O_2]^+$+$N_2$ reactions as a function of $[O_2]^+$ impact energy. ( ) pure $[O_2]^+(a^4\pi_u)$; ( ) pure $[O_2]^+(X^2\pi_g)$; ( ) mixed ion beams. Taken from reference [131].

It can be seen that the $a^4\pi_u$ state has a significantly higher charge transfer cross section than the $X^2\pi_g$ state, and the cross section for the former slowly decreases while the latter slowly increases with impact energy. To gain insight into the origin of the different reactivities of these two states Wilcox and Moran [131] calculated the energies and the overlaps for the $e^-+[O_2]^+(X^2\pi_g,v_o')\rightarrow O_2(X^3\Sigma_g^-,v'')$ and the $e^-+[O_2]^+(a^4\pi_u)\rightarrow O_2(X^3\Sigma_g^-)$ neutralizing "half reactions", which are illustrated in Fig.35. Positions of the lines denote transition energies, while the length of the lines give the magnitude of the vibrational overlaps. The corresponding $N_2(X^1\Sigma_g^+,v_o'=0)\rightarrow[N_2]^+(X^2\Sigma_g^+,v';A^2\pi_u,v';\ B^2\Sigma_u^+,v')$ half reactions are displayed similarly in Fig.35.

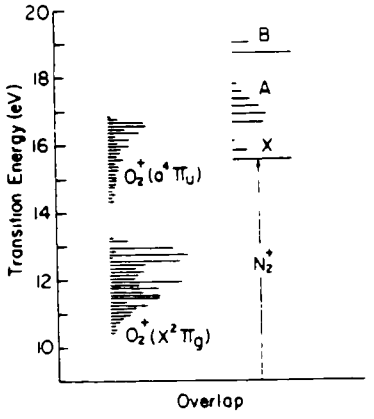


Figure 35. Transition energies for neutralization $[O_2]^+(X^2\pi_g, v_o')$ and $[O_2]^+(a^2\pi_u, v_o')$ ions and energies to form $[N_2]^+(X^2\Sigma^+_g, v')$, $[N_2]^+(A^2\pi_u, v')$, and $[N_2]^+(B^2\Sigma^+_g, v')$ state ions. The lengths of the horizontal lines designate magnitudes of the various vibrational overlaps. Taken from reference [131].

From the figure it is apparent that a close balance exists between energies liberated in the neutralization of $[O_2]^+(a^4\pi_u,v_o')$ and the energies required to form $[N_2]^+(X^2\Sigma_g^+,v';A^2\pi_u,v')$ product ions, whereas an energy deficit of several volts exists for the reactions of the ground state $[O_2]^+$. It is not surprising that cross sections for excited state reactions are significantly larger than those for ground

state reactant ions. The magnitude and kinetic energy dependence of $[O_2]^+(a^4\pi_u,v')$ cross sections, shown in Fig.32, is typical of resonant/near-resonant reactions, as expected from the data in Fig.35.

Cross sections for charge transfer reactions of polyatomic ions cannot be calculated theoretically in the same way as for diatomic ions because the calculations become too complex to handle with the present computing techniques. There have been experimental efforts to correlate cross sections for these reactions to the energy defects involved. Moran and coworkers [132-134] have determined charge transfer cross sections for a large number of polyatomic organic cations and neutral target molecules. The general conclusion from their experiments is that at a certain impact energy, reactions with zero energy defect have the highest cross section while reactions involving either positive or negative energy defects have increasingly lower cross sections. An example is shown in Fig.36, which shows the cross section of charge transfer as a function of energy defect for reactions involving ions generated by the 70eV EI of methanol and different targets.

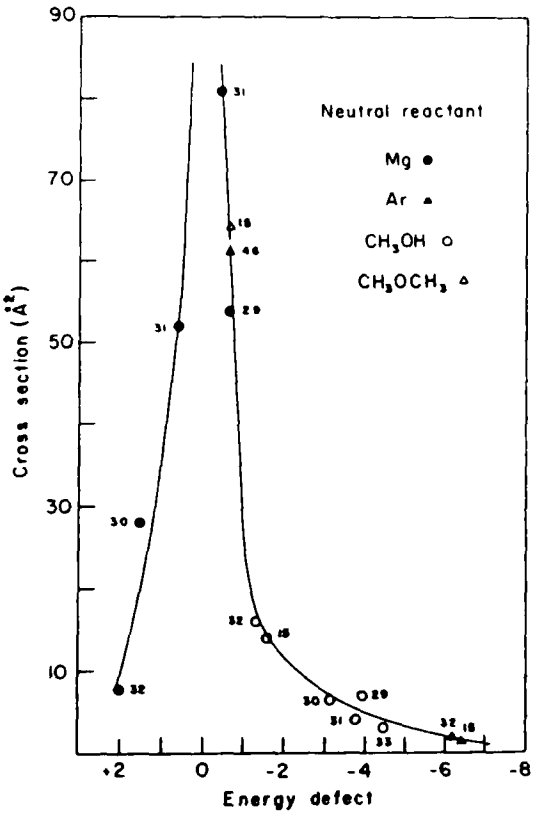


Figure 36. Charge transfer cross sections ($Å^2$) presented as a function of reaction energy defects (eV). Reactant ions were generated by the 70eV EI of methanol. Data points are labelled by the reactant ion m/z value. Taken from reference [133].

It must be noted that the diagram has to be considered with some caution, because it contains data obtained by two different methods and also uses low level MINDO calculations to obtain energy defects. The general trend it shows is probably valid, but the two orders of magnitude difference in cross section within a few eV range of energy defect is possibly exaggerated.

### 1.2.5. Neutralized Ion Beam Spectroscopy

This term was introduced by Porter and Gellene [135] who first systematically used the neutralization of fast ion beams to generate and study fast beams of neutrals. Porter and coworkers [136] developed an apparatus for the measurement of the angular profile of fast neutral beams generated by charge transfer collisions in order to obtain information about the dissociative properties of neutrals generated in the charge transfer process. The apparatus can be described briefly as follows.

An ion beam produced by EI or chemical ionization, is accelerated through 3-6keV, mass resolved by a magnet and focused into a collision chamber containing a low pressure of metal vapour (typically 1-5mtorr). Unreacted ions emerging from the chamber are swept out of the main beam direction by electrostatic deflection so that only neutral species continue their flight toward the electron multiplier detector. Translation of the detector normal to the beam axis samples beam intensity as a function of scattering angle ($I(\theta)$), giving rise to a neutral beam profile ($I(\theta)$ vs. $\theta$). Under their experimental conditions the transit time to reach the detector is between about $10^{-7}$ and $10^{-6}$s. If a neutral survives for a period longer than $10^{-6}$s , then the full width at half-maximum (FWHM) of its beam profile will be essentially the same as that of the primary ion beam. Alternatively, a neutral that dissociates on a time scale shorter than $10^{-7}$s will give rise to a broadened profile due to the components of the fragment's velocity normal to the

beam axis. A combination of these events will give rise to a composite profile as will a single dissociation process occurring on the time scale between $10^{-6}$ and $10^{-7}$s (metastable species). In order to interpret the beam profile of a neutral species some prior knowledge of its characteristics is generally necessary. When a neutral undergoes dissociation, as evidenced by beam broadening, the laws of conservation of energy and momentum allow the calculation of the fragmentation energy (more precisely, the kinetic energy released upon dissociation) by the relation [135]

$$FE = -\tfrac{1}{2} M_1 \{1 + (M_1/M_2)\}(V_{cm} \sin \theta_{max})^2 \qquad (1.36)$$

where FE is the maximum value of fragmentation energy, $M_1$ is the mass of the observed fragment at the maximum laboratory scattering angle $\theta_{max}$, $M_2$ is the mass of the other fragment, and $V_{cm}$ is the center of mass velocity. Use of equation (1.36) requires a knowledge of the fragment masses (i.e. dissociation pathway), which can be uniquely determined if $I(\theta)$ for both masses is observed.

This method has been used to gain information on several systems, such as:

(1) To study dissociative properties of $CH_n$ (n=1-4) formed by charge transfer between the corresponding fast $[CH_n]^+$ ions and metal targets of different ionization energies [137].

(2) To study the classical and bridged structures of the ethyl radical [138]. Assuming, that the dissociative state of the ethyl radical populated by charge transfer, with the hydrogen positioned between the two carbon atoms, can be thought of as a transition state for 1,2 hydrogen migration in the ethyl radical, Gellene et al. [138] obtained an upper bound for the energy of this transition state at 2.2eV. Similar studies [139] on charge transfer neutralization of $[C_2H_3]^+$ and $[C_2H_2]^{+\cdot}$ ions gave information on the transition state for 1,2-H migration in the

$C_2H_3$· radical and on the excited states of the $C_2H_3$· radical and the $C_2H_2$ molecule.

(3) To obtain information on the stability and dissociation properties of a number of small hypervalent radicals, such as $H_3$ [140]; $CH_5$, $NH_4$, $H_3O$ [141]; $CH_3NH_3$ [142]; $NH_4(NH_3)_n$ [143]; $CH_3NH_3(NH_3)_n$ [144]; $D_2F$ [145]; $D_3O$ [146,147].

(3) To study the rare gas dimers, $He_2$, $Ne_2$ and $Ar_2$ [148], and the rare gas hydrides, HeH, NeH, ArH, KrH and XeH [149].

In order to obtain information more specific to the stability and/or dissociation pathways of these neutral species, Gellene and Porter [150] introduced a new feature to their apparatus described above. This consists of a second cell located after the ion beam deflecting electrodes into which collision gas (usually $NO_2$) can be admitted in order to reionize the neutral species emanating from the neutralization chamber. A very limited resolution mass spectrum of these ions was obtained by detecting their deflection in a uniform electric field created between two parallel electrodes. To illustrate the kind of result obtained, Fig.37 shows the neutral beam profile and the mass spectra of the neutral species formed in $[CH_5]^+$($[CD_5]^+$)/Na charge transfer.

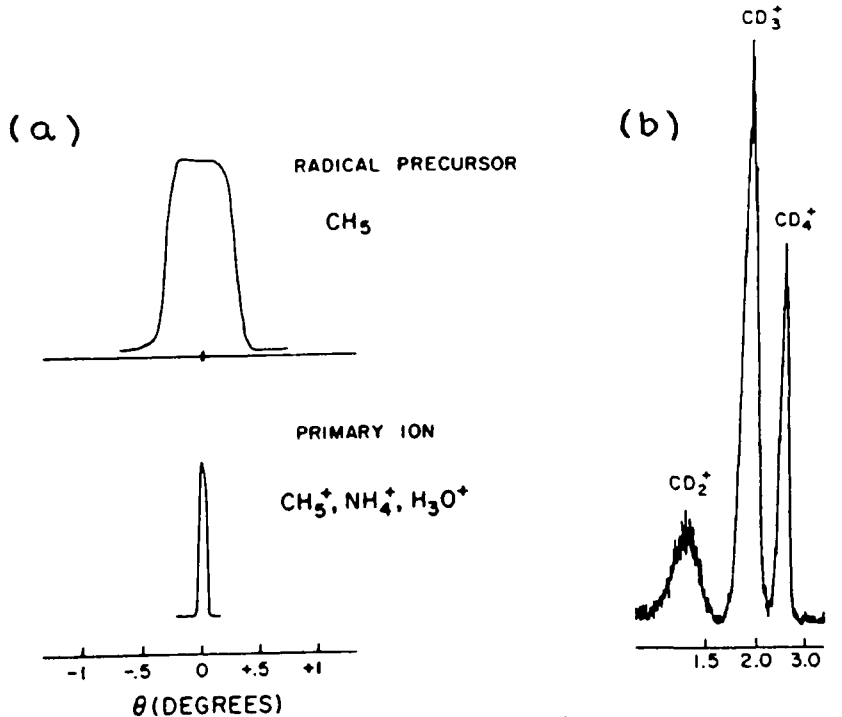


Figure 37. (a) Beam profiles for primary $[CH_5]^+$ ions and neutralized fragments from $[CH_5]^+$/Na reactions, [141]. (b) Collisional ($NO_2$) reionization spectrum of neutralized (Na) $[CD_5]^+$ of 3keV kinetic energy, [150].Using the deuterated analogue of $[CH_5]^+$ improved the fragment peak

The neutral beam profile for the $[CH_5]^+$/Na reaction contains no narrow component indicating the generation of no metastable $CH_5$. From the extrema of the angular profile Gellene and Porter [141] calculated 2.65±0.15eV as the maximum value of kinetic energy released for the dissociation of the unstable $CH_5$ into $CH_4$+H. The collisional reionization spectrum, which is a potentially more sensitive observation for surviving neutrals than the neutral beam profile measurement (because the fragments are separated from the recovery peak), also does not indicate the presence of surviving $CD_5$ species. The $[CH_5]^+/CH_5$ system will be discussed and investigated later in this thesis.

Some of the hypervalent molecules referred to above have been shown to have non-bonding ground states, but bound Rydberg states with a geometry similar to that of the bound ground state of the corresponding ion. In a recent review of these species Herzberg [151] suggested naming them "Rydberg molecules" (or radicals). Of the polyatomic Rydberg radicals so far only $H_3$ and $NH_4$ have been well characterized spectroscopically [151], although there have been unsuccessful efforts to observe optical spectra of $H_2F$, $H_3O$ and $CH_5$ [151].

A more sophisticated version of this technique has been developed in Amsterdam by de Bruijn and Los [152] to study predissociations of bound excited states of small molecules. The primary molecular ion beam applied in the experiment is focused onto the centre of a position and time sensitive double detector. A very short collision chamber (length 1mm) is located at a fixed position along the ion beam path. Neutralization takes place by charge transfer from alkali metal targets for which resonant charge transfer results in an excited (electronically and/or vibrationally) neutral molecule, which can then dissociate via different mechanisms. The two fragments will acquire opposite momenta in the c.o.m. frame of the molecule, as a consequence of which they proceed along their path with different

laboratory velocities. If two particles arrive within a narrow time interval (typically 100ns) at opposite halves of the detector, their mutual distance R and flight-time difference $\tau$ are measured. For every event, from the values of R and $\tau$, the released kinetic energy $\epsilon$ and the recoil angle $\theta$ can be calculated. The energy resolution of the apparatus is excellent, better than 1%. To illustrate the capabilities of this technique Fig.38 shows the measured released kinetic energy spectrum, in the 7-10.5eV interval, for the dissociation of $H_2$ molecules generated in $[H_2]^+$/Na charge transfer [153].

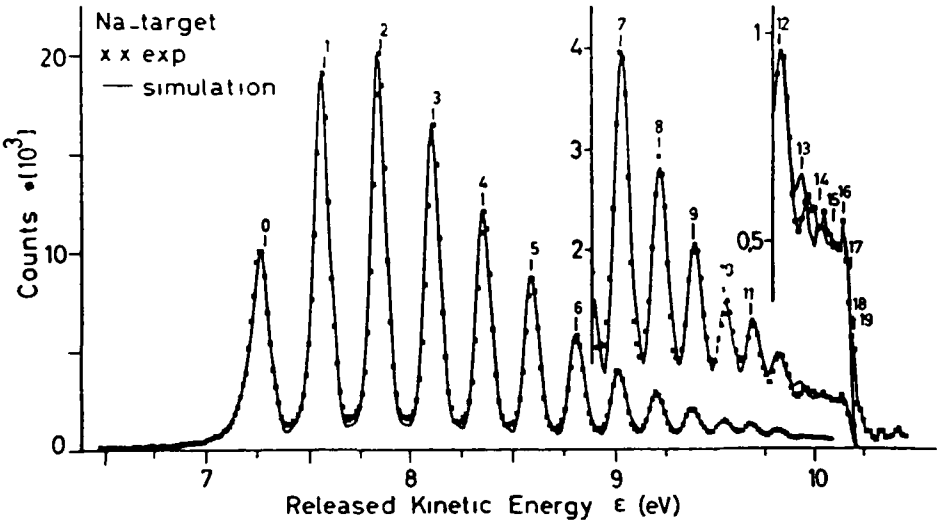


Figure 38. Kinetic energy release spectra for the fragmenting $H_2$ molecules generated in 7keV $[H_2]^+$/Na collisions. The vertical bars with numbers indicate the positions of the specific vibrational levels of the (predissociating) $c^3\pi_u$ state of $H_2$. Taken from reference [153].

The narrow peaks corresponding to discrete values of $\epsilon$ have been assigned to the predissociation of the vibrational levels of the $c^3\pi_u$ state of $H_2$. Vibrational energy levels for the v=0-19 states could be determined and found to agree with theoretical calculations within the 5meV experimental accuracy.

Spectroscopic quality measurements on the predissociation of the $^{1,3}\pi_g$ Rydberg

states of $O_2$ (converging to the $[O_2]^+(X^2\pi_g)$ ground state) [154], and the $A^2\Sigma^+$ and $B^2\pi$ excited states of HeH [155] also have been carried out by this technique.

### 1.2.6. Neutralization-Reionization Mass Spectrometry

Neutralization reionization mass spectrometry (NRMS) is a recently developed mass spectrometric technique to study neutral species in a mass spectrometer. The term and the technique (in the more recent and general sense) has been introduced by McLafferty and coworkers [156,11] who first modified a tandem mass spectrometer in order to investigate large neutral species by placing tandem collision cells in a field-free region. The general layout of a NRMS experiment is schematically illustrated in Fig.39.

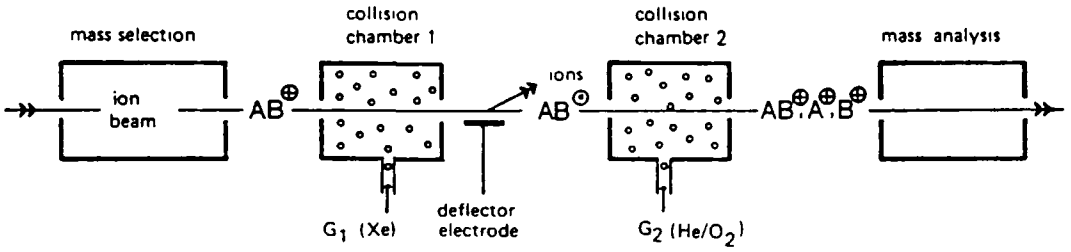


Figure 39. Schematic diagram of a NRMS experiment. Taken from reference [12].

The general processes that are involved in this method can be divided into two steps as illustrated by equations (1.37a,b) and (1.38).

(1) Neutralization

$$AB^+ + N \rightarrow AB + N^+$$

$$\rightarrow A + B \qquad (1.37a)$$

and/or

$$AB^+ + N \rightarrow A^+ + B + N \qquad (1.37b)$$

(2) Reionization

$$AB + R \rightarrow AB^{+} + R$$
$$\rightarrow A+ , B^{+}, \text{etc.} \qquad (1.38)$$

In the first step, neutral species are generated by charge transfer collision between a mass selected ion of keV translational energy and a neutral target gas introduced into the first collision cell (see Fig.37). Some of the neutral AB molecules formed by charge transfer can have sufficient internal energy to dissociate into neutral fragments. This is especially true for targets having lower ionization energy than the recombination energy of the projectile ion (such as alkali metal atoms versus cations of organic molecules), in which case a resonant charge transfer process results in highly excited neutrals. If the AB molecule is produced entirely in an unstable state only neutral fragments are generated. It is obvious that CID processes can also generate neutral (fragment) species (see equation (1.37b)).This is usually undesirable, because NRMS experiments are generally carried out to obtain information on the neutral counterpart of the projectile ion, but the neutral fragments of CID carry information about the ion. The importance of the CID can be suppressed by appropriately choosing the neutralization agent. Usually, targets of low ionization energy (such as Xe, or metal vapors) are poor CID and excellent charge transfer agents. McLafferty and coworkers [157] systematically investigated a range of gases and metal vapors as neutralization agents and found Hg to be optimal. Holmes and Terlouw and coworkers [158,159] have introduced the use of Xe as neutralization gas. It is not only an efficient electron transfer agent but is also more easily manipulated than metal vapors.

After the first collision cell there is an ion beam deflector electrode which

repels all ionic species out of the primary beam path so that only fast neutrals emanating from the cell will continue their flight through the apparatus. The second step (equation (1.38) takes place in the second collision cell located after the ion beam deflector. Here, the fast neutral species will collide with target gas molecules. These collisions can result in their ionization and/or dissociative ionization (equation (1.38)). Danis et al. [160] carried out systematic investigations on the effect of the reionization gas on the NR mass spectra. It was found that using He as collision gas maximized the contribution of the dissociative reionization to the spectra, which can be desirable if one wants to gain information about the structure of the reionized species. A group of target gases, $O_2$, NO, $Cl_2$ and $NO_2$, was found to maximize the cross section for reionization without dissociation and to minimize the cross section for dissociative reionization. This effect was attributed to the ability of these molecules to accept an electron in the reionization process, a reaction that should have a lower energy requirement and must be accompanied by less excitation energy being deposited in the reionized species than removing electrons into the continuum by a more violent collision.

To interpret a NR mass spectrum can be a difficult task, because the peaks in it can have many possible origins. The information (seemingly) simplest to obtain is that of the stability of the neutral counterpart of the primary ion. At keV kinetic energies the interaction time for a charge transfer collision is usually shorter than a characteristic vibrational period of the molecule. Therefore, neutralization is generally assumed to be vertical in the sense that the neutral species formed will retain the structure of the ion. If there is a peak in the NR mass spectrum corresponding to the mass of the primary ion (recovery peak) it indicates that this neutral species survives longer than the time of flight between the first and second

cells (usually in the order of $10^{-7}$-$10^{-6}$s). However, the structure of the neutral species surviving long enough to be reionized can be in doubt for three reasons.

(1) The neutral species originally formed by charge transfer can rearrange into a more stable form.

(2) A small fraction of the ions in the primary beam may have a different (isomeric) structure than that of the majority and the observed recovery peak can be due to this minor "impurity".

(3) Interference from the natural isotopic abundance of ions of lower mass. This latter type of interference can become especially important when the cross sections for the neutralization of ions of lower mass are large and at the same time the neutral counterpart of the ion intended to be studied is unstable or has a very small cross section for formation. Examples for this interference will be discussed later in this thesis.

The fragment peaks of the NR mass spectrum may provide information about the structure of the neutral, because reionization should also be a vertical process and so dissociative reionization will correspond to the CID of the ion having the structure of the neutral. However, the fragment peak spectrum can often be ambiguous, especially when the recovery may be due to an isomer making up only a few percent of the projectile ion beam. A good example of the difficulties discussed above is the work related to the stability of the neutral ylide, $CH_2ClH$.

$[CH_2ClH]^{+\cdot}$, the ylid isomer of $[CH_3Cl]^{+\cdot}$ was reported to be stable in the gas phase in 1982 [161]. It was generated by EI of chloroacetic acid, $ClCH_2COOH$ through the reaction

$$[ClCH_2COOH]^{+\cdot} \rightarrow [CH_2ClH]^{+\cdot} + CO_2 \qquad (1.39)$$

One of the most specific structure characteristic feature in its CA mass spectrum was found to be the abundant doubly charged ion resulting from the charge stripping reaction (CS)

$$[CH_2ClH]^{+\cdot} \rightarrow [CH_2ClH]^{2+\cdot} \qquad (1.40)$$

The conventional isomer $[CH_3Cl]^{+\cdot}$ does not have a doubly charged molecular ion in its CA mass spectrum [161]. In 1983 Danis et al [162] presented a NR mass spectrum (Zn, neutralization/He,reionization) of $[C,H_3,Cl]^{+\cdot}$ ions formed by EI of $ClCH_2COOH$. It contained a recovery peak which was taken to be indicative of the generation of a stable neutral ylide $CH_2ClH$. In 1985 Holmes, Terlouw and coworkers [158] presented a Xe/He NR mass spectra of the ylid ion. In general the Xe/He results agreed with the Zn/He NRMS experiments. In addition, Holmes et al. [158] were able to record the charge stripping part of the NR spectrum, which contained no doubly charged molecular ion, thereby questioning the structure of the recovered $[C,H_3,Cl]^{+\cdot}$ ion in the NRMS experiments. Another, more detailed study from the laboratory of McLafferty appeared in 1986 [163]. In this work Hg neutralization and He or $O_2$ reionization (at low overall transmissions of 10-30%) of the m/z52 ion from EI of $ClCH_2COOH$ was shown to produce a recovery signal. Also, very low transmission (10%) spectra contained doubly charged molecular ion peaks. Based on the m/z37 and 38 peaks Wesdemiotis et al. [163] estimated that ca. 50% of the recovered m/z52 ions had the ylid structure. This result was found to be in contradiction with state of the art ab initio molecular orbital theory calculations of Radom and his coworkers [164] which showed that the ylide, $CH_2ClH$, resides in a very shallow well with only 17kJ/mol required to dissociate it into $CH_2$+HCl or $CH_2Cl$+H. Other calculations of the same group [165] predicted that upon vertical

neutralization, $[CH_2ClH]^+$ ions would produce $CH_2ClH$ neutrals having an excess energy of 84kJ/mol, which well exceeds the energy for dissociation. This controversy initiated a thorough reinvestigation of this system in the laboratories of Holmes and Terlouw [166]. In that work it was shown in a variety of experiments, that the m/z52 ion beam from the EI of $ClCH_2COOH$ contained a small amount (estimated to be ca. 14%) of the conventional $[CH_3Cl]^{+\cdot}$ isomer. Xe/He and $Xe/O_2$ NRMS experiments were carried out with m/z52 ion beams having different conventional isomer contents. The results were in keeping with the assumption that only neutrals having the conventional structure and originating from the neutralization of the conventional isomers in the primary ion beam, survived the flight time between the first and second cells. Also, high transmission (80%) NRMS experiments, in which only single collision events were sampled, showed the presence of no doubly charged molecular ions. This latter observation points out the importance of working under single collision conditions, as it was shown that $52^{++}$ ions were generated but only in a multiple collision sequence in the reionization step [166]. The $52^{++}$ ion generated in this way was not characteristic of the structure of the surviving neutral. In order to further prove the structure of the $[C,H_3,Cl]$ neutral species the structure of the reionized m/z52 species was examined by low energy (30eV) CID experiments by the triple sector instrument at the University of Toronto. Within experimental uncertainty the CA mass spectra of the neutralized-reionized $[CH_3Cl]^{+\cdot}$ and $[C,H_3,Cl]^{+\cdot}$ ions from chloroacetic acid were identical. It was therefore concluded that the recovered m/z52 ions in the $Xe/O_2$(He) NR mass spectra had the $[CH_3Cl]^{+\cdot}$ structure. At the same time that these results appeared in the literature, Wesdemiotis et al. [167] published a report in which they presented the high energy (10keV) CA mass spectra of $Hg/O_2$ neutralized-reionized $[CH_3Cl]^{+\cdot}$ and $[C,H_3,Cl]^{+\cdot}$ from the EI of chloroacetic acid.

From these experiments it was concluded that ca. 50% of the m/z 52 recovery peak in the case of chloroacetic acid as precursor molecule had the $[CH_2ClH]^{+\cdot}$ structure. It appears that when Hg vapour is used for neutralization stable $CH_2ClH$ is formed by charge transfer neutralization of the $[CH_2ClH]^{+\cdot}$ ion, whereas in the case of Xe as neutralization agent no stable $CH_2ClH$ formation can be observed. This is very surprising, considering that the difference in the ionization energies of Hg (IE=10.4eV) and Xe (IE=12.1eV) is rather small. Another possible source of the different conclusions reached by the groups at Cornell and at Ottawa can be the difference in the apparatuses used. This possibility can be tested by carrying out the measurements with one of the apparatuses using both Hg and Xe as neutralization gas.

**In summary. It was shown in section 1.2.4 that there has been considerable progress in the understanding of charge exchange collisions between simple ions (mono- and diatomic) of keV translational energy and neutral targets. There were two major factors found to influence the relative importance of a particular charge exchange channel. These are the energy defect associated with the particular channel and the vibrational overlaps between the initial and final states. In sections 1.2.5 and 1.2.6 it was seen that charge exchange neutralization of fast ion beams provides an effective method for observing neutral species that are difficult to study by more conventional methods because of their inherent instability. However, it was also pointed out that there are experimental difficulties associated with this novel method, which require further understanding and continuous attention by the experimentalists in this field.**

# 2.1 Field Ionization of High Velocity Neutral Species

## 2.1.1 Introduction

The application of an electric field to an atom or molecule distorts the atomic or molecular potential. It creates a saddle point at which an electron of sufficiently high potential can escape; electrons having lower potential energy than the height of the saddle point can also escape by tunneling through the barrier of finite width.

The ionization of ground-state atoms and molecules requires very high electric fields of the order of $10^8$ $Vcm^{-1}$, which can be achieved only by specially constructed electrodes. This places experimental limitations on the use of field ionization. However, field ionization of ground state species has long been used as a means of ionization in the ion source of mass spectrometers [168,169], and a neutral beam detector has been built, based on upon the phenomenon of field ionization [170].

The ionization of high Rydberg (HR) states of atoms and molecules requires much weaker electric fields than ground state species, (of the order of $10^3 Vcm^{-1}$). These can be achieved relatively easily, placing fewer limitations on the design of such field ionization devices. Field ionization has therefore been widely used for the detection of HR atoms [171], HR molecules [172-175], and HR fragments formed in the dissociative excitation of molecules [175]. The method can also be used to identify Rydberg states [176] and to determine the populations [171,177] of different principal quantum number states.

In this chapter are described the modifications made to a double focusing mass spectrometer of reversed geometry (VG Analytical ZAB-2F), to permit the field ionization of fast, HR species. The test experiments involved neutral Ar atoms generated by collisional electron transfer from Xe as target gas.

### 2.1.2 Experimental

The experiments were performed with a VG Analytical ZAB-2F double focusing mass spectrometer modified as described below. The second field-free region contains two collision cells with a deflector electrode between them. The layout of this and other accessories are shown in Fig.3 in the introduction of this thesis (chapter 1.1). To generate ions by field ionization, two movable nickel meshes were installed in the position shown in Fig.3. The nickel meshes were obtained from Buckbee-Mears Operation (245, East 6th St, St Paul, Minnesota, USA). They had 8 wires per mm in a rectangular grid and a transmission of 78%. Fig.40 shows the position of the meshes with respect to the ion lenses and earthed plates attached to the second collision cell. The mesh was spot-welded directly onto stainless-steel rings attached to support rods. The assembly was held in alignment by means of bolted ceramic clamps (see insert, Fig.40); the latter were mounted on a bellows drive so that the meshes could be in or out of the ion beam path, as desired. Connecting wires to the mesh support were also clamped to the mesh support assembly, to avoid any torsional stress during movement of the bellows drive which might change the alignment of the system. The meshes were parallel to each other, at right angles to the ion beam path and 0.7mm apart. Electrical connections for the meshes were carried through insulated seals on the flange, which normally supports the conversion dynodes for the electron multiplier installed as shown in the second field- free region. The second collision cell was the standard VG-Analytical assembly; the bellows, which carries the field ionization meshes normally carries a Z-axial variable restrictor plate.

It was found during preliminary experiments that the bare ion beam deflector electrode mounted between the collision cells [178] was unsatisfactory because field

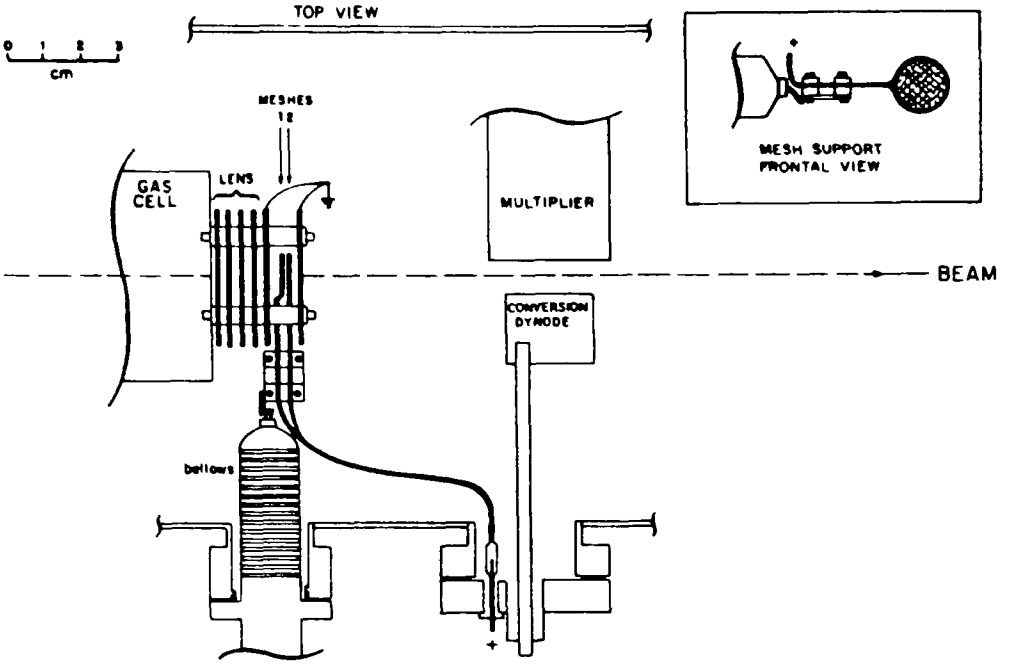


Figure 40. Partial scale drawing of the field ionization assembly and the second collision cell. The cell, multiplier and dynode are not to scale.

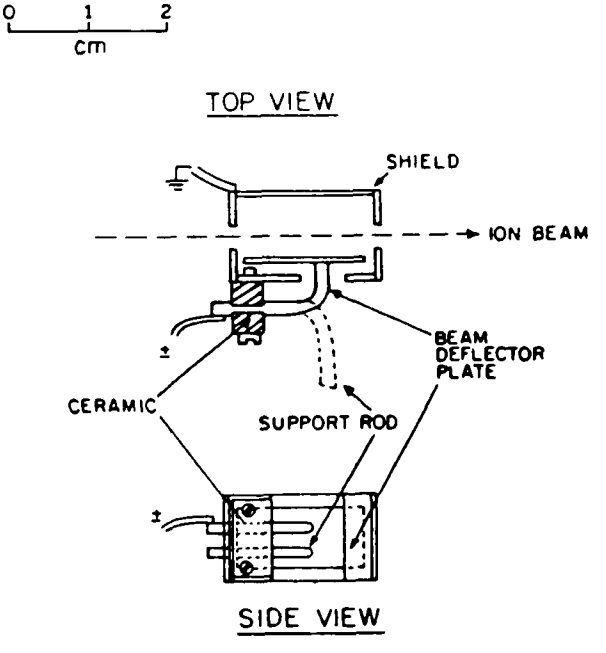


Figure 41. Ion beam deflector electrode, mounted in an earthed metal box.

penetration caused irreproducible translational energy shifts in neutralization-reionization (NR) mass spectra [158,159]. Accordingly, a new shielded electrode was built, as shown in Fig.41; this arrangement was entirely satisfactory. Field ionization experiments were performed as described below. The resolving power of the mass spectrometer was normally adjusted such that the half-height width of a beam of transmitted ions was 2eV or less at an accelerating voltage of 8000V. Gases were obtained from Air Products and were all of research grade. Mesh and electrode voltages were taken from high-precision power supplies, Fluke 412B.

### 2.1.3 Results and Discussion

To test the operation of the field ionization assembly the following experiments were performed. $Ar^+$ ions, having a translational energy corresponding to 8kV, were mass selected by the magnet. Xe was admitted into the first collision cell at a measured pressure of $1x10^{-5}$Torr. This pressure was read on the ion gauge mounted above the diffusion pump, situated just before the first collision cell. This Xe pressure was sufficient to reduce an ion beam by ca. 15%. Equation 2.1 describes the ion-atom charge transfer process:

$$Ar_i^+ + Xe_l \rightarrow Ar_k + Xe_m^+ + \Delta E_{kl} \qquad (2.1)$$

where i, k, l and m are different quantum states of the reactants and products and $\Delta E_{kl}$ is the kinetic energy change of the projectile (Ar) and is equal to the internal energy difference between products and reactants. $Ar^+$ ions emerging from an EI ion source are known to contain ions in metastable, excited electronic states (MEES) [179]. Their lifetimes are typically $10^{-4}$s, so they survive acceleration and mass

analysis, arriving unchanged at the detector. With 50eV ionizing electron energy, these excited atoms make up ca. 3.5% of the ion beam [180]. It is known that electron transfer between fast MEES $Ar^+$ ions and a variety of target atoms and molecules gives neutral Ar in HR states; the cross section for such processes have been proposed to be large [181-185]. The electron transfer processes of greatest importance between $Ar^+$ and Xe can be represented by the equations

$$Ar^+_g + Xe_g \rightarrow Ar_g + Xe^+_g + \Delta E_{k2} \qquad (2.2)$$

$$Ar^+(MEES) + Xe_g \rightarrow Ar(HR) + Xe^+_g + \Delta E_{k3} \qquad (2.3)$$

where g denotes ground state. It is the HR Ar atoms that can readily be field ionized.

In the first series of experiments, 8keV $Ar^+$ ions were mass selected into the second field-free region of the mass spectrometer. Xe was admitted to the first collision cell and a potential of +600V was applied to the ion beam deflector electrode. The surviving $Ar^+$ ions were thus deflected away and only a weak signal remained for species having ca. the same translational energy as that of the primary ion beam ($E_o$); this arose from collisional reionization of fast, neutral Ar by the small amount of Xe that had diffused into the region beyond the ion beam deflector electrode. When the meshes, both grounded, were made to intersect the neutral beam, the weak residual $Ar^+$ signal was reduced by ca. 40%, in keeping with the mesh transmission. The ion kinetic energy spectrum (obtained by scanning the electric sector) is shown in Fig.42(a). Two signals were present. A narrow peak, A in Fig.42(a), displaced to the high energy side of the main ion beam position ($E_o$) by 5±0.3eV. This small kinetic energy gain (see below for translational energy calibration) agrees well with the value reported by Aparina et al. [185] for the

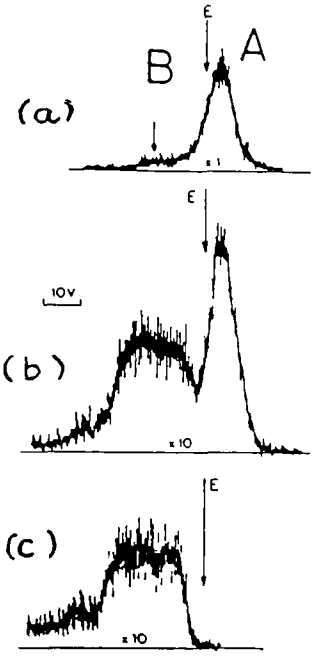


Figure 42. Ionization of Ar atoms by diffused Xe. Ion source accelerating voltage, $E_s$=7999V. Ionizing electron energy (a) c.50eV (b) c.30eV (c) c.15eV

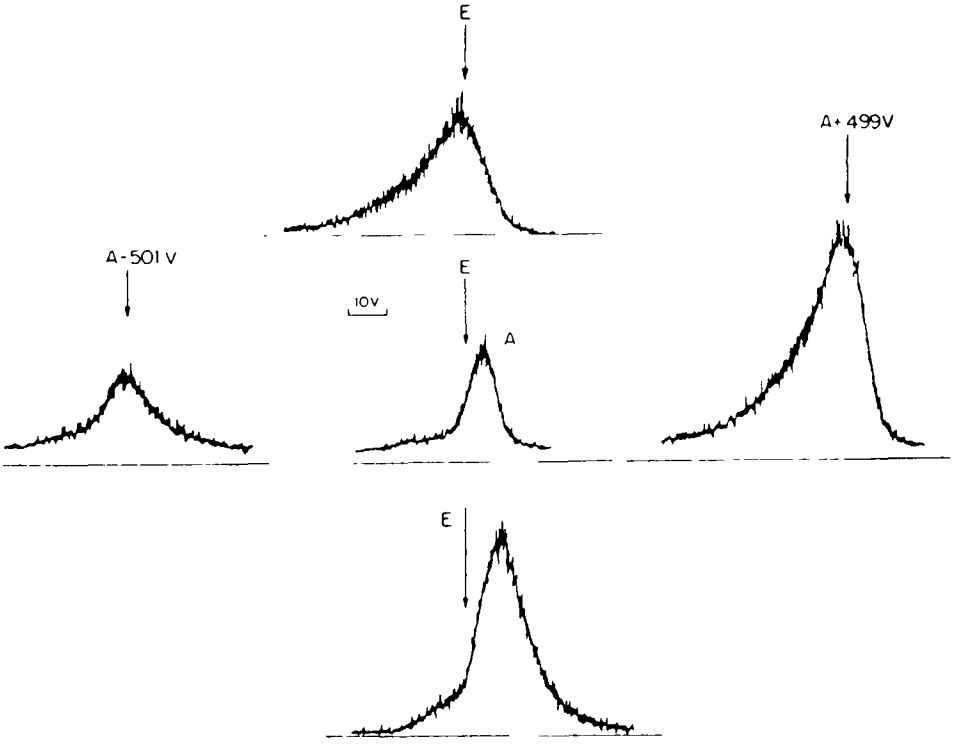


Figure 43. Field ionization of HR Rydberg Ar atoms. (a) Residual collisional signal, corresponding to 42(a); see text for the discussion of (b)-(e).

generation of HR Ar atoms by reaction (2.3), primary beam translational energy being 100eV. A weak, broad peak (B) was also apparent. When the ionizing electron energy was reduced from (nominal) 50eV, peak A decreased in intensity, see Fig.42(b) and (c), and disappeared at ca. 15eV, an energy well below the appearance energy for MEES $Ar^+$ ions, 32eV [179]. The weak, broad peak is proposed to arise from the collisional reionization of ground-state Ar atoms.

Next, the effects of applying a potential difference between meshes M1 and M2 (see Figs.2 and 40) were examined. Voltages were applied M1 and M2 in the following sequences.

(i) M1 positive potential, +QV; M2 earthed. In the resulting ion kinetic energy spectra, a well-defined peak appeared, displaced by +QV from the position of peak A, the residual collisional reionization peak in Fig.42(a) described above. The new peak intensity increased with increase of +Q; Fig.43(b) shows the peak for Q=+500V. The maximum was at A+499V and the peak tailed towards lower energies. The peak arises from field ionization of HR atoms at or close to M1, the tailing being produced by HR Ar atoms that have ionized a short distance down the potential gradient between M1 and M2. This "delayed" field ionization is probably due to ionization by tunneling through the potential barrier created by the external electric field. Note that the collision induced reionization peak A was ca. 18% of the field ionization peak obtained in this mode at Q=+1200V.

(ii) M1 negative potential, -QV; M2 earthed. The field is now of opposite sign to that in (i). The peak for Q=-500V is shown as in Fig.5(c). It was centered at A-501V and tailed towards higher translational energies; some weak, poorly defined structure appeared at lower energies (see below). The origin of the main peak is as for (i) and the tailing towards higher energies again arises from atoms that are field ionized a short distance down the potential gradient such ions receiving less

deceleration.

(iii) M1 earthed; M2 positive potential, +QV and (iv) M1 earthed ; M2 negative potential, -V. In these experiments, there was no electric field between S1 (the earthed plate before M1, see Fig.40)) and M1, the high field gradient still lay between M1 and M2, and there was now a low field gradient between M2 and S2 (the earthed plate after M2).

In these modes of operation, the peak corresponding to residual collisional reionization increased in intensity and in width as Q is increased. Only weak signals appeared at A±Q, about one-third the intensity of the residual (collision-induced) reionization peak (at Q=0); they did not change greatly in intensity with the voltage on M2 and so they probably arose from some surface-induced ionization on M2 [186]. Some observations are shown in Fig.43; 43(d) and 43(e) are for Q=+500V and -500V, respectively. Each peak tailed, the former towards high energies, the latter towards lower energies.The peaks arose from the field-induced ionization of HR Ar atoms as they entered the high field gradient region between M1 and M2; they then suffered deceleration (for Q-+500V0 followed by acceleration (between M2 and S2), and vice versa for Q=-500V.

*In summary, the experiments described above all yielded $Ar^+$ from field-ionized HR Ar atoms, ionization having taken place at the first mesh, M1. Experiments (iii) and (iv) showed that there must be very little contribution from surface-induced ionization. In all cases, the signal intensity increased with the magnitude of Q.* Fig.44 shows a plot of field-generated $Ar^+$ as a function of +Q. *M1 charged, M2 earthed, the mode that gave the most intense and best-defined peak.* Using the relationship [187] between the effective quantum numbers, n*, of the states that are ionized and the electric field gradient, F($Vmm^{-1}$),

$$n^* > [(5x10^7)/F]^{1/4} \qquad (2.4)$$

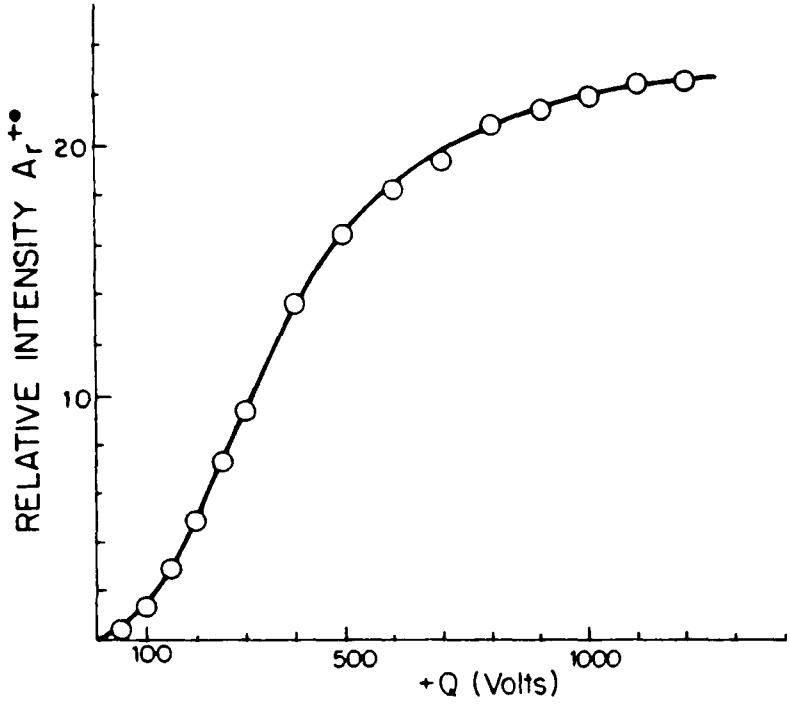


Figure 44. Intensity of field ionization of HR Ar atoms as a function of field gradient. At Q=+1000V the field-induced $Ar^+$ signal is c. $10^{-5}$ of the primary $Ar^+$ ion beam.

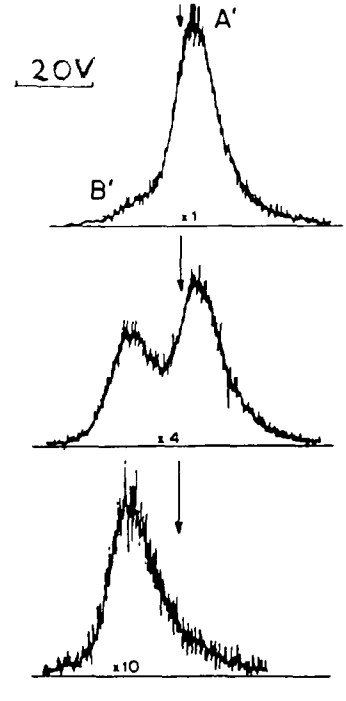


Figure 45. Field ionization of HR Ar atoms produced from ground state $Ar^+$.

it can be calculated that between 60 and 1200V on M1, states having 27>n*>13 are ionized. Between the ion beam deflector electrode (normally at +600V) and its surrounding earthed plates (see Fig.41) there will also be a field gradient, although of smaller magnitude than that between the FI meshes. Charging the electrode at 600V gives rise to ca. $75Vmm^{-1}$ field gradient between the deflector and the parallel wall of the surrounding metal box. In principle therefore, this electrode could field-ionize HR states of very high principal quantum number and deflect them away from the beam path. This possibility was investigated as follows. With 1200V on M1 and M2 earthed, the FI $Ar^+$ peak is observed at $E_o$+1200V. The peak increased by no more than ca. 1% when the beam deflector electrode voltage was gradually reduced from 600V to zero, showing that few Ar atoms having n*>29 (obtained from eq.(2.4)) are present. However, when the beam deflector voltage was raised from 600 to 1500V, corresponding to a ca. $190Vmm^{-1}$ field gradient across the beam path, the FI signal decreased by 25%. It is concluded therefore, that some 25% of the HR Ar atoms have 29>n*>22.

One final observation should be described. In Fig.43(c) and (d) there appears to be some structure at the lower energy side of the peak (in these two cases the peaks tail towards higher energies due to the ionization between M1 and M2). This could arise from HR atoms having a kinetic energy different from those formed by reaction (2.3). To investigate this possibility the following experiment was carried out. M1 was raised to +100V while M2 was charged at +QV. This produced a field ionization peak removed by 100V from the residual collision gas signal A; the intensity of the FI peak increased with increase in Q. Fig.45 shows the result, at Q=+700V, of reducing the ionizing electron energy from nominal 50eV in Fig.45(a) to 30eV in Fig.45(b) and to 15eV in Fig.45(c). Two peaks were clearly observed, the higher energy peak (A') being removed at low ionizing electron energies; this must

have resulted from the removal of MEES $Ar^+$ ions from the primary ion beam. The intensity of the lower energy peak (B') did not change relative to the primary beam intensity, and it is proposed that it resulted from reaction (2.5)

$$Ar^+ + Xe \rightarrow Ar(HR) + Xe^+ - 12.1eV \qquad (2.5)$$

in which HR atoms are produced from ground state ions. The relative cross sections for reactions (2.3) and (2.5) can be estimated as follows. At 50eV ionizing electron energy, the ion beam contains ca. 3.5% MEES $Ar^+$ [180] and the ratios of the two peaks in Fig.45(a) was approximately 10:1; thus the cross section for reaction (2.3) must be at least 280 times greater than that for reaction (2.5). The separation between the two peaks was measured to be 19±1eV. In Table 1 are given the energies, above the ground state of $Ar^+$, of the MEES of $Ar^+$; two MEES lie 19.1eV above the ground state and so presumably these are responsible for peak A' in Fig.45(b).

**Table 1. Metastable electronic excited states of $Ar^+$**

| State | Excitation energy above ionic ground state (eV) |
|---|---|
| $^4D_{7/2}$ | 16.4 |
| $^4F_{9/2}$ | 17.6 |
| $^4F_{7/2}$ | 17.7 |
| $^2F_{7/2}$ | 18.5 |
| $^2G_{9/2}$ | 19.1 |
| $^2G_{7/2}$ | 19.1 |

**In summary, it has been shown that charged, fine metal meshes can be used in a conventional double-focusing mass spectrometer to field-ionize fast, high-Rydberg species, yielding well defined ion beams.**

## 2.2 Measurement of the Translational Energy Loss for Neutralization-Reionization Mass Spectra

The neutralization of beams of fast ions by electron transfer from Xe target gas and their reionization by collision with a second gas (typically He or $O_2$) has been described elsewhere [158,159] and is a variation of the method described by McLafferty et al. [162], who used metal vapors as the electron transfer targets. In experiments reported from this laboratory [158,159], the reaction of an ion with Xe can be written:

$$M^{+\cdot} + Xe \rightarrow M + Xe^{+} + \Delta E_n \qquad (2.6)$$

where $\Delta E_n$ is the kinetic energy loss of the projectile ion and is equal to the internal energy difference between the reactants and products, neglecting any energy loss by radiation. After this process, which takes place in the first cell, all ions are deflected away by the electric field of the charged deflector electrode and the species M enter the second collision cell, wherein they can be reionized by collision:

$$M + T \rightarrow M^{+\cdot} + T + e^{-} \quad E_e + \Delta E_r \qquad (2.7)$$

T is the target gas, $\Delta E_r$ is the internal energy change in the reaction and $E_e$ is the kinetic energy of the electron lost by M. The net kinetic energy change for the

neutralization-reionization (NR) process is $\Delta E_{nr}$ and is given by the equation:

$$\Delta E_{nr} = E(M^{+\cdot})_{nr} \quad E(M^{+\cdot})_o = \Delta E_n + \Delta E_r - E_e \qquad (2.8)$$

where $E(M^{+\cdot})_o$ is the kinetic energy of $M^{+\cdot}$ before entering the first collision cell and $E(M^{+\cdot})_{nr}$ is that of the reionized $M^{+\cdot}$. Experiments to measure $\Delta E_{nr}$ have been described [159], in which the displacement of the reionized beam from the primary main ion beam voltage was recorded and equated to $\Delta E_{nr}$. It was reported [159] that $\Delta E_{nr}$ measured this way was equal or close to the ionization energy of the charge exchange target gas, Xe. However, further experiments showed that although $\Delta E_{nr}$ was constant under a single set of experimental conditions, its value changed significantly (e.g. ±3eV) from day to day and even upon merely retuning the mass spectrometer for optimum energy resolution. It was therefore deemed necessary to develop a calibration technique, using a beam translational energy displacement of known, independently verifiable magnitude.

A potential difficulty with NR experiments such as those described above, is that the magnitude of $E_e$ is indeterminate. For example, Barat et al. [188] found that when fast (keV) ground-state He atoms are ionized by collision with thermal He atoms as targets, the most probable value for $E_e$ was several eV and its magnitude depended upon the kinetic energy of the projectile atoms and the angular displacement of the products. This problem of the unknown contribution of $E_e$ in equations (2.7) and (2.8) can be avoided by producing HR species in the neutralization step and reionizing them by collision (or by field ionization), where $E_e$ is now <0.1eV. A suitable system is the interaction between fast $Kr^+$ ions and Ar as target gas. Aparina et al. [183,184] showed that metastable electronic excited states of ionized Kr, similar to those observed for $Ar^+$ [179,180], capture electrons from Xe (and a variety of molecular targets) to give HR Kr. The cross-section for

this reaction was proposed to be very large at $Kr^+$ energies from 10 to 100 eV. There are four important metastable excited electronic states of $Kr^+$, $^4D_{7/2}$, $^4F_{9/2}$, $^4F_{7/2}$ and $^2F_{7/2}$, lying 14.9, 15.6 15.9 and 16.3 eV, respectively, above the ground state of $Kr^+$; they make up ca. 3% of a $Kr^+$ ion beam generated by 40eV EI [180]. These lie close to the ionization energy of Ar, 15.7eV, and so the electron transfer processes

$$Kr^+(MEES) + Ar \rightarrow Kr(HR) + Ar^+(G) + \Delta E \qquad (2.9)$$

can take place with high probability, giving HR Kr atoms that need very little excitation to ionize them. Figs.46(a) and (b) shows the (Ar) neutralization (He) reionization mass spectra of $Kr^+$ ions for ionizing electron energies of (nominal) 40 and 15eV. Each spectrum contains an asymmetric extended peak, designated as B, and Fig.46(a) displays a sharp peak, A. The former has its maximum ca. 43eV below peak A and a shoulder ca. 21eV below peak A. This structure in B is essentially unaffected by the change in ionizing electron energy, but the sharp peak A is only present at the higher electron energy, when MEES $Kr^+$ ions are present. This peak is near the original main $Kr^+$ beam energy. Peak B is typical of interactions between ground-state atoms and He target gas [188]. It is proposed that peak A arises from MEES $Kr^+$ ions, which, on electron transfer from Ar, become HR Kr atoms. The sharp peak has no observable structure and must be produced by reionization of long-lived HR states long-lived enough to traverse the distance between the collision cells, flight time ca. 1μs. It is proposed that the sharp peak A results from the reactions

$$Kr^+(MEES) + Ar \rightarrow Kr(HR) + Ar^+ \qquad (2.10a)$$

$$Kr(HR) + He \rightarrow Kr^+ + He + e \qquad (2.10b)$$

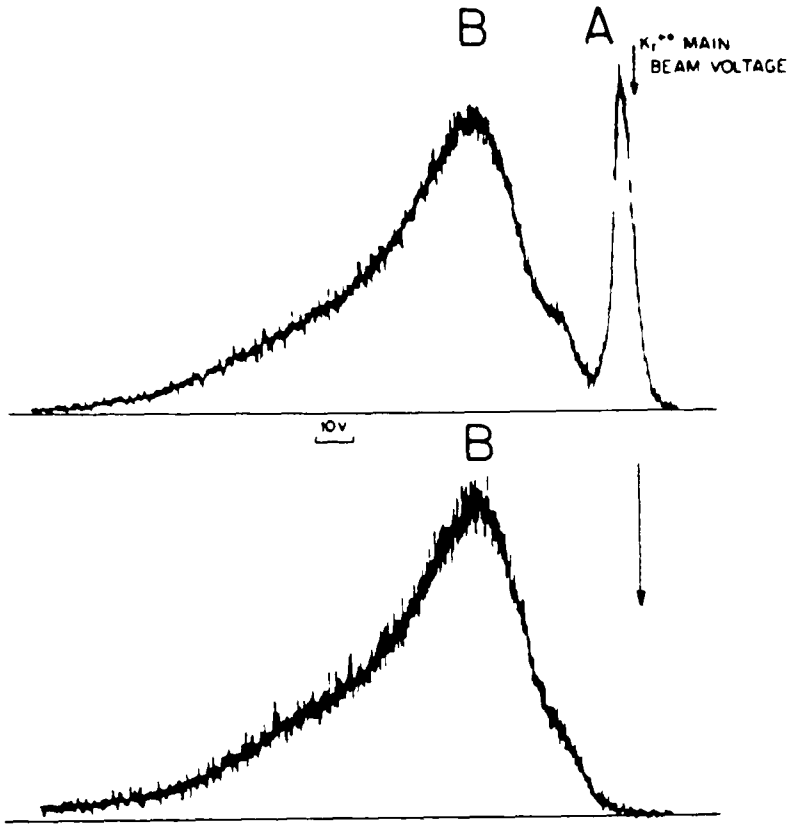


Figure 46. Collision induced reionization signals (He target) for fast Kr atoms generated from $Kr^+$ by charge exchange with Ar atoms. Nominal ionizing electron energy (a) 40eV (b) 15eV.

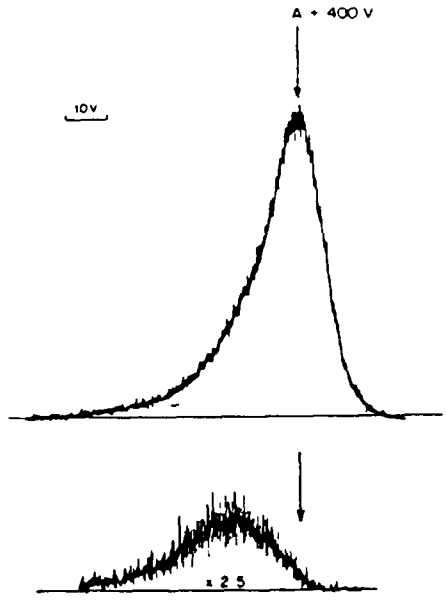


Figure 47. Field ionization peaks corresponding to Fig.47(a) and (b). See text for discussion.

That the above proposal was correct, was established as follows. Fig.47(a) shows the kinetic energy spectrum corresponding to Fig.46(a) but without He in the second cell and with mesh M1 charged at +400V and M2 earthed. The peak is ca. 2.5 times as intense as A in Fig.46(a); its summit is at A+400V and must result from the field ionization of HR Kr atoms having the same kinetic energy as the species producing peak A in Fig.46(a). Fig.47(b) shows the result of lowering the ionizing electron energy to ca. 15eV, below the energy required to produce MEES $Kr^+$. The weak residual signal has its summit at A+384V. Therefore, it is concluded that the major part of the peak in Fig.47(a) arises from Kr(HR) produced in reaction (2.10a). The peak displacement in Fig.47(b) (16V below the FI peak summit in Fig.47(a)) can be represented by the equation

$$Kr^+(G) + Ar \rightarrow Ar^+(G) + Kr(HR) \quad 15.7eV \qquad (2.11)$$

From the above observations it is concluded that peak A in Fig.46(a) arises from reactions (2.10a and 2.10b). The range of excitation energies among the four MEES $Kr^+$ produced by 40eV EI is 1.4eV (see above). For two of the four MEES of $Kr^+$, the charge transfer reaction (2.10a) is very near to resonant (the energy defect for the $^4F_{9/2}$ state is 0.1eV and that for the $^4F_{7/2}$ state is -0.2eV); as the most probable processes, they will determine the position of the summit of the reionization peak. We propose that the position of the summit corresponds to a kinetic energy change of 0±0.3eV. Any further displacement represents the correction term necessary to obtain the true value of $\Delta E_{nr}$ at the particular instrument setting. For example, in Fig.46(a), the observed displacement from the main $Kr^+$ ion beam energy was 4.6eV. Typically, from a number of observations, the correction term had a range of ±5eV. Note that the correction remained constant

provided that no changes were made to the ion source and beam focusing controls.

The above $Kr^+$/Ar/He experiments are not very convenient for everyday use and so a secondary standard was chosen. This was the neutralization-reionization of $[H_2O]^+$ molecular ion, an experiment easy to perform routinely during a series of NRMS experiments. Between each $H_2O$ measurement, a $Kr^+$ NR mass spectrum was performed and the relative energies of the summit of peak A from the $Kr^+$/Ar/He experiments and that for m/z 18 from $[H_2O]^+$/Xe/He measurements were carefully compared. From several series of experiments over a period of weeks, the peak displacement $\Delta E(H_2O)_{nr}$ for the $[H_2O]^+$ NR mass spectrum relative to the $Kr^+$ ion peak was measured to be -15.8eV with a reproducibility of ±0.3eV. From equations (2.7) and (2.8) it can be seen that if the kinetic energy of the electron ($E_e$) ejected in the reionization step was zero, then $\Delta E_{nr}$ should be equal to the ionization energy of the neutralization target, i.e. for the $[H_2O]^+$/Xe/He system $\Delta E_{nr}$ should be -12.1eV. *The large difference between this value and the actually observed one (3.7eV) shows that the electron ejected in the reionization step had a substantial kinetic energy, indicating that reionization by He collision gas requires violent collisions characterized by small values of impact parameter. The above experiments were repeated for the Xe/$O_2$ neutralization-reionization of $[H_2O]^+$. In this case a $\Delta E(H_2O)_{nr}$ value of -13.6±0.3eV was obtained, which is quite close to the ionization energy of Xe, indicating that reionization by $O_2$ involves collisions of relatively large impact parameter. These observations are in keeping with the conclusions reached before about the nature of He and $O_2$ as reionization gases [9].*

# 2.3 Kinetic Energy Spectroscopy of High-Rydberg Fragments from keV Collisions of $[H_2]^+$ and $[D_2]^+$ with Rare-Gas Atoms and Diatomic Molecules

## 2.3.1 Introduction

Since the first report by Kupriyanov et al. in 1965 [189], many measurements have been made on the dissociation of molecules by electron impact (EI) to give high-Rydberg (HR) fragments. Most of these experiments used translational spectroscopy and appearance energy measurements as diagnostic methods. A comprehensive review of this research has been published [175]. An important general conclusion from these experiments was that dissociation processes which lead to HR fragments, in EI excitation, can generally be explained by the so-called ion-core model , which has been extensively discussed in the literature [190-192]. In brief, the main principle of this model is that the HR fragments in the EI dissociative ionization of molecules originate from the dissociation of HR molecular states, which can be described as a singly charged molecular ion core surrounded by a distant electron in a HR orbit. The high-lying Rydberg electron can be treated as a spectator orbiting the molecule at distances so large (hundreds of ångströms) that it leaves the core ion relatively unperturbed. It is therefore the repulsive states of the molecular core ion which determine the dissociation processes. This model has been extended to the HR states of singly charged molecular ions, which are described as a Rydberg electron bound to a doubly charged molecular core ion.

In this section we will describe the measurements of field-induced ion kinetic-

energy spectra HR fragments originating from collisions between molecular ions having keV kinetic energy and thermal target gas atoms (or molecules). (The first such experiments have been reported from this laboratory [193].) Analysis of the kinetic-energy spectra have been carried out by the application the ion-core model described above. There were two major single-collision processes for the production of HR fragments, one of which has unique importance when He is the target gas.

### 2.3.2 Experimental

All measurements were made with a VG Analytical ZAB-2F double focusing mass spectrometer modified as described in section 2.1.2 of this thesis. Measurements were performed as follows. $[H_2]^+$ and $[D_2]^+$ ions were generated by EI by admitting the molecular gas to the ion source. The ionizing electron energy was 70eV. The resolving power of the mass spectrometer was adjusted such that the half height width of a beam of transmitted ions was 10V or less. The ions were accelerated from the source to a particular value of kinetic energy and were mass selected by the magnet into the second field-free region. Collision gas was admitted into the first collision cell to a pressure sufficient to achieve ≈15% beam attenuation. The deflector electrode was usually charged at -700V to deflect ionic species. Mesh M1 was at +1000V and mesh M2 was grounded. The electric field between the two meshes was ca. 1.5kV/mm. Using equation 2.4 we estimate that in this mode of operation HR states having principal quantum numbers $14<n^*<28$ are field ionized. Field ionization takes place at mesh M1 as the fast HR neutrals enter the high electric field gradient and therefore the resulting ions will be accelerated by 1000V. A kinetic energy spectrum of the fast ionic species was obtained by scanning the electric sector in the usual way. For homonuclear diatomic projectile ions, the

signal corresponding to the field ionized HR atomic fragments (generated via collisions in the first cell) will be centered near $(1/2E_s+1000)$eV in the kinetic energy spectrum, where $E_o$ is the translational energy of the main beam. Such signals are therefore removed from the translational-energy regions where the collisional reionization signals (resulting from collision gas which has diffused to regions beyond the deflector) appear. A test was also carried out to confirm that the "field-induced" signals really corresponded to field ionization of HR species. This consisted of raising the voltage on the deflector electrode. As described above (section 2.1.3) there is an electric field between the deflector electrode and the parallel wall of its surrounding cage and this can ionize certain HR species and the resulting ions will be deflected away. Therefore raising the voltage on the deflector is expected to decrease the intensity of the observed "field-induced" signal. Indeed, increasing the voltage from -700V to -2500V decreased the intensity of the signals appearing around $(1/2E_o+1000)$eV by ca. 40%, indicating that such fraction of the atomic HR fragments have effective principal quantum numbers $20<n^*<28$. In general, signals arising from HR fragments are $\approx 10^{-3}$ of the intensity of the ionic products of collision-induced dissociations obtained using the same collision gas pressures.

### 2.3.3 Results and Discussions

The field-induced ion kinetic-energy spectra of the H(HR) fragments from $[H_2]^+$/He collisions are shown in Figs.48(a) for 10keV impact energy and in Fig.48(b) for 5keV impact energy. The intensity of the signals was found to be proportional to the collision gas pressure over the range of from 3% to 30% beam attenuation, indicating that features in the spectra arise from single collision processes. All the spectra contain two major components. One is a central narrow peak, designated as peak A.

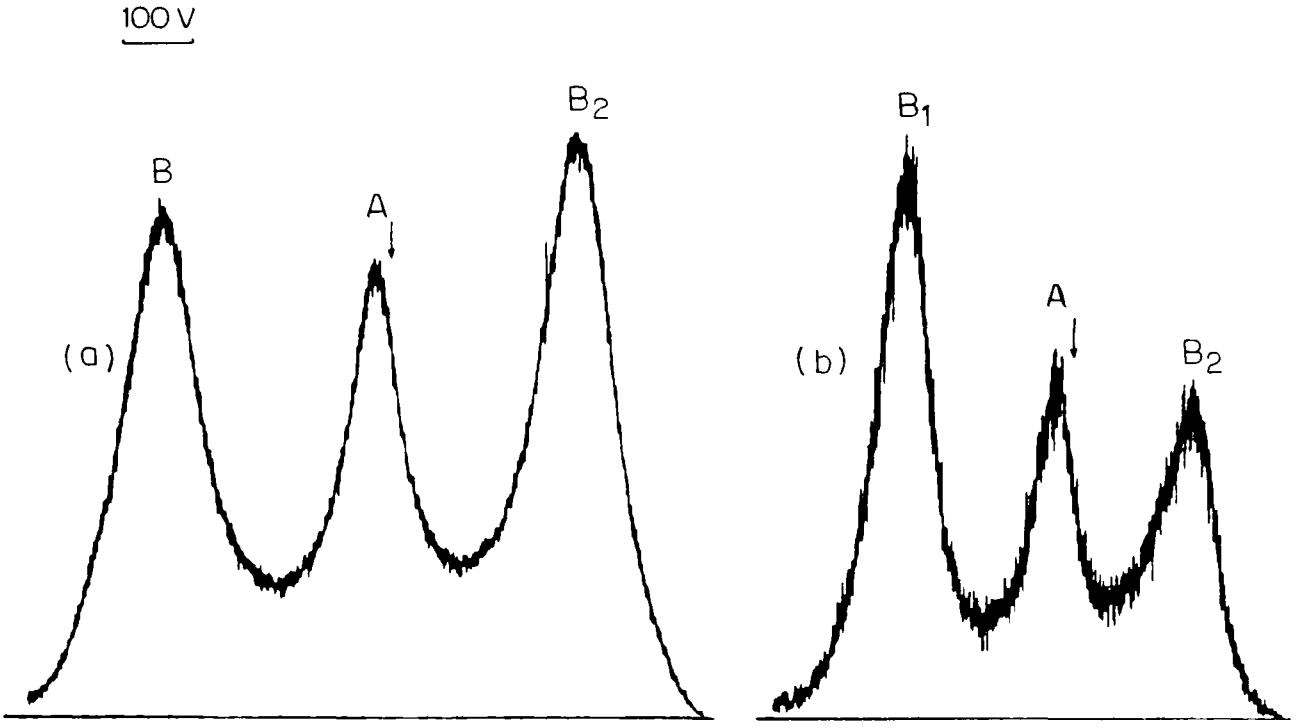


Figure 48. Field-induced ion kinetic-energy spectra of H(HR) fragments $[H_2]^+$/He collisions The arrow shows the energy ((1/2)$E_o$+1000)eV. (a) $E_o$=9987V (b) $E_o$=5009V.

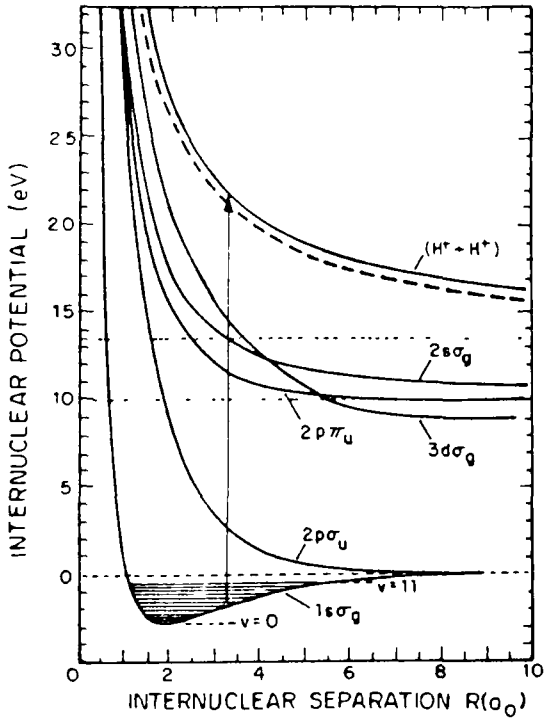


Figure 49. Potential curves for $[H_2]^+$.; the broken curve indicates the $[H_2]^+$(HR) region.

The summit of peak A is located at a kinetic energy value that is lower by 22±5eV than $(1/2E_o+1000)$eV, (the value expected if there was no kinetic energy loss involved in the collision event generating the H(HR) fragment), indicating that the process responsible for the observations has an endothermicity of that magnitude. The width of this peak indicates that the dissociation process associated with it involves a small amount of kinetic energy release (KER), less than 100meV. Based on the observations we propose the following single collision process for the origin of peak A. Upon collision the $[H_2]^+$ projectile captures an electron from a He target atom into a HR orbit and the $[H_2]^+$ core is simultaneously excited vibrationally either by momentum transfer or by the Russek mechanism (see section 1.2.1.) above its dissociation limit. This event must take place in ca. $10^{-16}$s, which is the characteristic collision time at these impact energies. The $[H_2]^+$ core will dissociate in the time frame of $10^{-14}$s and as the $H^+$ and H fragments separate the HR electron will join one $H^+$ giving an H(HR) fragment. The overall process can be described by the equation

$$[H_2]^+ + T \rightarrow T^+ + H_2(HR)^* \rightarrow H(HR) + H(1s) \qquad (2.12)$$

where $H_2(HR)^*$ is high-Rydberg $H_2$, vibrationally excited and T is the target species (in this case He). This mechanism is in keeping with the observation that collision-induced vibrational dissociation of $[H_2]^+$ gives a narrow KER distribution, and also reaction (2.12) would be endothermic by ca. 26eV (see Fig.49) which is in keeping with the observed kinetic-energy displacement for peak A.

The other major feature in the spectra in Fig.48 is a pair of peaks, $B_1/B_2$ which symmetrically flank peak A. This kind of feature, so-called "dished peak", appear in the kinetic energy spectra obtained by electrostatic sector energy

analyzers when fragmentations associated with large KER values (>2eV) take place as described in section 1.2.2. We calculate the most probable value of the KER by substituting into equation (1.24) the distance across the maxima of the dished peaks. (Although this analysis of the dished peaks may appear to be oversimplified on the basis of some recent theoretical investigations of this problem [194-196], it will however be shown below, that the most probable values for KER obtained in this way are in good agreement with the results of accurate, independent measurements.) Using equation (1.24) we obtained 8.2±0.3eV as the most probable value of KER associated with peak $B_1/B_2$. The error limit gives the largest observed fluctuation in the measured value and also is the estimated accuracy of the experimental method. On examining the potential curves for the $[H_2]^+$ system, shown in Fig.49, it was concluded that the fragments associated with large KER must originate from excitation of an $[H_2]^+$ ion core to one of the repulsive states shown in Fig.49. It is known that an $[H_2]^+$ ion beam emerging from an EI ion source contains an Franck-Condon distribution of vibrational states peaked around v=2-3 [197]. The only vertical transition giving the observed magnitude of KER from an internuclear distance near the outer turning points of these states is to the $H^+ + H^+$ curve. We propose that the feature $B_1/B_2$ originates from a vertical transition from the ground electronic state of $[H_2]^+$ into to a HR state of $[H_2]^+$, a system consisting of an electron in a far removed orbit around the $[H_2]^{2+}$ core. The two protons will repel each other receiving practically all the available KER; as they separate, the HR electron will join one of them giving a H(HR) fragments which is responsible for peaks $B_1/B_2$. The process can be described by the equation

$$[H_2]^+ + T \rightarrow T + [H_2]^+(HR) \rightarrow H(HR) + H^+ \qquad (2.13)$$

This assignment is supported by the independent observations of Meierjohann and Vogler [26], who by a coincidence method, measured the KER distribution of $H^+$+$H^+$ fragments from 10keV collisions between $[H_2]^+$ and He. The $H^+$+$H^+$ fragment pairs detected in coincidence must be due to vertical excitation of the ground state $[H_2]^+$ to the $H^+$+$H^+$ repulsive curve, which is nearly the same as the potential curve for $[H_2]^+$(HR) except for the very small binding energy (<0.2eV) of the HR electron. They obtained a maximum in the KER distribution at 8.7eV. Considering that a HR electron can have a binding energy of up to 0.2eV, we conclude that the 8.2±0.3eV value obtained in the present work is in excellent agreement with the result of Meierjohann and Vogler. This supports the above interpretation of the origin of $B_1/B_2$ peaks in Fig.48 and also shows that this method for obtaining the most probable value of KER associated with a dished peak in the kinetic energy spectrum is reasonably correct.

The pair of peaks that constitute a dished peak correspond to fragments that are scattered forward (higher energy peak) and backward (lower energy peak) relative to the main ion beam direction. In the apparatus used in these experiments large-kinetic-energy-release processes involving the dissociation of diatomic ions produce dished peaks that are asymmetric in the forward direction. This is caused by instrumental discrimination effects. If the process involved gives forward and backward scattered products with the same probability, the forward scattered part of the dished peak is ca. 25% higher than the backward scattered. From Fig48.(b) it is apparent that at 5keV impact energy the backward scattered peak in the field-induced ion kinetic-energy spectrum of H(HR) fragments from $[H_2]^+$/He collisions is much higher than the forward scattered one, indicating that in these collisions backward scattered H(HR) fragments must be produced by a much greater probability than forward scattered ones. To investigate this effect the

forward/backward ratios, scaled by the factor for the instrumental discrimination effects, were determined for the dished peaks in the field-induced ion kinetic-energy spectra of H(HR) fragments from $[H_2]^+$/He collisions as a function of impact energy. Table 2 shows the results

**Table 2. The ratio of forward/backward scattered H(HR) fragments from $[H_2]^+$/He collisions as a function of the impact energy.**

| impact energy (keV) | forward/backward |
|---|---|
| 10 | 1:1.1 |
| 9 | 1:1.2 |
| 8 | 1:1.4 |
| 7 | 1:1.7 |
| 6 | 1:2.0 |
| 5 | 1:2.2 |

It is apparent that the slower the $[H_2]^+$ projectile the more pronounced the forward/backward asymmetry. Putting it another way, the longer the collision time the larger the effect, which indicates that interactions within the $[H_2]^+$...He collision complex are responsible for the observed asymmetry. Because only forward or backward scattered fragments are observed under the present experimental conditions, the collision complex is a $[H_2]^+$-He species aligned along the primary beam direction. The promotion of the electron of the $[H_2]^+$ into a HR orbit takes place within this complex and the two protons will be repelled in opposite directions, forward and backward relative to the main direction. It appears that as

the collision time decreases the proton repelled backwards, being farther from the He atom, tends to carry away the HR electron. A possible explanation for this effect is that the proton closer to the He atom is shielded in some degree by the He electrons.

Field-induced ion kinetic-energy spectra of D(HR) fragments from $[D_2]^+$/He collisions have also been recorded and those obtained at 10keV and 6keV collision energies are shown in Figs.50(a) and 50(b), respectively. $[D_2]^+$ ions of 10keV kinetic energy has the same velocity as that of 5keV $[H_2]^+$ ions and the forward/backward ratio for 10keV $[D_2]^+$ projectiles is the same (1:2.1) as that for 5keV $[H_2]^+$ projectiles. This observation supports our proposal that the asymmetry in the dished peaks is related to the lifetime of the collision complex. It is also apparent from Fig.50 that between 10keV and 6keV impact energies the extent of the forward/backward asymmetry does not change significantly. (Spectra were recorded, although not shown, at 8, 9 and 7keV kinetic energies and they showed no change in this ratio.)

The present observations, which clearly arise from Rydberg states, should be contrasted with those obtained in the collision-induced generation of $H^+$ from $[H_2]^+$. The ion kinetic-energy spectra of $H^+$ fragments from collisions between 10 and 5keV $[H_2]^+$ incident on a He target are shown in Figs.51(a) and 51(b), respectively. The spectra in these figures consists of a central narrow peak and an extended, very broad dished peak. The appearance of the dished part of the spectra are completely different from those in Figs.48 and 50. These have broad maxima corresponding to KER of 3-4eV and it has been concluded that they mainly arise from vertical electronic excitation from the ground electronic state to the repulsive $2p\sigma_u$ state, (see section 1.2.1). There is extended tailing towards higher values of KER starting at around 8eV, a feature attributed to collision-induced vertical ionization of the

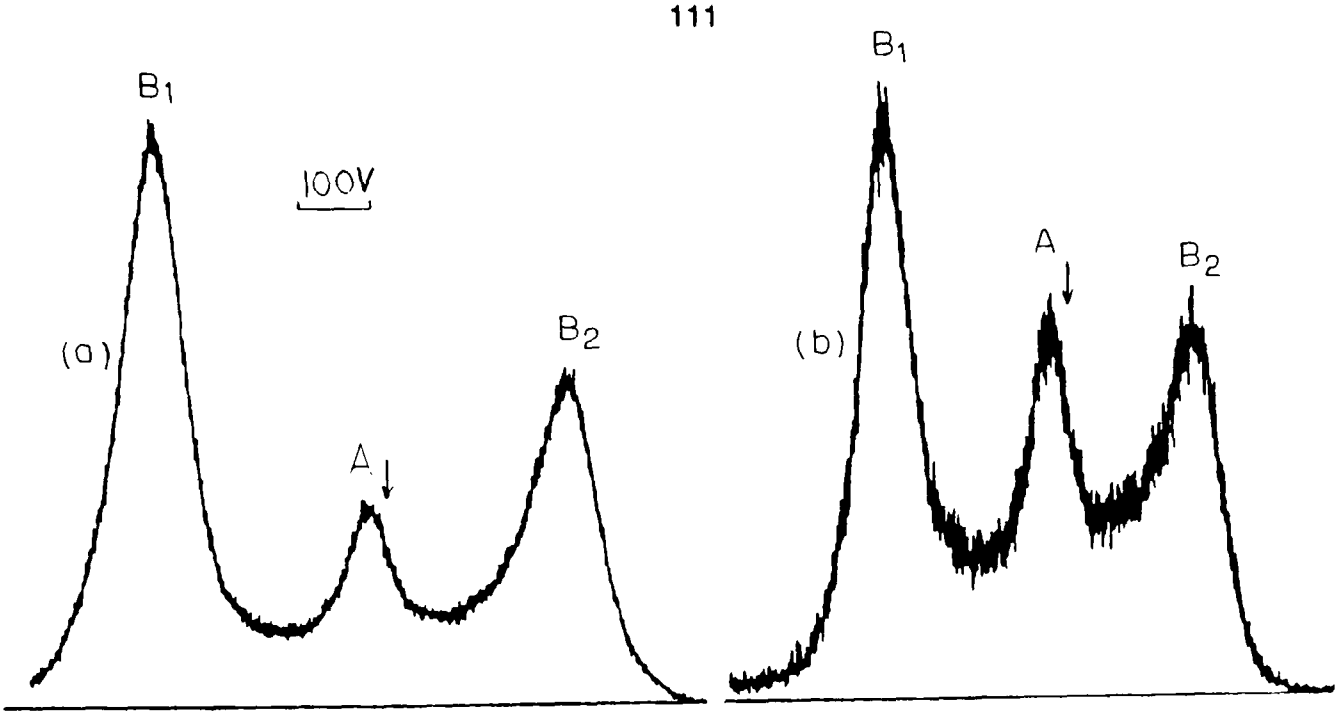


Figure 50. Field-induced ion kinetic-energy spectra of D(HR) fragments from $[D_2]^+$/He collisions. The arrow shows the energy $((1/2)E_o+1000)V$. (a) $E_o$=9994V; (b) $E_o$=5997V.

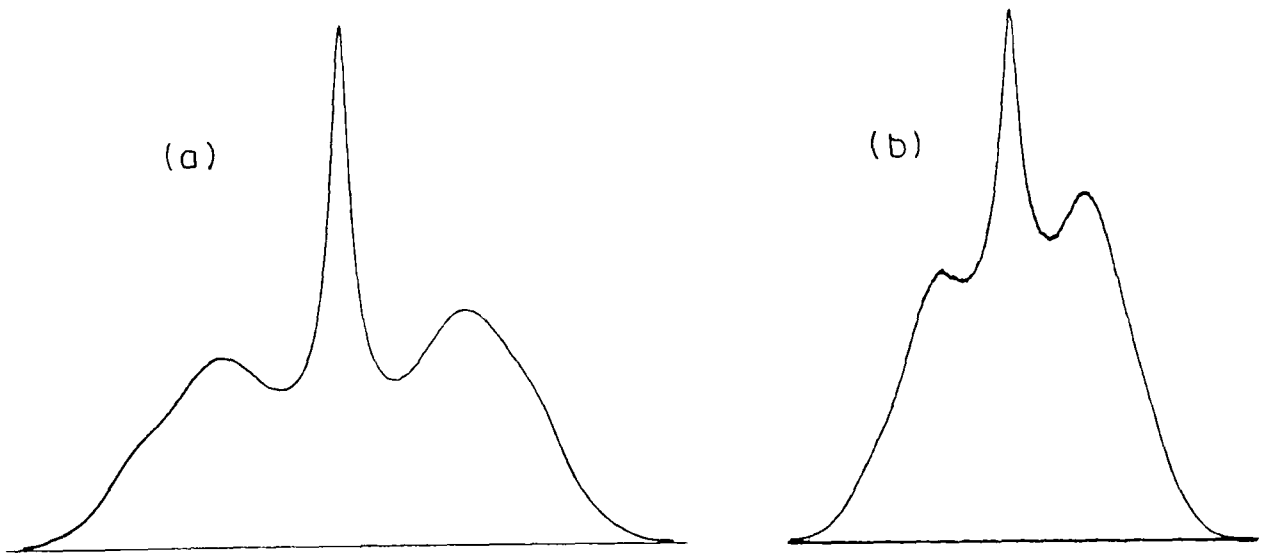


Figure 51. Kinetic energy spectra of $H^+$ fragments from $[H_2]^+$/He collisions. (a) $E_o$=9986V; (b) $E_o$=5010V.

$[H_2]^+$ ion [198].

Field-induced ion kinetic-energy spectra of H(HR) fragments from collisions between 8keV $[H_2]^+$ and a number of collision gases other than He have also been recorded. Fig.52 contains the spectra for Ne, Ar, Kr and Xe as collision gases and Fig.53 shows the spectra corresponding to $H_2$, $N_2$, $O_2$ and NO targets. From Fig.52 it can be seen that in the case of rare gases as targets the relative importance of reaction (2.13), i.e. the broad component in the spectra, decreases as the ionization energy (I.E.) of the target species decreases. This trend can be rationalized by considering that reaction (2.13) involves the same energy defect (ca. 26eV) regardless of the nature of the collision gas, but the endothermicity of reaction (2.12) is dependent on it; it is the sum of the I.E. of the target species and the dissociation energy of $[H_2]^+$. The calculated energy defects for reaction (2.12) are, for He 27.2eV, for Ne 24.2eV, for Ar 18.4eV, for Kr 16.6 eV, for Xe 14.7eV. Another noteworthy observation is that for Ne as collision gas the asymmetry, present for He target and favoring the backward scattered fragments no longer appears in the dished component of the H(HR) fragment peak.

In contrast to what was observed for the rare gases, in the case of diatomic species the relative importance of reaction (2.12) and (2.13) shows no significant dependence on the I.E. of the targets even though they differ quite widely, (I.E.($H_2$)=15.4eV; I.E.($N_2$)=15.6eV; I.E.($O_2$)=12.1eV; I.E.(NO)=9.4eV).

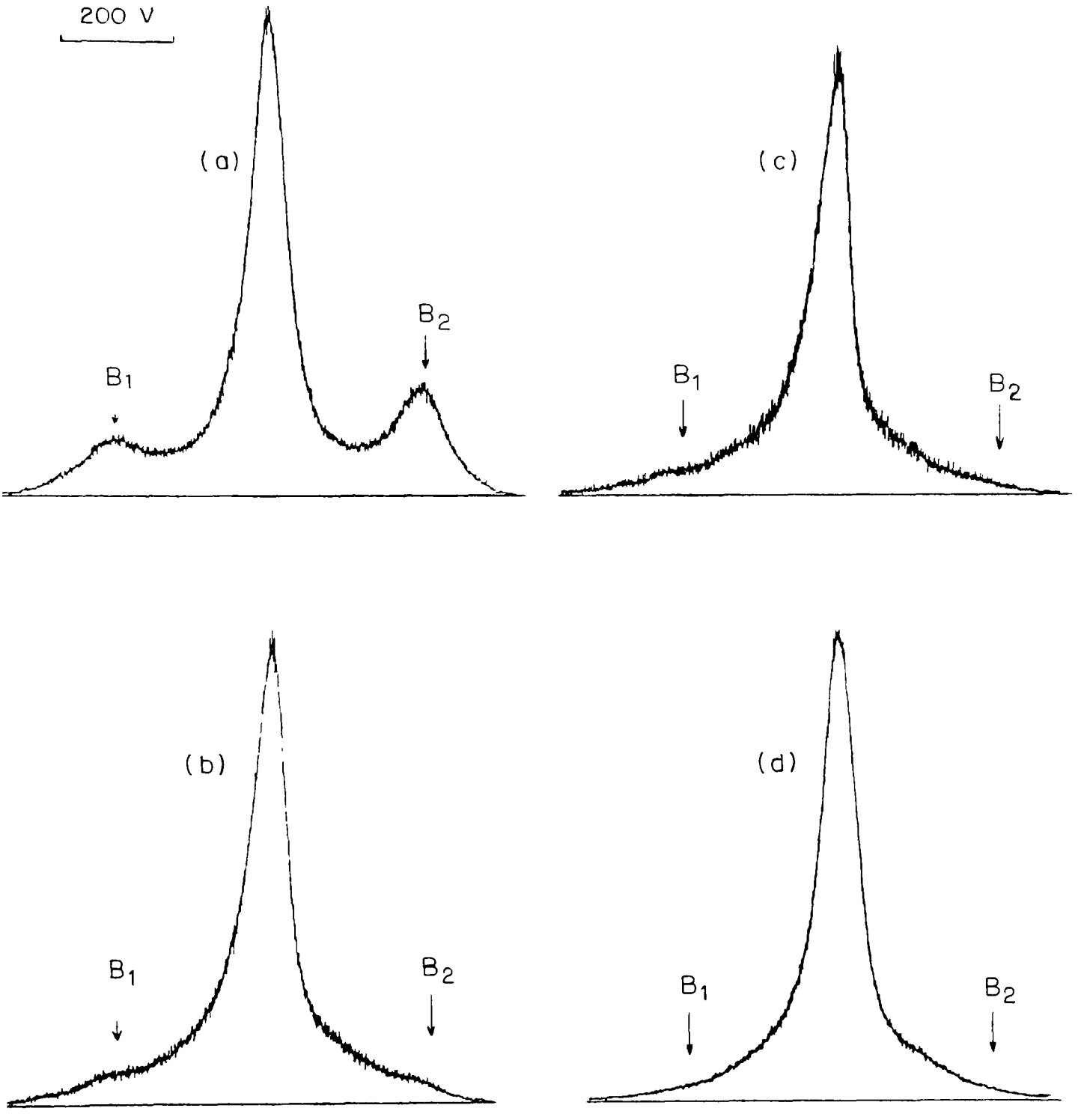


Figure 52. Field-induced ion kinetic-energy spectra of H(HR) fragments from collisions between $[H_2]^+$ ions and (a) Ne, (b) Ar, (c) Kr and (d) Xe target gases. $E_o$=8keV.

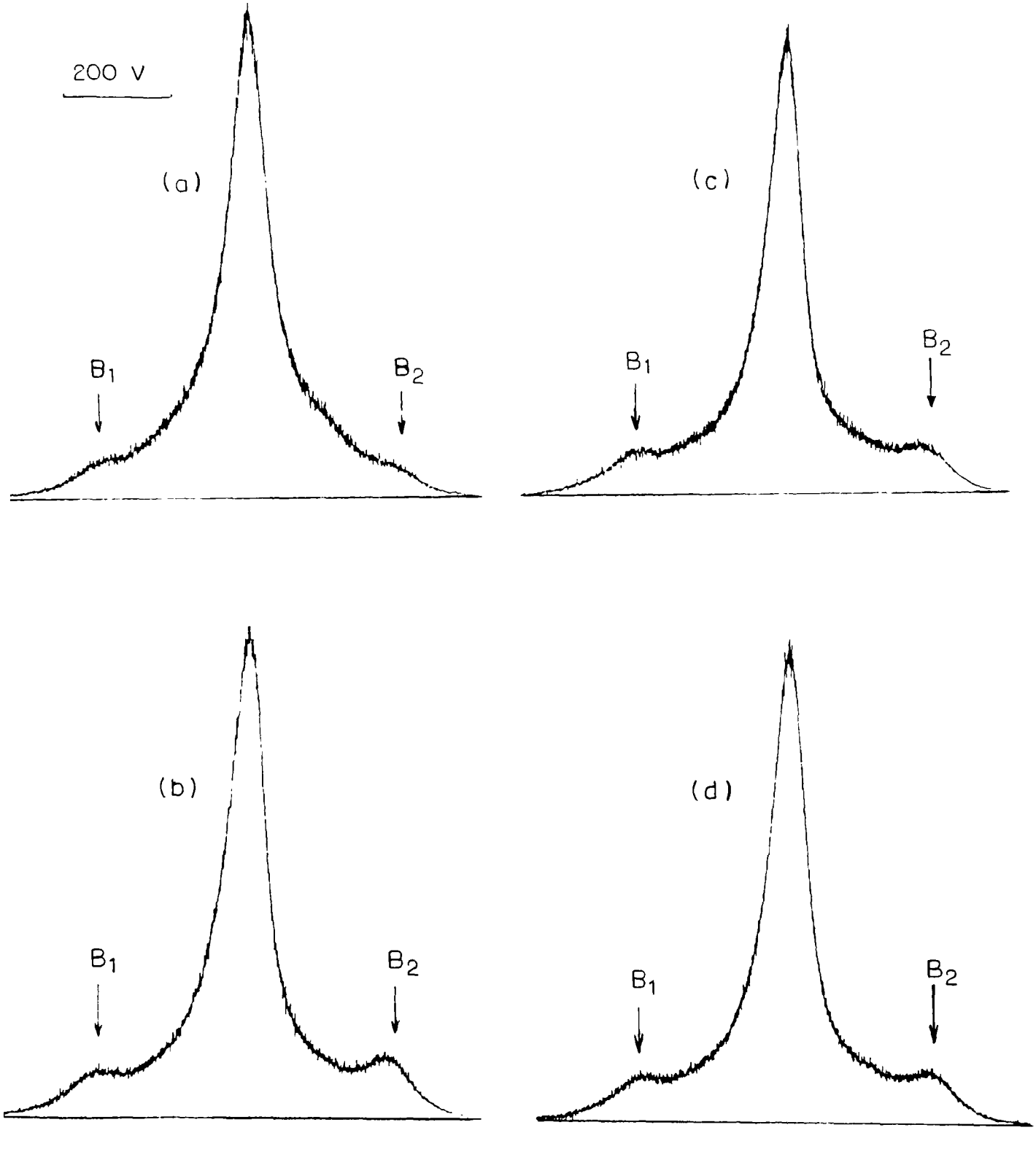


Figure 53. Field-induced ion kinetic-energy spectra of H(HR) fragments from collisions between $[H_2]^+$ and (a) $H_2$, (b) $N_2$, (c) $O_2$ and (d) NO collision gases. $E_o$=8keV.

**In summary. The field-induced ion kinetic-energy spectra of H(HR) fragments from keV collisions between $[H_2]^+$($[D_2]^+$) and a variety of collision gases were recorded. From the analysis of the spectra two distinct single collision processes have been identified that give rise to H(HR) fragments in the above collision systems. They can be generally described by equations (2.12) and (2.13). Helium as target was found to be unique in two respects. (i) For He reaction (2.13) was the overwhelmingly most important process for the generation of H(HR) fragments. (ii) There was a projectile velocity range found, which strongly favored the generation of backward scattered H(HR) fragments in $[H_2]^+$/He collisions.**

# 2.4 Characterization of the Vibrational Energy Distribution in $[H_2]^+$ Ion Beams

## 2.4.1 Introduction

In 1984 Brenton et al. [33] described a method to determine vibrational state distributions in $[H_2]^+$ ion beams. They measured the distributions of released kinetic energy received by the $H^+$ fragments from 6keV $[H_2]^+$/He collisions. Assuming that only excitations to the $2p\sigma_u$ state of $[H_2]^+$ were involved, they fitted distributions of vibrational states to reproduce the observed KER distributions. This method indicated only small variations in the vibrational populations of the $[H_2]^+$ beams generated by 70eV EI of $H_2$, $H_2O$ and $CH_4$ and other hydrocarbons. We believe that the kinetic-energy spectrum of $H^+$ fragments from keV $[H_2]^+$/He collisions is too insensitive to the vibrational energy states of $[H_2]^+$ ions for such an analysis. The basic reason is that there are other collision processes which generate $H^+$ ions with different ranges of KER values (both higher and lower), than the transition to the $2p\sigma_u$ state. They are (i) excitation to the $2p\pi_u$ state of $[H_2]^+$ (14% of all processes [199]), (ii) ionizing transitions to the $H^+$+$H^+$ curve (≈10% of all processes, giving rise to 20% of the $H^+$ signal because of *double* detection of this event [26]). Analysis of the kinetic energy spectra of H(HR) fragments from keV $[H_2]^+$/He collisions appears to be a more sensitive method to probe the vibrational energy distribution in $[H_2]^+$ ion beams, because the dished part of the kinetic energy peak originates from a *single* process involving transition to the $H^+$+$H^+$ curve (giving rise to large KER

values, >4eV. even at an internuclear distance of 3Å, the outer turning point of the v=12 level of $[H_2]^+$). The KER distribution is very sensitive to the internuclear separation in $[H_2]^+$ because the $H^+$+$H^+$ potential curve is strongly repulsive. In order to test this possibility we recorded the kinetic energy spectra of H(HR) fragments from 9keV collisions with He collision gas, for $[H_2]^+$ obtained by 70eV EI of $H_2$, $H_2O$, $H_2S$ and $CH_4$.

### 2.4.2 Results and Discussion

In Figs. 54(a),(b),(c) and (d) are shown the kinetic energy spectra of H(HR) fragments from collisions between He target gas and 9 keV $[H_2]^+$ ions originating from the 70 eV EI of $H_2$, $H_2O$, $CH_4$ and $H_2S$, respectively. We focus attention on the dished peaks of these spectra. The kinetic energy releases calculated from the maxima of these structures are 8.2±0.3 eV for $H_2$, 10.8±0.3 eV and 4.4±0.3 eV for $H_2O$, 5.2±0.3 eV for $CH_4$, and 4.5±03 eV for $H_2S$ as precursor molecules. As has already been discussed for the case of $H_2$ precursor, section 2.4, the observed kinetic energy release is associated with a mechanism described by reaction (2.13), involving transition to the $H^+$+$H^+$ repulsive curve, and is characteristic of the vibrational distribution the $[H_2]^+$ ion beam. In Fig.55 are shown the excitations responsible for the observed kinetic energy releases.

Von Busch and Dunn [197] determined experimentally the vibrational distribution in a $[H_2]^+$ ion beam generated by electron impact of $H_2$ molecules. They found a somewhat different distribution than that expected on the basis of the vibrational overlaps for $H_2$(v=0) $[H_2]^+$(v'=0-18) transitions. Their results, for the v'=0-10 levels, are shown in Table 3 together with the energies of the vertical transitions to the $H^+$+$H^+$ curve.

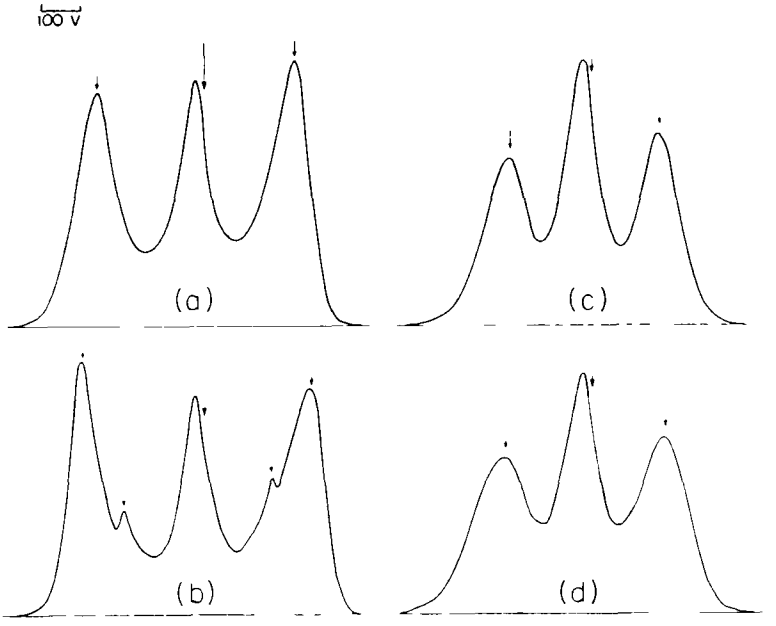


Figure 54. Field-induced ion kinetic-energy spectra of H(HR) fragments from $[H_2]^+$/He collisions. (a) $H_2$ precursor, (b) $H_2O$ precursor, (c) $CH_4$ precursor, (d) $H_2S$ precursor. $E_o$=8996V.

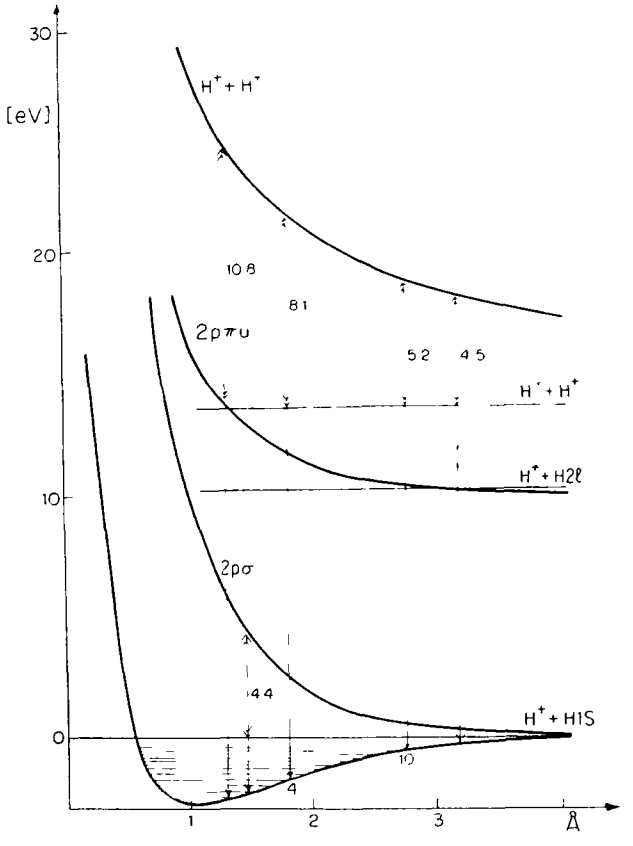


Figure 55. Potential curves for $[H_2]^+$ The arrows indicate the transitions discussed in the text.

**Table 3. Population (P) of vibrational state (v') in $[H_2]^+$(from [197]) and the vertical excitation energy (E) to the $H^+$+$H^+$ curve from the outer turning points of the particular states.**

| v' | P(v') | E(eV) |
|---|---|---|
| 0 | 0.119 | 30.1 |
| 1 | 0.190 | 25.9 |
| 2 | 0.188 | 24.9 |
| 3 | 0.152 | 23.9 |
| 4 | 0.125 | 23.1 |
| 5 | 0.075 | 22.4 |
| 6 | 0.052 | 21.8 |
| 7 | 0.037 | 21.2 |
| 8 | 0.024 | 20.6 |
| 9 | 0.016 | 20.1 |
| 10 | 0.011 | 19.6 |

As shown in Fig.55, the transition responsible for a 8.2eV kinetic energy release corresponds to an internuclear distance which lies between the outer turning points of the v'=3 and v'=4 vibrational levels. This observation indicates that transitions from these two states have the greatest, and approximately equal, importance. Inspecting Table 3 it can be seen that the v'=3 state has a ca 18% higher population that the v'=4, but the transition from the latter to the $H^+$+$H^+$ curve is 0.8eV less endothermic than that from the former. This can explain why the two transitions have approximately equal importance in our spectrum. It is also apparent from Table 3 that the most highly populated states are the v'=1 and v'=2 states, but, probably because of the higher endothermicity, the transitions from these states are less

important than those from the v'=3 and v'=4 levels. Considering the populations of the v'>4 vibrational levels we estimate, using the data in Table 3, that when a higher vibrational level is less populated by ca 50% than the most highly populated, though lower lying state, transitions from the former make no major contribution to the observed spectrum.

The large KER obtained for $H_2O$ as precursor corresponds to an internuclear distance which is smaller than the outer turning point of the v'=1 state, indicating that EI of $H_2O$ produces $[H_2]^+$ ions of very low vibrational energy content. We estimate that at least 2/3 of the $[H_2]^+$ ions must be in the v'=0 or v'=1 state. The smaller kinetic energy release (inner pair of peaks) can be attributed to electron capture by the $[H_2]^+$ projectile into a HR orbit together with excitation of the core into the repulsive $2p\sigma_u$ state. This process can be described as a modified version of reaction (2.12), where the ion core was dissociated by vibrational excitation. The signal in Fig.54(b) corresponding to the 4.4±0.3eV KER is very weak, the reaction generating it is more 20 times less probable than reaction (2.13) giving the 10.8±0.3eV KER. This is not surprising when one considers that the former is more endothermic by 3.7eV than the latter.

The kinetic energy releases obtained for $CH_4$ and $H_2S$ as precursors indicate that the EI of these molecules generates vibrationally hot $[H_2]^+$ ions. The value for $CH_4$ corresponds to a transition from the outer turning point of the v'=11 state, that for $H_2S$ precursor from the outer turning point of the v'=14 state. In the last case the pair of peaks are significantly broader than in all other such spectra indicating that a number of vibrational states are similarly densely populated around v'=14.

**The above results show that the field-induced ion kinetic-energy spectrum of the H(HR) fragments from $[H_2]^+$/He collisions is a quite sensitive diagnostic tool for the characterization of vibrational energy content of $[H_2]^+$ ion beams.**

# 2.5 Kinetic Energy Spectra of HR Fragments from keV Collisions between Small Ions and Inert Gas Atoms

## 2.5.1 Introduction

It has been shown in section 2.3 that H(HR) fragments from keV collisions between $[H_2]^+$ and gas targets are produced via two mechanisms, which were identified by applying the ion core model of molecular HR states to explain of the features in the field-induced ion kinetic-energy spectra of these fragments. In this section are presented the field-induced ion kinetic-energy spectra of HR fragments from collisions between a variety of diatomic (and some polyatomic) ions and rare gas targets in order to investigate the possibility of applying the ion core model for the HR molecular state for these more complicated systems and to attempt to extend the processes identified for $[H_2]^+$ projectiles to larger systems. The processes that have been observed for $[H_2]^+$ projectiles have been generalized as follows.

**Process 1.** Electron capture by the projectile ion ($XY^+$) from the target gas atom (N) into a HR orbit, accompanied by a simultaneous vibrational and/or electronic excitation of the ion core into the dissociative continuum. The excited ion core dissociates, the HR electron joins the ionic fragment and that resulting HR species can then be field ionized. When the ion core is dissociated by vibrational excitation it gives rise to a single narrow peak in the ion kinetic energy spectra. When the core is dissociated by electronic excitation it gives rise to broad, sometimes dished peaks. The overall process can be described by the following equation

$$XY^+ + N \rightarrow N^+ + XY(HR)^* \rightarrow X(HR) + Y + N^+$$
$$\rightarrow Y(HR) + X + N^+ \qquad (2.14)$$

where XY(HR)* is HR XY with a vibrationally and or electronically excited $XY^+$ core.

**Process 2.** The vertical electronic excitation of the projectile ion upon collision, into a HR state of the ion which converges to a dissociative electronic state of the doubly charged ionic core. The transition is illustrated in Fig.56.

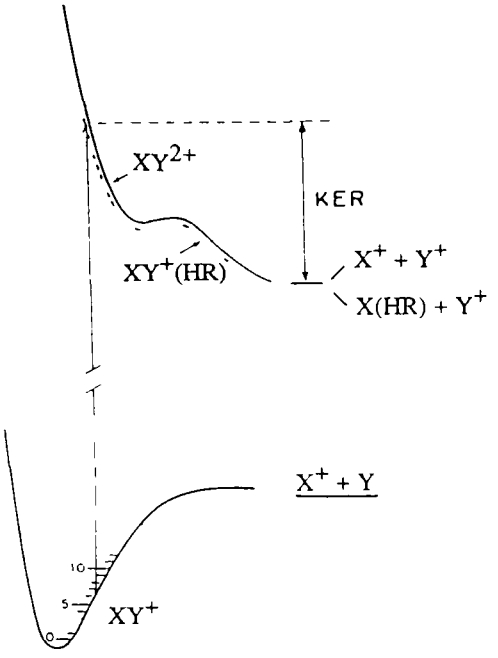


Figure 56 Generalized illustration of the transition giving rise to process 2 See text for discussion.

The doubly charged core dissociates into two ionic fragments and the HR electron joins one of them. The kinetic energy spectrum for this latter field ionizable atom shows a KER of the order of 5-10 eV in the centre of mass system, giving rise to a dished peak, i.e. a pair of peaks separated by hundreds of volts due to the amplification when the centre of mass framework is transformed to the laboratory framework. The observed KER should reflect the vibrational energy state of the original diatomic molecular ion. When the potential curve is known for the doubly charged electronic state to which the diatomic ion was excited by collision, then

the internuclear distance for the dissociating species can be determined from the kinetic energy release for process 2, provided that the transition occurs to a repulsive part of the potential curve. The transition to that state must be a vertical process because the collision time is much shorter than a vibrational or rotational period of the molecule. This calculated internuclear distance is that for the outer turning point of the most highly populated vibrational state in the molecular ion beam, and so the vibrational energy distribution in the projectile ion beam can be characterized.

Here we extend our studies to a variety of projectile ions. The observed kinetic energy spectra of the HR fragments were analyzed in the framework of the ion core model of HR molecules and molecular ions using the available theoretical and experimental data for the ionic core species.

### 2.5.2 Experimental

All measurements were made with the VG Analytical ZAB-2F double focusing mass spectrometer of reversed geometry, which has been modified as described before.

Measurements were performed as follows. Ions were generated by 70 eV electron impact unless otherwise stated. For $[N_2]^+$, $[O_2]^+$, $[NO]^+$,$[CH_4]^+$ and $[CD_4]^+$, the corresponding molecular gases were used, $[CH]^+$ was generated from $CH_4$, $[CD]^+$ from $CD_4$, $[OH]^+$ from $H_2O$, and $[NH]^+$ from $NH_3$. The ions formed in the ion source were accelerated to 9 or 10 keV and were mass selected by the magnet into the second field free region. The energy resolution of the apparatus was adjusted so that the main ion beam had a width of 10V at half height. Collision gas was admitted into the first collision cell to a pressure corresponding to 50% transmission of the main ion beam. The deflector electrode was usually charged to -700V to

deflect ionic species. The first mesh was at +1200V (except for $[NO]^+$ when it was at +1500V) and the second mesh was grounded. The electric field between the two meshes, ca 20 kV/cm, is sufficient to ionize HR species having an effective principal quantum number of n*>12. A kinetic energy spectrum of the resulting ion beam was obtained by scanning the electric sector in the usual way. The data were signal averaged [200] to obtain a better signal to noise ratio. In this mode of operation peaks appear in the kinetic energy spectra centered near $((m_f/m_p)*E_o + Q)$eV where $E_o$ is the primary ion beam kinetic energy, $m_p$ is the mass of the ions transmitted by the magnet, $m_f$ is the mass of the HR fragment and Q is the voltage on the first mesh.

To confirm that the field induced ion signals corresponded to field ionization of HR states the deflector voltage was raised from 700V to 2500V. This attenuated the field induced signal of HR states by ca 40%, whereas the very weak signals due to the interaction of non-Rydberg species with the mesh surface are not affected by this operation.

HR species could, in principle, be generated by two successive collisions, the first producing a fragment ion which captures an electron into a HR orbit on the second encounter. However, this would generate field-induced ion kinetic-energy spectra which should resemble the kinetic-energy spectra of the ionic fragments from these collisions. The spectra reported here are wholly dissimilar to the appropriate ion kinetic-energy spectra. Moreover, the net cross section for the consecutive events could only account for less than 1% of the observed signal intensities.

### 2.5.3 Results and Discussion

#### $[N_2]^+$, $[O_2]^+$ and $[NO]^+$ projectiles

The field-induced ion kinetic-energy spectra of N(HR) fragments for 10keV $[N_2]^+$/Xe and $[N_2]^+$/He collisions are shown in Figs.57(a) and 57(b), respectively.

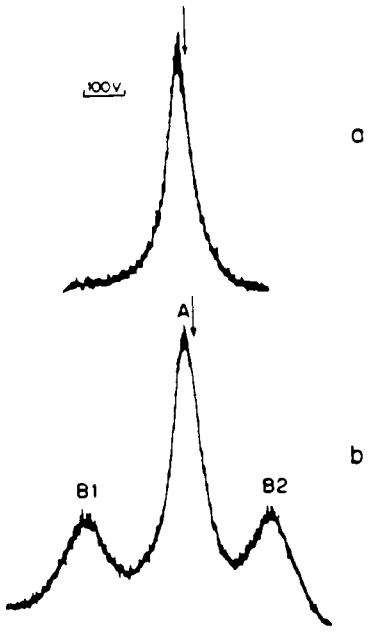


Figure 57. Field-induced ion kinetic energy spectra. (a) $[N_2]^+$/Xe, (b) $[N_2]^+$/He. The arrows show the energy $(1/2)E_o$+1200V. $E_o$=8keV.

With Xe as collision gas there is only a single narrow peak in the kinetic-energy spectrum. It is concluded that for this target the only mechanism generating N(HR) fragments is process 1. In the case of He collision gas the same narrow peak as for

Xe (peak A in Fig.57(b)) is also prominent indicating that process 1 also plays an important role. But in addition, there is a dished peak present ($B_1/B_2$), for which we calculated a most probable KER value of 6.8±0.3eV. This feature is proposed to be due to a process 2 type reaction, i.e. excitation of the $[N_2]^+$ projectile into one of its HR states. Based on the observed KER we assign a transition to the HR series converging to the $A^3\pi_g$ of $[N_2]^{2+}$, which has been found by other methods [201,202] to dissociate into two $N^+(^3P)$ fragments with 6.7eV KER.

The kinetic energy spectra of O(HR) fragments from the $[O_2]^+$/Xe and $[O_2]^+$/He systems are shown in Figs.58(a) and 58(b), those of the N(HR) and O(HR) fragments from the $[NO]^+$/Xe and $[NO]^+$/He systems are shown in Figs.59(a) and 59(b). It has been shown that 70eV EI of $O_2$ produces an $[O_2]^+$ ion beam in which 50% of the ions are in the $X^2\pi_g$ ground state and 50% of them are in the $a^4\pi_u$ excited state (ca 4 eV above the ground state) [203]. The 70eV EI of NO is also known to generate a mixture of the electronic states of $[NO]^+$ in which 1/3 of the ions are in the $X^1\Sigma^+$ ground state and 2/3 of them are in the $a^3\Sigma^+$ excited state (ca 6 eV above the ground state) [203]. Both the $a^4\pi_u$ state of $[O_2]^+$ and the $a^3\Sigma^+$ state of $[NO]^+$ have lifetimes in the order of seconds [203] and so there is no doubt that they would survive the flight time between the source and the collision cell (ca. 6μs) in our apparatus. Therefore in order not to populate these metastable excited states we generated the $[O_2]^+$ and the $[NO]^+$ ion beams by 12±1eV EI on their molecular gases.

With Xe as collision gas the kinetic energy spectra for the O(HR) fragments from $[O_2]^+$/Xe collisions, and N(HR) and O(HR) fragments from $[NO]^+$/Xe collisions contain only narrow peaks. It is concluded that the only mechanism generating HR fragments in these systems is process 1.

In the case of He collision gas the same narrow peaks as for Xe were also

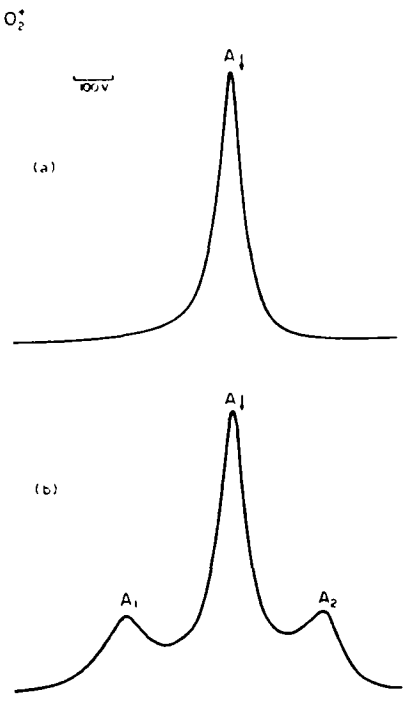


Figure 58. Field induced ion kinetic energy spectra. (a) $[O_2]^+$/Xe
(b) $[O_2]^+$/He. The arrow shows the energy ((1/2)$E_o$+1200)eV.$E_o$=9989V.

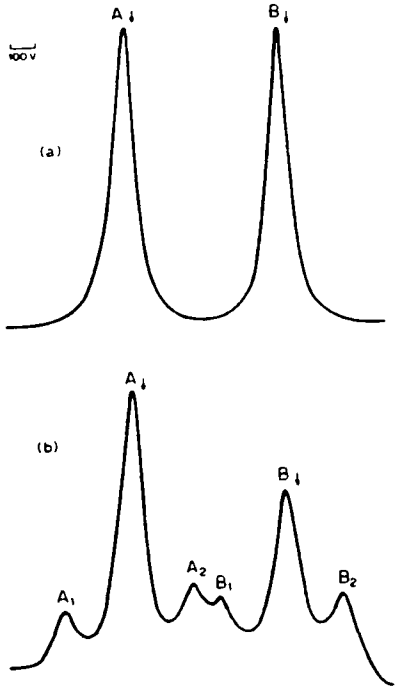


Figure 59. Field-induced ion kinetic-energy spectra. (a) $[NO]^+$/Xe,
(b) $[NO]^+$/He. The arrow at A shows the energy ((14/30)$E_o$+1500)eV;
the arrow at B shows the energy ((16/30)$E_o$+1500)eV. $E_o$=9998V.

prominent (peak A in Fig.58(b) and peaks A and B in Fig.59(b)) indicating that process 1 also plays an important role. But in addition there are dished peaks present; $A_1/A_2$ in Fig.58(b), $A_1/A_2$ and $B_1/B_2$ in Fig.59(b). The KER values calculated from the distances between the maxima of the peak pairs, using equation (1.24) are 7.3±0.3eV for $A_1/A_2$ in Fig.58(b) (O(HR) fragments), and 7.2±0.3 eV for both $A_1/A_2$ (N(HR) fragments) and $B_1/B_2$ (O(HR) fragments)in Fig.59(b). The only likely origin of these large kinetic energy releases is the dissociation of a doubly charged ionic core, generating HR atoms by process 2. The reaction involves vertical excitation of the projectile ion into one of its Rydberg series. In order to identify, on the basis of the observed kinetic energy release, the electronic state of the doubly charged ion to which the intermediate HR ionic state converges, it is necessary to know the most probable value (or at least a range of values) of the internuclear distance in the projectile ion beam. Ionization by electron impact is Franck-Condon in nature and so the appropriate internuclear distance is the equilibrium bond length in the ground state molecule, (and the Franck-Condon region around it). The equilibrium bond length of the ion is smaller than that of the molecule, for both projectiles, and so vertical ionization involves transitions to the outer turning points of the vibrational levels of the ion. The best available theoretical calculations for the electronic potential curves of $[O_2]^{2+}$ are those of Beebe et al. [204]. Considering that the equilibrium (ground state) bond length in $O_2$ is 1.207Å [205], the most likely electronic state of the doubly charged ion giving rise to the 7.3±0.3eV kinetic energy release, is the lowest $^3\pi_g$ state. Only the lower electronic states are considered, because the progressively increasing endothermicity of transitions to higher excited states makes them much less probable. Excitation to the $a^3\pi_g$ state would give a predicted kinetic energy release of 7 eV. The $a^3\pi_g$ state of $[O_2]^{2+}$ correlates to $O^+(^4S)+O^+(^2D)$ products. If upon dissociation of this

core the HR electron joined the ground state $O^+(^4S)$ ion, the resulting O(HR) atom can survive on the μs time scale and so can reach the field ionization region. However, if the electron joined the excited $O^+(^2D)$ the resulting HR species should autoionize before reaching the field ionization regions. *(The rate of allowed autoionization for a HR atom with an electrically excited core is $10^{11}n^{-3}s^{-1}$ or faster [206]. The autoionization of the Rydberg series, converging to the $^2D$ state of $O^+$, into the $O^+(^4S)+e^-$ continuum is not forbidden by any selection rule [207]. Therefore, only Rydberg states of principal quantum number n>48 survive 1μs or longer, but under our experimental conditions , HR states of that high n are not detected.)* This may explain the relatively low intensity of the dished peak in Fig.58(b).

We repeated the experiments for the $[O_2]^+$/Xe and the $[O_2]^+$/He systems with an $[O_2]^+$ projectile beam generated by the 70eV EI of $O_2$ gas, i.e. when 50% of the ions were in the $a^4\pi_u$ excited electronic state. The same kinetic energy spectra were obtained as those shown in Figs.58(a) and 58(b). The KER value obtained from the dished peak of the spectrum of the $[O_2]^+$/He system, 7.3±0.3 eV, also did not change. This latter observation is not unexpected if the transition, in process 2, from the $a^4\pi_u$ state also occurs to the $a^3\pi_g$ state of the $[O_2]^{2+}$. The $a^4\pi_u$ state of $[O_2]^+$ has an equilibrium bond distance of 1.38Å [208] which is longer than that of the ground state neutral molecule and so the characteristic internuclear distance is different for this state than that for the $X^2\pi_g$ ground state of the ion, but the potential curve of $[O_2]^{2+}(a^4\pi_g)$ changes very little (has a shallow minimum) in this region.

In 1986 Wetmore and Boyd [209] calculated the potential curves of the doublet and quartet electronic states of $[NO]^{2+}$. The doubly charged core electronic state the transition to which gives rise to the observed 7.2±0.3eV KER associated with

both the N(HR) and O(HR) fragments from $[NO]^+$/He collisions, has to satisfy the following conditions. (i) It has to correlate with ground state $N^+$ and $O^+$ products. If one of them was not in the ground state it could not give rise to a field-induced ion signal, because the corresponding HR state fragment would autoionize before reaching the field ionization detector. (ii) The transition cannot occur to a quartet state of $[NO]^{2+}$ from the singlet ground state of $[NO]^+$ because of spin-conservation rules, (see section 1.2.2). Considering the theoretical potential curves of Wetmore and Boyd [207] and the above conditions, the only likely $[NO]^{2+}$ state to which the transition occurs is the $A^2\pi$ state. Transition to this state at an internuclear distance of 1.04Å [205] (very close to the 1.06Å equilibrium internuclear distance of $[NO]^+$) would give 7.2eV KER.

The experiments were repeated with an $[NO]^+$ projectile beam obtained by the 70eV EI of NO gas, i.e. when 2/3 of the ions are in the $a^3\Sigma^+$ excited state. We obtained generally similar spectra to those in Figs.59(a) and 59(b). There were however some differences for the dished peaks obtained for the $[NO]^+$/He system. In the latter experiments the intensity of the dished peaks relative to the central peaks were by ca. 20% higher and the KER was 7.9±0.3 eV, for both N(HR) and O(HR) fragments. This latter value of the kinetic energy release is significantly higher than the 7.2±0.3 eV obtained when the projectile ion beam consisted only of ground state $[NO]^+$. The equilibrium bond distance of the $a^3\Sigma^+$ state of $[NO]^+$ is 1.29Å [205], greater than that of ground state NO. Therefore the characteristic internuclear distance for the $a^3\Sigma^+$ state is greater than that for the ground state of $[NO]^+$, and so if the triplet state were also excited to a Rydberg series converging to the $A^2\pi$ state of $[NO]^{2+}$, which is repulsive in this region, we should obtain a kinetic energy release smaller than 7.2 eV. That the observed kinetic energy release is *greater* than this value indicates that the $a^3\Sigma^+$ state of $[NO]^+$, upon collision with

He, must be excited to another state of $[NO]^{2+}$. In this case spin-conservation does not forbid transitions to the quartet states of $[NO]^{2+}$. Based on the potential curve given by Wetmore and Boyd [209] we conclude that there is no appropriate doublet state of $[NO]^{2+}$, i.e. which can give rise to the observed kinetic energy release and which correlates to ground state $N^+(^3P)$ and $O^+(^4S)$. Transition to the $A^4\pi$ state appears to be the best candidate, it dissociates at an internuclear distance of 1.5Å (corresponding to slightly vibrationally excited $[NO]^+(a^3\Sigma^+)$) with 7.9eV KER.

### $[CH]^+$, $[CD]^+$, $[OH]^+$, and $[NH]^+$ projectiles

Figs60(a) and (b) show the field-induced ion kinetic-energy spectra of C(HR) and H(HR) fragments from $[CH]^+$/Xe and $[CH]^+$/He collisions; Fig.60(c) shows the field-induced ion kinetic-energy spectra for C(HR) and D(HR) fragments from $[CD]^+$/He collisions. Those for the N(HR) and H(HR) fragments for $[NH]^+$/Xe and $[NH]^+$/He systems are shown in Figs.61(a) and 61(b), and those of the O(HR) and H(HR) for the $[OH]^+$/Xe and $[OH]^+$/He systems are shown in Figs.62(a) and 62(b). In the case of Xe collision gas the spectra contain almost exclusively a single narrow peak for each fragment, although for the heavy fragments N(HR), (peak B in Fig. 61(a)), and O(HR), (peak B in Fig.62(a)), some minor broad features are observable, the origin of which will be discussed later. We conclude again, that with Xe as collision gas, process 1 is the major mechanism for the generation of HR fragments.

In the case of He collision gas, the kinetic energy spectra of H(HR) fragments, for all three projectiles, contain a central narrow peak (peaks A in Figs. 60(b), (c), 61(b) and 62(b)) flanked by a dished peak (structures $A_1/A_2$ in Figs. 60(b), (c), 61(b) and 62(b)). The central peaks have width and position similar to the single narrow peaks observed with Xe as collision gas; all these we identify as arising

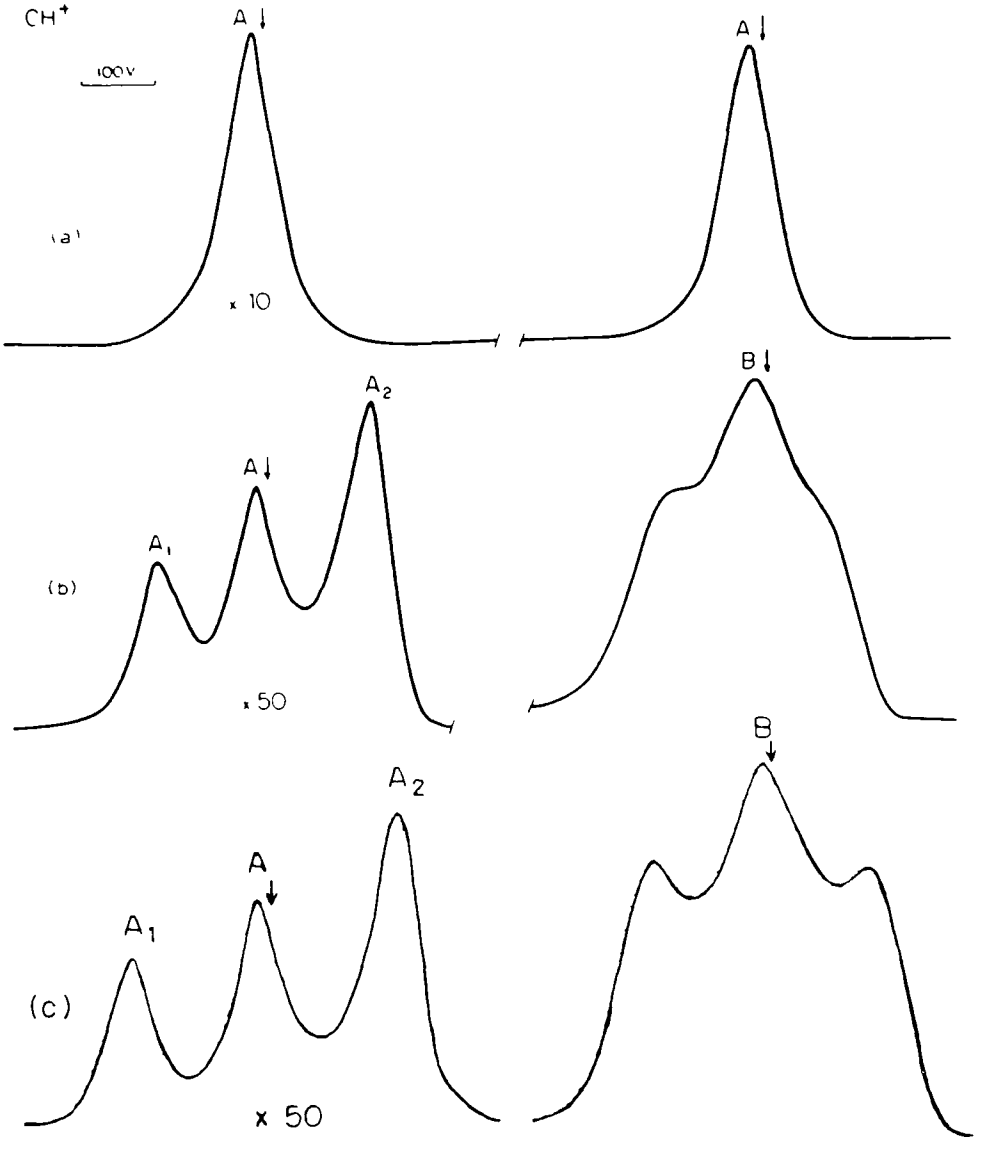


Figure 60. Field-induced ion kinetic-energy spectra. (a) $[CH]^+$/Xe, (b) $[CH]^+$/He, (c) $[CD]^+$/He. The arrow at A shows the energy $((1/13)E_o+1200)$eV;the arrow at B shows the energy $((12/13)E_o+1200)$eV. $E_o$=9004V.

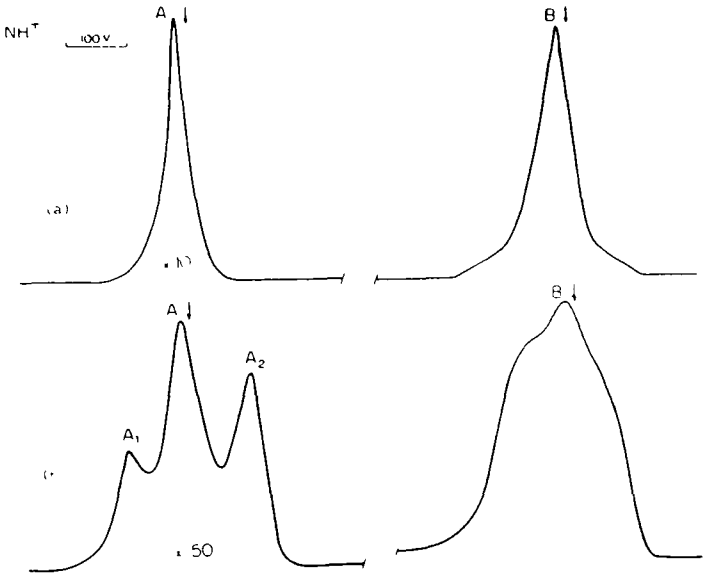


Figure 61. Field-induced ion kinetic-energy spectra. (a) $[NH]^+$/Xe
(b) $[NH]^+$/He. The arrow at A shows the energy $((1/15)E_o+1200)$eV;
the arrow at B shows the energy $((14/15)E_o+1200)$eV. $E_o$=8996V.

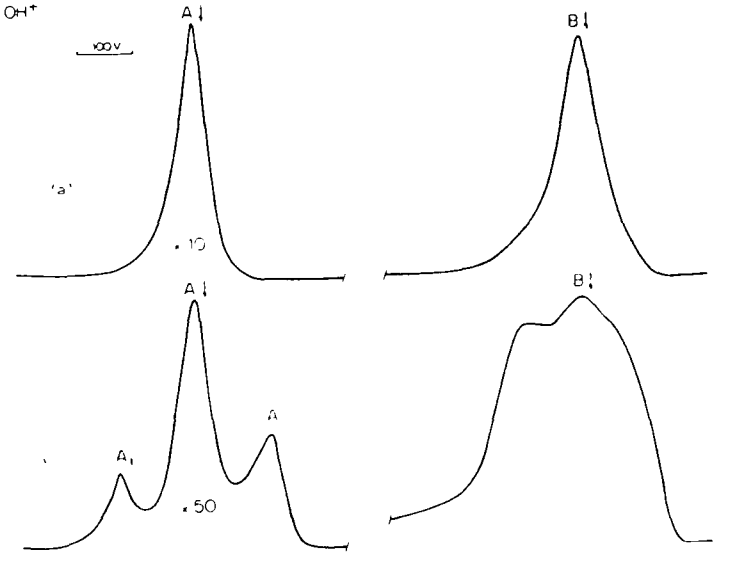


Figure 62. Field-induced ion kinetic-energy spectra. (a) $[OH]^+$/Xe,
(b) $[OH]^+$/He. The arrow at A shows the energy $((1/17)E_o+1200)$eV;
the arrow at B shows the energy $((16/17)E_o+1200)$eV. $E_o$=9998V.

from process 1. The kinetic energy releases calculated from the distances between the maxima of the dished peaks are, 8.0±0.3 eV for $[CH]^+$, 8.5±0.3eV for $[CD]^+$, 7.5± 0.3 eV for $[NH]^+$, and 9.1±0.3 eV for $[OH]^+$. The magnitude of these values shows that these peaks must originate from process 2. Potential energy curves of the lower electronic states of $[CH]^{2+}$ are available from the high level ab initio calculations of Wetmore et al. [210]. From their results we conclude that the electronic state of the doubly charged ion to which the transition occurs must be the lowest $^2\pi$ state, which is the only state that can give rise to 8eV kinetic energy release at a reasonable internuclear distance, i.e. equal to or greater than the equilibrium internuclear distance in the $[CH]^+$ cation. Transition to the $a^2\pi$ state at 1.2Å internuclear distance gives a calculated kinetic energy release of 8eV. For $[NH]^{2+}$ the only available calculations are those for the deprotonation energy of the dication at two different internuclear distances. Koch and Schwarz [211] calculated a 5.9eV deprotonation energy at 1.249Å internuclear distance, and the calculations of Pope et al. [212] gave a 9.0eV deprotonation energy at 1.07Å, the internuclear distance for ground state $[NH]^+$. The present experimental value of 7.5±0.3eV, falls between the calculated values.

Schwarz et al. [213] calculated the ground state potential curve of $[OH]^{2+}$ using Moller-Plesset perturbation theory terminated at the second order, applied to a 6-31G** basis set. Vertical transition to this curve would give 11.1eV KER, even at the extremely large internuclear distance of 3.4Å. The accuracy of this calculation, however, is questionable. This is shown by the fact that the recalculation of the energy at a single geometry at a much higher level of theory (MP4SDTQ/6-311++G**) lowers it by 1.8 eV.

The kinetic energy spectra of the heavier fragments from collision with He are very different from those of the corresponding light H(HR) fragment, for all three

projectile ions, see structures B in Figs.60(b), (c), 61(b) and 62(b). These generally contain a central narrow peak of minor importance, which must arise from process 1. Around the central peak is a broad rectangular feature, not a dished peak as in the case of the H(HR) fragment, (except for $[CD]^+$ primary ions). This, in itself, is not surprising. The heavier fragment carries away the major fraction of the kinetic energy of the projectile ion and therefore the relative importance of the velocity component gained in the z-axial direction is much smaller than in the case of H(HR) fragment. This makes the heavier fragment much less sensitive to the instrumental z-axial discrimination, which as shown by Szulejko et al. [195], is the source of the "dishing" in peaks associated with a large KER in the center of mass framework. (For $[CD]^+$ as projectile, Fig.60(c), the dishing also appear in the spectrum of the heavier fragment probably because in this case the ratio of the masses of the light and heavy fragments is larger than for the other.) However, there are two features which show that the broad component of peak B in Figs. 60(b),(c), 61(b) and 62(b) cannot originate from the same process as the $A_1/A_2$ structures in the same figures. The first is that the rectangular peaks are positioned *asymmetrical* about the narrow peaks *towards lower energies*, whereas the dished peaks are asymmetric towards *higher* energies. The process which generates X(HR) atoms (X can be C, N and O atom) in $[XH]^+$/He collisions with a large kinetic energy release is more endothermic (by ca 5 eV), than the process involving electron capture into a HR orbit accompanied by vibrational excitation of the ion core into its dissociative continuum for X(HR) generation. Just the opposite is true for the H(HR) fragments, the dished peak is generated in a process which is less endothermic by ca 5 eV than that which gives rise to the narrow peak. The second reason is that the kinetic energy release calculated from the distances across the shoulders of the rectangular peaks, 5.0±0.5 eV for $[CH]^+$ and $[CD]^+$; 4.0±0.5 eV for $[NH]^+$; 4.5±0.5 eV for $[OH]^+$, are

significantly different from those obtained above for the dished peaks. Note also that the spectra of HR fragments from $[CD]^+$/He collisions contain *completely different, dished* peaks for the D(HR) and the C(HR) fragments.

We propose the following mechanism, which can explain all observations, for the production of X(HR) species associated with large kinetic energy release in $[XH]^+$/He collisions and which is common for all three projectiles. This is a process which involves electron capture by the $[XH]^+$ ion from the He target into a HR orbit with the simultaneous excitation of the singly charged core into a repulsive electronic state which correlates to the ground state $X^+$ ion and H atom. All three projectile possess such states, and high level theoretical calculations are available for them [214-216]. This mechanism can give rise to the kinetic energy releases obtained above and also explains the asymmetry of peaks B because, for a given $[XH]^+$ projectile, this process is more endothermic by the amount of the released energy, than electron capture into HR orbit with the simultaneous vibrational excitation into the $X^+$+H dissociative continuum.

Sun and Freed [214] calculated the valence state potential curves of $[CH]^+$. The only repulsive state, which converges to the $C^+(^2P)$ + $H(^2S)$ limit, is the lowest $^3\Sigma^+$ state. Transition to this state would lead to 5eV energy release at 1.3Å internuclear distance. This is in reasonable agreement with the 1.2Å characteristic internuclear distance for $[CH]^+$ ions obtained above, by assuming that the H(HR) fragments were formed by process 2 involving a transition to the $a^2\pi$ state of $[CH]^{2+}$. For $[NH]^+$ electron capture into HR a orbit with transition to the $2^4\Sigma^-$ state [215], and for $[OH]^+$ electron capture into a HR orbit with excitation to the $2^3\Sigma^-$ state [216] are the most likely processes to give rise to the observed rectangular peaks.

The relatively high cross section for this process is somewhat surprising, it being greater than that for the process generating the central narrow parts of features B,

(see above), in spite of being more endothermic by 4-5 eV. We also identify the minor broad features around peaks B in Figs.61(a) and 62(a) as originating from the same kind of process as the rectangular peaks in Figs.61(b) and 62(b).

### $[CH_4]^+$ and $[CD_4]^+$ projectiles

Figs.63(a) and 63(b) show the kinetic energy spectra of H(HR) and $CH_3$(HR) fragments from $[CH_4]^+$/Xe and $[CH_4]^+$/He collisions, those for the $CD_3$(HR) and D(HR) fragments from $[CD_4]^+$/He collisions are shown in Fig.63(c). The observation of the polyatomic $CH_3$ fragment as a field-ionizable species in our experimental conditions shows that in collisions between $[CH_4]^+$ ($[CD_4]^+$) ions and rare gas targets, long lived (at least 1μs) tetratomic $CH_3$(HR) ($CD_3$(HR)) fragments are formed. The observation of the long lived polyatomic HR fragment may seem to be unexpected, because the additional degrees of freedom (rotational and vibrational) of a molecule make such species susceptible to fast, radiationless decay, such as autoionization and predissociation into non-Rydberg fragments (for a detailed discussion see ref.[217]). It has however been shown theoretically by Band [218] that if the HR electron has a large orbital angular momentum (l>4) radiationless decay processes can become slower than radiative decay of the HR state, due to the decreased penetration of the core by the electron. A small number of di- and polyatomic molecules have been observed in long lived HR states (for a review see ref. [175]). Long lived $CH_3$(HR) species have already been observed as fragments from the electron impact dissociative excitation of methane [219], but the present work is the first report of production of long lived polyatomic HR fragments in keV ion-neutral collisions.

In the case of Xe collision gas (Fig.63(a)) we observed a single narrow peak for

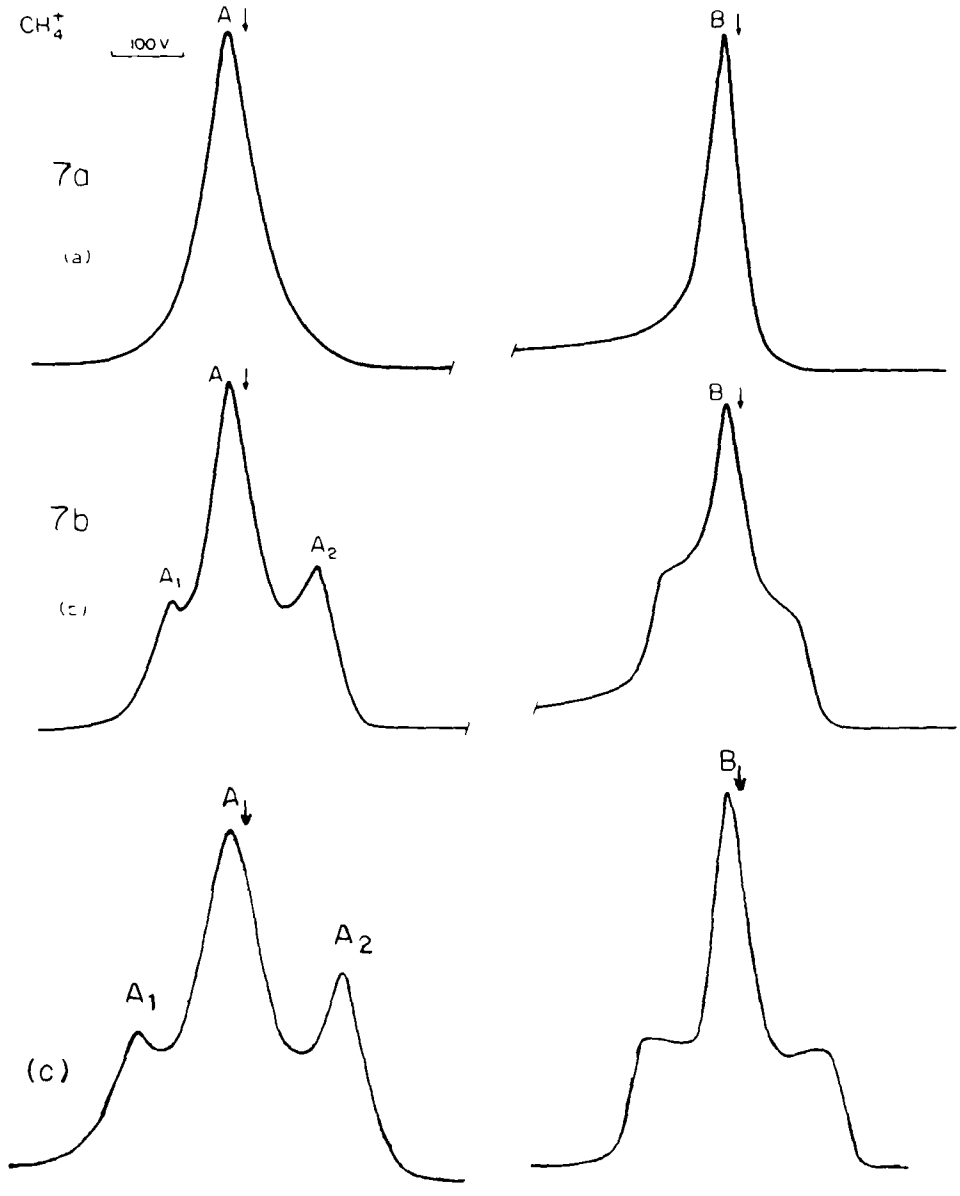


Figure 63. Field-induced ion kinetic-energy spectra (a) $[CH_4]^+$/Xe, (b) $[CH_4]^+$/He, (c) $[CD_4]^+$/He. The arrow at A shows the energy $((1/16)E_o+1200)$eV; the arrow at B shows the energy $((15/16)E_o+1200)$eV. $E_o$=9002V.

both the H(HR) (peak A) and $CH_3$(HR) (peak B) fragments. We assign a process 1 type mechanism to them; i.e. electron capture by the $[CH_4]^+$ projectile from the Xe target into a HR orbit and simultaneous vibrational and/or electronic excitation to give either the $H^+$+$CH_3$ or the $[CH_3]^+$+H dissociation products. In the case of He collision gas (Fig.63(b) and (c)), the same processes also occur, giving rise to the narrow central peaks, A and B. In addition there is the $A_1/A_2$ dished peak for the H(HR), (D(HR)), fragments and a rectangular peak around peak B for the $CH_3$(HR) fragments, the peak for the $CD_3$(HR) fragments is slightly dished reflecting the higher mass ratio between light and heavy fragments in this case. The kinetic energy release calculated from the distance between the $A_1/A_2$ structure is 4.7±0.3 eV for both $[CH_4]^+$ and $[CD_4]^+$. The same kinetic energy release was obtained from the distance across the shoulders of the rectangular peaks in Figs.63(b) and (c). We propose that these features are due to a process 2 type reaction, i.e. excitation of the $[CH_4]^+$ projectile upon collision into a HR state with a doubly charged core which dissociates into $H^+$ and $[CH_3]^+$ in its ground state. When the HR electron joins the $H^+$ a H(HR) atom is produced and when it joins the $[CH_3]^+$ ion the $CH_3$(HR) fragment is generated.

Siegbahn [220] and Pople at al. [221] have carried out high level ab initio calculations for $[CH_4]^{2+}$. They calculated the deprotonation energy of the dication and the height of the energy barrier to deprotonation. The difference of these two values should give the minimum expected kinetic energy release for $[CH_4]^{2+}$ dissociation into $H^+$ and ground state $[CH_3]^+$. These expected minimum values are 5.5eV [220] and 5.3eV [221]. Both values are somewhat higher than the observed kinetic energy release in our experiment. This may indicate that the above calculations somewhat overestimate the height of the energy barrier to deprotonation. It seems unlikely that the $[CH_3]^+$ core has 0.6-0.9eV rovibrational

energy and the corresponding $CH_3$(HR) is still metastable on the μs time scale.

**In summary. It has been shown in this chapter that the processes described in section 2.5.1 give rise to HR fragments in keV collisions between the projectile ions studied here and Xe and He targets. For Xe as collision gas, which has a relatively low ionization energy (IE=12.1eV) process 1 is the only important process generating HR fragments. For the high ionization energy (IE=24.6eV) He target, both process 1 and process 2 are operative in the generation of HR fragments. Table 4 contains a summary of the various collisional excitations assigned to features in the field-induced ion kinetic energy spectra analysed in this chapter.**

**Table 4.**

Designated excitations leading to fragments with a large kinetic energy release

| Precursor | Ion | Designated transitions [a] | Kinetic energy release (eV) | Figure (structure) |
|---|---|---|---|---|
| $O_2$ | $[O_2]^+$ | $O_2^+(X^2\pi_g) \rightarrow [O_2^{2+}(A^3\pi_g)](HR)$ | $7.3 \pm 0.3$ | 2(b) ($A_1/A_2$) |
| NO | $[NO]^+$ | $NO^+(X^1\Sigma^+) \rightarrow [NO^{2+}(4^3\pi)](HR)$ | $7.2 \pm 0.3$ | 3(b) ($A_1/A_2$, $B_1/B_1$) |
| $CH_4$ | $[CH]^+$ | $CH^+(X^1\Sigma^+) \rightarrow [CH^{2+}(A^2\pi)](HR)$ | $8.0 \pm 0.3$ | 4(b) ($A_1/A_2$) |
| | | $CH^+(X^1\Sigma^+) \rightarrow [CH^+(1^3\Sigma^+)](HR)$ | $5.0 \pm 0.5$ | 4(b) ($B^b$) |
| $NH_3$ | $[NH]^+$ | $NH^+(X^4\Sigma^-) \rightarrow [NH^{2+}](HR)$ | $7.5 \pm 0.3$ | 5(b) ($A_1/A_2$) |
| | | $NH^+(X^4\Sigma^-) \rightarrow [NH^+(2^4\Sigma^-)](HR)$ | $4.0 \pm 0.5$ | 5(b) ($B^b$) |
| $H_2O$ | $[OH]^+$ | $OH^+(X^3\Sigma^-) \rightarrow [OH^{2+}](HR)$ | $9.1 \pm 0.3$ | 5(b) ($A_1/A_2$) |
| | | $OH^+(X^3\Sigma^-) \rightarrow [OH^+(2^3\Sigma^-)](HR)$ | $4.5 \pm 0.5$ | 6(b) ($B^b$) |
| $CH_4$ | $[CH_4]^+$ | $CH_4^+ \rightarrow [CH_4^{2+}](HR)$ | $4.6 \pm 0.3$ | 7(b) ($A_1/A_2$; $B^b$) |
| $H_2$ | $[H_2]^+$ | $H_2^+(1s\sigma_g, v'=3) \rightarrow [H_2^{2+}](HR)$ | $8.1 \pm 0.2$ | 8(a) |
| $H_2O$ | $[H_2]^+$ | $H_2^+(1s\sigma_g, v'=1) \rightarrow [H_2^{2+}](HR)$ | $10.8 \pm 0.2$ | 8(b) |
| | | $H_2^+(1s\sigma_g, v'=1) \rightarrow [H_2^+(2p\sigma_u)](HR)$ | $4.4 \pm 0.2$ | 8(b) |
| $CH_4$ | $[H_2]^+$ | $H_2^+(1s\sigma_g, v'=1) \rightarrow [H_2^{2+}](HR)$ | $5.2 \pm 0.2$ | 8(c) |
| $H_2S$ | $[H_2]^+$ | $H_2^+(2s\sigma_g, v'=13) \rightarrow [H_2^{2+}](HR)$ | $4.5 \pm 0.2$ | 8(d) |

[a] The species in square brackets is the core ion orbited by the HR electron.
[b] Rectangular component of peak B.

# 2.6 keV Collisions of $[H_3]^+$ and Isotopomer Ions

## 2.6.1 Introduction

The $[H_3]^+$ molecule was discovered by J.J. Thomson in 1912 [222]. It is the simplest polyatomic molecule and has therefore been the subject of much experimental and theoretical work. Its chemistry has been studied extensively by mass spectrometric methods [223-226]. The dynamics of proton transfer reactions between $[H_3]^+$ and neutral molecules, the most important type of reaction of this ion, were investigated by Futrell and coworkers [227,228]. $[H_3]^+$ is also considered to be abundant in interstellar clouds and its significance in interstellar chemistry has been discussed in a recent review by Smith [229]. A large number of lines in the IR spectra of the active fundamental bands of $[H_3]^+$ and isotopomers have been observed in this decade. The ground state equilibrium geometry was found to have $D_{3h}$ symmetry. A recent paper by Watson et al [230] gives an extensive account of the experimental and theoretical work in this field. Carrington and Kennedy [231] observed a surprisingly large number of transition lines (ca 27,000) in the IR predissociation spectra of $[H_3]^+$. Their results indicated that a large number of metastable resonance states of $[H_3]^+$ exist above its dissociation limit. These observations have motivated theoretical work which promises to give new insights into molecular behaviour near the dissociation limit [232,233].

There have been several calculations on the excited electronic potential surfaces of $[H_3]^+$. The most thorough and accurate of these is the study of Schaad and Hicks [234]. They carried out configuration interaction calculations on the lowest five states of each symmetry $^1A'$, $^3A'$, $^1A''$ and $^3A''$, in the search for a stable excited state of $[H_3]^+$. All geometries having bond lengths between 1.2 and

3.6a.u. were examined. In addition, calculations were made at longer bond lengths to determine the dissociation limit of each potential surface. They also presented potential curves of the excited states for the equilateral triangle ($D_{3h}$) geometry. The two lowest singlet states of $[H_3]^+$ (the lower is the ground state) have received special attention by theoreticians because there is an avoided intersection between these states [235]. It was shown that nonadiabatic coupling along this intersection gives rise to the charge exchange products in $H^+ + H_2$ reactions. Tully has [236] reviewed the experimental and theoretical work related to that interaction.

There have been a number of investigations of the collisions between $[H_3]^+$ of keV translational energy and different target gases. Measurements were carried out to determine cross sections for H(n=2,3) production in order to obtain information relevant to the study of proton aurora in planetary atmospheres and to the diagnostics of high power beams of neutral hydrogen used in the supplementary heating of plasmas in Tokamak devices [237-240]. Goh and Swan [240] obtained the kinetic energy spectra of $[H_2]^+$ fragments from keV $[H_3]^+$/He collisions. They used their results to determine the binding energy of $[H_3]^+$. In 1985 Yenen and Jaecks [241] measured the polarization of $L_\alpha$ radiation (associated with H(n=2) production) in coincidence with the scattered $[H_2]^+$ resulting from the process:

$$[H_3]^+ + He \rightarrow ([H_3]^+)^* + He \rightarrow [H_2]^+ + H(n=2) + He \qquad (2.15)$$

for specific laboratory angles. They identified two processes which lead to the simultaneous generation of $[H_2]^+$ and H(n=2). These were the excitation of the fast $[H_3]^+$ upon collision with He into its $1^1A_2''$ and $2^1E'$ electronic states.

In the present work the kinetic energy spectra of $H^+(D^+)$ and $[H_2]^+([D_2]^+$, $[DH]^+)$ fragments from collisions between 9.9 keV $[H_3]^+([D_2H]^+)$ ions and rare gas targets will be presented. The analysis of these spectra provides new information

about processes leading to $H^+ + H_2$ fragments. We report the first observation of the involvement of a nonadiabatic transition in the collision induced dissociation of a polyatomic ion and on the validity of Wigner's spin-conservation rule in the electronic excitation of a polyatomic ion in ion-neutral collisions at keV energies. We also present and analyze kinetic energy spectra of metastable high-Rydberg (HR) fragments from 9.9 keV collisions between $[H_3]^+$, $[D_2H]^+$ and $[H_2D]^+$ projectiles and He target gas, and identify the processes generating them.

### 2.6.2 Experimental

All measurements were made with a VG Analytical ZAB 2F mass spectrometer of reversed geometry, which has been modified as described before.

Measurements were performed as follows. $[H_3]^+$ ions were generated by the 70 eV electron impact of $H_2$ gas through the reaction $[H_2]^+ + H_2 \rightarrow [H_3]^+ + H$. $[D_2H]^+$ and $[H_2D]^+$ ions were obtained by the 70 eV electron impact of a 1:1 mixture of $H_2$ and $D_2$ gases. Ions were generated under "high" and "low" source pressure conditions. These correspond to ca 1 torr and 0.01 torr ion source pressures, respectively. The ions were accelerated to 9.9 keV and were mass selected by the magnet into the second field free region of the mass spectrometer. Collision induced dissociation of $[H_3]^+$ and isotopomer ions was achieved by admitting collision gases (He, Ne, Ar, Kr and Xe respectively) into the first collision cell at a pressure that caused no more than 10% attenuation of the main ion beam. The kinetic energy spectra of the ionic fragments from these collisions were obtained by scanning the electric sector of the mass spectrometer in the usual way. Energy resolution was such that the main ion beam width at half height was 3V. Field ionization experiments, to obtain the kinetic energy spectra of HR fragments from

$[H_3]^+([D_2H]^+, [H_2D]^+)$/He collisions, were carried out with the meshes intersecting the ion beam path, the first mesh being charged to +1100V and the second mesh grounded, creating a 18 kV/cm field gradient between them. The main beam width at half height for these experiments was 10V, the lower energy resolution being necessary for sensitivity reasons. The data were signal averaged to get better signal to noise ratio. He collision gas was admitted to the first cell at a pressure corresponding to 20% beam attenuation. The deflector electrode was charged to +700V. The kinetic energy spectra of the ions resulting from field ionization were taken by scanning the electric sector. In this mode of operation, peaks due to fast, field ionizable species appear in the kinetic energy spectra centered near $[m_f/m_p+1100]$V where $m_f$ is the fragment mass and $m_p$ is the mass of the projectile ion. The same tests as described in section 2.5.2 were carried out to ensure that the field induced ion signals corresponded to HR species generated in single collision events.

### 2.6.3 Results and Discussion

#### The generation of ionic fragments

Fig.64(a) shows the kinetic energy spectra of ionic fragments from 9.9 keV $[H_3]^+$/He collisions, $[H_3]^+$ having been generated at "low" source pressure conditions. Fig.64(b) contains those for "high" source pressure conditions. The $[H_3]^+$ ions are formed in the ion source by the reaction $[H_2]^+ + H_2 \rightarrow [H_3]^+ + H$, which is exothermic by 40 kcal/mol. For this reason and because a substantial fraction of the $[H_2]^+$ ions formed by electron impact is vibrationally excited, the $[H_3]^+$ ions formed in "low" source pressure conditions will have a wide range of internal energies and are mostly vibrationally- rotationally highly excited. For these conditions the kinetic

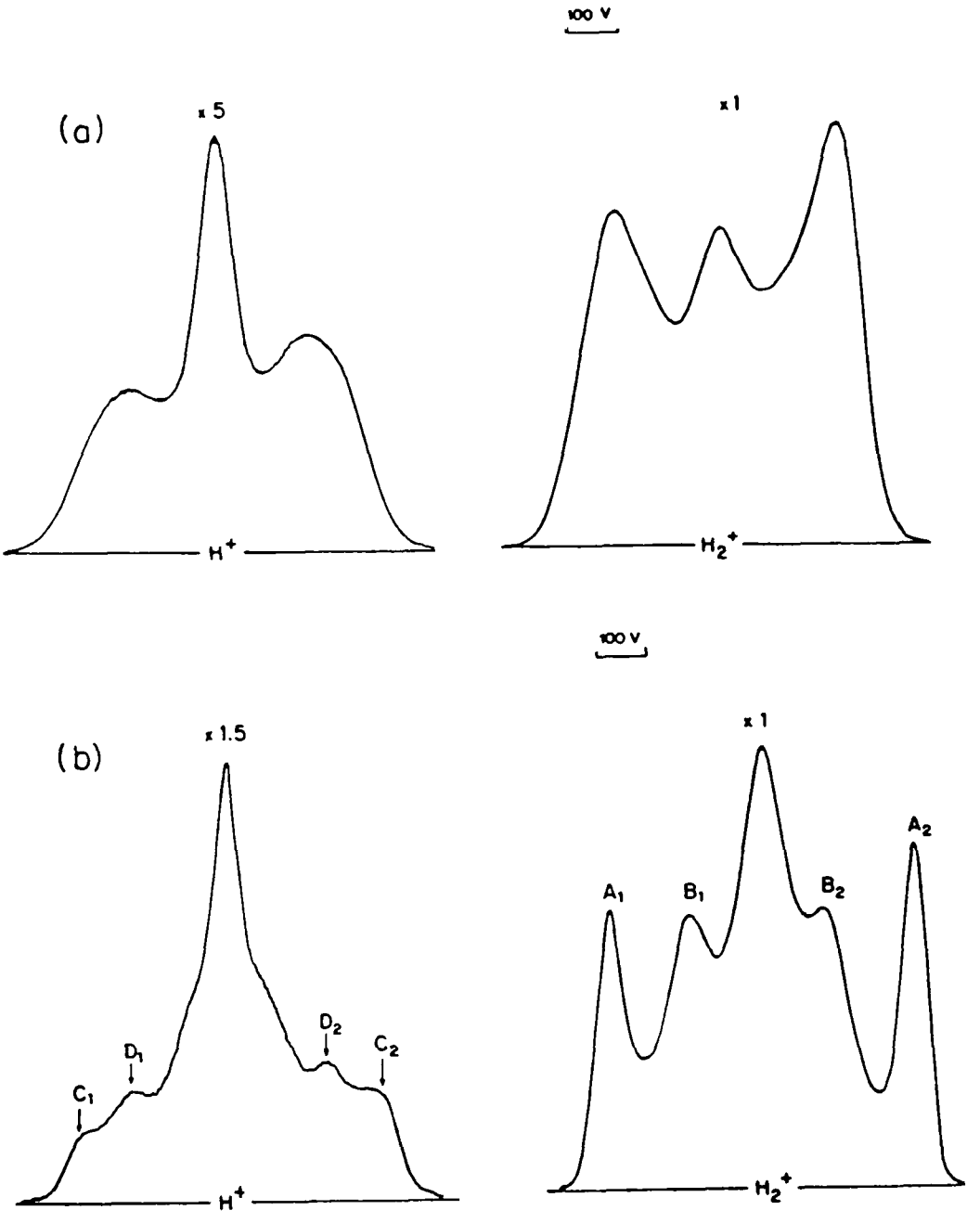


Figure 64 (a)Kinetic energy spectra of ionic fragments from 9.9 keV $[H_3]^+$/He collisions. $[H_3]^+$ ions were generated under "low" ion source pressure conditions. See text for discussion.
(b) Kinetic energy spectra of ionic fragments from 9.9 keV $[H_3]^+$/He collisions. $[H_3]^+$ ions were generated under "high" ion source pressure conditions. See text for discussion.

energy spectra of all fragment ions contained a central peak flanked by a dished peak. Central narrow peaks were present in all the spectra presented in this work. They originate from dissociations involving small amounts of KER (<0.2 eV), such as vibrational dissociation, and their intensity is overestimated by at least an order of magnitude relative to the dished peaks in the spectra as a result of instrumental discrimination effects. *The following discussions therefore will concentrate on the dished peaks in the spectra.* The distance across the maxima of the dished part of the $[H_2]^+$ peak corresponds to 5.3±0.3 eV KER. The presence of the dished component indicates that transitions to the repulsive electronic states of $[H_3]^+$, giving rise to a large KER, play an important role in generating ionic fragments. Because the internal energy of the projectile molecular ions is badly defined, it is not possible on the basis of fragment ion kinetic energy spectra, to determine which electronic states are involved.

It has been observed that the vibrationally highly excited $[H_3]^+$ ion can relax rapidly into its lower vibrational levels in collisions with $H_2$ molecules. "High" source pressure conditions will therefore favour such a process. Blakley et al. [242] characterized the degree of deexcitation in $[H_3]^+$ ions obtained from a chemical ionization source containing $H_2$ gas at pressures of 0.1 torr and 0.5 torr. Under "high" pressure conditions there is ca 1 torr pressure in the ion source of our apparatus. The vibrational energy distribution in the $[H_3]^+$ beam under these conditions must be similar to that shown in Table 5. (Note that the vibrational energy content is not precisely defined because there is no differentiation between the three normal modes of $[H_3]^+$, two of which are degenerate. Only the number of an average vibrational quantum is given.) From Table 5 it can be seen that in this case the internal energy content of the $[H_3]^+$ ion beam is quite well defined; ca 80% are in their vibrational ground state or contain only one vibrational quantum. The

spectra in Fig.64(b) show well defined features. The spectrum of the $[H_2]^+$ fragment contains two dished peaks $A_1/A_2$ and $B_1/B_2$, which correspond to most probable KER values of 10.0±0.2 eV and 2.0±0.2 eV, respectively. In 1981 Goh and Swan [66] showed that in keV $[H_3]^+$/He collisions the process generating $[H_2]^+$ ions with the largest KER is vertical excitation of the $[H_3]^+$ projectile into its first singlet excited electronic state which dissociates into $[H_2]^+$+H(1s).

**Table 5 Distribution of vibrational excitation energy in $[H_3]^+$ ion beams generated in a electron impact ion source at 0.5 torr pressure, as obtained from the analysis of translational exoergicity distributions for the endoergic reaction $[H_3]^+$+Ar→$H_2$+$[ArH]^+$, taken from ref.228. (a) Number of mean quanta in $[H_3]^+$ reactant with $[H_3]^+$ represented as a triply degenerate harmonic oscillator. (b) Vibrational excitation energy of $[H_3]^+$, not including zero point energy, assuming a mean quantum of 0.4 eV.**

| $n([H_3]^+)^a$ | $E^{*b}$ | Fractional population |
|---|---|---|
| 0 | 0 | 0.51 |
| 1 | 0.4 | 0.29 |
| 2 | 0.8 | 0.14 |
| 3 | 1.2 | 0.06 |

We therefore assign the $A_1/A_2$ peak to this process. It will be shown below that dissociation over the $C_{2v}$ potential surface of the first singlet excited electronic state of $[H_3]^+$ must almost exclusively lead to $[H_2]^+$(v=0)+H(1s) products, because the trajectories leading to vibrationally excited $[H_2]^+$ fragments cross over to the ground state potential surface. On the basis of this information the energy of the dissociative state can be obtained from the measured KER. Furthermore, because the

collision induced electronic transitions are vertical at these relative velocities (collision time $10^{-16}$ s), information about the initial state of the projectile ion can be inferred. As mentioned in the introduction, Schaad and Hicks [234] have published the potential curves for excited electronic states of $[H_3]^+$ for the equilateral triangle geometry ($D_{3h}$ symmetry) as a function of the length of the side of the triangle. Using their diagrams we determined that transition to the $1^1E'$ state at an equilateral triangle geometry with sides of 1.1Å will give rise to $[H_2]^+(v=0)+H(1s)$ products with a KER of 10.0eV. $[H_3]^+$ has equilateral triangular geometry with sides of 1.1Å at the outer turning point of the $1\nu_1$ (symmetric stretch) vibrational state [243]. We propose, for the $A_1/A_2$ structure in Fig.64(b), that vertical transition from the outer turning point of the $1\nu_1$ vibrational state into the $1^1E'$ electronic state is responsible for the 10.0±0.2 eV KER. This is in keeping with the vibrational distribution of Table 5; note that although the vibrational ground state is the most populated, electronic transitions at the equilibrium internuclear distance of the ground state are much more endothermic and therefore have a smaller probability than those from the outer turning point of the $1\nu_1$ state. Based on the above discussions we have chosen an equilateral triangle with sides of 1.1Å as the characteristic ground state geometry for $[H_3]^+$ produced under "high" ion source pressure conditions and from which vertical excitations to higher, dissociative electronic states occur upon collision. This selection is also in agreement with results of the Coulomb explosion experiments of Gaillard et al. [244], who obtained a most probable geometry in a beam of $[H_3]^+$ ions corresponding to an equilateral triangle with ca. 1Å sides. Using the selected geometry as a parameter and the potential curves of Schaad and Hicks [233] we can determine the expected KER received by the fragments resulting from collisional excitation to a given excited state. Table 6 lists the first five singlet and the first

Table 6 Energetics of the collision induced dissociation of $[H_3]^+$ (geometry: equilateral triangle, 1.1 Å sides) through vertical electronic excitation. See text for discussion.

| Dissociative states and transition energy (eV) | | Dissociation products | Maximum KER (eV) | Minimum KER (eV) |
|---|---|---|---|---|
| $1\,^1E'$ | 15.5 | $2H(1s) + [H]^+$ | 7.2 | 7.2 |
| | | $[H_2]^+(X^2\Sigma_g^+) + H(1s)$ | 10.0 | 7.4 |
| $1\,^1A_2''$ | 18.9 | $[H_2]^+(X^2\Sigma_g^+) + H(2p)$ | 3.2 | 0.6 |
| $2\,^1A_1'$ | 20.9 | $H_2(B^1\Sigma_u^+) + [H]^+$ | 6.0 | 2.5 |
| $2\,^1E'$ | 23.8 | $[H_2]^+(X^2\Sigma_g^+) + H(2s)$ | 8.0 | 5.4 |
| $1\,^1E''$ | 23.8 | $H_2(C^1\pi_u) + [H]^+$ | 7.7 | 5.2 |
| | | $H_2(I^1\pi_g) + [H]^+$ | 6.1 | 4.9 |
| $1\,^3E'$ | 10.3 | $[H_2]^+(X^2\Sigma_g^+) + H(1s)$ | 5.2 | 2.6 |
| $1\,^3A_2''$ | 17.2 | $H_2(c^3\pi_u) + [H]^+$ | 1.8 | 0.0 |
| $1\,^3A_1'$ | 19.6 | $H_2(a^3\Sigma_g^+) + [H]^+$ | 4.1 | 1.2 |
| $2\,^3E'$ | 23.2 | $[H_2]^+(X^2\Sigma_g^+) + H(2s)$ | 7.4 | 4.8 |
| $1\,^3E''$ | 23.8 | $[H_2]^+(X^2\Sigma_g^+) + H(2p)$ | 8.0 | 5.4 |
| | | $H_2(i^3\pi_g^+) + [H]^+$ | 6.2 | 5.0 |

five triplet states. It includes the energy requirement for transition to a given state, the products to which that state can lead, and the maximum (no vibrational excitation in the molecular fragment ) and minimum (determined by the dissociation energy of the molecular fragment, taken from [245]) amount of KER they can receive. In the following discussions we will rely on this table to relate observed KER's to particular excitation processes. From Table 6 it is clear that only excitation into the $1^1A_2''$ electronic state, dissociating into $[H_2]^+$(v=2)+H(1s), can give rise to the 2.0±0.2 eV KER associated with the $B_1/B_2$ structure in Fig.64(b). We note that Yenen and Jaecks have already shown that this process plays an important role in keV $[H_3]^+$ collisions [241].

The two most important processes for $[H_2]^+$ production involve transitions to the two lowest singlet states of $[H_3]^+$, in spite of the fact that excitation to the first triplet state ($1^3E'$) is less endothermic than that to the $1\ ^1E'$ or $1\ ^1A_2''$ states by 4.8eV and 8.6eV respectively. Based on the possible range of KER for the $1^3E'$ state (see Table 6), excitation to this state should give rise to a pair of peaks in the kinetic energy spectrum in Fig.64(b) that would fall between $A_1$ and $B_1$, and $B_2$ and $A_2$. There is no sign of the presence of such a structure. These observations imply that in keV $[H_3]^+$/He collisions, the Wigner total-spin-conservation rule [52,53] is strictly obeyed.

There have been no previous investigations of the processes leading to $[H]^+$ fragments in keV collisions of $[H_3]^+$. Fig.64(b) contains the kinetic energy spectrum of the $H^+$ fragments from 9.9keV $[H_3]^+$/He collisions, ($[H_3]^+$ generated under "high" ion source pressure conditions). The central part has two components, a narrow Gaussian type peak and a broad extended peak. The narrow part, corresponding to KER<0.1 eV, is most probably the result of dissociation due to vibrational excitation. We propose that the broad part originates from the three body dissociation of $[H_3]^+$

from the $1^1E'$ excited state into $2H(1s)+H^+$. Because this is a three body dissociation there are very few restrictions on the shape of the $H^+$ peak in the kinetic energy spectrum corresponding to this process. That this broad feature is absent for collision gases which do not cause excitation to the $1^1E'$ state (see Fig.68 below) supports our assignment. There are also two dished peaks present, $C_1/C_2$ and $D_1/D_2$ in the $H^+$ spectrum in Fig.64(b). The maxima of the $D_1/D_2$ structure are separated by 390V. For a two body dissociation (into $H_2+H^+$ fragments) the corresponding KER is 4.3±0.2 eV. From the data in Table 6 the origin of this KER must be excitation to the $2^1A_1'$ state, dissociating into $H_2(B^1\Sigma_g^+,v=10)+H^+$. The $C_1/C_2$ structure can be deconvoluted from $D_1/D_2$ to give a dished peak having maxima separated by 595V, i.e. equal to that for the $A_1/A_2$ peak. That this is indeed reasonable can be seen more clearly in the spectra for $[D_2H]^+$/He (see Fig.66 below) and $[H_3]^+$/Ne collisions (see Fig.68 below). The separation of 595V in the kinetic energy spectrum for the forward and backward scattered $H^+$ fragments, corresponds to 10 eV KER for a two body dissociation (a three body dissociation would require a much larger KER). There is no excited state of $[H_3]^+$ correlated to $H_2+H^+$, which could support a KER of this magnitude. Excitation into the ground state $[H_3]^{2+}$ surface could give 10eV KER for $[H_2]^+ + H^+$ products (the ground state potential energy surface for $C_{2v}$ $[H_3]^{2+}$ is shown later, see Fig.70). However, there is very strong evidence that this cannot be the case. First, using the results of Rumpf et al. [246], who calculated the discrimination against slower fragments in a mass spectrometer having similar dimensions to our apparatus, we estimate that $C_1/C_2$ has the same absolute intensity as $A_1/A_2$. This means that if the $H^+$ fragments forming $C_1/C_2$ originate from the process

$$[H_3]^+ + He \rightarrow [H_3]^{2+} + He + e^- \rightarrow [H_2]^+ + H^+ + He + e^- \qquad (2.16)$$

then the $[H_2]^+$ fragments forming $A_1/A_2$ should also solely be generated by this mechanism. That would contradict the experimental results of Goh and Swan [240] discussed above. More compelling evidence against the above mechanism is contained in the results relating to the production of high-Rydberg (HR) fragments which are discussed in the third section below. It will be shown that the H(HR) fragment from keV $[H_3]^+$/He collisions originates from vertical excitation of $[H_3]^+$ into a HR state having a $[H_3]^{2+}$ ionic core. Therefore the H(HR) kinetic energy spectrum and that of $H^+$ fragments generated directly from excitation into $[H_3]^{2+}$ should be the same. However it will be seen (Fig.69(b)) that the separation between the maxima of the dished peak for H(HR) fragments is only 450V and not 595V (see above), because the $[H_3]^{2+}$ core dissociates into three species $2H^+$+H(1s).

Returning to Table 6 we observe that excitation into the $1^1E'$ state could give a maximum KER of 11.8eV if it dissociated into $H_2(X^1\Sigma_g^+,v=0)+H^+$, ($H_2(X^1\Sigma_g^+)+H^+$ is lower in energy by 1.8 eV than $[H_2]^+$+H(1s)). The first singlet excited state of $[H_3]^+$ does not correlate adiabatically to the former products. However, there is an avoided intersection between the first singlet excited state and the ground state of $[H_3]^+$, along which there is strong nonadiabatic coupling between these two states [247]. Thus, when the trajectory of the dissociating $[H_3]^+$ over the first singlet excited state hypersurface crosses the region of the avoided intersection, a transition to the ground state surface can take place. The ground state is bound for small internuclear distances, but is repulsive in the region of the avoided intersection leading into $H_2(X^1\Sigma_g^+)+H^+$. Fig.65 shows a part of the first singlet excited state potential surface for isosceles triangle geometry ($C_{2v}$ symmetry) as calculated by Bauschlicher et al. [236].

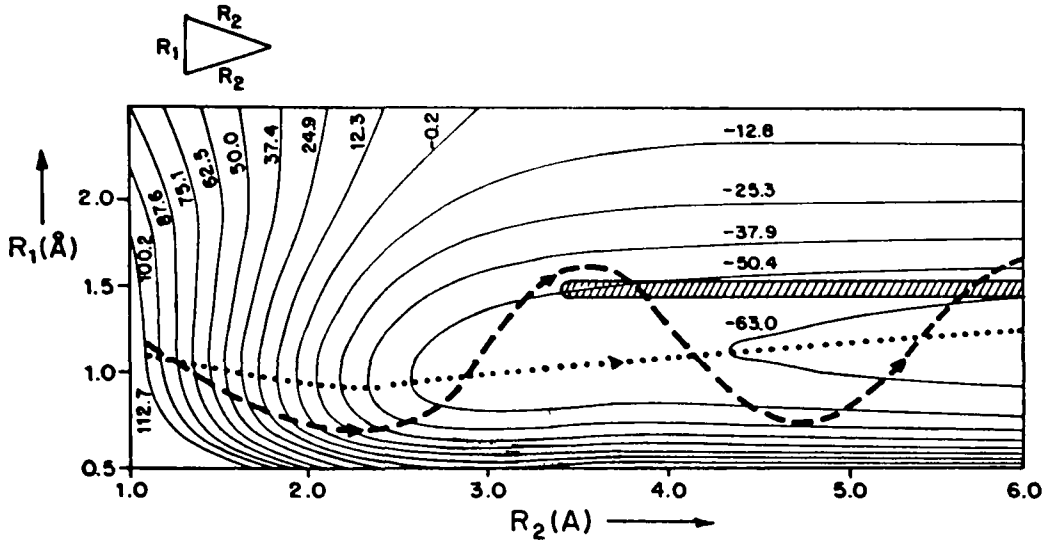


Figure 65. Potential diagram for the $1\,^1A_1$ state of $[H_3]^+$. Energy is given in $kcalmol^{-1}$

The shaded area is the region for which the probability of transition to the ground state surface is close to unity. Two hypothetical trajectories are drawn over the surface. One (dotted line) leads to $[H_2]^+(v=0)+H(1s)$ products; the other (broken line) leads to $[H_2]^+(v=1)+H(1s)$ products. It can be seen that the trajectory giving $[H_2]^+$ with one quantum of vibrational excitation crosses the shaded region and therefore has a large probability for crossing to the lower surface. Trajectories leading to $[H_2]^+$ fragments containing more than one vibrational quantum would also cross over to the lower surface with high probability. Only the trajectory giving $[H_2]^+$ in its vibrational ground state does *not* cross the region of large nonadiabatic interaction. We therefore expect that all the available internal energy of the collisionally generated $[H_3]^+(1\,^1E')$ will appear as KER for the fragmentation into $[H_2]^+$+H(1s). Another noteworthy feature is that the region of large transition probability is restricted to a narrow area corresponding to 1.32Å H-H distance and with the third nucleus being far removed ($R_2$>3.2 Å). 1.32 Å is the internuclear distance at the

outer turning point of the v=4 vibrational state of $H_2(X^1\Sigma_g)$. It is very likely that from these crossing points to the ground state potential surface, i.e. for which the H-H distance is always 1.32 Å, the $[H_3]^+$ dissociates into $H_2(X^1\Sigma_g,v=4)+H^+$ products which are 1.85eV above the $H_2(X^1\Sigma_g,v=0)+H^+$ products. This energy is equal to the difference between the measured KER (10.0eV) and the total available energy (11.8eV) for the translational excitation of the fragments.

The kinetic energy spectra of the ionic fragments from 9.9keV $[D_2H]^+$/He collisions, shown in Fig.66, supply additional evidence that the nonadiabatic transition between the first excited and ground singlet states plays an important role in generating hydrogen ions. For $[D_2H]^+$ in its symmetric stretch vibrational mode, the characteristic geometry is an isosceles triangle because the light H nucleus will oscillate about its equilibrium position with a greater amplitude than the heavier D nuclei. However, after analyzing the kinetic energy spectra we found that the same processes are operative in $[D_2H]^+$/He as in $[H_3]^+$/He collisions.

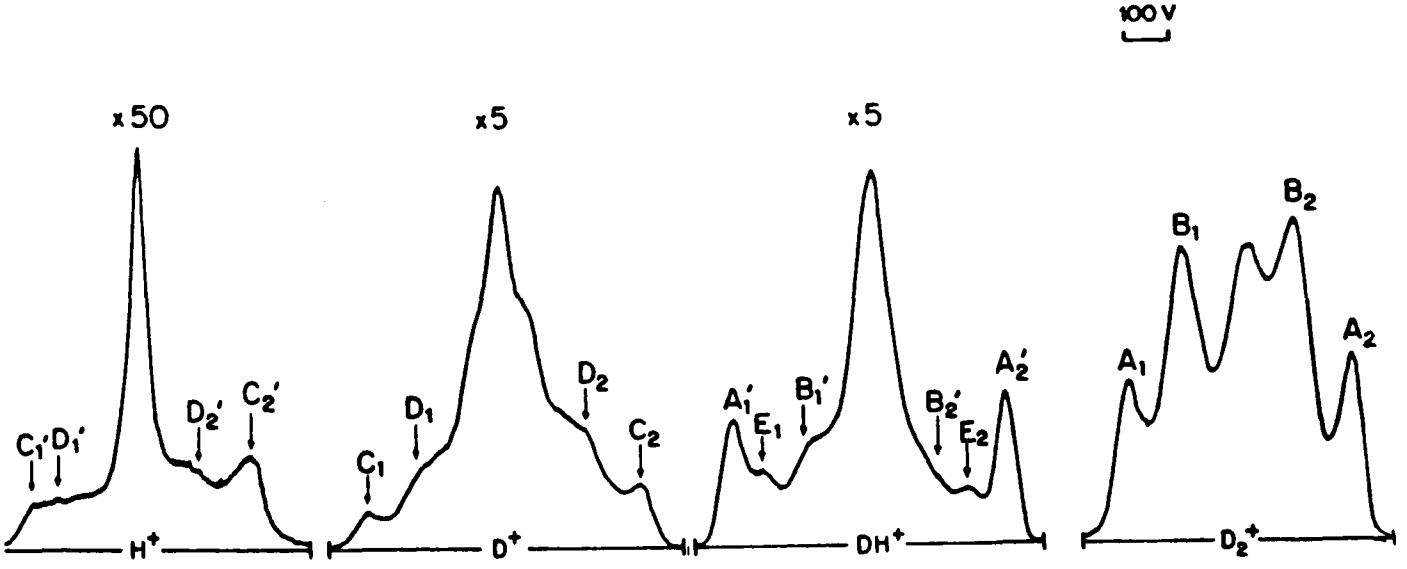


Figure 66. Kinetic energy spectra of ionic fragments from 9.9 keV $[D_2H]^+$/He collisions. $[D_2H]^+$ ions were generated under "high" ion source pressure conditions.

The KER's for the dished peaks in the $[D_2]^+$ and $[DH]^+$ spectra are: 9.8±0.2 eV for $A_1/A_2$, 10.0±0.2eV for $A_1'/A_2'$, 2.3±0.2 eV for $B_1/B_2$ and $B_1'/B_2'$. Comparing these data with those for the $[H_2]^+$ spectrum in Fig.64(b) we conclude that the same processes lead to the generation of $[D_2]^+$ and $[DH]^+$ fragments in keV $[D_2H]^+$/He as for $[H_2]^+$ generation in $[H_3]^+$/He collisions. These are excitation to the first and second singlet excited states respectively. If discrimination effects for ionic fragments of different mass [246] are taken into account, it can be shown that dissociation from the first singlet excited state gives ca equal amounts of $[D_2]^+$ and $[DH]^+$; on the other hand dissociation from the second singlet excited state gives at least ten times more $[D_2]^+$ than $[DH]^+$. In the $[DH]^+$ spectrum there is also a weak new feature (not seen in Fig.64(b)), $E_1/E_2$ which corresponds to a 5.7±0.3eV KER. We assign this feature to excitation to and dissociation from the fourth singlet excited state (2 $^1E'$ in $D_{3h}$ symmetry), a process which has been shown by Yenen and Jaecks [241], to be operative in generating $[H_2]^+$+H(2s) fragment pairs in keV $[H_3]^+$/He collisions. The $E_1/E_2$ feature is very weak, which is not surprising considering that the transition involved in its production is so much more endothermic than those corresponding to other features (see Table 6). The KER for $D_1/D_2$ and $D_1'/D_2'$ is 4.3±0.3eV, the same as for $D_1/D_2$ in Fig.64(b) and we conclude that the mechanisms involved are also the same. In the $D^+$ spectrum there is a well defined dished peak, $C_1/C_2$ having the same separation across its maxima as that for $A_1'/A_2'$ in the $[DH]^+$ spectrum, and in the $H^+$ spectrum the distance between $C_1'/C_2'$ is the same as that between $A_1/A_2$ in the $[D_2]^+$ spectrum. The appearance of dished peaks in the kinetic energy spectra of $D^+$ and $H^+$ fragments corresponding to such large separations can only be due to the process described above for the generation of $C_1/C_2$ structure in Fig.64(b)

**The dependence of the validity of Wigner's total-spin-conservation rule on the nature of the collision gas**

Fig.67 shows the kinetic energy spectra of $[H_2]^+$ fragments from collisions between $[H_3]^+$ ions (generated under "high" ion source pressure conditions) having 9.9 keV translational energy and Ne,Ar,Kr and Xe targets. For Ne as target, the same features as for He can readily be observed. However, the spectra for Ar,Kr and Xe targets are completely different. The major new feature is $A_1'/A_2'$ in all three and $A_1/A_2$, which was important for He and Ne, is now only a minor signal. There is a KER of 4.6±0.2 eV associated with this new dished peak. *Only* a transition to the $1^3E'$ *triplet* state, followed by dissociation into $[H_2]^+$+H(1s) can give rise to a KER of this magnitude. Transition to the $1^3E'$ state is 4.8eV less endothermic than that to the $1^1E'$ state but is forbidden by Wigner's total-spin-conservation rule [52,53] and was not observed for He and Ne targets. Apparently the spin-conservation rule breaks down for Ar, Kr and Xe and the less endothermic process becomes the more important. An alternative explanation is that the targets are excited simultaneously to a triplet state. In this case the total spin would be conserved, but the first such excited state lies 11.5eV above the ground state for Ar, 9.9eV for Kr and 8.3eV for Xe, [248]. Therefore these latter alternatives would be *more* endothermic, by 6.7eV for Ar, 5.1eV for Kr and 3.5eV for Xe, than excitation to the $1^1E'$ state and therefore are very unlikely to be responsible for the observations.

The same behaviour is observable in the $H^+$ spectra which are shown in Fig.68. The spectrum for Ne is again very similar to that for He, but those for Ar, Kr and Xe are completely different. There is a new feature ($B_1'/B_2'$), the importance of which increases from Ar to Xe, associated with a KER of 1.7±0.3eV . The best candidate for its origin is again a spin-forbidden transition to the $1^3A_2''$ state, which dissociates into $H_2(c^1\pi_u)$+$[H]^+$ (see Table 6). This transition is less

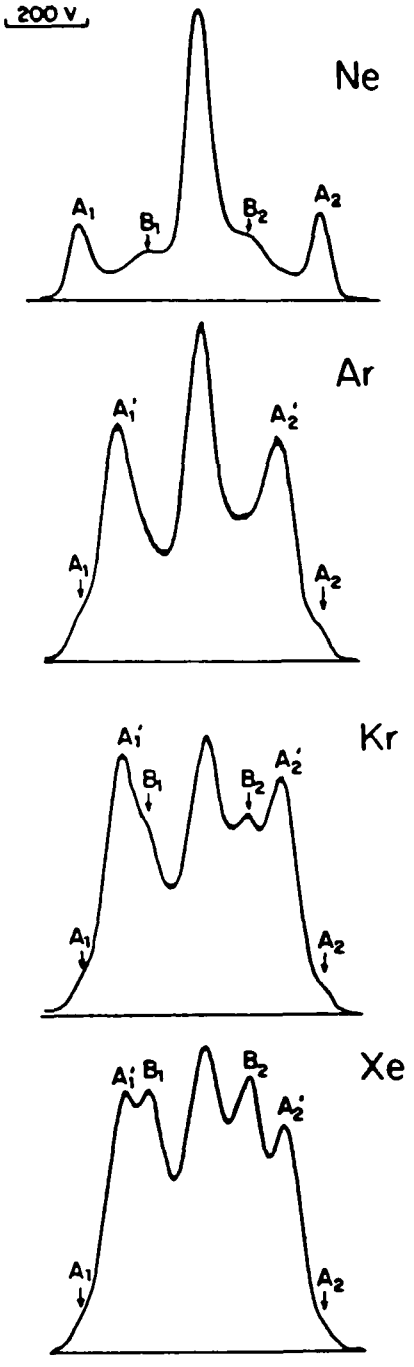


Figure 67 Kinetic energy spectra of the $[H_2]^+$ fragment from 9.9 keV collisions between $[H_3]^+$ ions and rare gas targets (Ne, Ar, Kr, Xe). $[H_3]^+$ ions were generated under "high" ion source pressure conditions. See text for discussion.

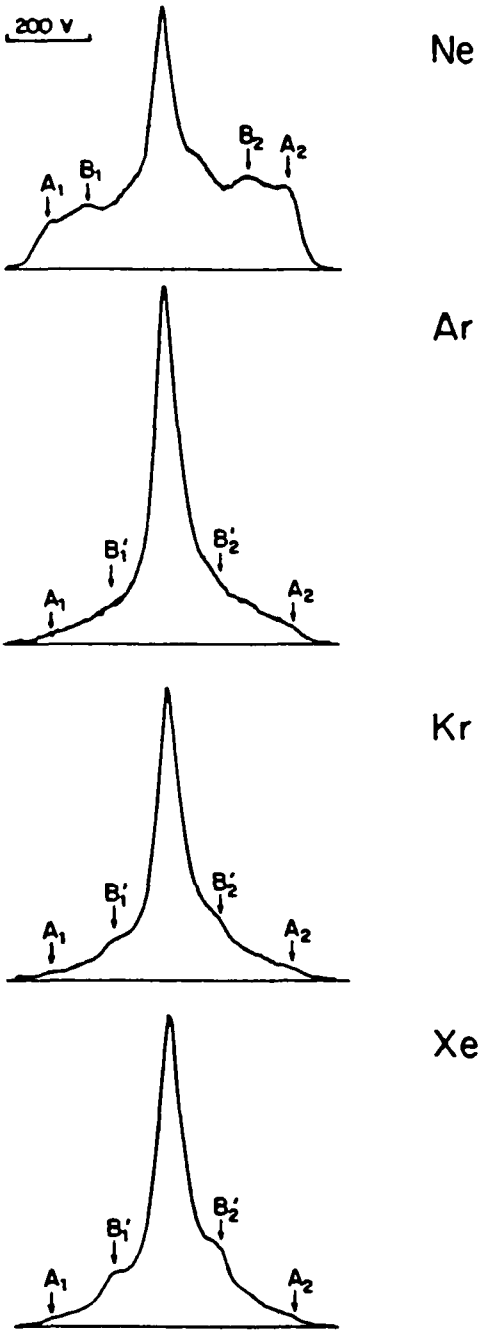


Figure 68 Kinetic energy spectra of the $H^+$ fragment from 9.9 keV collisions between $[H_3]^+$ ions and rare gas targets (Ne, Ar, Kr, Xe). $[H_3]^+$ ions were generated under "high" ion source pressure conditions. See text for discussion.

endothermic by 3.7eV than that leading to the $2^1A_1$' state. Wigner's spin-conservation rule would be obeyed for this process only if there were a simultaneous excitation to the triplet states of the rare gas targets. However, such an excitation would be more endothermic, by 7.8eV for Ar, 6.2eV for Kr and 4.6eV for Xe, than the excitation to the $2^1A_1$' state and is therefore again considered to be very unlikely.

We have also recorded kinetic energy spectra of ionic fragments from collisions between $[H_3]^+$ ions of 9.9keV translational energy and the diatomic targets, $H_2$, $D_2$, $N_2$. The spectra obtained were closely similar to those obtained for Ar as target gas. To our knowledge the present results provide the first observation relating to the validity of Wigner's total-spin-conservation rule in collisions between *polyatomic* ions and neutral targets. Formerly, Moore [50,51] carried out experiments to examine Wigner's total-spin-conservation rule in keV collisions between $N^+$ atoms and a variety of targets. He found that for He, Ne, Ar and $N_2$ targets the spin-conservation rule strongly holds, but for heavier targets (Kr, Xe, $O_2$) spin-nonconservative transitions can occur with high probability. This was attributed to the change from the (L,S) coupling which is valid for lighter atoms, to (j,j) coupling which applies to heavier atoms.

### Generation of HR fragments

Fig.69(a) shows the kinetic energy spectra of HR fragments from 9.9keV $[H_3]^+$/He collisions for $[H_3]^+$ generated under "low" source pressure conditions; those for "high" source pressure conditions can be found in Fig.69(b). An unusual feature of the spectra of the $H_2$(HR) fragments is that the baseline at the low energy end of the peak is considerably higher than that at the high energy end; for H(HR) it is at approximately the same level on both sides. We explain this observation as follows:

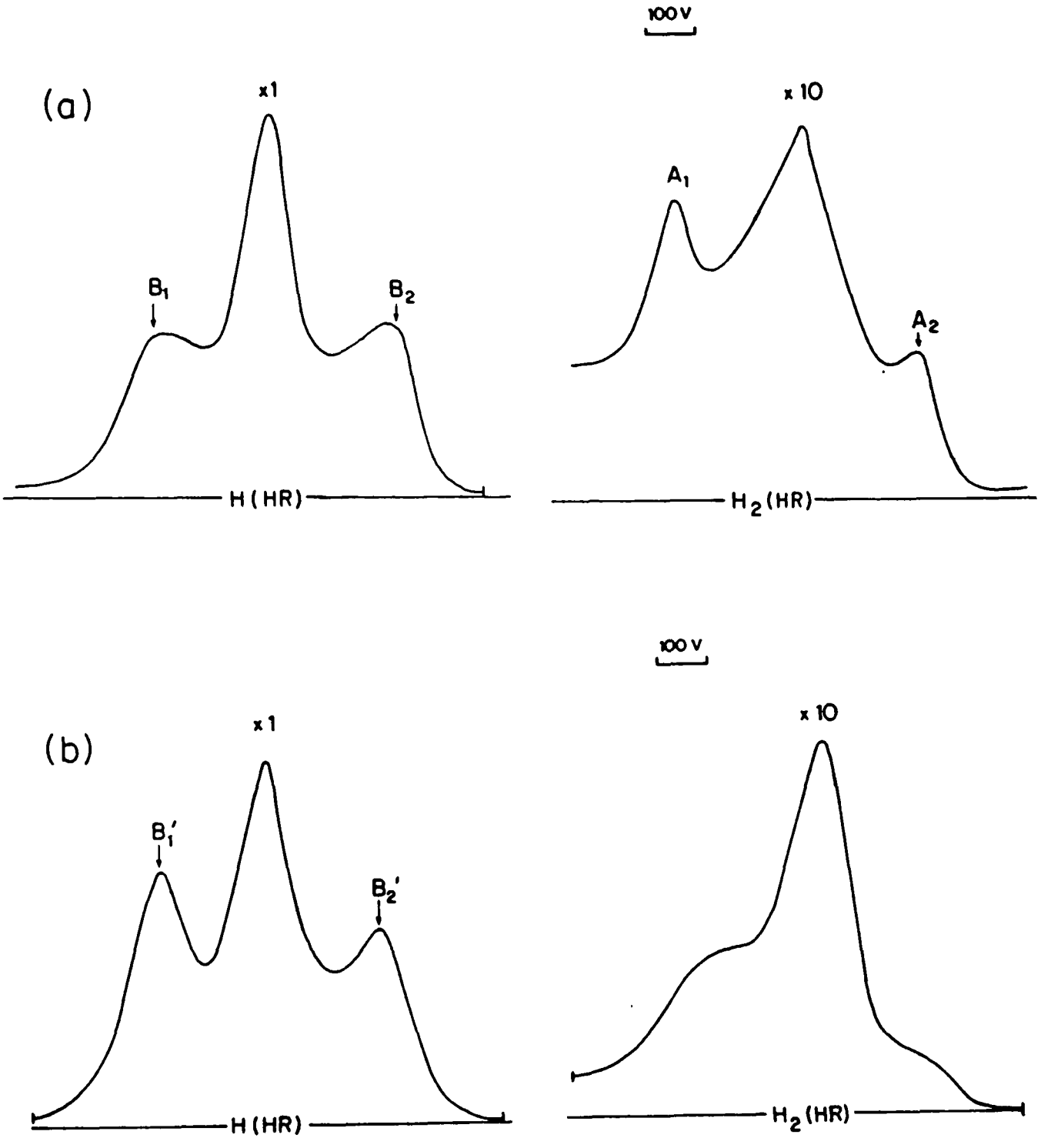


Figure 69 (a) Field induced ion kinetic energy spectra of HR fragments from 9.9 keV $[H_3]^+$/He collisions. $[H_3]^+$ ions were generated under "low" ion source pressure conditions. See text for discussion.
(b) Field induced ion kinetic energy spectra of HR fragments from 9.9 keV $[H_3]^+$/He collisions. $[H_3]^+$ ions were generated under "high ion source pressure conditions. See text for discussion.
The potential energy is in hartrees. See text for discussion.

A $H_2$(HR) molecule can be very well described as consisting of a $[H_2]^+$ ionic core with an electron in a far removed orbit (hundreds of angstroms in diameter, binding energy<0.2 eV). The $[H_2]^+$ core can be rotationally and vibrationally excited; the HR electron has a very small but finite probability to be at the $[H_2]^+$ core, a situation in which it can receive some of the core's rovibrational energy, thus leading to ionization. It has been shown theoretically by Band [218] that the rate of this autoionization process depends strongly on the rovibrational state of the core and on the angular momentum of the HR electron, resulting in a wide range of possible lifetimes for the $H_2$(HR) molecules. Field ionization in our apparatus takes place at the first mesh, where the fast HR species enter the high electric field gradient between the meshes. Ions formed at the first mesh will be accelerated by 1100V (the potential between the first and second mesh). However, some of the autoionizing $H_2$(HR) molecules can have lifetimes corresponding to their passage between the first mesh and the grounded plate preceding it. $[H_2]^+$ ions thus generated will receive less acceleration than those generated at the first mesh, and will give a continuous background signal which falls off sharply at the high energy side of the peak. All the spectra in Figs.69(a) and 69(b) contain two components, a narrow central peak flanked by a broad dished structure. In the forthcoming discussion we will concentrate on the broad features in these spectra.

The $H_2$(HR) spectrum in Fig.69(a) ("low source pressure conditions) contains an extended dished peak $A_1/A_2$ associated with a most probable KER of 7.8±0.3 eV. In the kinetic energy spectrum of the H(HR) fragments there is also a dished structure $B_1/B_2$. The arrows at $B_1/B_2$ are the same distance apart as those at $A_1/A_2$. We propose that the origin of $A_1/A_2$ and the major part of $B_1/B_2$ is as follows. Some of the $[H_3]^+$ projectiles upon collision with the He target will be excited into one of their HR states, which can be described as an $[H_3]^{2+}$ ionic core surrounded by

an electron in HR orbit. The $[H_3]^{2+}$ core will dissociate into $[H_2]^+ + H^+$ giving rise to the observed KER; when the fragments are separated, the HR electron will join either the $[H_2]^+$ or $H^+$ giving rise to $H_2$(HR) and H(HR), respectively. Fig.70 shows the ground state ($1^2A_1$) potential energy surface of $[H_3]^{2+}$ for isosceles triangle geometry, as calculated by Conroy [249].

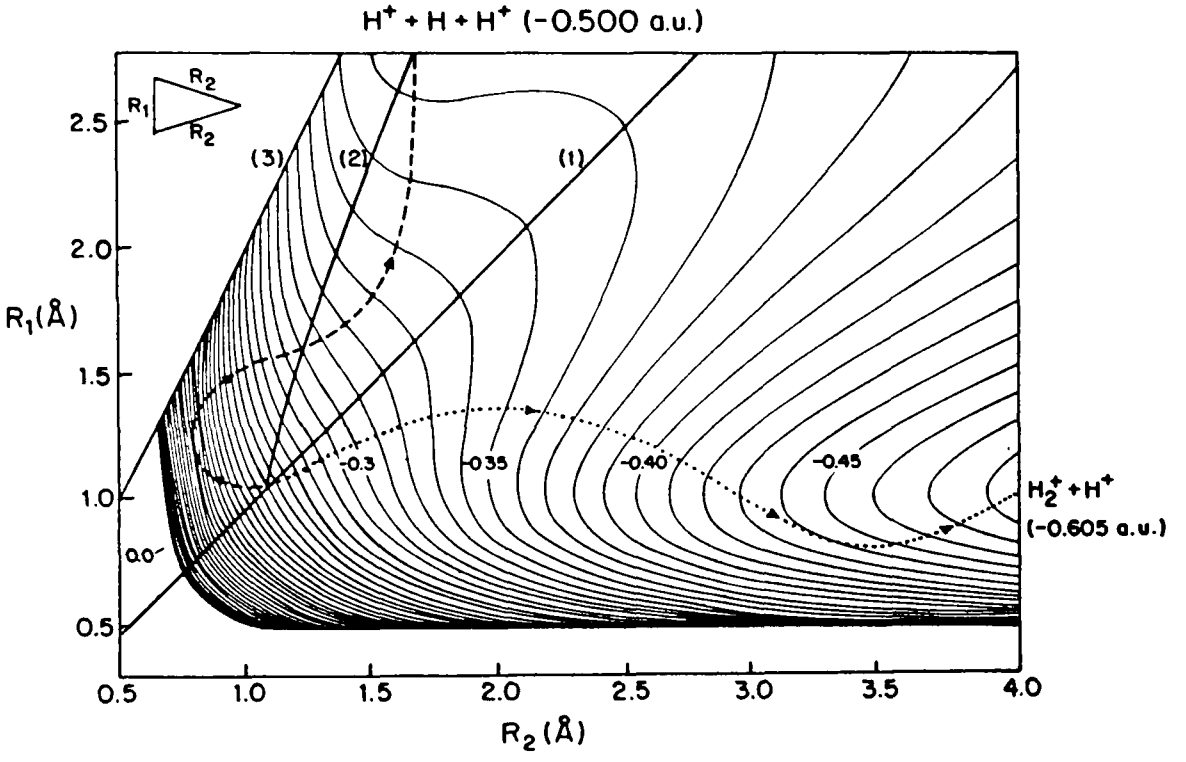


Figure 70. Potential energy diagram for the ground, $1^2A_1$, state of $[H_3]^{2+}$ The energy is given in hartrees.

It can be seen that dissociation over this surface into $[H_2]^+ + H^+$ can easily support a 7.8±0.3 eV KER. The mechanism described above is also in keeping with the conclusions reached in other sections of this thesis (2.5.3 and 2.5.5) in which we presented and analysed kinetic energy spectra of HR fragments from keV collisions between small ions ($[H_2]^+$, $[N_2]^+$, $[CH]^+$, $[CH_4]^+$ etc.) and rare gas targets (He, Xe). It was found that in the case of He as target gas, excitation to HR states converging to repulsive doubly charged states of the projectile ions, (designated as

process 2), always generated HR fragments. The potential surface in Fig.70 is divided into two parts by line(1) (joining the points on the surface that correspond to equilateral triangle geometry), the area above it leads to a plateau corresponding to $2H^+$+H(1s) and the area below it to $[H_2]^+$+$H^+$. The $B_1/B_2$ structure is less dished than $A_1/A_2$ in Fig.69(a) which indicates that in some cases the vertical excitation of $[H_3]^+$ will lead to HR states, the $[H_3]^{2+}$ core of which, dissociates into three fragments $2H^+$+H(1s). In this case the $[H_3]^+$ projectiles can have a wide range of vibrational states and so vertical transitions from many different nuclear geometries can contribute to the kinetic energy spectra.

The kinetic energy spectra in Fig.69(b), obtained for "high" source pressure conditions, are very different from those of Fig.69(a). As was shown in the first discussion section, the characteristic nuclear geometry of $[H_3]^+$ generated under "high" source pressure conditions, (from which vertical electronic transitions occur upon collisions), is an equilateral triangle with 1.1Å sides. Vertical excitation from this geometry to the $[H_3]^{2+}$ surface will end at line(1). The initial momenta of the nuclei of this species will determine their dissociation into $[H_2]^+$+$H^+$ or $2H^+$+H(1s) fragments over the $1^2A_1$ surface. The ground state $[H_3]^{2+}$ ion having the characteristic geometry, has an internal energy that should yield at least 7.5eV KER when it dissociates into $[H_2]^+$+$H^+$ ($[H_2]^+$ being produced just below its dissociation limit). Using equation (1.24), it can be calculated that $H_2$(HR) and H(HR) fragments corresponding to the dissociation of such an ionic core would give rise to dished peaks with *at least* 510V between their maxima. However, in the spectrum of H(HR) in Fig.69(b) there is a strongly dished structure $B_1'/B_2'$ with maxima separated by only 450V. This implies that the major part of $B_1'/B_2'$ must originate from the dissociation of the $[H_3]^{2+}$ core into $2H^+$+H(1s). The internal energy available to translational degrees of freedom is 7.2eV in this case. The maximum separation

between forward and backward scattered H(HR) in the kinetic energy spectrum, $\Delta E_{max}$, results if all the available internal energy is shared between two fragments from the dissociation of the $[H_3]^{2+}$ core (e.g.the $2H^+$) the third nucleus receiving no translational energy. Applying the laws of conservation of momentum and energy, $\Delta E_{max}$ is given by

$$\Delta E_{max} = (8/3 x V_0 x W)^{1/2} \qquad (2.17)$$

where $V_0$ is the translational energy of the projectile and W is the available internal energy. Substituting 7.2eV for W in equation(2) we obtain 435V for $\Delta E_{max}$, somewhat smaller than the distance between $B_1'/B_2'$ (450V) in Fig.69(b), (450V requires 7.6eV of available internal energy). The energy deficit can be made up from momentum transfer to nuclei in the $[H_3]^+$ ion during collision. There are two trajectories drawn over the potential surface in Fig.70. The dotted line belongs to the initial geometry being a 1.1 Å sided equilateral triangle and with all three nuclei having zero initial momenta. It can be seen that such initial conditions would lead to $[H_2]^+ + H^+$ products, which is not in keeping with the observations presented above. Moreover, from the qualitative features of this surface, it is clear that in order for the dissociation to lead to $2H^+ + H(1s)$ products, one of the nuclei of the $[H_3]^{2+}$ core must have an appreciable initial momentum, greater than those of the other two atoms. This condition can be realized if the vertical electronic excitation to the intermediary $[H_3]^+(HR)$ species involves a simultaneous momentum transfer to one of the nuclei. The broken line in Fig.70 gives a characteristic trajectory characteristic for such an excitation mechanism. A dissociation process, during which *two* of the nuclei of the $[H_3]^{2+}$ core moved away from each other in opposite directions with the third remaining at rest, would result in only the first two nuclei

receiving *all* the available KER. For such process a relationship between $R_1$ and $R_2$ can be found by using simple geometrical considerations, which must be satisfied during the entire dissociation. For isosceles triangle initial geometries, the following general relationship was obtained: $R_2^2=A+R_1^2/4$, where A is a parameter depending on the initial geometry. Line (2) in Fig.70 joins the points satisfying this equation for a 1.1Å sided equilateral triangle as the initial geometry. This line does not belong to a reasonable trajectory over the surface. However the trajectory given by the broken line asymptotically reaches it. It is therefore feasible that dissociation along this trajectory will result in the partitioning of all the available internal energy into the translational energy of only *two* of the fragments. The $H_2$(HR) spectrum in Fig.69(b) contains a weak, poorly defined, broad component which can be due to a small fraction of the dissociative intermediate $[H_3]^+$(HR) dissociating into $H_2$(HR)+$H^+$.

Fig.71(a) contains the kinetic energy spectra of HR fragments from 9.9keV $[H_2D]^+$/He collisions for "low" source pressure conditions; those for "high" source pressure are shown in Fig.71(b). For "low" source pressures the m/z 2 fragment in the kinetic energy spectrum is almost entirely due to D(HR) fragments from $[D_2]^+$/He collisions. The appearance of this peak is in keeping with our previous results on that system, section 2.4.3. The DH(HR) and the H(HR) spectra contain dished peaks $A_1/A_2$ and $B_1/B_2$, respectively. Both features are associated with a characteristic KER of 7.8±0.3eV, implying that they are due to the same process as $A_1/A_2$ and $B_1/B_2$ in Fig.69(a). The kinetic energy spectra for "high" source pressure conditions in Fig.71(b) again reflect the same processes as those for the $[H_3]^+$/He system in Fig.69(b). For an $[H_2D]^{2+}$ core dissociating into $2H^+$+D(1s), and with only the $2H^+$ fragments receiving KER, $\Delta E_{max}$ has the form:

$$\Delta E_{max} = (2xV_0xW)^{1/2} \qquad (2.18)$$

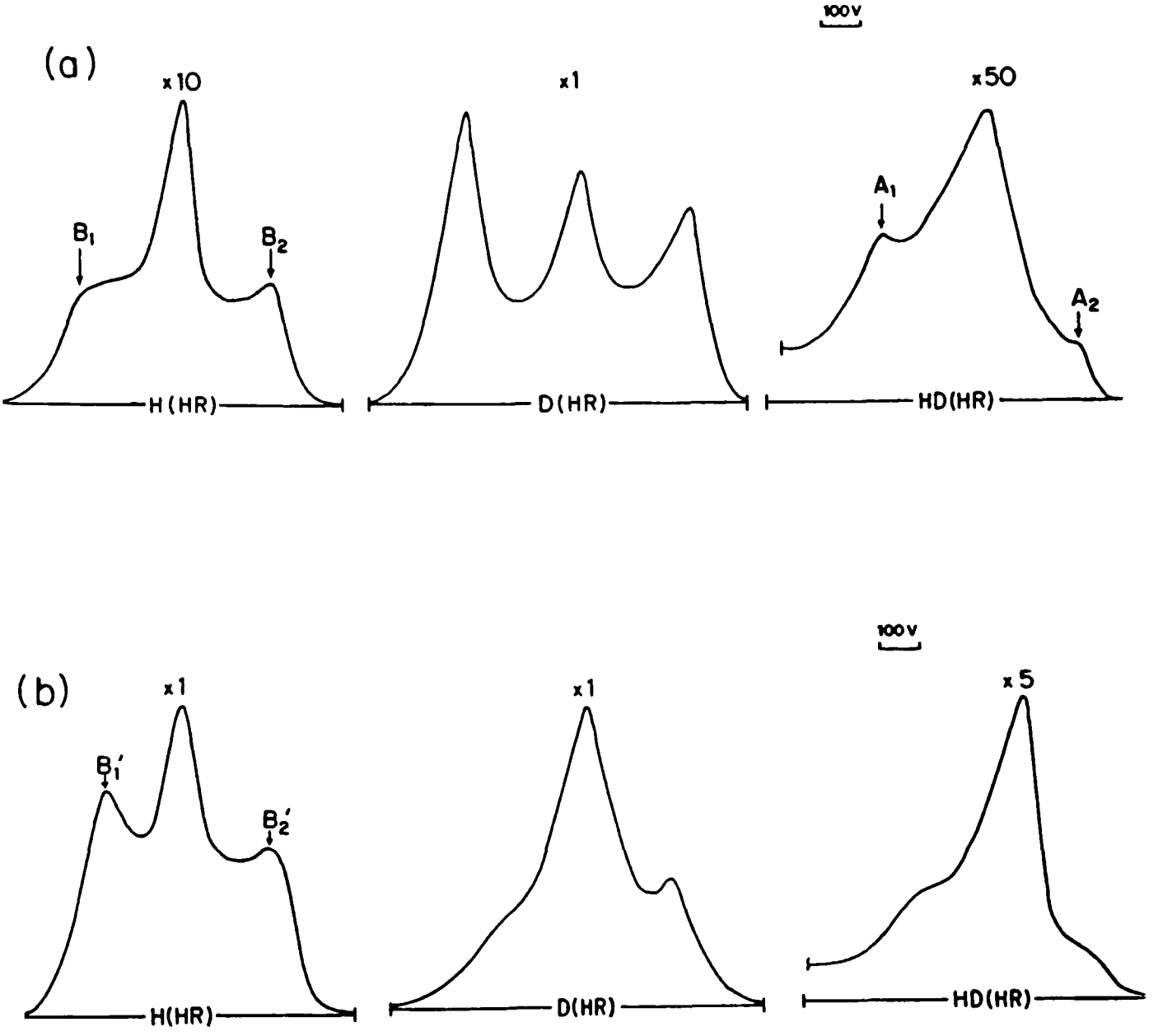


Figure 71 (a) Field induced ion kinetic energy spectra of HR fragments from 9.9 keV $[H_2D]^+$/He collisions. $[H_2D]^+$ ions were generated under "low" ion source pressure conditions. See text for discussion.
(b)Field induced ion kinetic energy spectra of HR fragments from 9.9 keV $[H_2D]^+$/He collisions. $[H_2D]^+$ ions were generated under "high" ion source pressure conditions. See text for discussion.

There is a well defined dished structure in the spectrum of the H(HR) fragments $B_1'/B_2'$. The distance across the maxima is 400V, corresponding to 8.0±0.3eV as the available internal energy in the dissociating $[H_2D]^{2+}$ core. Based on these observations we propose that $B_1'/B_2'$ is due to a mechanism similar to that described for the origin of $B_1'/B_2'$ in Fig.69(b). There is a poorly defined broad component in the kinetic energy spectrum of D(HR) fragments. We estimate, using the results of Rumpf et al. [246], that it is ca. 20 times less intense than the dished component in the H(HR) spectrum. The width of this broad feature is in keeping with a process involving dissociation of a $[H_2D]^{2+}$ core into $H^+$+$D^+$+H(1s), the $H^+$ and $D^+$ fragments receiving the major fraction of the KER. There is a very weak broad component in the HD(HR) spectrum, which is possibly due to a very small fraction of the $[H_2D]^+$(HR) intermediates dissociating to HD(HR)+$H^+$.

The kinetic energy spectra of HR fragments from 9.9keV $[D_2H]^+$/He collisions, shown in Fig.72(a), contain dished peaks which must be due to the dissociation of the $[D_2H]^{2+}$ core of $[D_2H]^+$(HR) species into ($[D_2]^+$+$H^+$) and ($[DH]^+$+$D^+$), yielding $D_2$(HR),H(HR) and DH(HR),D(HR) fragments, respectively. From the distance across the maxima of the corresponding dished peaks we obtain a most probable KER of 8.4±0.3eV for $D_2$(HR) and H(HR) and 7.3±0.3eV for the fragments DH(HR) and D(HR). The kinetic energy spectra of HR fragments from $[D_2H]^+$/He collisions, when the $[D_2H]^+$ is generated under "high" source pressure conditions, are shown in Fig.72(b). The $[D_2H]^+$ ion, at the outer turning point of its symmetric stretch vibration, has acute angled isosceles triangle geometry in which the D-H distance is greater than the D-D distance. Vertical excitation from this geometry to the potential surface of the $1^2A_1$ doubly charged state, shown in Fig.70, will result in dissociation only into $[D_2]^+$+$H^+$ fragments. Therefore, vertical excitation, (without any significant momentum transfer), of $[D_2H]^+$ into $[D_2H]^+$(HR) converging to the $1^2A_1$ doubly

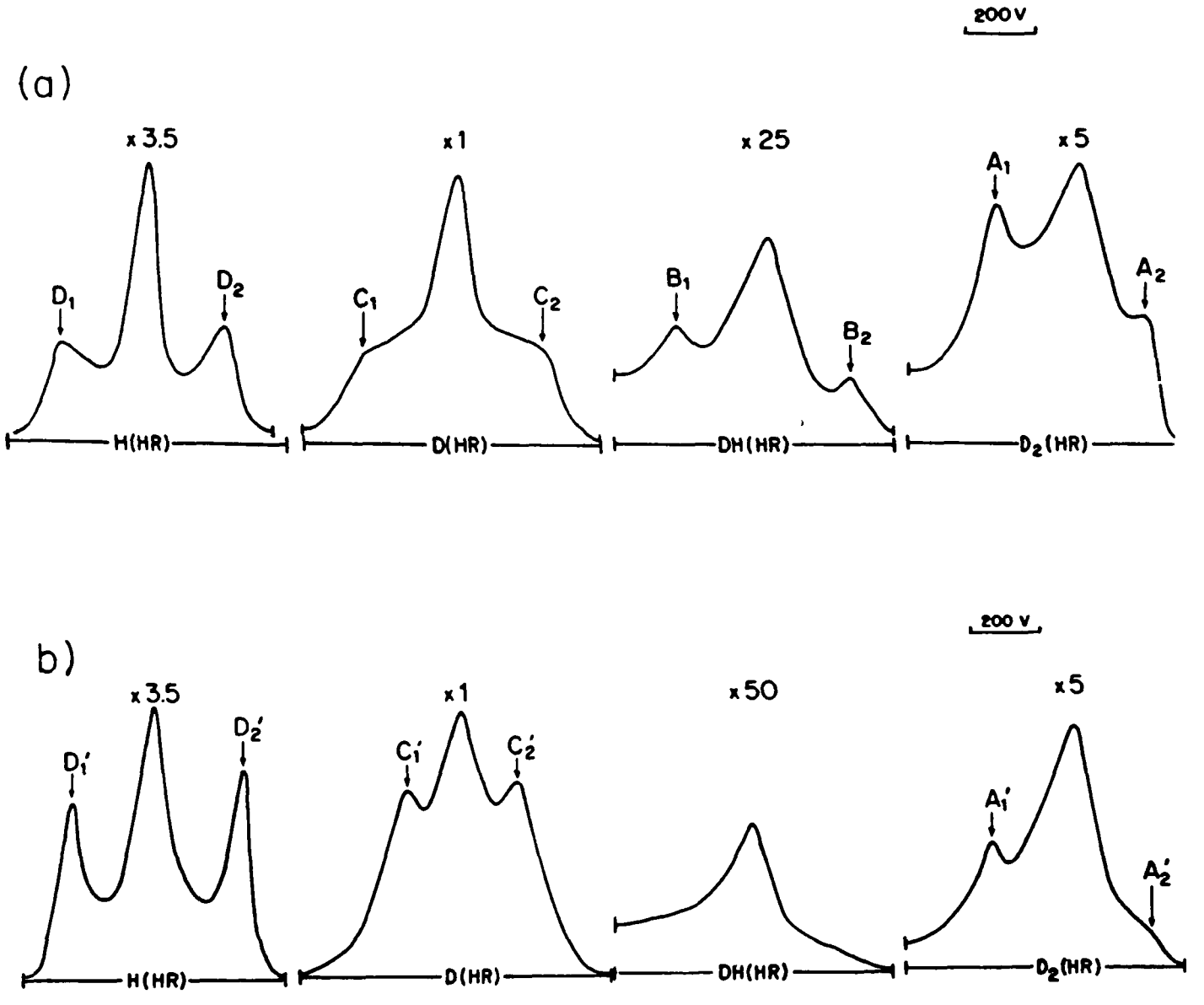


Figure 72 (a) Field induced ion kinetic energy spectra of HR fragments from 9.9 keV $[D_2H]^+$/He collisions. $[D_2H]^+$ ions were generated under "low" ion source pressure conditions. See text for discussion.
(b) Field induced ion kinetic energy spectra of HR fragments from 9.9 keV $[D_2H]^+$/He collisions. $[D_2H]^+$ ions were generated under "high" ion source pressure conditions. See text for discussion.

charged state, will give rise to only $D_2$(HR) and H(HR) fragments. Indeed, there is an intense, well defined dished peak in the H(HR) spectrum, $D_1$'/$D_2$', associated with 9.2±0.2eV KER and there is also a structure in the $D_2$(HR) spectrum, $A_1$'/$A_2$', associated with same KER. The DH(HR) signal is *extremely* weak and contains a barely visible broad component, in keeping with the above conclusion concerning the dissociation of a $[D_2H]^{2+}$ core. The D(HR) spectrum contains a dished component $C_1$'/$C_2$', separated by 310V across the maxima. Using the tables of reference [246], we estimate that the HR fragments associated with $C_1$'/$C_2$' have an absolute intensity of ca. 10% of that for $D_1$'/$D_2$'. Based on the magnitude of the separation of the forward and backward scattered fragments in the kinetic energy spectrum of D(HR) and the absence of any similar structure in the H(HR) spectrum, we conclude that the D(HR) fragments must come from a dissociation of the $[D_2H]^{2+}$ core of the $[D_2H]^+$(HR) intermediate into $2D^+$+H(1s) and with all three fragments receiving a substantial fraction of the available internal energy. Using the laws of the conservation of energy and momentum, we calculate that if the available internal energy is 7.2eV, 50% will be converted into the translational energy of the H(1s) fragment. We propose the following qualitative explanation for these observations. Simultaneous with the vertical electronic excitation of $[D_2H]^+$ into a HR state, there is momentum transfer in the hydrogen nucleus of the $[D_2H]^{2+}$ core. This enables the $[D_2H]^{2+}$ system to move to the region of the $1^2A_1$ surface which is connected to $2D^+$+H(1s) products.

## SUMMARY

**In this chapter we have presented an analysis of the kinetic energy spectra of ionic and HR fragments from 9.9 keV collisions between $[H_3]^+$ (and isotopomer ions) and rare gas targets. The $[H_3]^+$ ions generated under "high" source pressure conditions have a well defined reactive geometry, an equilateral triangle with 1.1Å**

sides, from which vertical excitations to dissociative electronic states take place. By combining the KERs associated with dished peaks in the kinetic energy spectra, the above geometry and results of theoretical calculations we were able to assign dissociation mechanisms to the major features in the spectra. For He and Ne targets the most important processes generating $[H_2]^+$ fragments were excitations to the $1^1E'$ and the $1^1A_2''$ states. The most important process for the generation of $H^+$ in collisions with He and Ne was transition to the first singlet excited state ($1^1E'$ in $D_{3h}$ symmetry) followed by a nonadiabatic transition to the ground electronic state which then dissociates into $H_2(X^1\Sigma_g^+)+H^+$. Another important process giving $H^+$ is dissociation from the $2^1A_1'$ state.

All the above transitions obey Wigner's total-spin-conservation rule, and there is no sign of transitions to triplet states for He and Ne as collision gases, even though the excitation to the lowest triplet state is 4.8eV less endothermic than the excitation to the lowest singlet excited state. However, for the heavier rare gases (and all diatomic targets), spin-forbidden processes involving excitations to triplet states of $[H_3]^+$, lead to most of the ionic fragments. The triplet states involved are the $1^3E'$ state which dissociates into $[H_2]^+$+H(1s) fragments and the $1^3A_2''$ state, giving $H_2(c^3\pi_u)+H^+$.

Broad features in the kinetic energy spectra of HR fragments from 9.9keV $[H_3]^+$($[H_2D]^+$,$[D_2H]^+$)/He collisions were attributed to excitation of the projectiles into a HR state converging to the $1^2A_1$ doubly charged state. The doubly charged ion core dissociates over this surface and after the fragments have separated the HR electron joins one of them, yielding the HR species. For the case of $[H_3]^+$ having equilateral triangle geometry, the kinetic energy spectrum of H(HR) fragments can only correspond to dissociation of the $[H_3]^{2+}$ core of the intermediate HR species into $2H^+$+H(1s) and only two of the fragments receive all the available

internal energy as translational energy. This is explained by proposing that vertical excitation into $[H_3]^+(HR)$ involves a simultaneous momentum transfer to one of the core nuclei giving rise to trajectories over the $1^2A_1$ surface which correspond to this particular partitioning of internal energy. The same mechanism appears to hold for $[H_2D]^+$ and $[D_2H]^+$ projectiles. In Table 7 we summarize observations related to the collision induced dissociation of $[H_3]^+$ ions having the characteristic geometry; it lists the excited states involved, the dissociation products and the observed KER.

Table 7 Summary of observations relating to the collision induced dissociation of $[H_3]^+$ ions (geometry: equilateral triangle, 1.1 Å sides). See text for discussion. (a) For the gases in brackets the particular process has only minor importance. (b) Non-adiabatic transition between the first singlet excited state and ground state of $[H_3]^+$. (c) HR state of $[H_3]^+$ converging to $[H_3]^{2+}(1^2A_1)$.

| Collision gas[a] | Dissociation process | KER (eV) |
|---|---|---|
| He,Ne,(Ar,Kr,Xe) | $[H_3]^+(1^1E') \rightarrow [H_2]^+(v=0)+H(1s)$ | 10.0±0.2 |
| He,Ne,(Ar,Kr,Xe) | $[H_3]^+(1^1E') \xrightarrow{b} [H_3]^+(1^1A_1) \rightarrow H_2(X^1\Sigma_g^+,v=4)+H^+$ | 10.0±0.2 |
| He,Ne,(Ar,Kr,Xe) | $[H_3]^+(1^1A_2'') \rightarrow [H_2]^+(v=2)+H(2p)$ | 2.0±0.2 |
| He,Ne,(Ar,Kr,Xe) | $[H_3]^+(2^1A_1') \rightarrow H_2(B^1\Sigma_u^+,v=10)+H^+$ | 4.3±0.3 |
| Ar, Kr, Xe | $[H_3]^+(1^3E') \rightarrow [H_2]^+(v=1)+H(1s)$ | 4.6±0.2 |
| Ar, Kr, Xe | $[H_3]^+(1^3A_2'') \rightarrow H_2(c^3\pi_u,v=0)+H^+$ | 1.7±0.3 |
| He | $[H_3]^+(HR)^c \rightarrow H(HR)+H^++H(1s)$ | 7.6±0.3 |

# 2.7 The Effect of Projectile Vibrational Energy Content on the Neutralization Reionization Mass Spectra of $[H_2]^+$ Ions

## 2.7.1 Introduction

Neutralization reionization mass spectrometry (NRMS) is a technique which permits the production of novel neutral species [11,12]. The basic features of this kind of experiment are illustrated in Fig.39 in section 1.2.6. Neutrals are generated in collisions between mass selected beams of fast ions and a stationary target gas in the first collision chamber. The beam of fast neutrals obtained is analyzed, after the ions have been deflected away by an electric field, by collisional reionization in a second collision cell and recording the kinetic energy spectrum of the resulting ions. These observations provide information about the stability of the neutral species, and/or about its dissociation properties. There is very little information presently available on the details of the neutralization and reionization processes. One detail of possible importance is how NRMS is effected by the vibrational energy content of the projectile ion. Here we report results of experiments performed with $[H_2]^+$ ion beams of different, known vibrational energy content.

In section 2.4 we described experiments that permit the characterization of the vibrational energy distribution in $[H_2]^+$ ion beams generated by 70 eV electron impact (EI) of different molecules. It has been established that 70 eV EI of $H_2O$ produces $[H_2]^+$ ions mainly in the v=0 and v=1 vibrational states, and 70 eV EI of $CH_4$ generates $[H_2]^+$ ions, populating vibrational levels around the v=11 state. It had been determined formerly that 70 eV EI of $H_2$ gives a Franck-Condon distribution of $[H_2]^+$ vibrational states, i.e. the v=1 and the v=2 are the most populated states

but the v=0,3,4 levels are also populated with comparable importance [197].

The potential energy diagram for molecular hydrogen (Fig.73) shows that the equilibrium internuclear distance in the ion is greater than in the neutral species (0.75 → 1.1Å), but that vertical ionization/neutralization from the ground state of each leads to stable products. Note also that $[H_2]^+$ resides in a fairly deep potential well of 2.75eV. Thus the $[H_2]^+/H_2$ system provides a useful model to examine how NR mass spectrometric phenomena are effected by the vibrational energy content of the projectile ions.

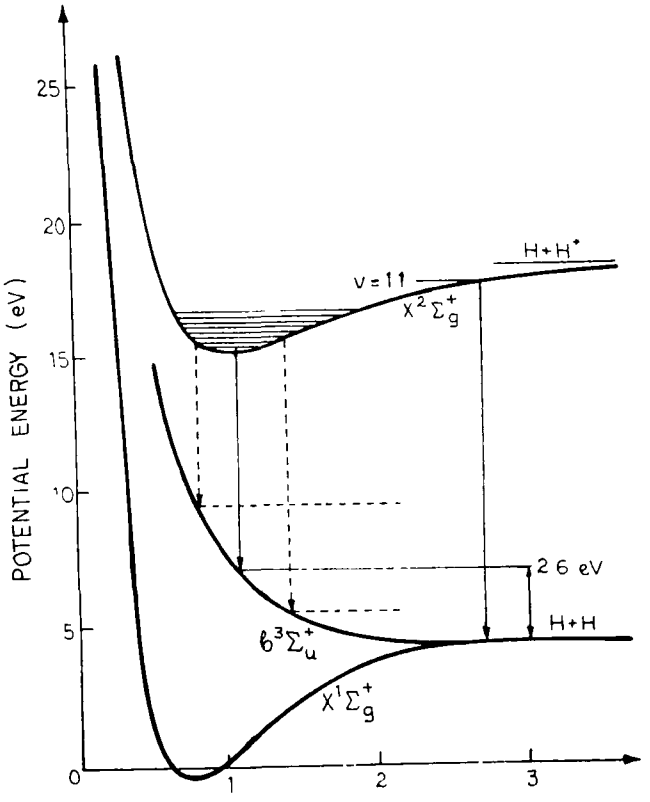


Figure 73 Potential energy diagram for $H_2$, $[H_2]^+$.
See text for discussion.

### 2.7.2 Results and discussion

We carried out experiments using a ZAB 2F mass spectrometer modified for NRMS experiments, with $[H_2]^+$ ion beams generated by the reactions described in the introduction. We used six combinations of neutralization/reionization gases: Xe/He, $Xe/O_2$, $H_2$/He, $H_2/O_2$, Ne/He, $Ne/O_2$. The pressure of gases in the collision cells were adjusted to cause a 10% attenuation of the projectile ion beam. The experimental results for $[H_2]^+$ yields from NR of $[H_2]^+$ ions of different vibrational energy content are shown in Table 8 and the corresponding results for $H^+$ yields are given in Table 9.

**Table 8. Relative $[H_2]^+$ NR mass spectrometric yields as a function of $[H_2]^+$ ion vibrational energy and of target gases. Numbers in parentheses indicate populated vibrational energy states in the $[H_2]^+$ beam; those in square brackets are the ratios $[H_2]^+$ NR mass spectrometric yield:$[H_2]^+$ input flux, relative to that for $H_2/O_2$ NR mass spectrometry, for which the absolute ratio is $2x10^{-4}$.**

| Precursor molecule | NR gas | | | | | |
|---|---|---|---|---|---|---|
| | $H_2$/He | $H_2/O_2$ | Xe/He | $Xe/O_2$ | Ne/He | $Ne/O_2$ |
| $H_2O$(0,1) | 1.0 | 1.0 | 1.0 | 1.0 | 1.0 | 1.0 |
| | [0.82] | [1.0] | [0.95] | [0.90] | [0.65] | [0.50] |
| $H_2$(0,1,2,3,4) | 0.94 | 0.97 | 0.87 | 0.92 | 0.86 | 0.94 |
| $CH_4$(≈11) | 0.66 | 0.63 | 0.64 | 0.72 | 0.60 | 0.68 |

**Table 9.** **$H^+/[H_2]^+$ yields in NR mass spectrometry of $[H_2]^+$ ions having different vibrational energy content (shown in parentheses).**

| Precursor molecule | NR gas | | | | | |
|---|---|---|---|---|---|---|
| | $H_2$/He | $H_2/O_2$ | Xe/He | $Xe/O_2$ | Ne/He | $Ne/O_2$ |
| $H_2O$(0,1) | 0.12 | 0.10 | 0.15 | 0.18 | 0.14 | 0.18 |
| $H_2$(0,1,2,3,4) | 0.26 | 0.15 | 0.23 | 0.30 | 0.23 | 0.24 |
| $CH_4$(≈11) | 0.44 | 0.44 | 0.52 | 0.52 | 0.70 | 0.74 |

For all collision gas combinations the intensity of recovered $[H_2]^+$ ions after neutralization-reionization decreased with increasing vibrational energy content in the primary $[H_2]^+$ ion beam. There can be two reasons for that:

(i) A decreasing cross section for neutralization. There are theoretical [123] and experimental [250] results which show a decrease of up to 40% for the cross section of $H_2$ production in keV $[H_2]^+/H_2$ collisions as the vibrational energy content of the $[H_2]^+$ beam increases.

(ii) Increased dissociation upon collisional reionization.

It should be noted that this decrease in recovery is not great. Even in the case when vibrational states around v=11 are populated, i.e. levels very close to the dissociation limit, there is less than 40% change relative to the case of a vibrationally very cold primary ion beam (v=0,1; $H_2O$ precursor). The other interesting feature is that changing the collision gas does not strongly influence the observed values. This is especially significant in the case of different neutralizing agents, where there is little difference between a neutralizing agent for which the

charge exchange reaction with $[H_2]^+$ is exothermic (Xe; IE=12.1 eV); resonant ($H_2$ gas); or endothermic (Ne; IE=21.5 eV); this will be further discussed below.

Table 9 contains the ratio of the fragment $H^+$ intensity to the recovered $[H_2]^+$ intensity. This ratio always increases with increasing projectile vibrational energy content. It probably results from the increasing importance of the following three processes:

$$[H_2]^+ + N \rightarrow N^+ + [H_2^*] \rightarrow H + H \rightarrow H^+ \qquad (2.19)$$

where N is the neutralization target gas and R is the reionization target gas; e.g. the broken arrows in Fig.73, showing this dissociative electron capture.

$$[H_2]^+ N \rightarrow N + H^+ + H \rightarrow H+ \qquad (2.20)$$

i.e. collision induced dissociation of the primary $[H_2]^+$ by the neutralization target gas.

$$[H_2]^+ + N \rightarrow N^+ + H_2 \rightarrow H^+ + H \qquad (2.21)$$

i.e. production of stable $H_2$ upon neutralization, but followed by collision induced dissociative reionization.

In order to discover more about the $H^+$ production in our experiments we recorded the kinetic energy spectra for this fragment. Fig.74 shows the results for $H_2/O_2$ and Fig.75 shows those for the $H_2$/He collision gas combination. If reaction (2.19) was of the greatest importance in producing $H^+$ fragments, then the $H^+$ ion kinetic-energy spectra would reproduce the kinetic energy distribution of the H

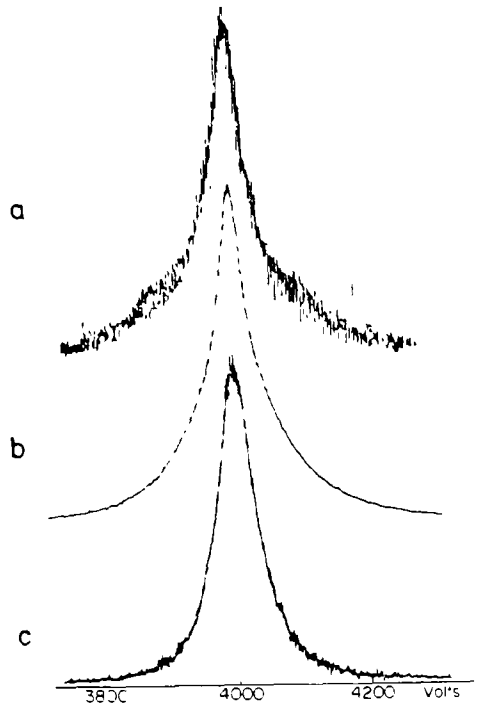


Figure 74 Kinetic energy spectra for $H_2$/He NR mass spectrometry of $[H_2]^+$ produced from (a) $H_2O$ (b) $H_2$ (c) $CH_4$

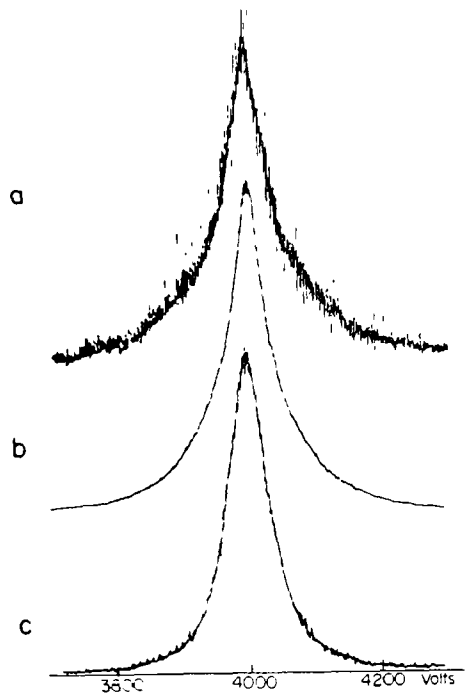


Figure 75 Kinetic energy spectra for $H_2/O_2$ NR mass spectrometry of $[H_2]^+$ produced from (a) $H_2O$ (b) $H_2$ (c) $CH_4$

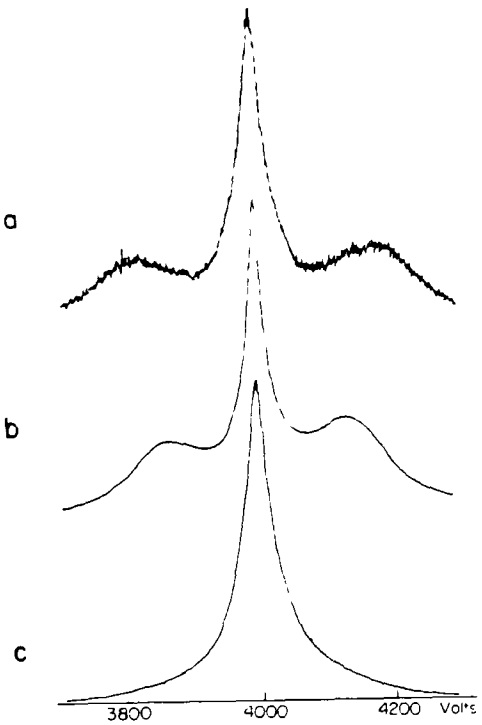


Figure 76 Kinetic energy spectra for $H^+$ from the $H_2$ CID of $[H_2]^+$ produced from (a) $H_2O$ (b) $H_2$ (c) $CH_4$

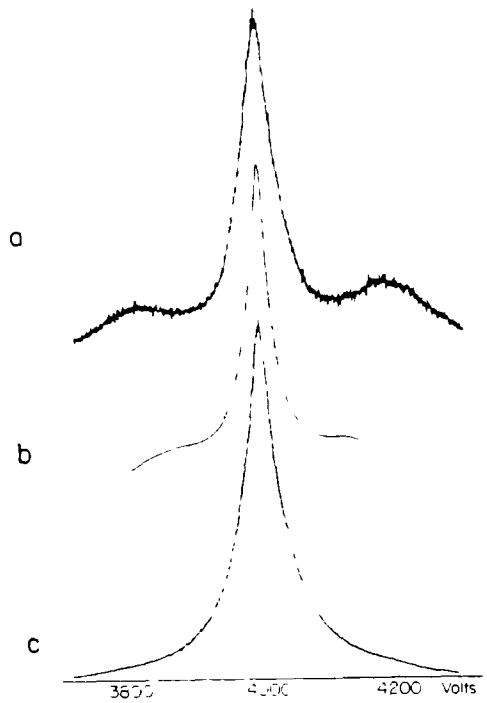


Figure 77 Kinetic energy spectra for $H^+$ from the $O_2$ CID of $[H_2]^+$ produced from (a) $H_2O$ (b) $H_2$ (c)$CH_4$

atoms produced by the dissociative electron capture. For $[H_2]^+$ ions of 10keV translational energy and stationary $H_2$ target gas, the velocity distributions (which are proportional to the kinetic energy distributions in the present work) were obtained by a coincidence method. They reflected the formation of H atom pairs resulting from charge transfer, leading to the repulsive $b^3\Sigma_u^+$ state of $H_2$. The transition involved are showed as broken lines in Fig.73. Thus, for example, the released kinetic energy is single valued for only v=0 in the $[H_2]^+$ ion; i.e. 2.6eV (see Fig.73). Higher vibrational levels yield ranges of larger and smaller kinetic energy releases which correspondingly broaden the kinetic energy release distribution. On the other hand, if processes (2.20) and (2.21) were the most important, then the observed $H^+$ kinetic energy spectra would be similar to those obtained for $H^+$ ions from the collision induced dissociation of $[H_2]^+$ by either the neutralization or the reionization gas. These spectra are shown in Figs.76 and 77; the former is for $H_2$ as collision gas, the latter is for $O_2$.

Note that the spectra in Figs.74(a) and (b) and 75(a) and (b) are markedly different from the corresponding spectra, Figs.76(a) and (b) and 77(a) and (b), in that the broad components in the latter are wholly absent in the former. This shows that process (2.2.19), i.e. dissociative electron capture followed by collisional reionization of the resulting H atoms, is the most important process generating $H^+$in the NR mass spectrometry of $[H_2]^+$ having low vibrational energy content (v=0-4). Indeed our spectra for these $[H_2]^+$ ions compares quite well with results of Vogler [26]. The exception lies in Figs.74(a) and 75(a), where the central regions of the peaks, which correspond to very small kinetic energy releases, are emphasized in the present work owing to discrimination (against large kinetic energy releases) in our apparatus.

In the case of highly vibrationally excited primary $[H_2]^+$ beams ($CH_4$

precursor), the kinetic energy distributions of the $H^+$ fragments from NR (see Figs.74(c) and 75(c)) are very closely similar to those obtained for $H^+$ generated in the CID of $[H_2]^+$ by either $H_2$ (Fig.76(c)) or $O_2$ (Fig.77(c)). This shows that processes (2.20) and (2.21) are much more important in this case than process (2.19). The kinetic energy spectra of $H^+$ fragments for the rest of the collision gas combinations were recorded, but because the spectra obtained for a particular $[H_2]^+$ precursor are closely similar to the corresponding results in Figs.74 and 75, they are not presented here. All the above observations clearly indicate that the phenomenology in these NR experiments does not depend on the nature of the collision gases.

**So far as NR mass spectrometric experiments are concerned, the major conclusions are that the recovery signal intensity is only markedly affected (reduced in this case) when vibrationally highly excited ions (near to their dissociation limit) are neutralized and reionized. Relative yields are only weakly dependent upon the endo- or exothermicity of the neutralization step and on the nature of the reionization gas. The relatively high recovery for $[H_2]^+$ (v=11) species (see Table 8) is in agreement with results obtained by Moran et al. [123] which showed that in keV charge exchange collisions the vibrational overlap between initial and final states is more important than their net energy difference. The present experiments show that a considerable yield of stable $H_2$ molecules must be produced, even for vibrationally "hot" $[H_2]^+$ projectiles, i.e. a variety of $H_2$ vibrational states must be accessible in the neutralization step. If this result can be extended to the NR of polyatomic ions, it is probable that highly vibrationally excited ions will yield neutral species of sufficient stability (lifetime) to be reionized and then detected.**

# 2.8 keV Collisions of Methonium Ions

## 2.8.1 Introduction

Neutralization reionization mass spectrometry (NRMS) [11,12] is a technique well suited to investigating the stability of hypervalent radicals, the neutral counterparts of the protonated first and second row hydrides having received considerable attention [139-148]; $CH_5$ is particularly interesting because of the contradictory results in the literature [141, 150, 251, 252].

In 1980 Williams and Porter [141] and in 1984 Gellene and Porter [148] investigated the methonium ( $CH_5$ ) radical by neutralized ion beam techniques. In the earlier report [141] the angular scattering of the neutral products from charge exchange between $[CH_5]^+$ and $[CD_5]^+$ ions having 5 keV translational energy and alkali metal vapors (Na and K) was measured. In the second report the neutral species from charge exchange between 6 keV $[CD_5]^+$ ions and K atoms were reionized by collisions with $NO_2$ target gas, and the resulting fast ions were mass analyzed by observing their deflection in a uniform electric field. These experiments showed, in keeping with theoretical predictions [253, 254], that $CH_5$ formed by the vertical neutralization of ground state $[CH_5]^+$ ions is not stable. It dissociated mainly into $CH_4$ + H products [150] with 2.65 ± 0.15 eV as the maximum kinetic energy release [141]. The *vertical* electron affinity of $[CH_5]^+$ was estimated to be 5.3±0.15 eV.

In conflict with these results Griffiths et al. [251] have recently reported the recovery of parent ions in NR experiments with 6 keV $[CH_5]^+$ and $[CD_5]^+$ ions. They used a modified double focussing mass spectrometer having B/E geometry (VG Analytical ZAB-2F). The modifications consisted of a collision gas cell preceded by ion beam deflector electrodes mounted in the second field free region of the

instrument. They admitted gases of high ionization energy, $N_2$ ( IE=15.6 eV), Kr (IE=14.0 eV) or Xe (IE=12.1 eV), into the collision cell. Gas diffused therefrom into the region between the magnet and the ion beam deflection plates acted as the neutralizing agent. The fast neutrals which were produced were then ionized by collisions with the gas in the collision cell. The resulting ions were mass analyzed via their kinetic energy spectrum obtained by scanning the electric sector of the mass spectrometer. The observation of a recovery signal for the parent ion led them to conclude that neutral $CH_5$ species, having a lifetime of at least 390 ns, were formed in charge exchange between the target gas atoms and the projectile ions. From the net kinetic energy loss undergone by the $[CH_5]^+$ ions in the neutralization-reionization process, they estimated the ionization energy for the metastable $CH_5$ species to be 8.0±0.5 eV. Only the kinetic energy spectrum of the $[CH_5]^+$ recovery peak was shown and no description was given of the fragment ion peaks $[CH_4]^+$, $[CH_3]^+$, etc., or those from $[CD_5]^+$ ions.

Motivated by these contradictory results Selgren and Gellene [252] have very recently repeated the experiments reported in references [141] and [150]. With Na atoms as neutralization target (IE=5.1 eV) they reproduced the results of references [141] and [150]. However with Zn atoms (IE=9.3 eV), as neutralizing agent they obtained completely different observations; the neutral beam profile showed a much larger kinetic energy release in the dissociation of $CH_5$ and $CD_5$ than when Na was the target. The $Zn/NO_2$ NR mass spectrum of $[CD_5]^+$ contained a recovery peak, which was the *most intense* peak in the spectrum. Moreover, the shape of the $[CD_4]^+$ fragment peak reflected a very large kinetic energy release in the dissociation $CD_5 \rightarrow CD_4 + D$. The poor energy resolution of their apparatus did not allow a precise determination of the released kinetic energy, but the results were compatible with 8 eV as the most probable value. It was considered that this

is the largest possible kinetic energy release for a fragmenting $CH_5$ neutral having slightly less energy than the difference between the ground state of $[CH_5]^+$ and the neutral dissociation products $CH_4$ + H (or $CH_3$ + $H_2$) ( $\Delta H_f[CH_5]^+$=912.5 kJ/mol [255]; $\Delta H_f[CH_4]$ + $\Delta H_f[H]$=143.1 kJ/mol [256]). Their explanation was that high Rydberg $CD_5$ molecules ($CD_5$(HR)) were formed in $[CD_5]^+$/ Zn collisions. Such a species can be metastable in the μs time scale and can predissociate into non-Rydberg fragments, $CD_4$ + D, giving up to 8 eV kinetic energy release. They argued that in the case of Na and other targets having a low ionization energy, resonant charge exchange leading to the unstable ground Rydberg level of $CH_5$ is the most important process. In the case of targets with higher ionization energy (IE>6-7 eV) the formation of metastable $CH_5$(HR) becomes the most important process.They thus attributed the recovery of the parent ion in the neutralization-reionization experiments of Griffiths et al. [251] to the formation of metastable $CH_5$(HR) radicals.

By exploiting specific features of our ZAB 2F mass spectrometer, which has been modified for NRMS experiments, we have investigated and augmented the results of Selgren and Gellene [252] and Griffiths et al. [251]. The resolution of our apparatus permits the determination of the kinetic energy released in the $CH_5 \rightarrow CH_4$ + H dissociation with ±0.2 eV precision. With the field ionization device, fast high-Rydberg species can selectively be ionized and detected . It can therefore unequivocally be determined whether metastable $CH_5$(HR), ($CD_5$(HR)) species are produced in collisions between $[CH_5]^+$ ($[CD_5]^+$) ions of keV translational energy and high ionization energy targets, such as Xe, Kr, NO, etc.

Collision induced dissociation experiments with $O_2$ as target gas were used to study the dissociative states of the $[CD_5]^+$ and $[CD_5]^{2+}$ ions. Kinetic energy spectra of the field ionizable HR fragments, (D(HR), $D_2$(HR) and $CD_3$(HR)),

resulting from collisions between $[CD_5]^+$ ions of 9.9 keV translational energy and He target gas were also obtained and mechanisms for their generation were determined.

### 2.8.2 Experimental

All measurements were made with a VG Analytical ZAB-2F double focusing mass spectrometer of reversed geometry, modified for NRMS experiments and for field ionization of fast HR species as described in sections 1.1.4 and 2.1.1. Measurements were performed as follows. Beams of $[CH_5]^+$, $[CD_5]^+$ and $[CD_4H]^+$ ions were generated by chemical ionization of $CH_4$, $CD_4$ and a 1:1 mixture of $CH_4/CD_4$ gases, respectively, and ion source pressures were varied to provide different degrees of protonation. In the NRMS experiments neutralization gas was admitted to the first collision cell and reionization gas to the second collision cell; the ion beam deflector was charged to +1 kV. Neutralization gases used were Xe, Kr, NO and $N_2$; $O_2$ and $NO_2$ were the reionization gases. The pressures of each collision gas were adjusted to cause no more than 10% attenuation of the main ion beam. The beams of $[CH_5]^+$,$[CD_5]^+$ and $[CD_4H]^+$ ions were accelerated to 8 kV. Energy resolution was such that the main ion beam width at half height was 5 V or less. Experiments were performed with primary ion beams generated under "high" and "low" source pressure conditions. For the $CH_4/CD_4$ mixture in the ion source, "high" source pressure refers to a $20^+/21^+$ ratio of 0.1 in the mass spectrum and low source pressure indicate a $20^+/21^+$ ratio of 15. For pure $CH_4$ or $CD_4$ admitted into the source, "high" source pressure corresponds to $16^+/17^+=20^+/22^+=0.02$ and "low" source pressure to $16^+/17^+=20^+/22^+=3$. The present "high" source pressure conditions correspond to ca 0.5 torr and 350K temperature, similar to those employed by Selgren and Gellene [251]. Collision induced dissociation of $[CD_5]^+$

ions of 9.9 keV translational energy was achieved by admitting $O_2$ gas into the second collision cell again at a pressure causing 10% beam attenuation. We estimated, using the results of Kim [256], that at this main beam attenuation the probability of double collision processes is less than 5% of that for single collision events. The main beam in this case had a width of 2 V at half height. Field ionization experiments were carried out with the meshes intersecting the ion beam path, the first mesh being charged to +1300 V and the second mesh grounded, creating a 2kV/mm field gradient between them. The $[CD_5]^+$ ion beams used in these experiments were accelerated to 9.9 kV translational energy and had a width at half height of 10 V, the lower energy resolution being necessary for sensitivity reasons. Collision gas, He, was admitted to the first cell at a pressure corresponding to 30% beam attenuation. The deflector electrode was charged to +700V. In this mode of operation, peaks due to fast, field ionizable species appear in the kinetic energy spectra centered near $[(m_f/22)x9900+1300]$ V where $m_f$ is the fragment mass. The same tests as described in section 2.5.2 were carried out to ensure that the field ionization signals corresponded to HR species generated in single collision events. The kinetic energy spectra of ions produced in the above three types of experiment were obtained by scanning the electric sector in the usual way.

### 2.8.3 Results and Discussions

#### (A) NRMS experiments

Figs.78(a), 79(a) and 80(a) show the full $Xe/O_2$ NRMS of $[CH_5]^+$, $[CD_5]^+$ and $[CD_4H]^+$ ions, respectively, generated at" high" source pressure conditions. Figs.78(c) and 80(c) contain the $Xe/O_2$ NRMS of $[CH_5]^+$ and $[CD_4H]^+$, respectively, generated at" low" source pressure conditions, where the degree of protonation is

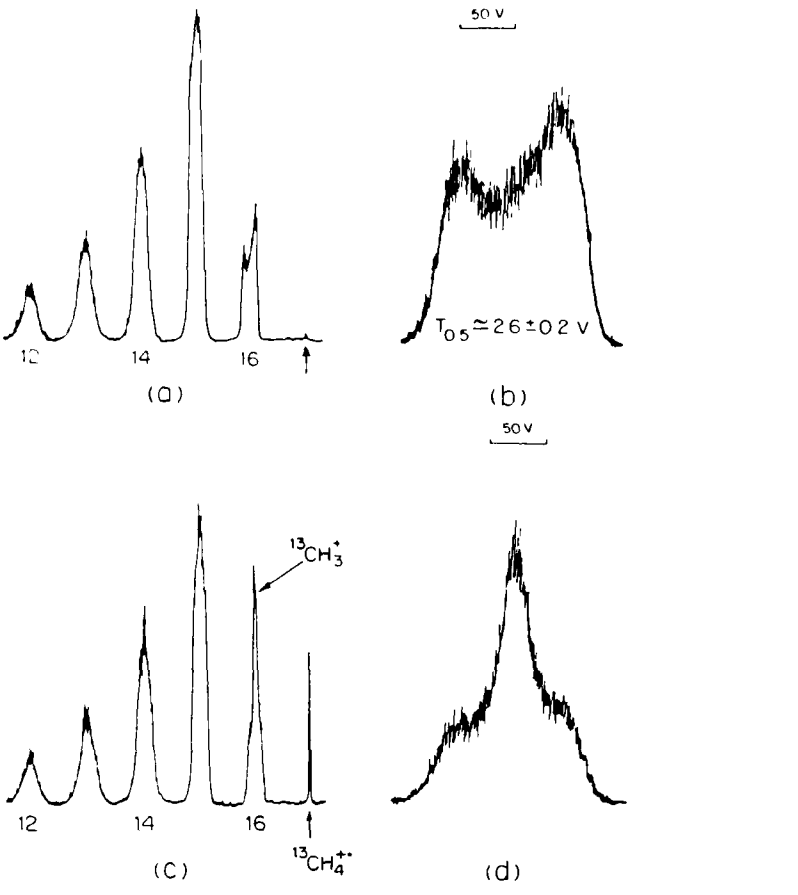


Figure 78 (a) $Xe/O_2$ NRMS of $[CH_5]^+$ ions; "high" source pressure conditions, $(16^+/17^+=0.02)$.
(b) The m/z=16 peak from (a) - see text for discussion.
(c) $Xe/O_2$ NRMS of $[CH_5]^+$ ions; "low" source pressure conditions, $(16^+/17^+=3)$.
(d) The m/z=16 peak from (c) - see text for discussion.

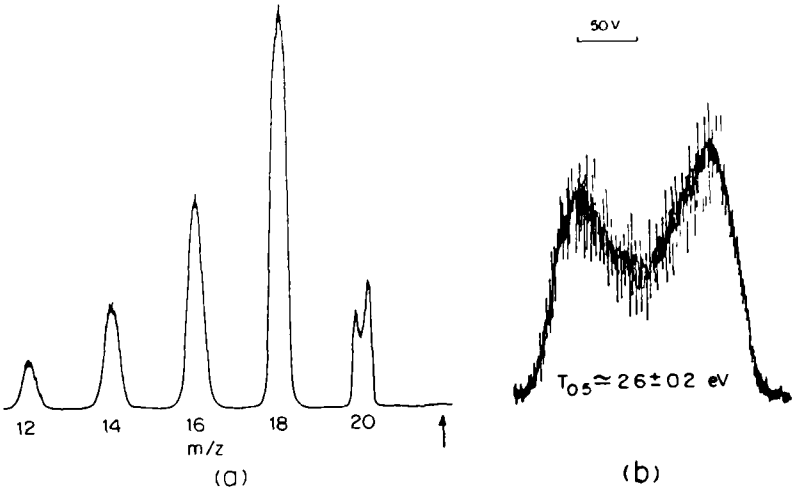


Figure 79 (a) $Xe/O_2$ NRMS of $[CD_5]^+$ ions; "high" source pressure conditions, $(20^+/22^+=0.02)$.
(b) The m/z=20 peak from (a) - see text for discussion.

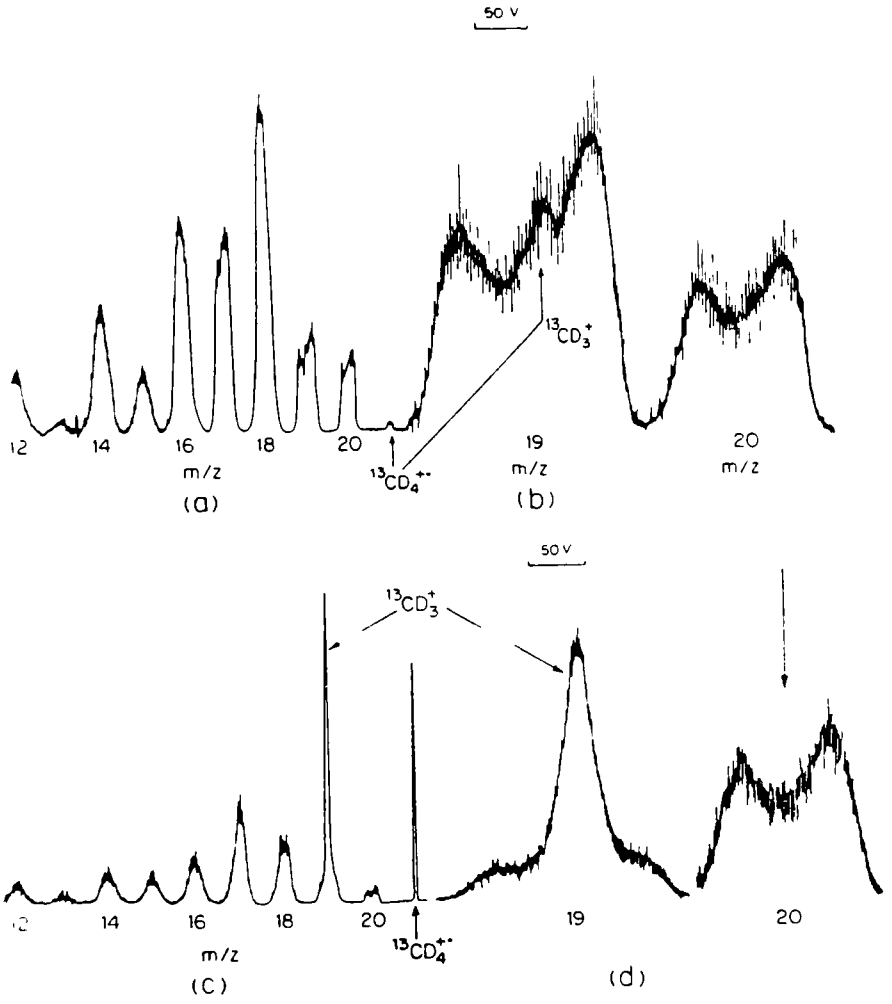


Figure 80 (a) $Xe/O_2$ NRMS of $[CD_4H]^+$ ions; "high" source pressure conditions, $(20^+/21^+=0.1)$.
(b) The m/z=20 and m/z=19 peaks from (a) - see text for discussion.
(c) $Xe/O_2$ NRMS of $[CD_4H]^+$ ions; "low" source pressure conditions, $(20^+/21^+=15)$.
(d) The m/z=20 and m/z=19 peaks from (c) - see text for discussion.

lower (see experimental). Figs.78(b), (d), 79(b) and 80(b), (d) also show in greater detail, the H and/or D loss peaks from the NR mass spectra.

At "high" ion source pressures there was no detectable $[CD_5]^+$ recovery (Fig.79(a)). For $[CH_5]^+$ and $[CD_4H]^+$ projectiles there were weak signals at the primary ion beam position (Figs. 78(a) and 80(a)), but these apparent recovery signals can (within experimental error) be completely ascribed to the presence of $[^{13}CH_4]^+$ and $[^{13}CD_4]^+$ ions in the m/z 17 and m/z 21 ion beams. The correction was made using established methods [166]. Thus there is no evidence in these experiments for the generation of $CH_5$, $CD_5$ or $CD_4H$ neutrals which are stable long enough to survive the flight time between the neutralization and the reionization cell (400 ns).

The peaks corresponding to H and/or D loss in the NR mass spectra are very broad and show extensive dishing (see Figs. 78(b),79(b) and 80(b)). This peak broadening must be due to the kinetic energy released upon dissociation of the neutrals produced by charge exchange between the fast primary ions and the Xe target atoms. The most probable value of the kinetic energy released in the center of mass frame was calculated using equation (1.24). The most probable kinetic energy release obtained for all three isotopomers was 1.4±0.2 eV. The kinetic energy release corresponding to the width at half height of these peaks ($T_{0.5}$) was 2.6±0.2 eV. The magnitude of these energies shows that neutralization of fast $[CH_5]^+$ (and isotopomer) ions by charge exchange with Xe probably creates the same dissociative state of $CH_5$ as was produced in the experiments with alkali metal targets [141,150].

A noteworthy feature of the dished peaks in Fig.80(b) is that the D loss peak contains a narrow component while the H loss peak does not. This is in keeping with our conclusion that the recovery signal is entirely due to the presence of $[^{13}CD_4]^+$ ions in the m/z 21 ion beam. The narrow component in the D loss peak is

due to the collision induced dissociative ionization of stable $^{13}CD_4$ neutrals; the H loss peak can only come from ionization of $CD_4$ generated via dissociative neutralization of $[CD_4H]^+$ , ($[^{13}CD_4]^+$ cannot give a m/z 20 fragment). This conclusion can be further tested by lowering the ion source pressure, thereby decreasing the degree of protonation and increasing the $^{13}C$ contributions to the m/z 17 and m/z 21 ion beams. The above argument predicts an increase in the apparent recovery signals and in the narrow component of the fragment ion peaks in the NR mass spectra; the results are shown in Figs.78(c),(d) and 80(c),(d). For the m/z 17 beam (Fig.78(c),(d)) there now is indeed a large recovery signal and the H loss peak contains a similarly large narrow component. The results for the m/z 21 projectiles are even more striking; there being a large recovery peak and a large narrow component in the D loss peak, but the H loss peak contains *no* narrow component, and is identical with the peak obtained at "high" source pressures, reflecting the kinetic energy release distribution in the dissociation $CD_4H \rightarrow CD_4+H$. In the case of $[CD_5]^+$ ions, "low" ion source pressure conditions did not produce spectra any different from those obtained at "high" source pressures (Fig.79(a),(b)) because in this case there is no possible $^{13}C$ contribution to the m/z 22 ion beam.

From the NR mass spectra in Figs.78(a), 79(a) and 80(a) it can be seen that the remaining fragment peaks show similar broadening to the H(D) loss peaks. Generally, fragment peaks arising from the neutralization and subsequent dissociative reionization of narrow primary ion beams are significantly narrower than the peaks in these spectra. For example compare the fragment ion peaks in Figs.78(a), 79(a) and 80(a) with those in the NR mass spectrum of $[CD_4]^+$ ions shown in Fig.81.

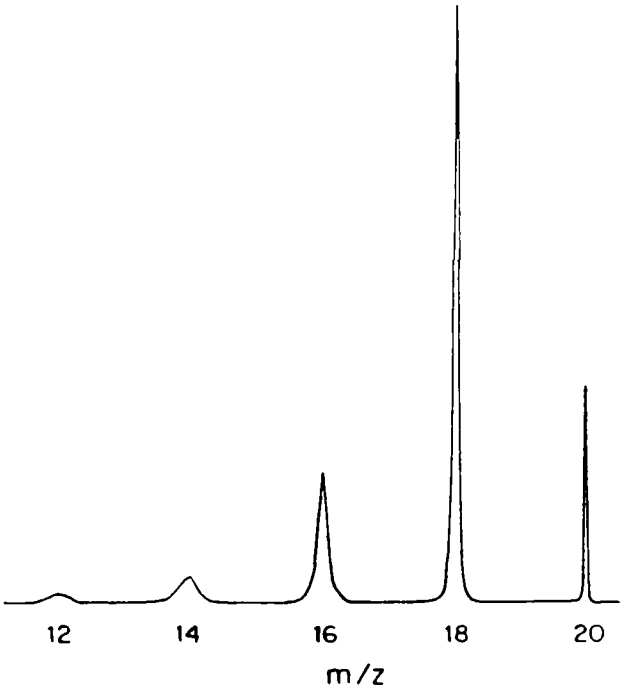


Figure 81. $Xe/O_2$ NRMS of $[CD_4]^+$ ions - see text for discussion.

That the width of the H(D) loss peaks is carried over to all the fragment peaks indicates that the entire NR mass spectrum results from the dissociative ionization of $CH_4$ ($CD_4$ and $CD_3H$) neutrals produced in the dissociative electron capture of $[CH_5]^+$ ( $[CD_5]^+$ and $[CD_4H]^+$) ions. The relative intensities of the fragment ion peaks also support this conclusion. The m/z 20/18 ratio in the NR mass spectrum of $[CD_5]^+$ ions (Fig.79(a)) is the same as that in the NR mass spectrum of $[CD_4]^+$ ions (Fig.81). The other fragment peaks are relatively higher for $[CD_5]^+$, but this effect was also observed when the collision induced dissociative ionization mass spectrum of $CH_4$ neutrals of 3 keV translational energy (obtained from metastable dissociation

of propane molecular ions in the second field free region of the mass spectrometer) were compared with the NR mass spectrum of $[CH_4]^+$ ions having the same kinetic energy [258]. The dissociative reionization mass spectra of the (3 keV) $CH_4$ beams generated as described above are expected to be dissimilar. The internal energy distribution in them differs widely; $CH_4$ species produced by the metastable dissociation of a molecular ion (e.g. $[C_3H_8]^{+\cdot}$) have a narrow range of internal energies near to the ground state. The $[CH_4]^+$ ions involved in the charge transfer neutralization, however, were generated by impact with 70 eV electrons; these ions will be vibrationally excited because of the significant geometry difference between the neutral molecule and the ion. Vertical neutralization will in turn lead to $CH_4$ molecules having a wide range of internal energies.

From the above results it is concluded that the charge exchange reaction between fast $[CH_5]^+$ ions and Xe target atoms produces unstable $CH_5$ radicals, which fragment into $CH_4$+H. Comparing our results with those in the literature, we conclude that upon Xe neutralization the same state is accessed as that from alkali metal neutralization. These conclusions are different from the predictions of Selgren and Gellene [252], who from their observations with Zn (IE=9.3 eV) as neutralization target, predicted that for neutralizing collisions between keV $[CH_5]^+$ ions and target molecules of high IE, the major processes should be (i) production of metastable $CH_5$(HR) molecules and (ii) predissociation of the $CH_5$(HR) molecules into ground state $CH_4$+H with a kinetic energy release of ca 8 eV. Experiments with our field ionization device (with Xe in cell 1, 10% beam attenuation), which selectively field ionizes fast HR species, showed no observable signal corresponding to metastable $CH_5$(HR) molecules even after increasing the amplification from that at which the NR spectra were usually obtained, by three orders of magnitude. Moreover, a dished $[CH_4]^+$ ($[CD_4]^+$) peak corresponding to an 8 eV kinetic energy

release, (the horns of which should be placed well beyond the tails of the dished peak of $T_{0.5}$=2.6 eV), was never observed in the NR mass spectrum of $[CH_5]^+$ ($[CD_5]^+$) even after increasing the amplification a thousand fold. In our apparatus discrimination against the fragments which receive greater kinetic energy release upon dissociation is expected. In 1986 Rumpf et al. [246] calculated the mass discrimination arising from energy release in dissociation in the second field free region of a double focussing mass spectrometer of reversed geometry which has the same or closely similar geometrical parameters as our apparatus. From their results we obtain that in the case of the dissociation process m/z 22 → m/z 20 + m/z 2, when the kinetic energy release changes from 2 eV to 10 eV the detection efficiency only decreases by a factor of 2. All our observations using Xe (IE=12.1 eV) are compatible with results obtained with alkali metal targets, indicating that NRMS phenomenology is only slightly affected by the nature of the collision gas, although the cross sections may vary widely. Furthermore, experiments with Kr (IE=14.0 eV) and $N_2$ (IE=15.6 eV) as neutralization gases, produced no noticeable differences from the spectra obtained with Xe. NO, which has an ionization energy,9.3 eV, very close to that of Zn, was also tried as neutralizing agent but the NR mass spectrum was similar to those for the other neutralizing agents (the m/z 12, 13, 14, 15 peaks had higher intensity relative to the m/z 16 peak than in Fig.78). Therefore the results of reference [252] for Zn must be considered to be very target specific. This specificity requires explanation, because considering the very large cross section observed for the production of metastable $CH_5$(HR) with Zn as target one could reasonably expect minor, but observable, signals corresponding to $CH_5$(HR) in the case of Xe,Kr and $N_2$ targets. In order to investigate any difference between $O_2$ (our regular agent) and $NO_2$ (used by Selgren and Gellene [252]) as reionization gases, Xe/$NO_2$ and NO/$NO_2$ NR mass

spectra of $[CH_5]^+$ were also measured. These differed negligibly from the $Xe/O_2$ (see Fig.78) and $NO/O_2$ NR mass spectra of $[CH_5]^+$.

The instability of $CH_5$ ($CD_5$) neutrals produced by charge exchange between fast $[CH_5]^+$ ($[CD_5]^+$) ions and Xe, Kr and $N_2$ targets disagrees with the results of Griffiths et al [251]. This contradiction is unexpected considering that they used the same mass spectrometer, except that their instrument did not have a separate collision cell for neutralization. A possible explanation is that they did not consider sufficiently carefully the presence of artifact recovery signals. In the case of $[CH_5]^+$ they argued, that their recovery signal was not due to $[^{13}CH_4]^+$ ions present in the m/z 17 primary beam, solely on the basis of the measured kinetic energy loss undergone by the recovered m/z 17 ions. However, Selgren and Gellene [252] have pointed out that the kinetic energy loss of the projectile ion in a NR process is characteristic of the neutralization target and not for the ionization energy of the projectile ion. Moreover, results from this laboratory (section 2.2) have shown a high sensitivity of the observed kinetic energy loss in NR experiments to ion beam focussing conditions. It therefore seems likely that their observed apparent recovery signal for $[CH_5]^+$ ions is indeed due to $[^{13}CH_4]^+$ ions.

Griffiths et al. [251] stated that they successfully repeated the experiments using $[CD_5]^+$ projectiles, and that the mean value obtained for the IE of $CD_5$ was, within experimental error, the same as that obtained for $CH_5$. In this case there is no possible isotopic interference which can produce a false recovery signal. However, we have observed, under certain conditions when working with $[CD_5]^+$ projectiles, another kind of interference. These observations can be described as follows. Under the conditions described in Fig.79., a small recovery peak was observed at m/z 22 when the amplifier gain was increased by 1000. The $CD_4$ pressure in the ion source was now systematically lowered. When m/z 20/22 was in

the range 100-1000, a recovery signal of smaller absolute intensity was observed; the fragment ion peak abundances (m/z 20, 18, 16, 14 and 12) were similar to that of m/z 22. Possibly, a *stable* $CD_5$ was now being generated, the low ion source pressure conditions preventing the collisional deenergization of $[CD_5]^+$ ions; i.e. energy rich $[CD_5]^+$ yielded a stable $CD_5$ radical. However, the NR mass spectral peaks were no longer singular, each (except for m/z 12) showing an additional narrow component on their low energy side. These neighboring narrow peaks were separated by 800V, an energy which corresponds to sequential D atom losses from an m/z 20 primary ion of 8 keV translational energy (the value for D loss from a m/z 22 ion, 727V, is significantly smaller than this). The relative intensities of the narrow peaks were closely similar to those in the NR mass spectrum of $[CD_4]^+$ ions. Furthermore, off-tuning the magnet from m/z 22 towards m/z 20 increased the intensity of these narrow signals. From this result we conclude that, in spite of selecting m/z 22 ions by the magnet, a very small number of m/z 20 ions were also transmitted through the apparatus giving rise to artifact peaks in the NR mass spectrum. (Note that the net NR cross section for $[CD_4]^+$ is ca 50 times that for $[CD_5]^+$ and that the $[CD_4]^+$ flux is 100-1000 times as intense as the $[CD_5]^+$ flux). We propose that some m/z 20 ions transmitted through the magnet (off focus) can be scattered back into focus by diffused collision gas. This interference is more serious when the beam collimation is less strict and when the neutralization gas pressure is significantly raised. In the experimental arrangement used by Griffiths et al [251], where there is no separate, differentially pumped collision cell for the neutralization gas, (collision gas leaking out of the single collision cell into the flight tube acted as neutralization agent), the above effect could become important even at high source pressure conditions.

**In summary, in these NRMS experiments using gases of high IE as**

**neutralization agents, the same processes were observed as those reported for alkali metal targets. The present results again emphasize the need for correcting the NR mass spectra for isotopic contributions, particularly because of the wide variations in neutralization-reionization efficiencies. Another possible source of interference signals was found, arising from ions of mass close to that selected by the magnet being scattered by diffused collision gas, so that they are transmitted through the instrument, giving rise to artifact peaks. This effect is particularly important if the interfering ion is of much greater abundance than the mass selected ion of interest and also has a much larger net cross section for NR. This interference can be avoided by either using double focussing mass selection or by careful collimation of the ion beam before and after mass selection.**

### (B) Collision induced dissociative processes of $[CD_5]^+$

Fig.82(a) shows the kinetic energy spectrum of the fragments from the $O_2$ collision induced dissociation of 9.9 keV $[CD_5]^+$ ions. Fig.82(b) shows the spectrum for the $D^+$, $[D_2]^+$, $[D_3]^+$ and $[CD_4]^+$ fragments in greater detail. In Fig.82(a) there is a very narrow signal at 5000V. This is due to stable $[CD_5]^{2+}$ ions formed by charge stripping upon collision with the $O_2$ target. In 1981 Proctor et al. [259] showed that $[CH_5]^{2+}$ ions can be generated by charge stripping with $N_2$. They determined a vertical ionization energy for $[CH_5]^+$ of 20.3±0.3 eV, by measuring the smallest kinetic energy loss involved in the reaction ($Q_{min.}$). In similar experiments, using $O_2$ as charge stripping agent, Stahl et al. [260] obtained a significantly greater value for $Q_{min,}$ 2.16±0.2 eV. They also presented the kinetic energy spectrum of the $[CH_4]^+$ fragment from the $[CH_5]^+/O_2$ collisions.

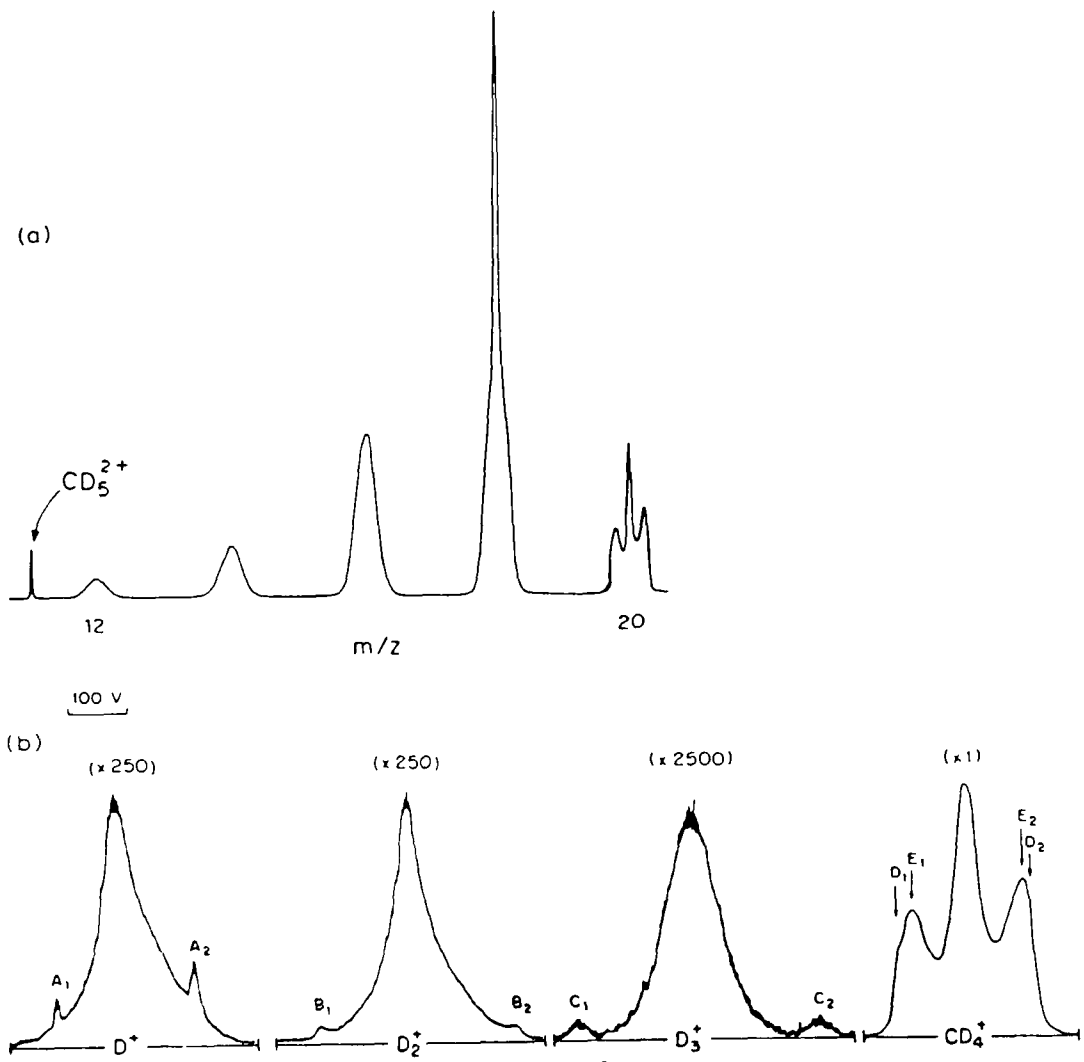


Figure 82 (a) Kinetic energy scan of ionic fragments from 9.9 keV $[CD_5]^+/O_2$ collisions.
(b) Kinetic energy spectra of $[D]^+$, $[D_2]^+$ and $[CD_4]^+$ fragments from 9.9 keV $[CD_5]^+/O_2$ collisions.

In 1972 Roussel and Julienne [261] measured the distribution of kinetic energy release received by the $[H]^+$, $[H_2]^+$ and $[H_3]^+$ fragments upon collisional dissociation of 40 keV $[CH_5]^+$ ions. They obtained for all three fragments a maximum in the distribution at ca 4-5 eV, which they attributed to the charge separation reactions:

$$[CH_5]^{2+} \rightarrow [CH_{5-x}]^+ + [H_x]^+ \quad (x=1,2,3) \qquad (2.22)$$

In the present work structures which contain additional information about the $[CD_5]^+$ and $[CD_5]^{2+}$ ions were observed in some of the fragment peaks: $[D]^+$, $[D_2]^+$, $[D_3]^+$ and $[CD_4]^+$ (see Fig.82(b)). All four peaks contain dished components indicative of large kinetic energy releases upon dissociation. For the $[D]^+$ fragment there must be a generating process which has a large, single valued release of kinetic energy, giving rise to the $A_1/A_2$ structure in Fig.82(b). The kinetic energy release in the center of mass frame, as calculated from the distance between the maxima of $A_1$ and $A_2$, was 4.6±0.2 eV. in good agreement with the earlier results of Roussel and Julienne [261]. An energy release of this magnitude likely involves a doubly charged ion. This is confirmed by the composite $[CD_4]^+$ fragment peak which contains *two* dished components ($D_1/D_2$ and $E_1/E_2$). Although convoluted by the sides of $E_1/E_2$, the $D_1/D_2$ component (which is more clearly observable in th analogous $[CH_4]^+$ peak, not presented here) has a kinetic energy release similar to that for $A_1/A_2$. We propose that structures $A_1/A_2$ and $D_1/D_2$ are due to the reaction:

$$[CD_5]^+ \xrightarrow{O_2} [CD_5]^{2+}(*) \rightarrow [CD_4]^+ + [D]^+ \qquad (2.23)$$

where $[CD_5]^{2+}(*)$ indicates a dissociative state of $[CD_5]^{2+}$. From the energy diagram (Fig.83) it can be seen that this state must lie at least, (assuming that the fragments are generated in their ground state), 22.8 eV above the $[CD_5]^+$ ground state, and 2.5 eV above the stable $[CD_5]^{2+}$ state reached vertically by charge stripping by Proctor et al. [258] or 0.8 eV above the one reached in the experiments of Stahl et al. [260].

In the $[CD_4]^+$ fragment peak there is also a *more intense, narrower* dished structure ($E_1/E_2$), corresponding to a kinetic energy release of a 3.0±0.1 eV. It has no counterpart in the $[D]^+$ peak. Thus there must be a repulsive state of $[CD_5]^+$ lying ca 8 eV above its ground state, which dissociates into $[CD_4]^+$ and D fragments (see the energy diagram). This is in keeping with the observation that the center of $E_1/E_2$ is displaced to a higher kinetic energy than that of $D_1/D_2$, by an amount which corresponds to the process generating $E_1/E_2$ being ca 15 eV less endothermic than that for $D_1/D_2$. In contrast to our $[CD_4]^+$ fragment peak (Fig.82(b))' the analogous $[CH_4]^+$ peak signal presented by Stahl et al. [260] does not contain dishing in the broad component, only a broad, rectangular feature. The kinetic energy release as derived from the width of the broad component at half height , was reported to be 4.7 eV; if estimated from the shoulders of the broad component, a much smaller value, ca 3 eV, is obtained. We therefore propose that their broad component corresponds with the intense $E_1/E_2$ component in Fig.82(b) and not as proposed by them, with the charge separation reaction (2.22), the weak $D_1/D_2$ feature in Fig.82(b). Stahl et al. [260] also carried out ab initio molecular orbital theory calculations for $[CH_5]^+$ and $[CH_5]^{2+}$, and obtained a reverse activation barrier of 4.78 eV for the reaction $[CH_5]^{2+} \rightarrow [CH_4]^+ + [H]^+$, which is in excellent agreement with the kinetic energy releases of the $A_1/A_2$ and $D_1/D_2$ features of the $[D]^+$ and $[CD_4]^+$ signals, respectively (see above).

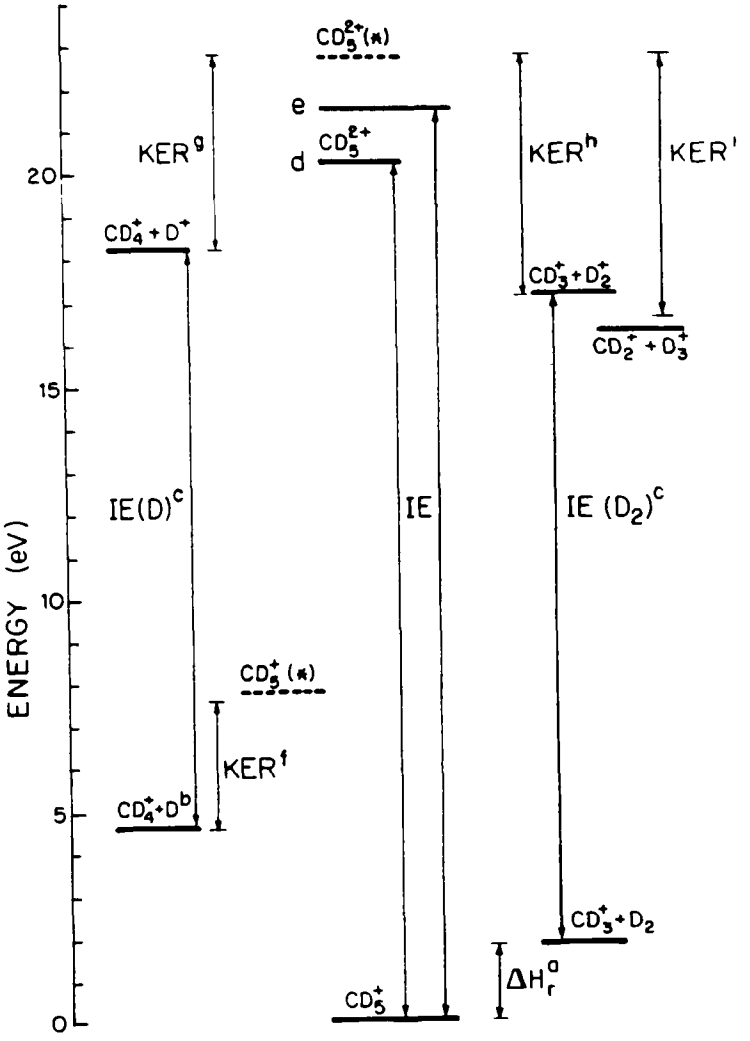


Figure 83 Energy diagram for the dissociative states and products of $[CD_5]^+$ and $[CD_5]^{2+}$. Broken lines indicate energy levels assigned to the dissociative states observed in this work.

[a] Ionization energies from [256].

[b] $\Delta H$ is determined as $\Delta H = \Delta H_1 + \Delta H_2$, where $\Delta H_1$ is the enthalpy change for the reaction $[CD_5]^+ = CD_4 + [D]^+$ [255] and $\Delta H_2$ is the enthalpy change for the reaction $CD_4 + [D]^+ = [CD_4]^+ + D$ [256].

[c] $\Delta H_r$ is the enthalpy change for the reaction $[CD_5]^+ = [CD_3]^+ + D_2$ [255].

[d] Vertical ionization energy of $[CD_5]^+$ from [259].

[e] Vertical ionization energy of $[CD_5]^+$ from [260].

[f] Kinetic energy release for peak $E_1/E_2$ in Fig.82(b).

[g] Kinetic energy release for peak $A_1/A_2$ in Fig.82(b).

[h] Kinetic energy release for peak $B_1/B_2$ in Fig.82(b).

[i] Kinetic energy release for peak $C_1/C_2$ in Fig.82(b).

In the kinetic energy spectrum of the $[D_2]^+$ fragments there is a relatively small, but clearly resolved dished structure $B_1/B_2$. The kinetic energy release involved was calculated to be 5.6±0.1 eV; its magnitude indicates that it too, arises from dissociation of $[CD_5]^{2+}$. There is no counterpart of this structure in the $[CD_3]^+$ peak, but this can be due to the collision induced dissociation into $[CD_3]^+$ + $D_2$ having so much larger a cross section that the tailing of the peak corresponding to this process completely obscures the counterpart of the $B_1/B_2$ dished peak. It must also be noted that the difference in kinetic energy release for $A_1/A_2$ and $B_1/B_2$ is 1.0 eV, which, within experimental error, is the difference between the energy of $[CD_4]^+$+$[D]^+$ and $[CD_3]^+$+$[D_2]^+$ see Fig.83. We conclude therefore that the $[CD_5]^{2+}$ ion dissociates over the same barrier into $[CD_4]^+$+$[D]^+$ and $[CD_3]^+$+$[D_2]^+$.

$[D_3]^+$ ions are also generated upon collision of $[CD_5]^+$ with $O_2$, albeit in smaller abundance than $[D_2]^+$ and $[D]^+$. This indicates that part of the $[CD_5]^+$ ions have the $C_{2v}$ structure, which could be considered as an ionized $D_2C$ $D_3$ complex. Ab initio molecular orbital theory calculations [262] predicted the $C_{2v}$ structure to be only 4 $kJmol^{-1}$ higher in energy than the most stable $C_S$ structure. Again there is a dished component present in the $[D_3]^+$ peak ($C_1/C_2$ in Fig.82(b)), originating from the charge separation reaction $[CD_5]^{2+} \rightarrow [CD_2]^+$+$[D_3]^+$. The measured kinetic energy release, 6.2±0.2 eV, shows that again the same barrier for dissociation is involved ( see the energy diagram in Fig.83).

### (C) HR Fragments

We have discussed observations on the generation of long-lived ( >1 μs) HR fragments in collisions between small ions having keV translational energy and rare gas target atoms, (Xe, He). General mechanisms were established for the production of the HR fragments based on the analysis of their kinetic energy spectra. In the

case of He as target, a common mechanism is the collisional excitation of the projectile ion into a dissociative HR state (described as process 2 in section 2.5.1). Such a state can be described as a doubly charged ionic core, (of a particular electronic state), surrounded by an electron in a distant orbit, hundreds of angstroms in diameter. The doubly charged core dissociates without being affected by the HR electron. When the fragments have fully separated, the HR electron joins one of them, giving rise to a neutral HR species. Therefore the HR fragments originating from this process reflect the dissociative properties of the electronic state of the doubly charged ion to which the intermediate HR state converges.

The kinetic energy spectra were recorded for the HR fragments from collisions between $[CD_5]^+$ ions of 9.9 keV translational energy and He target gas. The spectra are shown in Fig.84.

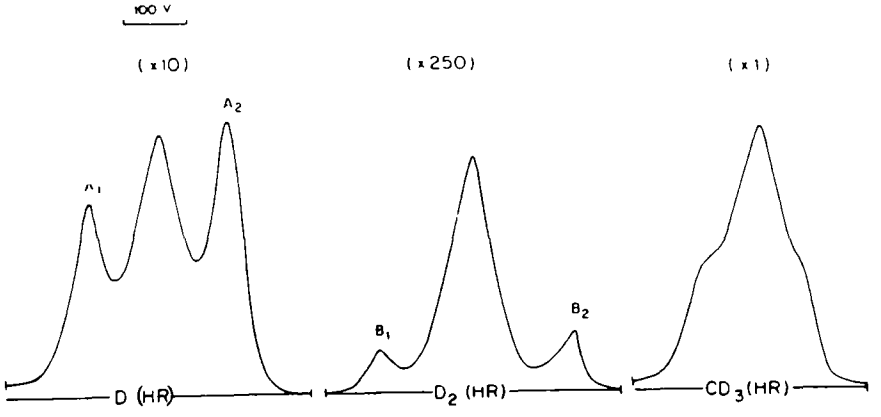


Figure 84. Field induced ion kinetic energy spectra of D(HR), $D_2$(HR) and $CD_3$(HR) fragments from 9.9 keV $[CD_5]^+$/He collisions - see text for discussion.

There are atomic (D(HR)), diatomic ($D_2$(HR)) and tetratomic ($CD_3$(HR)) metastable HR fragments observed. Rotational and vibrational degrees of freedom make di- and polyatomic HR species susceptible to fast radiationless decay processes, such as

autoionization and predissociation, (for a detailed discussion of these effects see reference [217]), which can explain the absence of other metastable HR fragments, e.g. $CD_4$(HR) etc., in these experiments. The possible reason for the stability of the observed HR species has been discussed in section 2.5.3. All the peaks in Fig.84 contain a central narrow component which must be generated by the process described as process 1 in section 2.5.1, namely electron capture into a HR orbit by $[CD_5]^+$ and simultaneous vibrational excitation of the ionic core into the dissociative continuum. The D(HR) and $D_2$(HR) fragment peaks have a dished component: $A_1/A_2$ and $B_1/B_2$, respectively. The kinetic energy release calculated from the distance between the maxima of $A_1/A_2$ is 4.6±0.2 eV and for $B_1/B_2$ is 5.4±0.2 eV. These values agree, within experimental error, with those obtained above for the $[D]^+$ and $[D_2]^+$ fragments in the $O_2$ collision induced dissociation of $[CD_5]^+$, and which were attributed to the dissociation of an electronic state of $[CD_5]^{2+}$ into $[CD_4]^+$+$[D]^+$ and $[CD_3]^+$+$[D_2]^+$. We therefore propose that the formation of an intermediate, dissociative HR state of $[CD_5]^+$ converging to the same doubly charged state, is involved in the production of HR fragments in keV $[CD_5]^+$/He collisions. The peak corresponding to $CD_3$(HR) fragments also contains a broad component. The released kinetic energy, estimated from the distance across the shoulders of the broad peak was 1.6 eV, indicating that this component must arise from a different mechanism than that which accounts for ($B_1/B_2$) of the $D_2$(HR) fragments. Note also that this broad feature is asymmetrically placed around the central narrow peak, lying towards lower energies, indicating that the process which generates it is more endothermic (ca 4 eV) than process 1 for $CD_3$(HR) generation. We have already observed similar features in the kinetic energy spectra of X(HR) (X=C, N or O) fragments from $[XH]^+$/He collisions, and have assigned a common mechanism to their generation (see section 2.5.3). We propose a similar process for the appearance of

the broad feature in the $CD_3$(HR) peak. It can be described as electron capture into a HR orbit by $[CD_5]^+$ upon collision with He together with the simultaneous excitation of the ionic $[CD_5]^+$ core into a repulsive electronic state which dissociates into $[CD_3]^+ + D_2$; after dissociation the HR electron joins the $[CD_3]^+$ fragment giving rise to a $CD_3$(HR) fragment.

# References


[1] R.P.Morgan, J.H.Beynon, R.H.Bateman and N.B. Green, *Int. J. Mass Spectrom. Ion Physics*, **28** 171 (1978).

[2] K.Levsen, *"Fundamental Processes in Organic Mass Spectrometry"*, Verlag Chemie, New York, 1978, pp. 42-47.

[3] H.M.Rosenstock, M.B.Wallenstein, A.L.Wahrhaftig and H.Eyring, *Proc. Nat. Acad. Sci.*, **38** 667 (1952).

[4] W.Forst, *"Theory of Unimolecular Reactions"*, Academic Press, New York, 1973.

[5] J.Bordas-Nagy, J.L.Holmes and A.A.Mommers, *Org. Mass Spectrom.*, **21** 629 (1986).

[6] F.W.Aston, *Proc. Cambridge Phyl. Soc.*, **19** 317 (1919).

[7] F.W.Aston, *"Mass Spectra and Isotopes"*, 2nd Edition, Arnold, London,1942.

[8] R.G.Cooks (Ed.), *"Collision Spectroscopy"*,Plenum Press, New York, 1978.

[9] F.W.McLafferty (Ed.), *"Tandem Mass Spectrometry"*, John Wiley and Sons, New York, 1983.

[10] J.L.Holmes, *Org. Mass Spectrom.*, **20** 169 (1985).

[11] C.Wesdemiotis and F.W.McLafferty, *Chem. Rev.*, **87** 485 (1987).

[12] J.K.Terlouw and H.Schwarz, *Ang.Chem.Int.Ed.Engl.*, **26** 805 (1987).

[13] J.Durup, in K.Ogata and T.Hayakawa (Eds.), *"Recent Developments in Mass Spectrometry"*, Univ. of Tokyo Press, Tokyo, 1970.

[14] J.Durup, P.G.Fournier and Pham Dong, *Int. J. Mass Spectrom. Ion Physics*, **2** 311 (1969).

[15] G.W.McClure and J.M.Peek, *"Dissociation in Heavy Particle Collisions"*, Wiley Interscience Series in Atomic and Molecular Collision Processes, Wiley Interscience, New York, 1972.

[16] J.Los and T.Govers, in R.G.Cooks (Ed.), *"Collision Spectroscopy"*, Plenum , Press, New York, 1978, pp. 289-356.

[17] J.Los, *Ber. Bunsen-Gesell. Phys. Chem.*, **77** 640 (1973).

[18] G.H.Dunn, *Phys. Rev. Lett.*, **8** 62 (1962).

[19] T.A.Green and J.M.Peek, *Phys. Rev.*, **183** 166 (1969).

[20] D.K.Gibson, J.Los and J.Schopman, *Physica*, **40** 385 (1968).

[21] G.W.McClure, *Phys. Rev.* , **A140** 769 (1965).

[22] I.Sauers, R.L.Fitzwilson, J.C.Ford and E.W.Williams, *Phys. Rev.*, **A6** 1418 (1972).

[23] M.Vogler and W.Seibt, *Z.Phys.*, **A210** 337 (1968).

[24] T.A.Green, *Phys. Rev.*, **A1** 1416 (1970).

[25] B.Meierjohann, *Physica*, **65** 41 (1973).

[26] B.Meierjohann and M.Vogler, *Z. Physik*, **A282** 7 (1977).

[27] W.Baldreich, W.W.Lotz and H.Ewald, *Z. Physik*, **A317** 23 (1984).

[28] R.Caudano and J.M.Delfosse, *J.Phys.*, **B2** 813 (1968).

[29] S.J.Anderson and J.B.Swan, *Phys. Lett.*, **A48** 435 (1974).

[30] S.J.Anderson, *J. Chem. Phys.*, **60** 3278 (1974).

[31] A.Russek, *Physica*, **48** 165 (1970).

[32] G.Comtet, P.G.Fournier and B.Lassier-Govers, *Chem. Phys.*, **101** 299 (1986).

[33] A.G.Brenton, P.G.Fournier, B.L.Govers, E.G.Richard and J.H.Beynon, *Proc. Roy. Soc. London*, **A365** 111 (1984).

[34] P.G.Fournier, A.G.Brenton, P.Jonathan and J.H.Beynon, *Int. J. Mass Spectrom. Ion Processes*, **79** 81 (1987).

[35] H.H.Michels, *J.Chem. Phys.*, **44** 3834 (1966).

[36] T.A.Green, H.H.Michels, J.C.Browne and M.M.Madsen, *J. Chem. Phys.*, **61** 5186 (1974).

[37] J.Schopman, P.G.Fournier and J.Los, *Physica*, **63** 518 (1973).

[38] J.Schopman and J.Los, *Physica*, **51** 132 (1971).

[39] J.C.Houver. J.Baudon, M.Abignoli, M.Varat, P.G.Fournier and J.Durup, *Int. J. Mass Spectrom. Ion Physics*, **4** 137 (1970).

[40] J.M.Peek, *Physica*, **60** 93 (1973).

[41] J.Schopman, J.Los and J.Maas, *Physica*, **51** 113 (1971).

[42] W.Seibt, *Abstracts VIth ICPEAC,* M.I.T. Press, Cambridge Massachusetts, 1969, p.803.

[43] Pham Dong and J.Durup, *Chem. Phys. Lett.*, **5** 340 (1970).

[44] J.T.Park, *Phys. Rev.*, **182** 152 (1969).

[45] J.T.Park, *Phys. Rev.*, **185** 152 (1969).

[46] J.H.Moore Jr. and J.P.Doering, *Phys. Rev. Lett.*, **23** 264 (1969).

[47] J.H.Moore Jr., *Bull. Am. Phys. Soc.*, **17** 1142 (1972).

[48] J.H.Moore Jr., *Phys. Rev.*, **A9** 2043 (1974).

[49] J.H.Moore Jr., *J.Geophys. Res.*, **77** 5567 (1972).

[50] J.H.Moore Jr., *Phys. Rev.*, **A8** 2359 (1973).

[51] J.H.Moore Jr., *Phys. Rev.*, **A10** 724 (1974).

[52] E.Wigner, *Nachr. Akad. Wiss. Goettingen, Math-Physik*, **Kl IIa** 375 (1927).

[53] H.S.W.Massey and E.H.S.Burhop, *"Electronic and Ionic Impact Phenomena"*, Oxford U.P., London, 1952, pp. 427-432, 522-524.

[54] J.H.Moore Jr., *J Phys. Chem.*, **76** 1130 (1972).

[55] J.P.Doering and J.H.Moore Jr., *J. Chem. Phys.*, **56** 2176 (1972).

[56] F.A.Herrero and J.P.Doering, *Phys. Rev. Lett.*, **29** 609 (1972).

[57] J.T.Park, in R.G.Cooks (Ed.), *"Collision Spectroscopy"*, Plenum Press, New York, 1978, pp. 19-90.

[58] N.Kobayashi, Y.Itoh and Y.Kaneko, *J.Phys. Soc. Japan*, **45** 617 (1978).

[59] F.Linder, in N.Oda and T.K.Takayanagi (Eds.), *"Electronic and Atomic Collisions"*, North-Holland, Amsterdam, 1980, pp. 535-546.

[60] Y.Itoh, N.Kobayashi and Y.Kaneko, *J. Phys.*, **B14** 679 (1981).

[61] A.J.Illies and M.T.Bowers, *Chem. Phys.*, **65** 281 (1982).

[62] A.O'Keefe, A.J.Illies, J.R.Gilbert and M.T.Bowers, *Chem. Phys.*, **82** 471 (1983).

[63] A.O'Keefe, R.Derai and M.T.Bowers, *Chem. Phys. Lett.*, **113** 93 (1985).

[64] A.O'Keefe, R.Derai and M.T.Bowers, *Chem. Phys.*, **91** 161 (1984).

[65] J.P.Maier and M.Rösslein, *J.Chem. Phys.*, **88** 4614 (1988).

[66] S.C.Goh and J.B.Swan, *Phys. Rev.*, **A24** 1624 (1981).

[67] J.L.Holmes and J.E.Szulejko, *Chem. Phys. Lett.*, **106** 292 (1984).

[68] J.M.Curtis and R.K.Boyd, *J. Chem. Phys.*, **80** 1151 (1984).

[69] J.M.Curtis and R.K.Boyd, *J. Chem. Phys.*, **81** 2991 (1984).

[70] R.W.Wetmore, R.J.LeRoy and R.K.Boyd, *J. Phys. Chem.*, **88** 6318 (1984).

[71] D.L.Cooper, *Chem. Phys. Lett.*, **132** 377 (1986).

[72] D.M.Curtis and J.H.D.Eland, *Int. J. Mass Spectrom. Ion Processes*, **63** 241 (1985).

[73] W.Koch, B.Liu, T.Weiske, C.B.L. Lebrilla, T.D. Drewello and H.Schwarz, *Chem. Phys. Lett.*, **142** 147 (1987).

[74] K.R.Jennings, *Int. J. Mass Spectrom. Ion Physics*, **1** 227 (1968).

[75] F.W.McLafferty and H.D.R.Schuddemage, *J. Am. Chem. Soc.*, **91** 1886 (1969).

[76] W.F.Haddon and F.W.McLafferty, *J. Am. Chem. Soc.*, **90** 4745 (1968).

[77] F.W.McLafferty, P.F.Bente III, R.Kornfeld, S.C.Tsai and I.Howe, *J. Am. Chem. Soc.*, **95** 2120 (1973).

[78] F.W.McLafferty, R.Kornfeld, W.F.Haddon, K.Levsen, I.Sakai, P.F.Bente,

S.C.Tsai and H.D.R.Schuddemage, *J. Am. Chem. Soc.*, **95** 3886 (1973).

[79] J.H.Beynon and R.G.Cooks, *Res. Develop.*, **22** 26 (1971).

[80] T.Wacks, P.F.Bente and F.W.McLafferty, *Int. J. Mass Spectrom. Ion Phys.*, **9** 333 (1972).

[81] R.G.Cooks, in R.G.Cooks (Ed.), *"Collision Spectroscopy"*, Plenum Press, New York, 1978, pp. 357-450.

[82] S.A.McLuckey, C.E.D.Ouwerkerk, A.J.H.Boerboom and P.G.Kistemaker, *Int. J. Mass Spectrom. Ion Processes,* **59** 85 (1984).

[83] B.Brehm, J.H.D.Eland, R.Frey and H.Schulte, *Int. J. Mass Spectrom. Ion Physics,* **21** 373 (1976).

[84] G.Bischof, V.Hermann, J.Krutein and F.Linder, *J. Phys.*, **B15** 249 (1982).

[85] G.L.Glisch, S.A.McLuckey, T.Y.Ridley and R.G.Cooks, *Int. J. Mass Spectrom. Ion Processes,* **41** 157 (1982).

[86] S.A.McLuckey, *Org. Mass Spectrom.*, **19** 544 (1984).

[87] H.S.W.Massey, *Rep. Prog. Phys.*, **12** 248 (1949).

[88] J.B.Hasted, *"Physics of Atomic Collisions"*, 2nd ed.,American Elsevier, Neww York, 1972, p. 621.

[89] M.S.Kim and F.W.McLafferty, *J. Am. Chem. Soc.*, **100** 3279 (1978).

[90] C.J.Proctor and F.W.McLafferty, *Org. Mass Spectrom.*, **18** 193 (1983).

[91] F.W.McLafferty and C.J.Proctor, *Org. Mass Spectrom.*, **18** 272 (1983).

[92] C.J.Porter, R.P.Morgan and J.H.Beynon, *Int. J. Mass Spectrom. Ion Processes,* **28** 321 (1978).

[93] F.W.McLafferty, A.Hirota, M.P.Barabalas and R.F.Pegues, *Int. J. Mass Spectrom. Ion Processes,* **35** 299 (1980).

[94] J.A.Laramee, P.Cameron and R.G.Cooks, *J. Am. Chem. Soc., 103* 12 (1981).

[95] R.D.Bowen, M.P.Barbalas, F.P.Pagano, P.J.Todd and F.W.McLafferty,

*Org. Mass Spectrom.*, **15** 51 (1980).

[96] J.L.Holmes, J.K.Terlouw, P.C.Burgers and R.T.B.Rye, *Org. Mass Spectrom.*, **15** 149 (1980).

[97] F.W.McLafferty, M.P.Barbalas and F.Turecek, J.Am. Chem. Soc., **105** 1 (1983).

[98] C.E.D.Overkerk, S.A.McLuckey, P.G.Kistemaker and A.J.H.Boerbom, *Int. J. Mass Spectrom. Ion Processes,* **56** 11 (1984).

[99] F.M.Bockhoff and F.W.McLafferty, *J. Am. Chem. Soc.*, **101** 1793 (1979).

[100] M.S.Kim, *Int. J. Mass Spectrom. Ion Procsses,* **50** 189 (1983).

[101] L.M.Bass and M.T.Bowers, *Org. Mass Spectrom.*, **17** 229 (1982).

[102] F.W.McLafferty and M.Bockhoff, *J. Am. Chem. Soc.,* **101** 1783 (1979).

[103] D.Rapp and W.E.Francis, *J. Chem. Phys.*, **37** 2631 (1962).

[104] J.B.Hasted, *Adv. At. Mol. Phys.*, **4** 237 (1968).

[105] E.F.Gurnee and J.L.Magee, *J. Chem. Phys.*, **26** 155 (1957).

[106] T.F.Moran, in *"Electron-Molecule Interactions and Their Applications"* Vol.2, Academic Press, New York, 1984, pp. 1-64.

[107] H.Hayden and N.G.Utterback, *Phys. Rev.*, **A135** 1575 (1964).

[108] W.N.Shelton and B.A.Stoicheff, *Phys. Rev.*, **A3** 613 (1971).

[109] F.L.Eisele and S.W.Nagy, *J. Chem. Phys.*, **65** 752 (1976).

[110] R.Hegeberg, T.Stefanson and M.T.Elford, *J. Phys.*, **B11** 133 (1978).

[111] B.L.Moiseiwitsch, *Proc. Phys. Soc. London,* **A69** 653 (1956).

[112] D.P.Hodgkinson and J.S.Briggs, *J.Phys.*, **B9** 255 (1976).

[113] D.P.Sural, S.C.Mukherjee and N.C.Sil, *Phys. Rev.*, **A164** 156 (1967).

[114] J.B.Hasted, in D.R.Bates (Ed.), *"Atomic and Molecular Processes",* Academic Press, New York, 1962,

[115] J.B.Hasted, *Proc. Roy. Soc. London,* **A205** 421 (1951).

[116] J.B.Hasted, *Proc. Roy. Soc. London,* **A212** 235 (1952).

[117] D.R.Bates and N.Lynn, *Proc. Roy. Soc. London,* **A253** 141 (1959).

[118] C.Reynaud, J.Pommier, Tuan Vu Ngoc and M.Barat, *Phys. Rev. Lett.,* **43** 579 (1979).

[119] T.O.Tiermann and C.Lifshitz, *Advances in Chemical Physics,* **45** 82 (1981).

[120] E.Pollack and Y.Jahn, *Adv. At. Mol. Phys.,* **22** 243 (1986).

[121] W.H.Cramer and A.B.Marcus, *J. Chem. Phys.,* **32** 186 (1960).

[122] O.Hollricher, *Z. Phys.,* **A187** 41 (1965).

[123] H.R.Rothwell, B.Van Zyl and R.C.Amme, *J. Chem. Phys.,* **61** 3851 (1974).

[124] T.F.Moran, M.R.Flannery and D.L.Albritton, *J. Chem. Phys.,* **62** 2869 (1975).

[125] D.R.Bates and R.H.G.Reid, *Proc. Roy. Soc.,* **A310** 1 (1969).

[126] M.R.Flannery, P.C.Cosby and T.F.Moran, *J. Chem. Phys.,* **59** 5494 (1973).

[127] T.F.Moran and M.R.Flannery, *J. Chem. Phys.,* **66** 370 (1977).

[128] R.H.Neynaber and G.D.Magnuson, *J. Chem. Phys.,* **59** 825 (1973).

[129] A.BLees and P.K.Rol, *J. Chem. Phys.,* **61** 4444 (1974).

[130] A.B.Lees and P.K.Rol, *J.Chem. Phys.,* **63** 2461 (1975).

[131] J.B.Wilcox and T.F.Moran, *J. Chem. Phys.,* **85** 989 (1981).

[132] G.C.Shields, L.Wendenberg, J.B.Wilcox and T.F.Moran, *Org. Mass Spectrom.,* **21** 137 (1986).

[133] G.C,Shields, P.A.Steiner, P.R.Nelson, M.C.Traumer and T.F.Moran, *Org. Mass Spectrom.,* **22** 64 (1987).

[134] J.B.Sedgewick, P.R.Nelson, P.A.SteinerIV and T.F.Moran, *Org. Mass Spectrom.,* **23** 256 (1988).

[135] G.I.Gellene and R.F.Porter, *Acc. Chem. Res.,* **16** 200 (1983).

[136] P.M.Curtis, B.W.Williams and R.F.Porter, *Chem. Phys. Lett.,* **65** 296 (1979).

[137] G.I.Gellene, B.W.Williams and R.F.Porter, *J.Chem. Phys.,* **74** 5636 (1981).

[138] G.I.Gellene, N.S.Kleinrock and R.F.Porter, *J. Chem. Phys.*, **78** 1795 (1983).

[139] D.M.Hudgins, A.B.Raksit and R.F.Porter, *Org. Mass Spectrom.*, **22** 375 (1988).

[140] S.J.Jeon, A.B.Raksit, G.I.Gellene and R.F.Porter, *J. Chem. Phys.*, **82** 4916 (1985).

[141] B.W.Williams and R.F.Porter, *J. Chem. Phys.*, **73** 5598 (1980).

[142] G.I.Gellene, D.I.Cleary and R.F.Porter, *J. Chem. Phys.*, **77** 3472 (1982).

[143] G.I.Gellene and R.F.Porter, *J. Chem. Phys.*, **88** 6680 (1984).

[144] S.J.Jeon, A.B.Raksit, G.I.Gellene and R.F.Porter, J. Am. Chem. Soc., **107** 4129 (1985).

[145] A.B.Raksit, S.J.Jeon and R.F.Porter, *J. Phys. Chem.*, **90** 2298 (1986).

[146] G.I.Gellene and R.F.Porter, *J. Chem. Phys.*, **81** 5570 (1984).

[147] A.B.Raksit and R.F.Porter, *Int. J. Mass Spectrom. Ion Processes,* **76** 299 (1987).

[148] G.I.Gellene and R.F.Porter, *High Temp. Science,* **17** 171 (1984).

[149] S.F.Selgren, D.E.Hipp and G.I.Gellene, *J. Chem. Phys.*, **88** 3116 (1987).

[150] G.I.Gellene and R.F.Porter, *Int. J. Mass Spectrom. Ion Processes,* **64** 55 (1985).

[151] G.Herzberg, *Ann. Rev. Phys. Chem.*, **38** 27 (1987).

[152] D.P.deBruijn and J.Los, *Rev. Sci. Instr.*, **53** 1020 (1982).

[153] D.P.deBruijn, J. Neuteboom and J.Los, *Chem. Phys.*, **85** 233 (9184).

[154] W.J.van der Zande, W.Koot, J.Petersen and J.Los, *Chem. Phys. Lett.*, **140** 175 (1987).

[155] W.J.van der Zande, W.Koot and D.P.deBruijn, *Phys. Rev. Lett.*, **57** 1219 (1986).

[156] F.W.McLafferty, P.J.Todd, D.C.McGilvery and M.A.Baldwin, *J. Am. Chem. Soc.*,

**102** 3360 (1980).

[157] P.O.Danis, R.Feng and F.W.McLafferty, *Anal. Chem.*, **53** 348 (1986).

[158] J.K.Terlouw, W.Kiefkamp, J.L.Holmes, A.A.Mommers and P.C.Burgers, *Int. J. Mass Spectrom. Ion Processes*, **64** 245 (1985).

[159] J.L.Holmes, A.A.Mommers,J.K.Terlouw and C.E.C.A.Hop, *Int. J. Mass Spectrom. Ion Processes*, **68** 249 (1986).

[160] P.O.Danis, R.Feng and F.W.McLafferty, *Anal. Chem.*, **53** 355 (1986).

[161] J.L.Holmes, F.P.Lossing, J.K.Terlouw and P.C.Burgers, *J. Am. Chem. Soc.*, **104** 2931 (1982).

[162] P.O.Danis, C.Wesdemiotis and F.W.McLafferty, *J. Am. Chem. Soc.*, **105** 7454 (1983).

[163] C.Wesdemiotis, R.Feng, P.O.Danis, E.R.Williams and F.W.McLafferty, *J. Am. Chem. Soc.*, **108** 5847 (1986).

[164] B.F.Yates, W.J.Bouma and L.Radom, *J. Am. Chem. Soc.*, **109** 2250 (1987).

[165] B.F.Yates, W.J.Bouma and L.Radom, *J. Am. Chem. Soc.*, **106** 5805 (1984).

[166] C.E.C.A.Hop, J.Bordas-Nagy, J.L.Holmes and J.K.Terlouw, *Org. Mass Spectrom.*, **23** 155 (1988).

[167] C.Wesdemiotis, R.Feng, M.A.Baldwin and F.W.McLafferty, *Org. Mass Spectrom.*, **23** 166 (1988).

[168] E.W.Muller, in L.Morton (Ed.), *"Advances in Electronics and Electron Physics"*, Academic Press, New York, 1960, Vol.13 , p. 87.

[169] H.D.Beckey, *"Field Ionization Mass Spectrometry"*, Pergamon Press, New York, 1971.

[170] W.D.Johnston and J.King, *Rev. Sci. Instrum.*, **37** 375 (1966).

[171] A.C.Riviere, *Methods of Experimental Physics*, **A7** 208 (1968).

[172] S.M.Tarr, J.A.Schiavonne and R.S.Freund, *Phys. Rev. Lett.*, **44** 1660 (1980).

[173] S.M.Tarr, J.S.Schiavonne and R.S.Freund, *J. Chem. Phys.*, **74** 2869 (1981).

[174] P.Hammond, F.H.Read and G.C.King, *J. Phys.* **B17** 2925 (1984).

[175] R.S.Freund, in R.F.Stebbings and F.B.Dunning (Eds.), *"Rydberg States of Atoms and Molecules"*, Cambridge University Press, Cambridge, 1983, pp.355-392

[176] F.G.Kellert, T.H.Jeys, G.B.McMillan, K.A. Smith, F.B.Dunning and R.F.Stebbings, *Phys. Rev.*, **A23** 1127 (1983).

[177] J.A.Schiavonne, D.E.Donahue, D.R.Derrick and R.S.Freund, *Phys.Rev.*, **A16** 48 (1977).

[178] J.L.Holmes and A.A.Mommers, *Org. Mass Spectrom.*, **19** 460 (1984).

[179] P.Varga and H.Winter, *Phys. Rev.* **A18** 2453 (1978).

[180] H.Hofer, W.Vanek, P.Varga and H.Winter, *Rev. Sci. Instrum.*, **54** 150 (1983).

[181] N.Kobayashi, T.Matsuo and Y.Kaneko, *J. Phys. Soc. Jpn.*, **49** 1195 (1980).

[182] J.Appel, J.Durup,, J.B.Ozenne, M.Durup and G.Parlant, *Chem. Phys.*, **25** 245 (1977).

[183] E.V.Aparina, A.A.Balakai, N.V.Kir Yakov and V.L.Tal'Roze, *Dokl. Akad. Nauk. SSSR*, **262** 630 (1982).

[184] E.V.Aparina, A.A.Balakai, N.V.Kir'Yakov and V.L.Tal'Roze, *Dokl. Akad. Nauk. SSSR*, **269** 395 (1983).

[185] E.V.Aparina, A.A.Balakai, N.V.Kir'Yakov and V.L.Tal'Roze, *Sov. J. Chem. Phys.*, **2** 2751 (1983).

[186] S.E.Kupriyanov, *Sov. Phys. JETP. Lett.*, **5** 197 (1967).

[187] P.R.Freeman, in D.Kleppner and F.M.Pimpkin (Eds.), *"Atomic Physics"*, Plenum Press, New York, 1981, pp. 209-229.

[188] M.Barat, D.H.Dhuicq, R.Francois, C.C.Lesech and R.McCaroll, *J.Phys.*,

**B6** 1206 (1973).

[189] S.E.Kupriyanov, *Zh. Eksp. Teor. Fiz.*, **48** 467 (1965).

[190] S.E.Kupriyanov, *Zh. Eksp. Teor. Fiz.*, **55** 460 (1968).

[191] R.S.Freund, *J. Chem. Phys.*, **54** 3125 (1971).

[192] K.C.Smyth, J.A.Schiavonne and R.S.Freund, *J. Chem. Phys.*, **59** 5225 (1973).

[193] J.Bordas-Nagy and J.L.Holmes, *Chem. Phys. Lett.*, **132** 200 (1986).

[194] J.E.Szulejko, A.Mendez-Amaya, R.P.Morgan, A.G.Brenton and J.H.Beynon, *Proc. Roy. Soc. London,* **A373** 1 (1980).

[195] A.Mendez-Amaya, A.G.Brenton, J.E.Szulejko and J.H.Beynon, *Proc. Roy. Soc. London,* **A373** 13 (1980).

[196] B.A.Rumpf and P.J.Derrick, *Int. J. Mass Spectrom. Ion Processes,* **82** 239 (1988).

[197] F.von Busch and G.H.Dunn, *Phys. Rev.*, **A5** 1726 (1971).

[198] R.Caudano and J.M.Delfosse, *J. Phys.*, **B2** 813 (1968).

[199] D.H.Jaecks, W.de Rijk and P.J.Martin, *Proc. 7th International Conf. Phys. Electr. Atomic Coll.*, 1971, p. 424

[200] J.C.Traeger and A.A.Mommers, *Org. Mass Spectrom.*, **22** 592 (1987).

[201] W.Schultz, B.Meierjohann, W.Seibt and H.E.Ewald, in K.Ogata and T.Hayakawa (Eds.), *"Recent Developments in Mass Spectrometry"*, University of Tokyo Press, Tokyo, 1970, p.939.

[202] W.C.Wells, W.L.Borst and E.C.Zipf, *Phys. Rev.*, **A14** 695 (1976).

[203] A.O'Keefe and J.R.McDonald, *Chem.Phys.* **103** 425 (1986).

[204] N.H.F.Beebe, E.W.Thulstrup and A.A.Andersen, *J.Chem.Phys.* **68** 2080 (1976).

[205] K.P.Huber and G.Herzberg, *"Constants of Diatomic Molecules"*, Van Nostrand Reinhold, New York, 1979.

[206] R.S.Berry, *Rec. Chem. Prog.*, **31** 9 (1970).

[207] M.E.Rudd and K.Smith, *Phys. Rev.*, **169** 79 (1968).

[208] P.H.Krupenie, *J. Phys. Chem. Ref. Data*, **1** 423 (1972).

[209] R.W.Wetmore and R.K.Boyd, *J. Phys. Chem.*, **90** 6091 (1986).

[210] R.W.Wetmore, R.K.Boyd and R.J.LeRoy, *Chem. Phys.* **89** 329 (1984).

[211] W.Koch and H.Schwarz, *Int. J. Mass Spetrom. Ion Processes*, **68** 49 (1986).

[212] S.A.Pope, I.M.Hillier, M.F.Grant and J.Kendric, *Chem. Phys. Lett.*, **95** 247 (1983).

[213] W.Koch, N.Heinrich, H.Schwarz, F.Maquin and D.Stahl, *Int. J. Mass Spetrom. Ion Processes*, **67** 305 (1985).

[214] H.Sun and K.F.Freed, *Chem. Phys. Lett.*, **78** 531 (1981).

[215] M.F.Guest and D.M.Hirst, *Mol. Phys.*, **34** 1611 (1977).

[216] M.F.Guest and D.M.Hirst, *Mol. Phys.*, **49** 1461 (1983).

[217] S.M.Tarr, J.A.Schiavone and R.S.Freund, *J. Chem. Phys.*, **74** 2869 (1981).

[218] Y.Band, *J. Phys.*, **B7** 2072 (1974).

[219] pp. 374-378 in reference [175].

[220] P.E.M.Siegbahn, *Chem. Phys.*, **66** 443 (1982).

[221] J.A.Pople, B.Tidor and P.von Schleyer, *Chem. Phys. Lett.*, **88** 533 (1982).

[222] J.J.Thomson, *Phyl. Mag.*, **21** 225 (1912).

[223] J.A.Burt, J.L.Dunn, M.J.McEwan, M.M.Sutton, A.E.Roche and H.I.Schiff, *J. Chem. Phys.*, **52** 6062 (1970).

[224] J.K.Kim, L.P.Theard and W.T.Huntress, *Int. J. Mass Spectrom. Ion Phys.* **15** 223 (1974).

[225] K.R.Ryan, *J. Chem. Phys.*, **61** 1559 (1974).

[226] A.B. Raksit, *Int. J. Mass Spectrom. Ion Processes*, **41** 185 (1982).

[227] M.L.Vestal, C.R.Blakley, P.W.Ryan and J.H.Futrell, *J.Chem.Phys.*, **64** 2094 (1976).

[228] C.R.Blakley, M.L.Vestal and J.H.Futrell, *J. Chem. Phys.*, **66** 2094 (1976).

[229] D.Smith, Phyl. *Trans. Roy. Soc. London,* **323** 269 (1987).

[230] J.K.Watson, S.C.Foster and R.W. McKellar, *Can. J. Phys.*, **65** 38 (1987).

[231] A.Carrington and R.A. Kennedy, *J. Chem. Phys.*, **81** 91 (1984).

[232] J.Tennyson and B.T.Sutcliffe, *J. Chem. Soc. Faraday Trans.*, **82** 1151 (1986).

[233] J.M.Gomez and E.Pollak, *Chem. Phys. Lett.*, **138** 125 (1987).

[234] L.J.Schaad and W.V.Hicks, *J. Chem. Phys.*, **61** 1934 (1974).

[235] C.W.Bauschlicher,Jr., S.V.O'Neil, R.K.Preston and H.F.Schaefer III, *J. Chem. Phys.*, **59** 1286 (1973).

[236] J.C. Tully, *Advances in Chemical Physics,* **42** 102 (1980).

[237] G.H.Dunn, R.Geballe, and D.Pretzer, *Phys. Rev.* **A128** 2200 (1962).

[238] E.W.Thomas, R.L.Fitzwilson, I.Savers and J.C.Ford, *J. Chem. Phys.*, **63** 4092 (1975).

[239] J.C.Ford, F.M.McCay, R.Conrads and E.W.Thomas, *Phys. Rev.*, **A5** 1705 (1972).

[240] F.B.Yousif, J.Geddes and H.B.Gilbody, *J .Phys.*, **B19** 217 (1986).

[241] O.Yenen and D.H.Jaecks, *Phys. Rev.*, **A32** 836 (1985).

[242] C.R.Blakley, M.L.Vestal and J.H.Futrell, *J. Chem. Phys.*, **66** 2392 (1977).

[243] P.G.Burton, E.von Nagy-Felsobukki,G.Doherty and M.Hamilton, *Mol. Phys.*, **55** 527 (1985).

[244] M.J.Gailard, D.S.Gemmel, G.Goldring, I.Levine, W.J.Pietsch, J.C.Poizat, R.J.Ratkowski, J.Remilleux, Z. Wager, and B.J.Zabrowsky, *Phys. Rev.*, **A17** 1797 (1978).

[245] T.E.Sharp, *At. Data,* **2** 119 (1971).

[246] B.A.Rumpf, C.E.Allison and P.J.Derrick, *Org. Mass Spectrom.*, **21** 294 (1986).

[247] J.C.Tully and R.K.Preston, *J. Chem. Phys.*, **55** 562 (1971).

[248] C.E.Moore, *"Atomic Energy Levels"*, National Bureau of Standards, 1949, 1952, 1958, Vol. 1-3.

[249] H.Conroy, *J. Chem. Phys.*, **51** 3979 (1969).

[250] F.Campbell, R.B.Browning and C.J.Latimer, *J. Phys.*, **B14** 3493 (1981).

[251] W.J. Griffiths, F.M. Harris, A.G. Brenton and J.H. Beynon, *Int. J. Mass Spectrom. Ion Processes,* **74** 317 (1986).

[252] S.F. Selgren and G.I. Gellene, *J. Chem. Phys.*, **87** 5804 (1987).

[253] W.A. Lathan, W.J.Hehre, L.A. Curtiss and J.A. Pople, *J.Am.Chem.Soc.*, **93** 6377 (1971).

[254] K. Morokuma and R.E. Davis, *J. Am. Chem. Soc.*, **94** 1060 (1971).

[255] A. Komornicki and D.A. Dixon, *J. Chem. Phys.*, **86** 5625 (1987).

[256] H.M. Rosenstock, K. Draxl, B.W. Steiner and J.T. Herron, *J. Phys. Chem.Ref.Data,* **6** Suppl. 1 (1977).

[257] C.E.C.A. Hop, J. Bordas-Nagy, J.L.Holmes and J.K.Terlouw, *Org. Mass Spectrom.*, **23** 155 (1988).

[258] C.E.C.A. Hop, Ph.D. Thesis, University of Utrecht, Utrecht The Netherlands, 1988, p. 43.

[259] C.J.Proctor, C.J.Porter, T.Ast, P.D.Bolton and J.H.Beynon, *Org. Mass Spectrom.*, **16** 454 (1981).

[260] D. Stahl, F. Maquin, T. Gaumann, H. Schwartz, P.A. Carrupt and P. Vogel, *J. Am. Chem. Soc.*, **107** 5049 (1985).

[261] M. Roussel and A. Julienne, *Int. J. Mass Spetrom. Ion Processes,* **9** 449 (1972).

[262] W.J.Hehre, L.Radom, P.v.R.Schleyer and J.A.Pople, *"Ab Initio Molecular Orbital Theory"*, John Wiley and Sons, New York, 1986, pp. 381-382 and references therein.